Electronic Structure of 3*d* Transition-Atom Impurities in Semiconductors

ALEX ZUNGER

Solar Energy Research Institute
Golden, Colorado 80401

I. Introduction 276
II. Phenomenology and Terminology 277
1. Impurity Oxidation and Charge States 277
2. Elements of Electronic Structure in T_d Symmetry 282
III. Observable Phenomena and Data 290
3. Types of Experiments 290
4. Stationary, Chemically Specific Techniques 291
5. Charge-Specific Techniques Involving a Single Electronic State 292
6. Techniques That Measure Interelectronic Transitions 303
7. Observations of the Lattice Symmetry around the Impurity 327
8. Trends in the Data 332
9. Puzzles and Dual Characteristics of 3*d* Impurities in Semiconductors 344
IV. Theoretical Content of Excitation and Ionization Energies 346
10. Mean-Field, Many-Electron, and Relaxation Contributions 346
11. Contemporary Approaches to Separation of MF and MC Effects 354
12. The Effective-Crystal-Field Approach 358
13. Chemical Trends in the Mean-Field Parameters 361
14. Chemical Trends in Excitation and Ionization Energies 370
V. Electronic-Structure Calculations in the Mean-Field Approach 377
15. The Point-Ion Crystal-Field Model 378
16. Ligand-Field and Cluster Models 380
17. Green's-Function Methods 388
VI. Results of First-Principles Green's-Function Studies 396
18. One-Electron Impurity Levels and Wave Functions 396
19. Charge Densities 413
20. The Self-Regulating Response 417
21. Effective Electronic Configurations 423
22. The Bulk Analog of 3*d* Impurities in Semiconductors 426
23. Breathing-Mode Lattice Distortions around the Impurity 429
24. Effects of Spin Polarization 431
25. *g* values 441
26. Donor, Acceptor, and Mott–Hubbard Energies 442
27. The Exchange-Correlation-Induced Negative "Effective U" 449

Copyright © 1986 by Academic Press, Inc.
All rights of reproduction in any form reserved.

28. Universal Trends in Impurity Binding Energies 457
29. Alloy Effects and Valence-Band Offsets 460
VII. Future Prospects 462

I. Introduction

The field of research on $3d$ impurities in semiconductors borders on the disciplines of solid-state physics, semiconductor technology, and inorganic chemistry. A quarter of a century has passed since Ludwig and Woodbury[1] published in this serial their (by now, classic) review on the paramagnetic resonance of $3d$ impurities in semiconductors. At that time, the basic theory of $3d$ ions in coordination compounds and ionic crystals was already developed; reviews on this subject were published in this series by Low[2] and by McClure.[3] Electronic-structure theory for semiconductors was, however, still in its infancy—even the band structure of most semiconductors was yet unknown. It is only natural that the intellectual tools used by Ludwig, Woodbury, and Ham[1,4] in their pioneering analyses of the properties of $3d$ impurities in *silicon* were rooted in those developed earlier for deep impurities in *ionic crystals* and $3d$ coordination compounds—crystal fields, ligand fields, empirical multiplet diagrams, etc. (reviewed in Refs. 5–9). The many new experimental techniques that have emerged in the intervening years and the application to this problem of numerous experimental methods rooted in semiconductor technology have generated a wealth of new data[10–15] and new puzzles. Semiconductor

[1] G. W. Ludwig and H. H. Woodbury, *Solid State Phys.* **13,** 223 (1962); H. H. Woodbury and G. W. Ludwig, *Phys. Rev.* **117,** 102 (1960).
[2] W. Low, *Solid State Phys. Suppl.* **2** (1960).
[3] S. S. McClure, *Solid State Phys.* **9,** 400 (1959).
[4] F. S. Ham and G. W. Ludwig, *Proc. Int. Conf. Paramagn. Reson., 1st, Jerusalem* 130 (1962).
[5] (a) C. J. Ballhausen, "Ligand Field Theory." McGraw-Hill, New York, 1962; (b) H. Watanabe, "Operator Methods in Ligand Field Theory." Prentice-Hall, New York, 1966.
[6] B. N. Figgis, "Introduction to Ligand Fields." Wiley, New York, 1967.
[7] J. E. Huhay, "Inorganic Chemistry," 3rd ed. Harper, New York, 1983.
[8] J. S. Griffith, "The Theory of Transition Metal Ions." Cambridge Univ. Press, London, 1971.
[9] S. Sugano, Y. Tanabe, and H. Kamimura, "Multiplets of Transition-Metal Ions in Crystals." Academic Press, New York, 1970.
[10] E. R. Weber, *Appl. Phys. A* **30,** 1 (1983).
[11] "Landolt-Börnstein Numerical Data and Functional Relationships in Science and Technology" (O. Madelung, ed.,) Vols. 17a and 17b Springer-Verlag, Berlin, 1982.
[12] U. Kaufmann and J. Schneider, *Adv. Electron. Electron Phys.* **58,** 81 (1983); U. Kaufmann and J. Schneider, *Festkörperprobleme* (*Adv. Solid State Phys*) **20,** 87 (1980).
[13] V. F. Masterov and B. E. Samorukov, *Sov. Phys. Semicond.* **12,** 363 (1978); V. F. Masterov, *Fiz. Tekh. Poluprovodn.* **18,** 3 (1984) [*Sov. Phys. Semicond.* **18,** 1 (1984)].
[14] B. Clerjaud, *J. Phys. C* **18,** 3615 (1985).
[15] H. J. Schulz, *J. Cryst. Growth* **59,** 65 (1982).

theorists have responded to the challenge posed by the new experimental findings by developing novel theoretical techniques (see some recent reviews in Refs. 13, 16, and 17) needed to describe localized impurities interacting with an itinerant network of covalent bonds—new cluster models, first-principles pseudopotentials, and self-consistent Green's-function approaches within the density-functional formalism. These techniques have now reached a point where clear, quantitative predictions of hitherto unobserved properties and phenomena are being made. In this article I review these recent developments *vis a vis* the new experimental methodologies and the classical phenomenological approaches[1–9] used earlier to understand deep $3d$ impurities. I will attempt to provide a coherent picture of our understanding of isolated $3d$ impurities in cubic semiconductors from the combined points of view of theoretical solid-state physics, semiconductor physics, and classical inorganic chemistry. My basic point of view will be to show how the valence-band resonances—the result of the covalent interaction of localized $3d$ states with itinerant semiconductor bands—lead to a qualitatively new physics relative to the classical theories, explain the results of many new experiments, offer new predictions, and demystify some of the early successes of the phenomenological approaches. I will emphasize in particular the role that recent self-consistent Green's-function methods played in advancing our understanding of such systems, and discuss the emerging theoretical picture in a way that emphasizes new challenging prospects in this field.

II. Phenomenology and Terminology

1. Impurity Oxidation and Charge States

Classical descriptions[1–9] of the electronic structure of $3d$ impurities in ionic solids and semiconductors rest on the tacit assumption that some of the electrons of the impurity atom are "active" (i.e., control the magnetic, optical, and electrical characteristics of the system) and the others are "passive." This separation is based on the empirical observation (discussed in Part III,6) that impurities with the same number of "active" electrons show similar properties in different chemical environments, including different host crystals. The "active" electrons are then used to describe the phenomenology of the system: its spin state, magnetic properties, and optical as well as thermal excitations. It is natural that we start by addressing the question of how many electrons are

[16] A. Zunger, *Annu. Rev. Mater. Sci.* **15,** 411 (1985).
[17] A. M. Stoneham, "Theory of Defects in Solids." Clarendon, Oxford, 1975; M. Jaros, *Adv. Phys.* **24,** 409 (1980).

necessary to usefully describe the phenomenology of the system. This partitioning of "active" and "passive" electrons has traditionally been effected on phenomenological grounds and has led to the development of various nomenclatures used in the literature to designate impurities with different numbers of "active" electrons. Since different nomenclatures have been developed independently by semiconductor device engineers, inorganic chemists, and solid-state physicists, it is only natural that they are not uniform (and often confusing). In this section I describe this classical phenomenology, present the jargon of the field, and define a (uniform) terminology. The basic phenomenology and its implications are first discussed noncritically, in the same way that they have been used in the literature. Clarifications and a critique follow.

The electrons introduced by the impurity atom into the host crystal traditionally have been separated into three groups: (1) core electrons, (2) "rebonding" electrons, and (3) "active impurity electrons." Only the last have been traditionally used to designate, identify, and analyze the electronic structure of the system; the significant role of the other two groups of electrons will be discussed in Part V. The number of "active" electrons depends on the particular lattice site taken up by the impurity atom, in a manner to be discussed next.

An impurity in the lattice is thought to have one or more stable locations in which it resides longer than the other locations through which it travels during its diffusion process. Usually, only high-symmetry sites are considered to be candidates for stable locations. These include the *substitutional* (s) and the *interstitial* (i) sites. In diamondlike and sphalerite semiconductors (Fig. 1), the substitutional site occurs either on the cation sublattice at the $\tau_1 = (0, 0, 0)a$

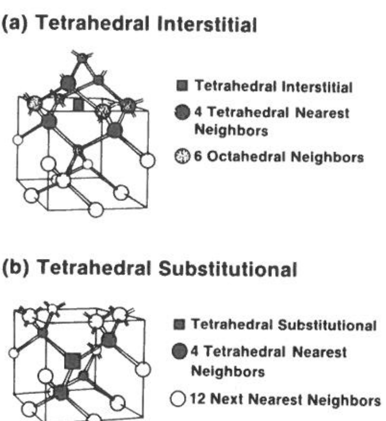

FIG. 1. Tetrahedral interstitial (a) and substitutional (b) sites in the diamondlike or zincblende lattice.

position (where a is the cubic lattice constant), or on the anion sublattice at the $\tau_2 = (\frac{1}{4}, \frac{1}{4}, \frac{1}{4})a$ position. All reports to date identify substitutional $3d$ impurities on the cation site alone, i.e., at τ_1. Two types of high-symmetry interstitial sites are available in face-centered cubic lattices: the *tetrahedral interstitial* (TI) and the *hexagonal interstitial* (HI). No report is available on $3d$ impurities in a stable HI site. In heteropolar tetrahedral binary semiconductors, there are two types of TI sites: the one nearest the anion at $\tau_3 = (\frac{1}{2}, \frac{1}{2}, \frac{1}{2})a$, and the one nearest the cation at $\tau_4 = (\frac{3}{4}, \frac{3}{4}, \frac{3}{4})a$. (Clearly, these two sites are crystallographically equivalent for homopolar diamondlike semiconductors). The TI site has been confirmed for $3d$ impurities in Si,[1,10] but no conclusive report exists for $3d$ impurities in a stable TI site in heteropolar semiconductors.[12,14] (See, however, the discussion of GaP:Fe in Table III, where the possibility of an interstitial site in III–V's has been raised recently.) The relevance of the lattice site taken up by the impurity to the determination of the number of "active" impurity electrons rests on the idea that some of the impurity electrons become chemically inert when they "repair" the hostlike broken bonds ("dangling bonds"). Unlike the case of a substitutional impurity, no bonds need to be reconstructed around a (previously empty) interstitial site.

Consider a neutral transition atom with atomic number Z and an electronic configuration [core]$3d^n4s^m$ (where "core" denotes the closed-shell rare-gas configuration) in free space. The *nominal impurity (I) atom valence* is defined as $N_I = n + m$. Denote the *nominal host atom valence* (i.e., for cations, its column number in the periodic table) as N_H. (For substitutional sites we have a nominal host valence $N_H^{(s)}$, where "s" stands for the valence of either the cation-substitutional site or the anion-substitutional site, whereas for empty interstitial sites, we have $N_H^{(TI)} = N_H^{(HI)} = 0$.) Before being inserted into the lattice, the impurity may have a nonzero *formal charge* q, hence, $N_I - q$ valence electrons (e.g., neutral $Fe^0\, d^6s^2$ with $N_I = 8$ and $q = 0$, or singly ionized $Fe^+\, d^6s^1$ with $N_I = 8$ and $q = 1$). Imagine the process of inserting such an impurity into the lattice as consisting of two steps: First, remove a host lattice site; then, insert the impurity atom with formal charge q into this site (with a compensating charge of $-q$ placed in the host bands to preserve overall charge neutrality). For a substitutional impurity, the first step removes $N_H^{(s)}$ host valence electrons, creating (in M-fold coordination) M "dangling bonds," each with an average of $N_H^{(s)}/M$ missing electrons; for an interstitial impurity this step does not alter the number of host electrons or bonds. The classical models then describe the second step as one in which (1) the $Z - N_I$ impurity core electrons form a chemically inert and electronically isolated set of states; (2) N_H out of the $N_I - q$ impurity valence electrons are used up to remake the broken host crystal dangling bonds, hence, becoming magnetically and optically inert; and (3) the remaining $N = N(q) = N_I - q - N_H$ "impurity electrons" are chemically unsaturated and hence, are pictured to be "active"

electrons, responsible for the optical, magnetic, and electrical activity of the system. They are thought to evolve from the impurity-atom d orbitals (for a reason to be discussed in Part VI,18). Hence, their electronic configuration is often denoted a "d^N." *The formal oxidation state* of the transition (T) atom is $N_H + q$ [denoted as $T^{(N_H+q)}$] and not to be confused with the *formal charge state* q of the "center" (i.e., impurity on a given site and charge state) A, [denoted A^q]. The formal charge q, used to designate impurities in the semiconductor literature,[18] represents the charge *relative to the bonded lattice*, whereas the formal oxidation state $N_H + q$, used in the chemical literature,[1–9] is meant to represent the *actual local charge on an impurity ion* (relative to vacuum). Different formal charge and oxidation states are divided into *stable* ones (i.e., those that can become the system's stationary ground state) and *unstable* ones (i.e., nonstationary states, including autoionization states inside the host crystal bands). The formal charge states A^+, A^{2+}, respectively, are referred to, in the semiconductor literature[18] as the empty single (or first) donor state, the empty second (or double) donor state, etc., since they are envisioned to represent products of a reaction in which a neutral center A^0 donated one or more electrons to its environment (i.e., acts as a Lewis acid). The charge states A^-, A^{2-}, are referred to, respectively, as the occupied single (or first) acceptor state, the occupied second (or double) acceptor state, etc. (i.e., acts as a Lewis base). To avoid confusion, yet to establish contact with notations in different sources, I use the complete designation $[T^{(N_H+q)}, d^N, A^q]$ (to be completed later by the notation for the particular electronic state). Figure 2 summarizes the relationship between the formal oxidation states, the formal charge states, and the nominal "d^N" configurations for all $3d$ impurities in a series of host crystals, e.g., $R^{I}X^{VII}$ (NaCl-type); $R^{II}X^{VI}$ (ZnS-type); $R^{III}X^{V}$ (GaAs-type); and $R^{IV}R^{IV}$ (Si-type). The reader might wish to consult this figure whenever an ambiguity appears. For example, consider an iron impurity in different crystals. In free space, its electronic configuration is d^6s^2 when neutral; hence, $N_I = 8$. Inserted in various crystals, it may exist in a series of oxidation states $N_H + q$, e.g., Fe^0, Fe^+, Fe^{2+}, and Fe^{3+}. Figure 2 shows that Fe^0 can occur either as an interstitial impurity ($N_H^{(TI)} = 0$) designated as $[Fe^0, d^8, A^0]$, or as a substitutional impurity. It can be substitutional in a monovalent ($N_H^{(s)} = 1$) NaCl-type crystal, in a divalent ($N_H^{(s)} = 2$) ZnS-type crystal, in a trivalent ($N_H^{(s)} = 3$) GaAs-type crystal, or in a tetravalent ($N_H^{(s)} = 4$) Si-type crystal. These different states are then denoted $[Fe^0, d^8, A^-]$, $[Fe^0, d^8, A^{2-}]$, $[Fe^0, d^8, A^{3-}]$, and $[Fe^0, d^8, A^{4-}]$, respectively. The notation established here for $3d$ impurities is an extension of the notation used for the more conventional sp-electron impurities in semiconductors;[18] e.g., neutral substitutional phosphorus in Si is $[P^{4+}, \mu^1, A^0]$, whereas its (empty) donor

[18] S. M. Sze, "Physics of Semiconductor Devices." Wiley (Interscience), New York, 1969.

N	Formal Oxidation States T^0	T^{1+}	T^{2+}	T^{3+}	T^{4+}	T^{5+}
1	K^0	Ca^{1+}	Sc^{2+}	Ti^{3+}	V^{4+}	Cr^{5+}
2	Ca^0	Sc^{1+}	Ti^{2+}	V^{3+}	Cr^{4+}	Mn^{5+}
3	Sc^0	Ti^{1+}	V^{2+}	Cr^{3+}	Mn^{4+}	Fe^{5+}
4	Ti^0	V^{1+}	Cr^{2+}	Mn^{3+}	Fe^{4+}	Co^{5+}
5	V^0	Cr^{1+}	Mn^{2+}	Fe^{3+}	Co^{4+}	Ni^{5+}
6	Cr^0	Mn^{1+}	Fe^{2+}	Co^{3+}	Ni^{4+}	Cu^{5+}
7	Mn^0	Fe^{1+}	Co^{2+}	Ni^{3+}	Cu^{4+}	Zn^{5+}
8	Fe^0	Co^{1+}	Ni^{2+}	Cu^{3+}	Zn^{4+}	Ga^{5+}
9	Co^0	Ni^{1+}	Cu^{2+}	Zn^{3+}	Ga^{4+}	
10	Ni^0	Cu^{1+}	Zn^{2+}	Ga^{3+}		
11	Cu^0	Zn^{1+}	Ga^{2+}			
12	Zn^0	Ga^{1+}				
13	Ga^0					

Site	Formal Charge States q					
Interstitial	A^0	A^+	A^{2+}	A^{3+}	A^{4+}	A^{5+}
$R^{I}X^{VII}$	A^-	A^0	A^+	A^{2+}	A^{3+}	A^{4+}
$R^{II}X^{VI}$	A^{2-}	A^-	A^0	A^+	A^{2+}	A^{3+}
$R^{III}X^{V}$	A^{3-}	A^{2-}	A^-	A^0	A^+	A^{2+}
$R^{IV}X^{IV}$	A^{4-}	A^{3-}	A^{2-}	A^-	A^0	A^+

FIG. 2. The relationship between the formal oxidation state (circles), and formal charge states (squares) for various d^N impurities in binary crystals. Lines connecting circles join the same impurity element in the various oxidation states. Lines connecting squares join a given oxidation state in various semiconductors. For example, all divalent (T^{2+}) impurities have the charge state A^{2+} when placed interstitially. When placed on a cation substitutional position in I-VII, II-VI, III-V, or IV-IV semiconductors, the divalent ions have the charge state A^+, A^0, A^-, and A^{2-}, respectively. Another example: Ni^{2+} has $N = 8$ d electrons and is neutral in II-VIs but positively charged in I-VIIs. Also, all A^- states in III-Vs are divalent (T^{2+}), all A^0 states are trivalent (T^{3+}), and all A^+ states are tetravalent (T^{4+}).

state is $[P^{5+}, \mu^0, A^+]$, where μ denotes the orbital carrying the "active" electron.

The utility of this terminology rests on the fact that a given formal oxidation state shows similar properties in different host crystals, and that the number $N = N_I - N_H - q$ of "active" impurity electrons determines the system's total spin S; e.g., substitutional phosphorus $[P^{4+}, \mu^1, A^0]$ acts as a donor in both Si

and Ge and shows a spin $S = \frac{1}{2}$. This nomenclature tacitly presupposes, however, that the N_H "rebonding" electrons reside in orbitals that are spatially and energetically removed from those of the N "active" electrons, making the former essentially inconsequential as far as low-energy chemical or external perturbations are concerned. This terminology is occasionally taken further to imply[3,6,7] that $N_H + q$ electrons are removed from the impurity's immediate environment, giving the T^{N_H+q} impurity the physical properties (e.g., ionic radius, chemical reactivity) of a $(N_H + q)$-fold ionized atom. Likewise, an A^q impurity is thought to have in its immediate environment λ fewer electrons than the $A^{q+\lambda}$ impurity, etc. While I will continue to use this classical terminology in this article, no such implications are made here. In fact, modern calculations to be discussed in Part VI show that the N_H "rebonding" electrons show up in semiconductors (but not in ionic systems) as hybridized valence-band resonances; while they are consequently spin paired (hence, they do not contribute to the *total* spin S), they can contribute significantly to the spin density as well as to optical excitations. Furthermore, they provide a source for efficient screening which controls many of the properties of the "active" electrons. Such calculations indicate that the *physical charge* that resides on an impurity atom in the solid is neither q nor $N_H + q$, but instead is smaller than either (i.e., the system is closer to charge neutrality). Since, however, the rebonding electrons form, together with the host crystal states, an electronic "closed shell," the total spin and momentum of the system is decided by the "active" electrons alone.

The total spin S depends on the manner in which the N "active" electrons distribute themselves between spin-up (N_+) and spin-down (N_-) states, with $S = (N_+ - N_-)/2$ and $N = N_+ + N_-$. Furthermore, the distribution of the N_+ and N_- electrons among different space orbitals decides the total angular momentum $L = 0, 1, 2 \ldots$ (denoted as the A, T, and $T + E$ multiplets, respectively) of the system. Together with S, this establishes the total angular momentum. Clearly knowledge of the manner in which the $N = N_I - N_H - q$ "active" impurity electrons distribute themselves in different spin and space orbitals requires an electronic-structure model. A description of the basic phenomenology surrounding such models follows.

2. Elements of Electronic Structure in T_d Symmetry

Both the substitutional and the tetrahedral interstitial sites in diamondlike and sphalerite crystals have the T_d point-group symmetry. This point group[5] sustains the $\alpha = a_1$, t_2, e, t_1, and a_2 irreducible representations. The total (electronic plus nuclear) potential $V(\mathbf{r})$ and charge density $\rho(\mathbf{r})$ around the impurity site in an undistorted cubic lattice must therefore transform

according to the totally symmetric a_1 representation of T_d; i.e.,

$$V(\mathbf{r}) = \sum_l V_l(|\mathbf{r}|) K_l^{a_1}(\hat{r}), \tag{2.1}$$

and

$$\rho(\mathbf{r}) = \sum_l \rho_l(|\mathbf{r}|) K_l^{a_1}(\hat{r}), \tag{2.2}$$

where for T_d symmetry, $l = 0, 3, 4, 6, 7, 8, \ldots$. Here, $V_l(|\mathbf{r}|)$ and $\rho_l(|\mathbf{r}|)$ are general scalar radial functions and $\{K_l^{a_1}(\hat{r})\}$ are the Kubic harmonics of angular momentum l in the a_1 representation of the symmetry group T_d. Unlike the O_h group, parity is no longer a good quantum number in the T_d point group. In a Cartesian coordinate system (x, y, z) with $r^2 = x^2 + y^2 + z^2$ we have, relative to the impurity site as an origin

$$K_0^{a_1}(x, y, z) = (1/4\pi)^{1/2}, \tag{2.3}$$

$$K_3^{a_1}(x, y, z) = \left(\frac{7}{4}\right)^{1/2} \left(\frac{15}{\pi}\right)^{1/2} \frac{xyz}{r^3}, \tag{2.4}$$

$$K_4^{a_1}(x, y, z) = \left(\frac{1}{4\pi}\right)^{1/2} \left(\frac{21}{4}\right)^{1/2} \left(1 - \frac{5(x^2y^2 + x^2z^2 + y^2z^2)}{r^4}\right), \tag{2.5}$$

$$K_6^{a_1}(x, y, z) = \left(\frac{1}{4\pi}\right)^{1/2} \left(\frac{13}{2}\right)^{1/2} \frac{1}{4} \left(\frac{7(x^6 + y^6 + z^6 + 30x^2y^2z^2)}{r^6} - 5\right), \tag{2.6}$$

$$K_7^{a_1}(x, y, z) = \left(\frac{1}{4\pi}\right)^{1/2} \left(\frac{455}{3}\right)^{1/2} \frac{3}{4} \frac{1}{r^7} xyz[11(x^4 + y^4 + z^4) - 5r^4], \tag{2.7}$$

$$K_8^{a_1}(x, y, z) = \left(\frac{1}{4\pi}\right)^{1/2} \sqrt{561}\, \frac{1}{8} \frac{1}{r^8} [x^8 + y^8 + z^8 - 14(x^6y^2 + x^6z^2 + y^6z^2 + x^2y^6 + x^2z^6 + y^2z^6) + 35(x^4y^4 + x^4z^4 + y^4z^4)]. \tag{2.8}$$

Notice that, unlike the octahedral point group O_h, in T_d symmetry the odd $l = 3$ and 7 terms in Eqs. (2.1) and (2.2) are nonzero; i.e., no inversion symmetry exists at the impurity site. Even though the potential of a free ion can be usefully described (in the central-field approach) as being spherical, that of an impurity is, in the same approximation, nonspherical, having acquired anisotropic $l = 3, 4, 6$, etc., components. Figure 3 shows the crystal potential $V(\mathbf{r})$ in Si, along the $\pm\langle 111 \rangle$ directions. Its resolution into angular momentum components [Eq. (2.1)] is shown in Fig. 3b and Fig. 3c–e for interstitial and substitutional sites, respectively, as obtained from a self-consistent pseudopotential band-structure calculation.[19,20] The nonspherical components are seen to be significant. This reduced symmetry relative to the continuous

[19] A. Zunger and U. Lindefelt, *Phys. Rev. B* **27**, 1191 (1983).
[20] A. Zunger, *Phys. Rev. B* **28**, 3678 (1983).

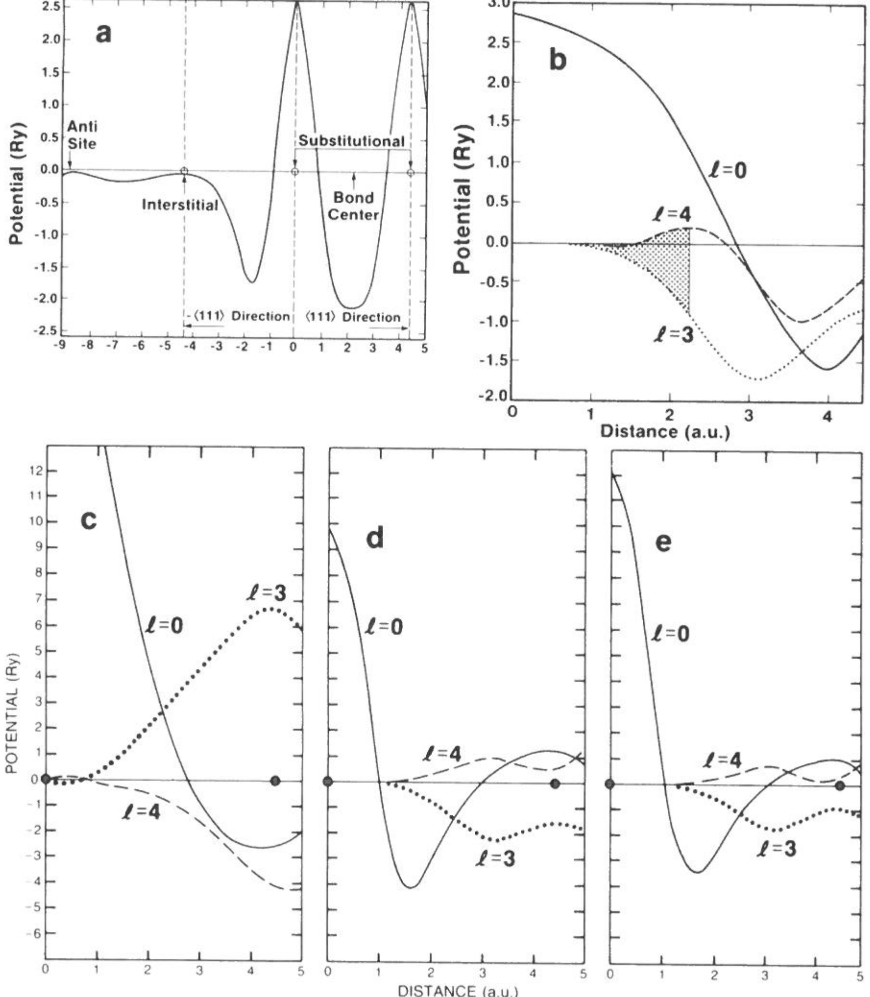

FIG. 3. The effective one-particle crystal pseudopotential in pure Si and its components. (a) The total self-consistently screened pseudopotential along the $\pm\langle 111\rangle$ crystal directions, showing the substitutional and interstitial lattice sites and the bond center position. (b) Decomposition of the total self-consistently screened pseudopotential around the *interstitial* site into angular momenta l [Eq. (2.1)]. Parts (c), (d), and (e) show a similar decomposition around the *substitutional* site of the Coulomb and exchange screening alone (c), the bare pseudopotential (d), and their sum (screened pseudopotential) in (e). After A. Zunger and U. Lindefelt, *Phys. Rev. B* **27**, 1191 (1983); and A. Zunger, *Phys. Rev. B* **28**, 3678 (1983).

rotation group implies that the permissible one-particle wavefunctions $\psi_{i,\sigma}^{\alpha,\lambda}(\mathbf{r})$ (level i, representation $\alpha = a_1$, t_2, e, t_1, or a_2, partner index λ, and spin σ) also have a lower symmetry; i.e., they can mix certain angular momentum components l which are orthogonal in the continuous rotation group. More specifically, expressed in terms of general radial orbitals $G_{i,l}^{\alpha,\sigma}(|\mathbf{r}|)$ of angular momentum l, spin σ, representation index α, and the Kubic harmonics $K_l^{\alpha,\lambda}(\hat{r})$ of partner index λ, the impurity wave functions have the following general form[21]

$$\psi_{i,\sigma}^{\alpha,\lambda}(\mathbf{r}) = \sum_{l=0} G_{i,l}^{\alpha,\sigma}(|\mathbf{r}|)K_l^{\alpha,\lambda}(\hat{r}). \tag{2.9}$$

References 5 and 21 give the Kubic harmonics $K_l^{\alpha,\lambda}(\hat{r})$ in T_d symmetry. The angular-momentum components allowed by symmetry to combine in the T_d impurity wave functions are

$$\psi_{i,\sigma}^{a_1,\lambda}(\mathbf{r}) = G_{i,0}^{a_1,\sigma}(r)K_0^{a_1,\lambda}(\hat{r}) + G_{i,3}^{a_1,\sigma}(r)K_3^{a_1,\lambda}(\hat{r}) + G_{i,4}^{a_1,\sigma}(r)K_4^{a_1,\lambda}(\hat{r}) + \cdots, \tag{2.10}$$

$$\psi_{i,\sigma}^{a_2,\lambda}(\mathbf{r}) = G_{i,6}^{a_2,\sigma}(r)K_6^{a_2,\lambda}(\hat{r}) + \cdots, \tag{2.11}$$

$$\psi_{i,\sigma}^{e,\lambda}(\mathbf{r}) = G_{i,2}^{e,\sigma}(r)K_2^{e,\lambda}(\hat{r}) + G_{i,4}^{e,\sigma}(r)K_4^{e,\lambda}(\hat{r}) + \cdots, \tag{2.12}$$

$$\psi_{i,\sigma}^{t_1,\lambda}(\mathbf{r}) = G_{i,3}^{t_1,\sigma}(r)K_3^{t_1,\lambda}(\hat{r}) + G_{i,4}^{t_1,\sigma}(r)K_4^{t_1,\lambda}(\hat{r}) + \cdots, \tag{2.13}$$

$$\psi_{i,\sigma}^{t_2,\lambda}(\mathbf{r}) = G_{i,1}^{t_2,\sigma}(r)K_1^{t_2,\lambda}(\hat{r}) + G_{i,2}^{t_2,\sigma}(r)K_2^{t_2,\lambda}(\hat{r}) + G_{i,3}^{t_2,\sigma}(r)K_3^{t_2,\lambda}(\hat{r}) + G_{i,4}^{t_2,\sigma}(r)K_4^{t_2,\lambda}(\hat{r}) + \cdots. \tag{2.14}$$

The degeneracies λ for a_1, a_2, e, t_1, and t_2 are 1, 1, 2, 3, and 3, respectively. Note that this general and rigorous expansion does not imply that $G_{i,l}^{\alpha,\sigma}(|\mathbf{r}|)$ has any simple form (e.g., atomic radial orbitals[4,5]) or that a given angular momentum l dominates another.[6,7] In particular, a_1 states need not be pure ($l = 0$) s states, but could include ($l = 3$) f character; the t_2 state can include both ($l = 1$) p character as well as ($l = 2$) d character ("hybridization"), etc. Note further that the general radial function $G_{i,l}^{\alpha,\sigma}(|\mathbf{r}|)$ may include contributions both from the impurity atomic orbitals as well as from ligand orbitals transforming around the central impurity site in an (α, σ, l) manner ("covalency").

A possible distribution of the N impurity electrons among different one-electron wave functions $\{\psi_{i,\sigma}^{\sigma,\lambda}(\mathbf{r})\}$ is referred to as a *one-electron configuration.* Hence, one needs to establish how many wave functions i are available to the N electrons to occupy, which (all or some) representations are to be considered, and what would be the relative order of their one-electron energies,

$$\epsilon_{i\sigma}^{\alpha} = \langle\psi_{i,r}^{\alpha,\lambda}(\mathbf{r})|\hat{T} + V(\mathbf{r})|\psi_{i,\sigma}^{\alpha,\lambda}(\mathbf{r})\rangle, \tag{2.15}$$

[21] U. Lindefelt and A. Zunger, *Phys. Rev. B* **26**, 846 (1982); *Phys. Rev. B* **24**, 5913 (1981).

(where $\hat{T}$ is the kinetic energy operator) to be followed in the occupation process (i.e., aufbau principle). In a mole of an impurity-containing crystal, there are $\sim 10^{23}$ levels with the properties denoted in Eqs. (2.10)–(2.14); however, most of them have an amplitude of $O(10^{-23})$ on the impurity site. The manner in which single d and s orbitals of the impurity atom distribute their amplitude over all $\sim 10^{23}$ available one-electron levels cannot be resolved in a qualitative manner (modern calculations, discussed in Parts V and VI, suggest that fewer than 10 groups of "levels" are involved). Most classical models, however, limit their discussion[1–7] to a few—usually one or two levels i for each representation, and to the t_2 and e representations alone (since these are the only ones to have an $l = 2$, d-like component). In this case the relative ordering of the one-electron levels can be characterized by only two parameters: the *one-electron crystal-field splitting* Δ_{CF} and the *one-electron exchange splitting* Δ_x. The former is defined as the spin average of the difference

$$\Delta_{CF}^{(i)} = \epsilon_i^e - \epsilon_i^{t_2}. \tag{2.16}$$

According to its definition in Eqs. (2.15) and (2.16), $\Delta_{CF}^{(i)}$ may include contributions from the difference in kinetic energies $\langle \psi_{i,\sigma}^{e,\lambda} | \hat{T} | \psi_{i,\sigma}^{e,\lambda} \rangle - \langle \psi_{i,\sigma}^{t_2,\lambda} | \hat{T} | \psi_{i,\sigma}^{t_2,\lambda} \rangle$, as well as the differences in potential energy. The latter term includes both contributions from the spherical potential $V_{l=0}(|\mathbf{r}|)$ in Eq. (2.1) [since the radial orbital $G_{i,l}^{e,\sigma}(|\mathbf{r}|)$ is, in general, different from $G_{i,l}^{t_2,\sigma}(|\mathbf{r}|)$], as well as from the nonspherical potential terms $V_{l\neq 0}(|\mathbf{r}|)$. Each of the space orbitals can be split further by the one-electron exchange (x) interaction into spin up (+) and spin down (−), giving the pairs $\{t_{2+}, t_{2-}\}$ and $\{e_+, e_-\}$, with energy separations of

$$\Delta_x^{t_2,i} = \epsilon_{i,+}^{t_2} - \epsilon_{i,-}^{t_2}; \qquad \Delta_x^{e,i} = \epsilon_{i,+}^{e} - \epsilon_{i,-}^{e}. \tag{2.17}$$

These are termed *one-electron exchange splittings*. Like $\Delta_{CF}^{(i)}$, they depend on the type i of wave function (e.g., bonding, antibonding, resonance, gap, etc.).

Limiting the discussion to the partially filled e and t_2 orbitals, a number of relative arrangements are possible, depending on the sign of Δ_{CF} and the relative magnitude of Δ_x and Δ_{CF} (cf. Fig. 4): (1) $\Delta_{CF} > 0$ and $\Delta_x > \Delta_{CF}$, resulting in a level ordering $t_{2+} < e_+ < t_{2-} < e_-$. This is referred to, for reasons that will be obvious later, as *interstitial high-spin-like* (I-HSL) level ordering, (or the "interstitial weak-field limit"). (2) $\Delta_{CF} > 0$ but $\Delta_x < \Delta_{CF}$, resulting in a level ordering $t_{2+} < t_{2-} < e_+ < e_-$. This is referred to as *interstitial low-spin-like* (I-LSL) level ordering (or "interstitial strong-field limit"). (3) $\Delta_{CF} < 0$ and $\Delta_x > \Delta_{CF}$ leads to an ordering $e_+ < t_{2+} < e_- < t_{2-}$. This is referred to as *substitutional high-spin-like* (S-HSL) level ordering (or "substitutional weak-field limit"). Finally, (4) $\Delta_{CF} < 0$ and $\Delta_x < \Delta_{CF}$ leads to a level ordering $e_+ < e_- < t_{2+} < t_{2-}$. This is referred to as a *substitutional low-*

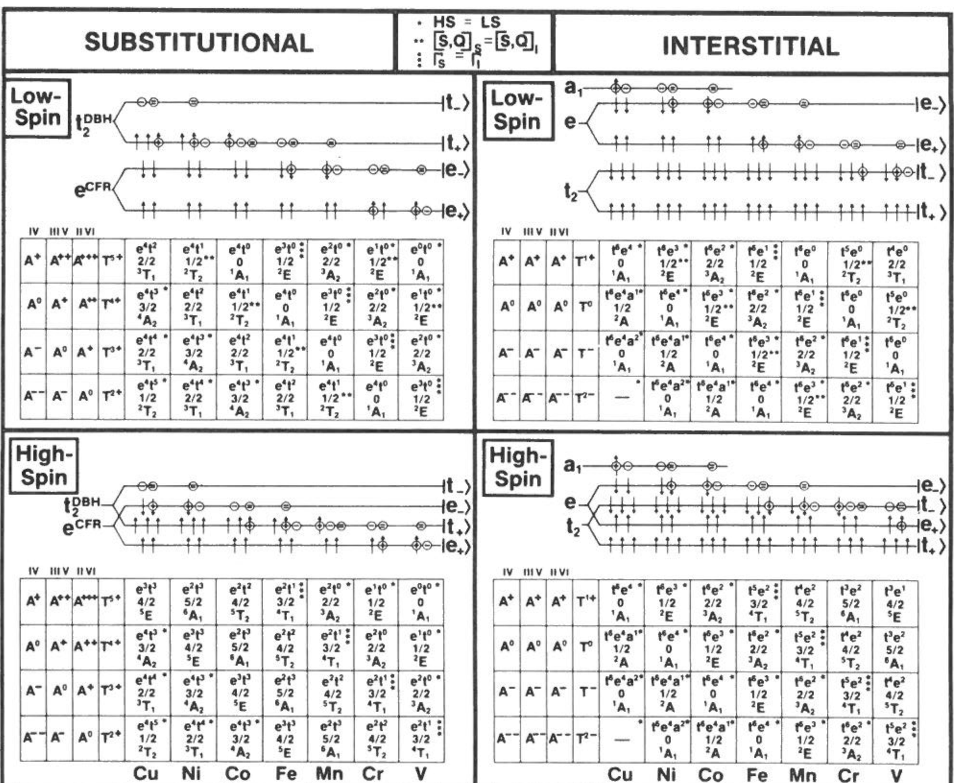

FIG. 4. Summary of one-electron energy levels (t_+, t_-, e_+, e_-) and many-electron multiplets for substitutional (left) and interstitial (right) 3d impurities in semiconductors. Formal charge states A^q are denoted for impurities in the host systems IV-IV as well as in III-V and II-VI semiconductors. T^{q+} denotes the oxidation state. A single asterisk (*) indicates that the high-spin and low-spin configurations give the same total spin S. A double asterisk (**) indicates that the spin S and charge q of the substitutional impurity are identical to those of the interstitial impurity. A triple asterisk (⁑) indicates that the multiplets for substitutional and interstitial configurations are identical. For example, substitutional V^{2+} has the high-spin configuration e^2t^1, a spin $S = \frac{3}{2}$, and a multiplet $^4T_1$. It is neutral (A^0) in II-VIs, negatively charged (A^-) in III-Vs and doubly negatively charged (A^{2-}) in IV-IV semiconductors. If it were in a low-spin state in substitutional geometry, its configuration would be e^3t^0, its spin $S = \frac{1}{2}$, and ground-state multiplet ^2E. The triple asterisk (⁑) denotes the fact that V can have the same multiplets in substitutional and interstitial positions: V^{2-} is also $^4T_1$ in an interstitial high-spin state with a configuration t^5e^2 and spin $\frac{3}{2}$. When V^{2+} is ionized, it forms V^{3+}. (Similarly, [Mn^{4+}, d^3, e^2t^1, $^4T_1$] in substitutional geometry has the same multiplet as [Mn^0, d^7, t^5e^2, $^4T_1$] in interstitial geometry.) In substitutional geometry V^{3+} has the same configuration and multiplets whether it is low spin or high spin (single asterisk), i.e., e^2t^0, $S = 2/2$, and $^3A_2$. The transition $V^{2+} \leftrightarrow V^{3+}$ is a $A^0 \leftrightarrow A^+$ donor-type in II-VIs, a $A^- \leftrightarrow A^0$ first acceptor in III-Vs, and a $A^{2-} \leftrightarrow A^-$ second acceptor in IV-IVs.

spin-like (S-LSL) level ordering (or "substitutional strong-field limit"). Clearly, if we could find which of the four level arrangements is pertinent to a given host-plus-impurity system, we could determine not only the spin S of the N impurity electrons, but also the angular momentum L, and consequently the total momentum. The picture could then be completed if a many-electron term corresponding to each dominant arrangement of one-electron levels could be established. Part of this task can be accomplished from symmetry considerations by observing the manner in which atomic many-electron terms transform into the many-electron terms of a lower site symmetry. For T_d, we have the correspondence[4,5,8]

$$\begin{aligned} &S, d^N \to A_1(t_2^n e^m),\\ &P, d^N \to T_1(t_2^n e^m),\\ &D, d^N \to T_2(t_2^n e^m) + E(t_2^{n\pm 1} e^{m\mp 1}),\\ &F, d^N \to T_1(t_2^n e^m) + T_2(t_2^{n\pm 1} e^{m\mp 1}) + A_2(t_2^{n\pm 2} e^{m\mp 2}), \end{aligned} \tag{2.18}$$

where $N = n + m$. In each case I indicate in parentheses the type of dominant one-electron configuration that gives rise to the appropriate many-electron multiplet. Table I illustrates this correspondence for d^1 through d^9 ions in substitutional and interstitial T_d symmetries. In each case I underline the high-spin many-electron configuration that, according to the phenomenological model, is likely to be the ground state. Also shown are the spin S and, when appropriate, the (weak-field) effective total angular momentum J of the ground electronic state. Using the correspondence rule of Eq. (2.18) and taking into account the degeneracies of the many-electron terms, one can define the *apparent many-electron (ME) crystal-field splitting* as the appropriate separation between crystalline terms that are degenerate in the free-ion limit; i.e., for D terms,

$$\Delta_{\text{ME}} = \left|E_T(^{2S+1}E) - E_T(^{2S+1}T_2)\right|, \tag{2.19}$$

and for F terms,

$$\Delta_{\text{ME}}^{(1)} = \left|E_T(^{2S+1}T_2) - E_T(^{2S+1}A_2)\right|, \tag{2.20}$$

or

$$\Delta_{\text{ME}}^{(2)} = \tfrac{5}{4}\left|E_T(^{2S+1}T_1) - E_T(^{2S+1}T_2)\right|. \tag{2.21}$$

The many-electron crystal-field splittings Δ_{ME} are different from the one-electron crystal-field splittings of Eq. (2.16).

The task of establishing which of the possible multiplets of Table I is the ground state is obviously not given by symmetry alone and is resolved using standard multiplet theory[8,9] (cf. Parts IV,11 and IV,12). Figure 4 depicts the result of such a procedure for all four possibilities listed above.

TABLE I. POSSIBLE SPLITTINGS OF THE FREE-ION MANY-ELECTRON TERMS INTO THE CRYSTALLINE MANY-ELECTRON TERMS IN T_d SYMMETRY[a]

Free-ion many-electron terms	T_d Crystalline many-electron terms	Ground state S	Ground state J
S Terms			
$Fe^{3+}, Cr^{+}, Mn^{2+}, d^5, {}^6S$	${}^6A_1(t^3e^2)$	$\frac{5}{2}$	$\frac{5}{2}$
D Terms			
$Sc^{2+}, d^1, {}^2D$	${}^2T_2(t^1e^0) + {}^2E(e^1t^0)$	$\frac{1}{2}$	
$Mn^{3+}, Cr^{2+}, d^4, {}^5D$	${}^5T_2(t^2e^2) + {}^5E(t^3e^1)$	2	1, 2, 3
$Co^{3+}, Fe^{2+}, d^6, {}^5D$	${}^5T_2(t^4e^2) + {}^5E(t^3e^3)$	2	0, $\frac{1}{2}$, 1
$Ni^{+}, Cu^{2+}, d^9, {}^2D$	${}^2T_2(t^5e^4) + {}^2E(t^6e^3)$	$\frac{1}{2}$	$\frac{1}{2}, \frac{3}{2}$
F Terms			
$V^{3+}, Ti^{2+}, d^2, {}^3F$	${}^3T_1(t^2e^0) + {}^3T_2(t^1e^1) + {}^3A_2(e^2t^0)$	1	
$Cr^{3+}, V^{2+}, d^3, {}^4F$	${}^4T_1(t^1e^2) + {}^4T_2(t^2e^1) + {}^4A_2(t^3e^0)$	$\frac{3}{2}$	$\frac{1}{2}, \frac{3}{2}, \frac{5}{2}$
$Ni^{3+}, Fe^{+}, Co^{2+}, d^7, {}^4F$	${}^4T_1(t^5e^2) + {}^4T_2(t^4e^3) + {}^4A_2(t^3e^4)$	$\frac{3}{2}$	
$Cu^{3+}, Ni^{2+}, d^8, {}^3F$	${}^3T_1(t^4e^4) + {}^3T_2(t^5e^3) + {}^3A_2(t^6e^2)$	1	0, 1, 2

[a] High-spin ground-state terms in substitutional (interstitial) symmetry are underlined by a solid (dashed) line. S denotes the ground-state spin and J is the (weak-crystal-field) effective total angular momentum into which the substitutional ground-state term is split by spin-orbit interaction in first order. The $J > 3/2$ of ${}^5E$ is further split in second order.

The classical phenomenological approaches that summarize a large body of experimental findings[1–4,10–12] have answered this question by establishing four empirical rules: (1) The $N = N_I - N_H - q$ "impurity electrons" occupy only e-like and t_2-like representations. (2) Only a single state i of each of these two representations is involved (hence, the index i is dropped)—the others are thought to belong to the inactive "rebonding" orbitals. (3) Interstitial $3d$ impurities in T_d symmetry (as well as substitutional, octahedrally coordinated impurities) have an I-HSL level arrangement. (4) Substitutional $3d$ impurities in T_d symmetry have an S-HSL level ordering.

These four empirical rules have been extracted over the past 40 years from an enormous data base of observations and have constituted the working paradigms of this field for years in interpreting EPR, luminescence, and absorption experiments. This approach to the problem, however, has not produced a quantitative theory that clarifies the phenomenology and provides quantitative predictions. Despite qualitative (but insightful) arguments in its favor (described below), its strength lies in its ability to unify a rather large

body of observations in terms of simple empirical rules. This article reviews the advances of the past few years towards demystifying the successful empiricism in this field, as applied to $3d$ impurities in semiconductors.

I next review the manner in which the central quantities appearing in the phenomenological models lend themselves to experimental observations.

III. Observable Phenomena and Data

3. Types of Experiments

Most experimental techniques in this field can be classified as either (1) those that measure the properties of an impurity in one or more electronic stationary states $[T^{(N_H - q)}, d^N, A^q]$, or (2) those that measure transitions between two different electronic stationary states (e.g., different charge and oxidation states). The first group includes such techniques as electron paramagnetic resonance (EPR), electron nuclear double resonance (ENDOR), Mössbauer spectroscopy, magnetic susceptibility, mass spectroscopy, extended x-ray-absorption fine structure (EXAFS), ion-implantation followed by back scattering and channeling measurements, and nuclear activation analysis (NAA). The second group includes techniques such as Hall effect, optically detected magnetic resonance (ODMR), deep-level transient spectroscopy (DLTS), thermally stimulated current (TSC) measurements, absorption, luminescence, and photoconductivity (PC). The first group of techniques can be further subdivided into (1) those that chemically identify the impurity element T (e.g., mass spectroscopy, neutron activation analysis), providing information on the identity of the impurity and the *total* impurity content (but not distinguishing one charge and oxidation state from the other), and (2) those that distinguish different stationary charge and oxidation states of the same chemical impurity (e.g., EPR, ENDOR). All the techniques belonging to group II can identify some fingerprints of different states of the same impurity [(2) above], but they are rarely chemically specific [(1) above].

This review does not attempt to describe the various experimental techniques. The interested reader is referred to a number of recent treatises[12,14,18,22] on this subject. Instead, I will indicate the property being measured by the various techniques, its relation to the quantities used to establish the phenomenology of these systems, and provide a critical compilation of the best data available, to be used in Parts III,8 and V in discussing models for the electronic structure.

[22] J. Bourgoin and M. Lannoo, "Point Defects in Semiconductors: Experimental Aspects." Springer-Verlag, Berlin, 1983.

4. Stationary, Chemically Specific Techniques

Normally, these are destructive experiments that measure the sum of all oxidation states $\sum_\mu T^{(\mu)}$ (where $\mu = N_H + q$) and chemical complexes associated with a given chemical impurity element T, and provide no information on distinct electronic levels i. Many of the solubility experiments have involved such techniques,[10] notably neutron activation analysis.[23] Detailed solubility data exist for $3d$ impurities in Si,[10,24] showing a maximum around $T \cong 1300$ K and a rapid decrease at lower temperatures. At 1000 K, Cu and Ni show the highest solubility ($\sim 5 \times 10^{17}$ cm^{-3}), whereas Co and Fe have a solubility of only 10^{14} cm^{-3} at this temperature. These low solubilities (more than five orders of magnitude smaller than that of conventional dopants such as B, As, and P) have made it quite difficult to chemically identify and characterize $3d$ impurities in semiconductors. The solubility of $3d$ impurities in III-Vs and II-VIs is somewhat greater[12]: maximum solubilities of 10^{17} cm^{-3} are typical of most $3d$ impurities in these materials, with the exception of Mn, which reaches a solubility of 10^{19} cm^{-3} in GaAs and forms continuous solid solutions with many II-VI compounds (e.g., $Cd_xMn_{1-x}Te$, or $Zn_xMn_{1-x}Te$). The solubilities of various impurities in Si have been systematized by Singh and Zunger[25] using the orbital radii concept,[26] but no microscopic theory yet exists for predicting these solubilities *a priori*. Ion implantation of various d-electron (and other) impurities in Si has been successfully accomplished.[27] Site locations have also been determined by backscattering and ion-channeling techniques, which show nonsubstitutional positions[25,27] in all cases. These site preferences have also been successfully predicted by orbital radii approaches.[25] EXAFS measurements have only recently been applied to $3d$ impurities in semiconductors (e.g., Si:Fe[28] and ZnSe:Cu[29]), providing information on the local lattice distortion around such impurities. Preliminary results for Si:Fe show[28] an outward breathing-mode distortion of the four silicon nearest neighbors of about 0.1 ± 0.05 Å. Magnetic susceptibility experiments are limited to highly soluble impurities

[23] N. Wiehl, U. Herpers, and E. Weber, *in* "Nuclear Physics Methods in Material Research" (K. Bethge, H. Baumann, H. Jex, and F. Rauch eds.), pp. 334. Vieweg, Braunschweig, 1980.

[24] F. A. Trumbore, *Bell Syst. Tech. J.* **39,** 205 (1962).

[25] V. A. Singh and A. Zunger, *Phys. Rev. B* **25,** 907 (1982).

[26] A. Zunger, *Phys. Rev. B* **22,** 5839 (1980).

[27] M. S. Duesbery and R. Taylor, *J. Phys. F* **9,** L19 (1979); E. N. Kaufmann, R. Vianden, T. E. Jackman, J. R. MacDonald, and L. Haggmarh, *J. Phys. F.* **9,** L23 (1979); S. T. Picraux, *in* "New Uses of Ion Accelerators" (J. F. Ziegler, ed.), p. 229. Plenum, New York, 1975; J. C. North and W. M. Gibson, *Appl. Phys. Lett.* **16,** 126 (1970).

[28] P. Pathikrit and B. A. Bunker, *Bull. Am. Phys. Soc.* **30,** 276 (Abstr. B02) (1985).

[29] A. J. Goldman, E. Canova, Y. H. Kao, B. J. Fitzpatrick, R. N. Bhargava, and J. C. Phillips, *Appl. Phys. Lett.* **43,** 836 (1983).

(e.g., GaAs:Mn) and have been used to deduce the probable spin state of such impurities.[30]

5. Charge-Specific Techniques Involving a Single Electronic State

Among these techniques EPR[1,2,31,32] and ENDOR[33] have played a crucial role in the area of $3d$ impurities. The EPR technique provides, among others, information on the spin S (e.g., from the number of fine-structure lines), the g value, and the hyperfine coupling constant A. Stress experiments and measurements of the anisotropy of these quantities can be further used[31] to extract the site symmetry of the center.

It is instructive to demonstrate how the observed EPR spin value has been used[1,10,12] to suggest the manner in which the N "active" impurity electrons distribute themselves among the various t_+, t_-, e_+, and e_- one-electron levels. The logic of the model is as follows: First, a "reasonable" site symmetry is assumed (e.g., interstitial for $3d$ impurities in Si, substitutional for the same impurities in GaAs), and the sign of Δ_{CF} compatible with this site symmetry according to classical crystal-field models is deduced (e.g., t_2 below e in tetrahedral interstitial symmetry, e below t_2 in tetrahedral substitutional symmetry). The site location also establishes the value of N_H, as discussed in Part II,1. Second, if the sample has been doped p type, it is assumed that positively ionized impurities exist ($q \geq 0$), whereas if it has been doped n type, the reverse ($q \leq 0$) is assumed to be true. Third, if the observed spin is S, then $2S$ spin-unpaired electrons are present, and the remaining $N - 2S = N_I - N_H - q - 2S$ must be spin paired. Hence, one selects a $t_+^n t_-^m e_+^{n'} e_-^{m'}$ configuration with $n + m + n' + m' = N$ such that $N - 2S$ electrons are spin paired and $2S$ are not. These levels are then occupied in an order consistent with the anticipated sign of Δ_{CF} and the ratio Δ_x/Δ_{CF}; standard multiplet theory[8] is used to assign a multiplet to this one-electron configuration.

For example, an $S = \frac{3}{2}$ EPR spectrum has been observed[1] in p-doped Si after Fe diffusion. Similar $S = \frac{3}{2}$ spectra have been also observed[1] for Si:Mn and Si:Cr in an intrinsic sample and for n-type doping, respectively. Assuming a TI site ($N_H = 0$, t_2 below e), one has $N_I = 8$, 7, and 6 and $q > 0$, $q = 0$ and $q < 0$ for the p-type, intrinsic, and n-type samples containing the Fe, Mn, and Cr impurities, respectively. Hence, one has to form $N_I - N_H - q - 2S$ paired electrons (i.e., 5-q, 4-q, and 3-q for Fe, Mn, and Cr, respectively) out of $N_I - N_H - q$ "active" electrons (i.e., $8-q$, $7-q$, and $6-q$, respectively). The similarity of all three spectra suggested[1] that all three impurities have the same "d^N" configuration. This implied a reasonable choice of $q = 1$, 0, and -1 for the samples containing Fe, Mn, and Cr, respectively, consistent with the type of doping. This yielded $N_I - N_H - q - 2S = 4$ paired electrons out of $N = 7$ "active" electrons in all three cases. The solution obtained was hence $t_+^3 t_-^2 e_+^2 e_-^0$. For an I-HSL configuration, the relevant multiplet[9] corresponding to this configuration (see Fig. 4) is $^4T_1$. The suggested states were hence $[Fe^+, d^7, A^-, t_2^5e^2, {}^4T_1]$, $[Mn^0, d^7, A^0, t_2^5e^2, {}^4T_1]$, and $[Cr^-, d^7, A^-, t_2^5e^2, {}^4T_1]$, all with $S = \frac{3}{2}$. This was consistent with the observed[1] g values. It is interesting to note that the assignment based on these data alone is not unique[19]: a substitutional assignment (e occupied before the t_2 level and $N_H = 4$) yields from the same considerations and data the configurations $[Fe^{5+}, d^3, A^+, e^2t_2^1, {}^4T_1]$, $[Mn^{4+}, d^3, A^0, e^2t_2^1, {}^4T_1]$, $[Cr^{3+}, d^3, A^-, e^2t_2^1, {}^4T_1]$, which are all consistent with observed S and L values (i.e., having the same multiplet as in the previous assignment) and the doping type, but which have a completely different electronic structure. Additional information (e.g., spin-orbit data[34]) is then needed to choose between the former I-HSL result and the latter S-HSL result. [However, the use of spin-orbit data to resolve this issue[34] is model dependent; a simplified linear combination of atomic orbitals (LCAO) model has been used[34]]. In Fig. 4, examples of identical multiplets for substitutional and interstitial sites are denoted by three asterisks (⁂). A single asterisk indicates that the high- and low-spin configurations have the same spin value. Two asterisks indicate that both the spin value and the formal charge q in the substitutional and TI sites are indistinguishable.

Additional information can be obtained from the EPR-observed g value. It is usually expressed in terms of three contributions[1,2,4,31,32]

$$g = g_S + g_L + \Delta g_{LS}, \tag{5.1}$$

where g_S and g_L are the electron-spin and orbital-angular-momentum parts, respectively, and Δg_{LS} is the spin-orbit contribution. The latter includes information on the effective crystal-field splitting Δ_{eff}, the spin-orbit coupling constant λ, and its reduction factor (relative to a free ion) k, since $\Delta g_{LS} \cong (n/m)\,\lambda k/\Delta_{eff}$. The angular-momentum part $g_L = \gamma(\mathbf{S}\cdot\mathbf{J})/(\mathbf{J}\cdot\mathbf{J})$ is proportional to the "covalency factor" $\gamma = \langle \psi_{t_2}^{\alpha,\lambda}(\mathbf{r}) | \hat{L} | \psi_{t_2}^{\alpha,\lambda}(\mathbf{r}) \rangle$; since $l = 1$ and 2 components of $\psi_{t_2}^{\alpha,\lambda}(\mathbf{r})$ have opposite contributions to γ, such a p-d mixing ("covalency") can "quench" g_L. A dynamic Jahn–Teller coupling can quench g_L too.[35]

[30] D. G. Andrianov, Yu. N. Bolsheva, G. V. Lazareva, A. S. Savelev, and S. M. Yakubenya, *Fiz. Tekh. Poluprovodn.* **17**, 810 (1983) [*Sov. Phys. Semicond.* **17**, 506 (1983)].

[31] G. D. Watkins, *in* "Point Defects in Solids" (J. H. Crawford and L. M. Silfkin, eds.), Vol. 2, pp. 333. Plenum, New York, 1975).

[32] E. G. Sieverts, *Phys. Status Solidi* **120B**, 11 (1983).

[33] G. Feher, *Phys. Rev.* **114**, 1219 (1959); A. Abragam and B. Bleaney, "Electron Paramagnetic Resonance of Transition Ions." Clarendon, Oxford, 1970; L. Kevan and L. D. Kispert, "Electron Spin Double Resonance Spectroscopy." Wiley, New York, 1976.

[34] L. F. Feiner, *J. Electron. Mater.* **14a**, 877 (1985).

[35] F. S. Ham, *in* "Electron Paramagnetic Resonance." (S. Geschwind, ed.), p. 1. Plenum, New York, 1972; F. S. Ham, *Phys. Rev.* **138**, A1727 (1965).

The central hyperfine coupling constant A (measured in units of cm^{-1}) includes three terms[36]: (1) the contribution A_c from Fermi contact interactions (including direct as well as core-polarization contact interactions), (2) the contribution A_L from interaction with the orbital magnetic moment of the electron, and (3) the contribution from the dipole–dipole interaction. The last contribution is normally very small.[36] A_c reflects the net spin density $\delta\rho(0)$ at the nucleus, and is given by[37,38]

$$A_c = \frac{8\pi}{3} g\mu_B g_N \beta_N \frac{\delta\rho(0)}{2S}, \tag{5.2}$$

where g and g_N are, respectively, the electron and nuclear g values, μ_B and β_N are the electron and nuclear Bohr magnetons, and S is the electron spin. The hyperfine field $H_{hf}^{(c)}$ (measured in units of kilogauss) associated with the contact hyperfine coupling constant A_c is $H_{hf}^{(c)} = (8\pi/3)\mu_B\,\delta\rho(0)$. Measurement of the central hyperfine field (often only its absolute magnitude is known experimentally) can hence be used to deduce the net spin density $\delta\rho(\mathbf{r}) = \Delta\rho_+(\mathbf{r}) - \Delta\rho_-(\mathbf{r})$ at the impurity nucleus $\mathbf{r} = 0$ (where $\Delta\rho_+$ and $\Delta\rho_-$ are, respectively, the spin-up and spin-down spin densities), if A_L and the other quantities in Eq. (5.2) can be evaluated independently. When experiments or calculations are available on the net spin density $\delta\rho_{atom}(0)$ of a free impurity atom (or ion), the ratio $\eta = \delta\rho(0)/\delta\rho_{atom}(0)$ can be used to infer the extent of delocalization of the impurity spin in the solid, relative to the free atom (ion).[39]

ENDOR data[40–46] can provide the net spin density $\delta\rho(\mathbf{r})$ both at the impurity site ($\mathbf{r} = 0$) and on the ligand sites. In general the spin density $\delta\rho(\mathbf{r})$

[36] A. J. Freeman and R. E. Watson, *in* "Magnetism" (G. Rado and H. Suhl, eds.), Vol. 2A, pp. 167. Academic Press, New York, 1965.

[37] C. P. Slichter, "Principles of Magnetic Resonance." Harper, New York, 1963; G. Lancaster, "Electron Spin Resonance in Semiconductors." Plenum, New York, 1967.

[38] S. Geschwind, *in* "Hyperfine Interactions" (A. J. Freeman and R. B. Frankel, eds.), pp. 225. Academic Press, New York, 1967.

[39] H. Katayama-Yoshida and A. Zunger, *Phys. Rev. Lett.* **53,** 1256 (1984); *Phys. Rev. B* **31,** 7877 (1985); *Proc. Mater. Res. Soc. on Microscopic Identification of Electronic Defects in Semiconductors*, p. 111 (1985), and unpublished results (1985).

[40] S. Greulich-Weber, J. R. Niklas, E. R. Weber, and J. M. Spaeth, *Phys. Rev. B* **30** 6292 (1984).

[41] (a) D. A. Van Wesep and A. J. Ammerlaan, *J. Electron Mater.* **14a,** 863 (1985); (b) D. A. Van Wezep, R. Van Kemp, E. G. Sievers, and C. A. J. Ammerlaan, *Phys. Rev. B* **32,** 7129 (1985).

[42] P. Van Engelen and S. G. Sie, *Solid State Commun.* **30,** 515 (1979); P. Van Engelen, *Phys. Rev. B* **22,** 3144 (1980).

[43] W. Teuerle and A. Hausmann, *Z. Phys. B* **23,** 11 (1976).

[44] V. I. Kirilov and V. V. Teslenko, *Fiz. Tverd. Tela (Leningrad)* **21,** 3209 (1979) [*Sov. Phys. Solid State* **21,** 1852 (1979)]; V. V. Teslenko, *Sov. Phys. Semicond.* **18,** 963 (1984) [*Fiz. Tekh. Polup.* **18,** 1536 (1984)].

[45] Y. Ueda, J. R. Niklas, J. M. Spaeth, U. Kaufmann, and J. Schneider, *Solid State Commun.* **46,** 127 (1983).

[46] J. Hage, J. R. Niklas, and J. B. Spaeth, *J. Electron. Mater.* **14a,** 1051 (1985).

may be contributed by[39] (1) the core states, which are exchange polarized[36] by the outer orbitals; (2) the impurity-induced valence-band resonances (VBR); and (3) the partially filled impurity-induced gap states

$$\delta\rho(\mathbf{r}) = \delta\rho_{core}(\mathbf{r}) + \delta\rho_{VBR}(\mathbf{r}) + \delta\rho_{gap}(\mathbf{r}). \tag{5.3}$$

It is important to emphasize[39] that although both the core states and the valence-band resonances are occupied by an equal number of spin-up and spin-down electrons (and hence contribute a zero *net* spin), their *spin densities* $\Delta\rho_+(\mathbf{r})$ and $\Delta\rho_-(\mathbf{r})$ need not compensate each other at arbitrary positions $\mathbf{r}$. Hence, although core and VBR states do not contribute to the *total spin*, both types of states can contribute to the *spin density* $\delta\rho(\mathbf{r})$. Unfortunately, all but the last term in Eq. (5.3) are commonly neglected in the experimental analysis (see, however, recent work in Ref. 41b).

Table II collects the observed EPR parameters of interstitial $3d$ impurities in Si[1,41a] and results of theoretical calculations of these quantities,[39] to be discussed in Part VI,25. Data are arranged in an isovalent series, according to the "d^N" configuration, to highlight regularities. It is remarkable that even 25 years after the original EPR work of Ludwig and Woodbury,[1] only a single entry[41a] (Si:Ti^+) has been added to their results. Similar data for $3d$ impurities in III-Vs and II-Vs are given in Tables III and IV, respectively (EPR in III-Vs is complicated by the fact that group-III and -V elements have only isotopes with nonzero nuclear spin, which often results in unresolved hyperfine interactions and broad signals). As was the case in Si:$3d$, most of the EPR data on $3d$ impurities in II-VIs (Table IV) were obtained in the "golden era of EPR," with only very few entries (e.g., ZnSe:Ti^{2+}, CdTe:Fe^{3+}, CdTe:Ni^+) measured more recently. The data in Tables II–IV illustrate both the overall similarity of the EPR parameters for the different members of each d^N group and distinct chemical variations within each such group.

ENDOR data are available for far fewer $3d$ impurities in semiconductors.[40–46] Such data can be used to estimate the extent of delocalization of the spin density in the system.[47] In Si:Fe_i^+ for example, recent experiments[40] suggest that at least 80% (72% in the analysis of Ref. 41b) of the spin density resides inside the impurity first-neighbor shell, and the remainder is distributed through at least five shells of Si atoms. A recent ENDOR experiment[41b] for Si:Ti_i^+ shows that only ~60% of the spin density resides in the impurity nearest-neighbor sphere. For GaAs:V^{3+}, recent data[46] suggest that ≈70% of the spin density is on the impurity site, 7% of the spin density is in the first shell, and 13% is in the second shell.

Whereas EPR and ENDOR provide information on the *spin* density at the impurity nucleus, in the cases where Mössbauer impurity nuclei are

[47] H. Katayama-Yoshida and A. Zunger, *Phys. Rev. B* **31,** 8317 (1985).

TABLE II. OBSERVED[a,b] AND CALCULATED[c] g VALUES AND HYPERFINE COUPLING CONSTANTS FOR INTERSTITIAL $3d$ IMPURITIES IN Si[d]

	Impurity	S	L	J	State	g_S	g_L	Δg_{LS}	g_{calc}	g_{expt}	A_c	A_L	A_{calc}	A_{expt} (10^{-4} cm^{-1})
d^1	$^{45}Sc^{2+}$	$\frac{1}{2}$	1	$\frac{1}{2}$	$^2T_2$	−0.6674	−0.1067	—	−0.7741	—	+5.1996	—	+5.1996	—
	$^{45}Sc^{2+}$	$\frac{1}{2}$	1	$\frac{3}{2}$	$^2T_2$	0.6673	−0.0533	—	0.6141	—	−5.1996	—	−5.1996	—
	$^{47}Ti^{3+}$	$\frac{1}{2}$	1	$\frac{1}{2}$	$^2T_2$	−0.6674	−0.2267	—	−0.8941	—	−1.9389	—	−1.9389	—
	$^{47}Ti^{3+}$	$\frac{1}{2}$	1	$\frac{3}{2}$	$^2T_2$	0.6674	−0.1133	—	0.5541	—	+1.9389	—	+1.9389	—
d^2	$^{45}Sc^{+}$	1	1	1	$^3T_1$	1.0012	0.0378	—	1.0390	—	−6.2673	—	−6.2673	—
	$^{45}Sc^{+}$	1	1	2	$^3T_1$	1.0012	0.0378	—	1.0390	—	−6.2673	—	−6.2673	—
	$^{47}Ti^{2+}$	1	1	1	$^3T_1$	1.0012	−0.0629	—	0.9383	—	+2.5845	—	+2.5845	—
	$^{47}Ti^{2+}$	1	1	2	$^3T_1$	1.0012	−0.0629	—	0.9383	—	+2.5845	—	+2.5845	—
	$^{51}V^{3+}$	1	1	1	$^3T_1$	1.0012	0.1212	—	1.1224	—	−21.1580	—	−21.1580	—
	$^{51}V^{3+}$	1	1	2	$^3T_1$	1.0012	0.1212	—	1.1224	—	−21.1580	—	−21.1580	—
d^3	$^{45}Sc^{0}$	$\frac{3}{2}$	0	$\frac{3}{2}$	$^4A_2$	2.0023	0.0	−0.0138	1.9885	—	−13.4504	−0.1519	−13.6023	—
	$^{47}Ti^{+}$	$\frac{3}{2}$	0	$\frac{3}{2}$	$^4A_2$	2.0023	0.0	−0.0111	1.9912	1.9986[b]	+4.6278	+0.0660	+4.6938	±5.224[b]
	$^{51}V^{2+}$	$\frac{3}{2}$	0	$\frac{3}{2}$	$^4A_2$	2.0023	0.0	−0.0292	1.9731	1.9892	−31.8998	−1.8550	−33.7548	−42.10
	$^{53}Cr^{3+}$	$\frac{3}{2}$	0	$\frac{3}{2}$	$^4A_2$	2.0023	0.0	−0.0391	1.9632	—	+5.2321	—	+5.2321	—
d^4	$^{47}Ti^{0}$	1	1	1	$^3T_1$	1.0012	0.0678	—	1.0690	—	+2.2094	—	+2.2094	—
	$^{47}Ti^{0}$	1	1	2	$^3T_1$	1.0012	0.0678	—	1.0690	—	+2.2094	—	+2.2094	—
	$^{51}V^{+}$	1	1	1	$^3T_1$	1.0012	−0.0408	—	0.9604	—	−15.6527	—	−15.6527	—
	$^{51}V^{+}$	1	1	2	$^3T_1$	1.0012	−0.0408	—	0.9604	—	−15.6527	—	−15.6527	—
	$^{53}Cr^{2+}$	2	0	2	^5E	2.0023	0.0	−0.0236	1.9787	—	+9.6581	+0.1884	+9.8465	—
	$^{55}Mn^{3+}$	2	0	2	^5E	2.0023	0.0	−0.0144	1.9879	—	−37.5687	−0.5020	−38.0707	—
d^5	$^{47}Ti^{-}$	$\frac{1}{2}$	1	$\frac{1}{2}$	$^2T_2$	−0.6674	0.0581	—	−0.6093	—	−1.5172	—	−1.5172	—
	$^{47}Ti^{-}$	$\frac{1}{2}$	1	$\frac{3}{2}$	$^2T_2$	0.6674	0.1163	—	0.7837	—	+1.9515	—	+1.9515	—
	$^{51}V^{0}$	$\frac{1}{2}$	1	$\frac{1}{2}$	$^2T_2$	−0.6674	0.0074	—	−0.6600	—	+13.9928	—	+13.9928	—
	$^{51}V^{0}$	$\frac{1}{2}$	1	$\frac{3}{2}$	$^2T_2$	0.6674	0.0148	—	0.6822	—	−14.4635	—	−14.4635	—
	$^{53}Cr^{+}$	$\frac{5}{2}$	0	$\frac{5}{2}$	$^6A_1$	2.0023	0.0	−0.0037	1.9986	1.9978	+10.9546	+0.0235	+10.9781	+10.67
	$^{55}Mn^{2+}$	$\frac{5}{2}$	0	$\frac{5}{2}$	$^6A_1$	2.0023	0.0	0.0024	2.0047	2.0066	−40.8465	+0.0730	−40.7735	−53.47
d^6	$^{53}Cr^{0}$	2	1	1	$^5T_2$	3.0035	0.0878	−0.0085	3.0828	2.97	+14.3214	—	+14.3214	±15.9
	$^{53}Cr^{0}$	2	1	2	$^5T_2$	1.6686	−0.0293	—	1.6393	1.72	+8.2939	—	+8.2939	—
	$^{53}Cr^{0}$	2	1	3	$^5T_2$	1.3349	−0.0585	—	1.2764	—	+6.1548	—	+6.1548	—
	$^{55}Mn^{+}$	2	1	1	$^5T_2$	3.0035	0.0887	0.0147	3.1069	3.01	−68.3008	—	−68.3008	±73.8
	$^{55}Mn^{+}$	2	1	2	$^5T_2$	1.6686	−0.0296	—	1.6390	1.68	−38.1214	—	−38.1214	±46.1
	$^{55}Mn^{+}$	2	1	3	$^5T_2$	1.3349	−0.0591	—	1.2758	1.34	−30.4064	—	−30.4064	—
d^7	$^{55}Mn^{0}$	$\frac{3}{2}$	1	$\frac{1}{2}$	$^4T_1$	3.3372	0.1583	0.0310	3.5265	3.362	−81.8557	+39.4493	−42.4064	±92.5
	$^{55}Mn^{0}$	$\frac{3}{2}$	1	$\frac{3}{2}$	$^4T_1$	1.4684	−0.0633	—	1.4051	1.46	−35.5471	—	−35.5471	—
	$^{55}Mn^{0}$	$\frac{3}{2}$	1	$\frac{5}{2}$	$^4T_1$	0.8009	−0.1424	—	0.6585	—	−16.0327	—	−16.0327	—
	$^{57}Fe^{+}$	$\frac{3}{2}$	1	$\frac{1}{2}$	$^4T_1$	3.3372	0.1531	0.0679	3.5582	3.524	−9.0434	+5.1798	−3.8636	±2.99
	$^{57}Fe^{+}$	$\frac{3}{2}$	1	$\frac{3}{2}$	$^4T_1$	1.4684	−0.0612	—	1.4072	—	−3.6112	—	−3.6112	—
	$^{57}Fe^{+}$	$\frac{3}{2}$	1	$\frac{5}{2}$	$^4T_1$	0.8009	−0.1378	—	0.6631	—	−1.7017	—	−1.7017	—
	$^{59}Co^{2+}$	$\frac{1}{2}$	0	$\frac{1}{2}$	^2E	2.0023	0.0	0.0374	2.0397	—	−18.3132	—	−18.3132	—
d^8	$^{55}Mn^{-}$	1	0	1	$^3A_2$	2.0023	0.0	0.0407	2.0430	2.0104	−49.6620	+0.5930	−49.0690	−71.28
	$^{57}Fe^{0}$	1	0	1	$^3A_2$	2.0023	0.0	0.0187	2.0210	2.0699	−5.4761	+0.2470	−5.2291	±6.98
	$^{59}Co^{+}$	1	0	1	$^3A_2$	2.0023	0.0	0.0577	2.0600	—	−16.4890	+2.7083	−13.7807	—
d^9	$^{59}Co^{0}$	$\frac{1}{2}$	0	$\frac{1}{2}$	^2E	2.0023	0.0	0.0834	2.0857	—	−21.6072	—	−21.6072	—

[a] H. H. Woodbury and G. W. Ludwig, *Phys. Rev.* **117**, 102 (1960); and *Solid State Phys.* **13**, 223 (1962).
[b] D. A. van Wezep and C. A. J. Ammerlaan, *J. Electron. Mater.* **14a**, 863 (1985).
[c] H. Katayama-Yoshida and A. Zunger, *Phys. Rev. B* **31**, 8317 (1985), and unpublished results (1985).
[d] For interstitial impurities, the oxidation state (given) is identical to the charge state.

TABLE III. OBSERVED g VALUES AND HYPERFINE CONSTANTS A OF SUBSTITUTIONAL IMPURITIES IN SI AND III-V SEMICONDUCTORS IN DIFFERENT FORMAL CHARGE STATES

	Systems	g_{expt}	S	L	A_{expt} (10^{-4} cm^{-1})
d^2, $^3A_2$	GaAs:$^{51}V^{3+}$, A^0	1.957[a]	1	0	± 54[a]; 55.1[a]
	InP:$^{51}V^{3+}$, A^0	1.96[a']	1	0	± 55[a']
	GaP:Cr^{4+}, A^+	1.985 – 1.986[b,c]	1	0	—
	GaAs:Cr^{4+}, A^+	1.993 – 1.995[b,c]	1	0	—
	InP:Cr^{4+}, A^+	1.999[c]	1	0	—
	Si:$^{53}Cr^{4+}$, A^0	1.9962[d]	1	0	± 12.54[d]
	Si:$^{55}Mn^{5+}$, A^+	2.0259[d]	1	0	-63.09[d]
d^3, $^4T_1$ OR[u]	GaAs:Cr^{3+}, A^0	$g'_x = 2.367$, $g'_y = 5.154$, $g'_z = 1.636$[b]			
	GaP:Cr^{3+}, A^0 (?)	$g'_x = 3.044$, $g'_y = 4.736$, $g'_z = 1.840$[a']			
d^4, $^5T_2$ TETR[v]	GaAs:Cr^{2+}, A^-	1.974 (∥); 1.997 (⊥)[e]			—
	InP:Cr^{2+}, A^-	1.978 (∥); 1.999 (⊥)[f]			
	GaP:Cr^{2+}, A^- (?)	1.981 (∥); 2.010 (⊥)[g] 1.78 ± 0.02 (∥)[g]			—
d^5, $^6A_1$	GaP:Cr^+, A^{2-}	1.999[h]	$\frac{5}{2}$	0	—
	GaP:$^{55}Mn^{2+}$, A^-	2.002[i], 2.003[i]	$\frac{5}{2}$	0	$-(53 - 54)$[i]
	GaAs:$^{55}Mn^{2+}$, A^-	2.003[j], 2.004[j]	$\frac{5}{2}$	0	-52.4[j]
	InP:$^{55}Mn^{2+}$, A^-	1.997[k]	$\frac{5}{2}$	0	-52.0[k]
	GaP:Fe^{3+}, A^0	2.026[l], 2.025[m]	$\frac{5}{2}$	0	—
	GaAs:$^{57}Fe^{3+}$, A^0	2.0453[n], 2.053[m]	$\frac{5}{2}$	0	$\simeq 10$[m]
	InP:Fe^{3+}, A^0	2.0235 – 2.024[g]	$\frac{5}{2}$	0	—
	InAs:Fe^{3+}, A^0	2.035[n]	$\frac{5}{2}$	0	—
	Si:$^{55}Mn^{2+}$, A^{2-}	2.0058[d]	$\frac{5}{2}$	0	-40.5[d]
d^7, $^4A_2$	GaP:Fe^{1+}, A^{2-}	2.133[o,m]	$\frac{3}{2}$	0	—
	GaP:Co^{2+}, A^-	2.164[p], 2.159[p]	$\frac{3}{2}$	0	—
	GaAs:Co^{2+}, A^-	2.189[q], 2.182[p]	$\frac{3}{2}$	0	—
	InP:Co^{2+}, A^-	2.192[r]	$\frac{3}{2}$	0	—
	GaP:Ni^{3+}, A^0	2.089[p]	$\frac{3}{2}$	0	—
	GaAs:Ni^{3+}, A^0	2.114[p], 2.106[n]	$\frac{3}{2}$	0	—
	InP:Ni^{3+}, A^0	2.098[p]	$\frac{3}{2}$	0	—
d^9, $^2T_2$	GaP:Ni^+, A^{2-}	$\lvert g \rvert = 0.94$[g]	$\frac{1}{2}$	1	—
	GaAs:Ni^+, A^{2-}	$g = -1.16$[t]	$\frac{1}{2}$	1	

[a] U. Kaufmann, H. Ennen, J. Schneider, R. Wörner, J. Weber, and F. Köhl, *Phys. Rev. B* **25**, 5598 (1982). A new experiment by J. Hage, J. R. Niklas, and J. M. Spaeth, *J. Electron. Mater.* **14a**, 1051 (1985) gives a hyperfine constant of 55.1.

[a'] B. Lambert, H. J. Von Bardeleben, and B. Deveaud, *J. Phys. C* **18**, L707 (1985).

[b] U. Kaufmann and J. Schneider, *Appl. Phys. Lett.* **36**, 747 (1980); G. H. Stauss, J. J. Krebs, S. H. Lee, and E. M. Swiggard, *Phys. Rev. B* **22**, 3141 (1980); G. H. Stauss and J. J. Krebs *Phys. Rev. B* **22**, 2050 (1980).

(continues)

Footnotes (*Continued*)

[c] N. K. Goswami, R. C. Newman, and J. R. Whitehouse, *Solid State Commun* **36**, 897 (1980). See also V. V. Teslenko, *Sov. Phys. Semicond.* **18**, 963 (1984) [*Fiz. Tekh. Poluprov.* **18**, 1536 (1984)], who gives the hyperfine tensor $A_{XX} = 70.15 \pm 0.05$ MHz, $A_{YY} = A_{ZZ} = 42.29 \pm 0.05$ MHz for GaP:Cr^{4+}.

[d] H. H. Woodbury and G. W. Ludwig, *Phys. Rev.* **117**, 102 (1960).

[e] J. J. Krebs and G. H. Stauss, *Phys. Rev. B* **16**, 971 (1977).

[f] R. J. Wagner, A. M. White, J. J. Krebs, and G. H. Stauss, *Inst. Phys. Conf. Ser.* **56**, 587 (1980).

[g] G. H. Stauss, J. J. Krebs, and R. L. Henry, *Phys. Rev. B* **16**, 974 (1977). For GaP:Cr^{2+}, C. A. Bates, J. Handley, A. Vasson, and A. M. Vasson, *J. Phys. C* **17**, L603 (1984), observed an EPR spectra with $g_{\parallel} = 1.78 \pm 0.02$, but it is not clear if this corresponds to isolated Cr^{2+}.

[h] U. Kaufmann and W. H. Koschel, *Phys. Rev. B* **17**, 2081 (1978).

[i] P. Van Engelen and S. G. Sie, *Solid State Commun.* **30**, 515 (1979); P. Van Engelen, *Phys. Rev. B* **22**, 3144 (1980); R. S. Title and T. S. Plaskett, *Appl. Phys. Lett.* **14**, 76 (1969).

[j] R. Bleekrode, H. Dieleman, and H. J. Vogter, *Phys. Lett.* **2**, 355 (1962); N. Almeleh and B. Goldstein, *Phys. Rev.* **128**, 1568 (1962).

[k] V. F. Masterov, Yu. V. Maltsev, and V. K. Sobolevskii, *Fiz. Tekh. Poluprovdn.* **15**, 2127 (1981) [*Sov. Phys. Semicond.* **15**, 1235 (1981).

[l] W. Teuerle, E. Blaschke, and A. Hausmann, *Z. Phys.* **270**, 37 (1974).

[m] V. I. Kirilov and U. V. Teslenko, *Fiz. Tverd. Tela* **21**, 3209 (1979); [*Sov. Phys. Solid State* **21**, 1852 (1979)].

[n] T. L. Estle, *Phys. Rev.* **136A**, 1702 (1964); M. DeWit and T. L. Estle, *Bull. Am. Phys. Soc.* **7**, 449 (1962), and *Phys. Rev.* **132**, 195 (1963).

[o] U. Kaufmann and J. Schneider, *Solid State Commun.* **21**, 1073 (1977). Recently it has been suggested by V. F. Masterov, L. P. Pasechnik, and K. F. Shtelmakh [*Sov. Phys. Semicond.* **19**, 391 (1985)] and V. F. Masterov, S. I. Markov, L. P. Pasechnik, and V. K. Sobolevskii [*Sov. Phys. Semicond.* **17**, 711 (1983)] that the $g = 2.131$ line observed in GaP:Fe is due to interstitial Fe^0 (d^8), not substitutional Fe^{1+}, d^7.

[p] U. Kaufmann and J. Schneider, *Solid State Commun.* **25**, 1113 (1978); K. Suto and J. Nishizawa, *J. Phys. Soc. Jpn.* **27**, 924 (1969); Y. Ueda, J. R. Niklas, J. M. Spaeth, U. Kaufmann, and J. Schneider, *Solid State Commun.* **46**, 127 (1983); See also D. G. Andrianov, N. I. Suchkova, A. S. Savelev, E. P. Rashevskaya, and M. A. Filippov, *Sov. Phys. Semicond.* **11**, 426 (1977) [*Fiz. Tek. Polup.* **11**, 730 (1977)] for EPR data on GaAs:Co^{2+} and GaAs:Ni^{3+}. The parameters for GaAs:Co^{2+} disagree with the results of others.

[q] M. Godlewski and A. M. Hennel, *Phys. Status Solidi* **88B**, K11 (1978).

[r] B. Lambert, B. Deveaud, Y. Toudic, and B. Clerjaud, *Physica* **116B**, 467 (1983).

[s] U. Kaufmann, W. H. Koschel, J. Schneider, and J. Weber, *Phys. Rev. B* **19**, 3343 (1979).

[t] W. Drozdzewicz, A. M. Hennel, Z. Wasilewski, B. Clerjaud, F. Gendron, C. Porte, and R. Germer, *Phys. Rev. B* **29**, 2438 (1984).

[u] OR denotes orthorhombic distortion.

[v] TETR denotes tetragonal distortion.

TABLE IV. g VALUES AND HYPERFINE CONSTANTS A OF SUBSTITUTIONAL $3d$ IMPURITIES IN II-VI SEMICONDUCTORS*

	System	g_{expt}	S	L	A_{expt} (10^{-4} cm^{-1})
$d^1, {}^2E$	$ZnS:{}^{45}Sc^{2+}, A^0$	1.934[a]	$\frac{1}{2}$		43.1[a]
$d^2, {}^3A_2$	$ZnS:{}^{47}Ti^{2+}, A^0$	1.9280[b]	1	0	12.7[b]
	$ZnS:{}^{51}V^{3+}, A^+$	1.9433[c]	1	0	63.0[c]
	$ZnSe:V^{3+}, A^+$	1.9483[d]	1	0	61.3[d]
	$ZnSe:Ti^{2+}, A^0$	1.924[e]	1	0	12.5[e]
	$CdS:V^{3+}, A^+$	1.93[f]	1	0	63[f]
	$CdS:Ti^{2+}, A^0$	~1.92[g]	1	0	13.5[g]
	$ZnTe:{}^{51}V^{3+}, A^+$	1.917[f]	1	0	57.8[f]
$d^3, {}^4T_1$ Trigonal	$ZnS:{}^{51}V^{2+}, A^0$	$g_\parallel = 1.961, g_\perp = 1.913$[h]	$\frac{3}{2}$	1	$A_\perp = 49.0, A_\parallel = 40.3$
$d^4, {}^5T_2$ TETR	$ZnS:Cr^{2+}, A^0$	$g_\parallel = 1.94, g_\perp = 1.98$[i]	2		—
	$CdS:Cr^{2+}, A^0$	$g_\parallel = 1.934, g_\perp = 1.970$[i]	2		—
	$ZnSe:Cr^{2+}, A^0$	$g_\parallel = 1.961, g_\perp = 1.98$[i]	2		—
	$ZnTe:Cr^{2+}, A^0$	$g_\parallel = 1.97, g_\perp = 1.99$[i]	2		—
	$CdTe:Cr^{2+}, A^0$	$g_\parallel = 1.980, g_\perp = 1.980$[i]	2		—
$d^5, {}^6A_1$	$ZnS:{}^{53}Cr^+, A^-$	1.9995[j,k]	$\frac{5}{2}$	0	13.4[j]
	$ZnS:{}^{55}Mn^{2+}, A^0$	2.0024[l]	$\frac{5}{2}$	0	−64.5[l]
	$ZnS:{}^{57}Fe^{3+}, A^+$	2.019[j]	$\frac{5}{2}$	0	7.69[j]
	$ZnSe:{}^{53}Cr^+, A^-$	2.0016[m,n]	$\frac{5}{2}$	0	13.27[n]
	$ZnSe:{}^{55}Mn^{2+}, A^0$	2.0055[l]–2.0069[m]	$\frac{5}{2}$	0	−61.77[n]
	$ZnSe:{}^{57}Fe^{3+}, A^+$	2.0469[m,n]	$\frac{5}{2}$	0	6.6[n]
	$ZnTe:{}^{53}Cr^+, A^-$	2.0026[o,n,m]	$\frac{5}{2}$	0	12.4[n]
	$ZnTe:{}^{55}Mn^{2+}, A^0$	2.0105[f,p,q]	$\frac{5}{2}$	0	−56.1[f]
	$CdS:{}^{55}Mn^{2+}, A^0$	2.0029[l,r,s], 2.0018	$\frac{5}{2}$	0	−65.3[r,s]
	$CdS:Fe^{3+}, A^+$	2.018[t]	$\frac{5}{2}$	0	—
	$CdSe:{}^{55}Mn^{2+}, A^0$	2.003[f,p,q,u]	$\frac{5}{2}$	0	−62.7[u]
	$CdTe:{}^{53}Cr^+, A^-$	1.9997[v]	$\frac{5}{2}$	0	+12.78[v]
	$CdTe:{}^{53}Mn^{2+}, A^0$	2.0069[f,p,s]	$\frac{5}{2}$	0	−57.3[f,s]
	$CdTe:Fe^{3+}, A^+$	2.084[w]	$\frac{5}{2}$	0	—
$d^7, {}^4A_2$	$ZnS:Fe^+, A^-$	2.2515[c]	$\frac{3}{2}$	0	—
	$ZnS:Co^{2+}, A^0$	2.248[x]	$\frac{3}{2}$	0	1.8[x]
	$ZnS:Ni^{3+}, A^+$	2.1480[c]	$\frac{3}{2}$	0	—
	$ZnSe:Co^{2+}, A^0$	2.270[x]	$\frac{3}{2}$	0	—
	$ZnSe:Ni^{3+}, A^+$	2.1978[y]	$\frac{3}{2}$	0	—
	$ZnTe:Fe^+, A^-$	2.280[n]	$\frac{3}{2}$	0	—
	$ZnTe:Co^{2+}, A^0$	2.2972[q,x]	$\frac{3}{2}$	0	17.5[q,x]
	$CdS:Co^{2+}, A^0$	2.27[f,z]	$\frac{3}{2}$	0	4.6[f,z]
	$CdTe:Co^{2+}, A^0$	2.31[x,aa]	$\frac{3}{2}$	0	23.4[x,aa]
$d^9, {}^2T_2$	$ZnS:{}^{61}Ni^+, A^-$	1.3991[bb]	$\frac{1}{2}$	1	80[cc,bb]
	$ZnSe:{}^{61}Ni^+, A^-$	1.4374[g]	$\frac{1}{2}$	1	81.4[y]
	$ZnS:Cu^{2+}, A^0$	$\lvert g \rvert = 0.71$[dd] (?)	$\frac{1}{2}$	1	—
	$ZnTe:Ni^+, A^-$	$\lvert g \rvert = 1.367$[ee,s]	$\frac{1}{2}$	1	—
	$CdTe:Ni^+, A^-$	$\lvert g \rvert = 1.425$[ff]	$\frac{1}{2}$	1	81.7[ff]
	$CdS:{}^{63}Cu^{2+}, A^0$	$g_\perp = 2.24, g_\perp = 1.75$[z] (?)	$\frac{1}{2}$	1	99[z]

We also give the many-electron term value in cubic symmetry. OR and TETR denote orthorhombic and tetragonal distortions, respectively.

Footnotes for Table IV

[a] Average spectrum due to motional effects observed by I. Broser and M. Schulz, *J. Phys. C* **7**, L147 (1974); A. O. Barksdale and T. L. Estle, *Phys. Lett.* **42A**, 426 (1973) reported low-temperature spectra (1.3–4.2 K) showing anisotropy: $g_1 = 1.929$, $qg_2 = -0.0370$, $A_1 = -42.8 \times 10^{-4}$ cm^{-1}, and $qA_2 = 17.4 \times 10^{-4}$ cm^{-1}. characteristic of a dynamic JT system.

[b] J. Schneider and V. A. Räuber, *Phys. Lett.* **21**, 380 (1966).

[c] W. C. Holton, J. Schneider, and T. L. Estle, *Phys. Rev. A* **133**, 1638 (1964). See also K. E. Tarkpea and A. Ots, *Phys. Status Solidi* **129B**, 799 (1985) for recent results on $ZnS:Fe^{1+}$.

[d] J. Dieleman, in "II-VI Semiconductor Compounds" (D. G. Thomas, ed.), p. 199. Benjamin, 1967.

[e] J. J. Davies, J. E. Nicholls, and D. J. Verity, *J. Phys. C* **13**, 1291 (1980).

[f] H. H. Woodbury and G. W. Ludwig, *Bull. Am. Phys. Soc.* **6**, 118 (1961).

[g] J. Dziesiaty and R. Böttcher, *Phys. Status Solidi* **26**, K21 (1968).

[h] J. Schneider, B. Dischler, and A. Räuber, *Solid State Commun.* **5**, 603 (1967).

[i] J. T. Vallin and G. D. Watkins, *Phys. Rev. B* **9**, 2051 (1974).

[j] R. S. Title, *Phys. Rev.* **131**, 623 (1963); H. D. Fair, R. D. Ewing, and F. E. Williams, *Phys. Rev.* **144**, 298 (1966); V. A. Raüber and J. Schneider, *Z. Naturforsch.* **17A**, 266 (1962).

[k] T. Taki and H. Bo, *J. Phys. Soc. Jpn.* **25**, 1324 (1968); J. Dieleman, R. S. Title, and W. V. Smith, *Phys. Lett.* **1**, 334 (1962).

[l] J. Schneider, S. R. Sircar, and A. Räuber, *Z. Naturforsch.* **18A**, 980 (1963).

[m] H. Röppischer, W. Elssner, and H. Böttner, *Phys. Status Solidi* **27A**, 375 (1975); R. S. Title, *Phys. Rev.* **133A**, 1613 (1964).

[n] T. L. Estle and W. C. Holton, *Bull. Am. Phys. Soc.* **10**, 57 (1965); *Phys. Rev.* **150**, 159 (1966).

[o] M. Z. Cieplak, M. Godlewski, and J. M. Baranowski, *Phys. Status Solidi* **70B**, 323 (1975); G. W. Ludwig and M. R. Lorentz, *Phys. Rev.* **131**, 601 (1963).

[p] S. Kunii, S. Tobita, and E. Hirahara, *J. Phys. Soc. Jpn.* **21**, 479 (1966); S. Kunii and E. Hirahara, *J. Phys. Soc. Jpn.* **19**, 1258 (1964).

[q] C. Kikuchi and G. M. Azarbayejani, *J. Phys. Soc. Jpn.* **17** (B-I), 453 (1962).

[r] P. B. Dorian, *Phys. Rev.* **112**, 1058 (1958); M. F. Deigen, V. M. Maevsky, V. Ya. Zevin, and N. I. Vitrikhovskii, *Sov. Phys. Solid State* **6**, 2193 (1965); A. P. Galushka and S. Z. Shulga, *Sov. Phys. Semicond.* **12**, 218 (1977).

[s] J. Lambe and C. Kikuchi, *Phys. Rev.* **119**, 1256 (1962).

[t] K. Morgaki and T. Hoshina, *J. Phys. Soc. Jpn.* **21**, 842 (1966); *Phys. Lett.* **17**, 86 (1965); see also J. Lambe, J. Baker, and C. Kikuchi, *Phys. Lett.* **3**, 270 (1959).

[u] O. Matumura, *J. Phys. Soc. Jpn.* **14**, 108 (1959); R. S. Title, *Phys. Rev.* **130**, 17 (1963).

[v] G. W. Ludwig and M. R. Lorenz, *Phys. Rev.* **131**, 601 (1963); see also M. Godlewski and J. M. Baranowski, *Phys. Status Solidi* **97B**, 281 (1980).

[w] G. Brunthaler, U. Kaufmann, and J. Schneider, *J. Appl. Phys.* **56**, 2974 (1984).

[x] F. S. Ham, G. W. Ludwig, G. D. Watkins, and G. D. Woodbury, *Phys. Rev. Lett.* **5**, 468 (1960); J. C. M. Henning, M. Van den Boom, and J. Dielman, *J. Phillips Rep.* **21**, 16 (1966) also observed $ZnSe:Co^{2+}$.

[y] R. K. Watts, *Phys. Rev.* **188**, 568 (1969).

[z] K. Morigaki, *J. Phys. Soc. Jpn.* **19**, 124 (1964) gives tentative results for $CdS:Cu^{2+}$; also, *ibid.*, **19**, 2064 gives results also for $CdS:Co^{2+}$. It is not obvious that the former corresponds to isolated Cu^{2+} (rather than complexes involving Cu).

[aa] T. P. P. Hall and W. Hayes, *J. Chem. Phys.* **32**, 1871 (1960).

[bb] M. Schulz and G. G. Wepfer, *Solid State Commun.* **10**, 405 (1972); Zeeman experiments for the ground as well as for the excited ${}^2E$ of $ZnS:Ni^+$ were reported by B. Clerjaud, A. Gelineau, F. Gendron, C. Porte, J. M. Baranowski, and Z. Liro, *J. Phys. C* **17**, 3837 (1984).

[cc] M. DeWit, T. L. Estle, W. C. Holton, and J. Schneider, *Bull. Am. Phys. Soc.* **9**, 249 (1964).

[dd] W. C. Holton, M. DeWit, R. K. Watts, T. L. Estle, and J. Schneider, *J. Phys. Chem. Solids* **30**, 963 (1969); M. DeWit, *Phys. Rev.* **177**, 441 (1969). It is not obvious that the spectra corresponds to isolated Cu^{2+} (rather than complexes).

[ee] B. Clerjaud, A. Gelineau, F. Gendron, C. Naud, and C. Porte, *J. Cryst. Growth* **72**, 351 (1985).

[ff] U. Kaufmann, J. Windscheif, and G. Brunthaler, *J. Phys. C* **17**, 6169 (1984).

considered, one can obtain through the measurement of the isomer shift (IS) information on the *charge* density (i.e., the sum of spin-up and spin-down contributions) at the impurity nucleus[48,49] $\Delta\rho(\mathbf{r}) = \Delta\rho_+(\mathbf{r}) + \Delta\rho_-(\mathbf{r})$. The isomer shift can be expressed as

$$\Delta_{IS} = \frac{2\pi e^2 Zc}{3E_\gamma}[\Delta\rho_a(0) - \Delta\rho_s(0)]\,\Delta\langle r_n^2\rangle, \tag{5.4}$$

where E_γ denotes the energy of the resonant γ ray, Z is the nuclear charge, $\Delta\langle r_n^2\rangle$ is the change in the second moment of the nuclear charge distribution accompanying nuclear excitation,[49] $\Delta\rho_s(0)$ is the electron charge density of source(s) nuclei at $\mathbf{r} = 0$ and $\Delta\rho_a(0)$ is the charge density of the absorber (a) at $\mathbf{r} = 0$. The values of $\Delta\rho_a(0) - \Delta\rho_s(0)$ for the same impurity in different charge states and different host crystals are then compared to infer the changes in *s*-electron density at the impurity nucleus. A number of Mössbauer experiments have been reported for Fe$\leftrightarrow$Co in Si[50,51], in III-V semiconductors[52], and in II-VI semiconductors[53], although their interpretation is clouded by the occurrence of complexes and impurity precipitates.[50,51] It has been noted[47] that such experiments in semiconductors suggest a surprisingly small change in the IS with the formal oxidation state relative to analogous experiments in ionic crystals. For example,[52,53] $\Delta_{IS}(\mathrm{GaAs{:}Fe^{2+}}) - \Delta_{IS}(\mathrm{GaAs{:}Fe^{3+}}) \simeq 0.23$ mm/sec; $\Delta_{IS}(\mathrm{GaP{:}Fe^{2+}}) - \Delta_{IS}(\mathrm{GaP{:}Fe^{3+}}) = 0.37$ mm/sec. In silicon[50] the difference is almost zero. By contrast, in ionic systems[48,49] (e.g., FeF_2, FeO_2 *vs.* FeF_3 and FeO_3) the corresponding difference is considerably larger ($\sim$0.93 mm/sec), suggesting that in ionic systems a larger fraction of *s* electrons is removed from the impurity site as Fe is ionized in the $Fe^{2+} \rightarrow Fe^{3+}$ process. The relative insensitivity of the IS to ionization of the *s*-electron in semiconductors provides an important clue to its electronic structure (Part VI,20).

6. Techniques that Measure Interelectronic Transitions

The foregoing discussion has indicated that 3*d* impurities can exist in different charge and oxidation states, each distinguished by the number of "active" electrons and by the way they are distributed in different orbitals. The complete notation, then, of a given state of a center is $[T^{N_H+q}, d^N, A^q, e^n t_2^m, {}^{2S+1}\Gamma]$, denoting, respectively, the formal oxidation state, the effective d^N configuration, the formal charge state, the dominant one-electron configuration, and the many-electron multiplet term. Absorption, luminescence, Hall effect, and photoconductivity experiments suggest that there are two types of electronic transitions between such states: those between different multiplets of the same formal charge (or oxidation) state, and those that alter the formal charge (or oxidation) state of the center.

a. Internal $d \rightarrow d^*$ Excitations

Internal transitions are electronic excitations within a fixed formal charge and oxidation state. They are often referred to as $d^N \rightarrow (d^N)^*$ internal transitions, or crystal-field excitons, and resemble similar transitions in the free ions,[8] where both the initial and the final state belong to the same formal charge and oxidation state, but the system changes its electronic configuration from one many-electron state to the other; i.e.,

$$[T^{N_H+q}, d^N, A^q, e^m t_2^n, {}^{2S+1}\Gamma] \rightarrow [T^{N_H+q}, d^N, A^q, e^{m'} t_2^{n'}, {}^{2S'+1}\Gamma']. \tag{6.1}$$

The change in the total many-electron energy can be written as[54]

$$\Delta^{(ij)} = E_T^{(j)}[e^{m'} t_2^{n'}] - E_T^{(i)}[e^m t_2^n], \tag{6.2}$$

where $E_T^{(j)}[e^{m'} t_2^{n'}]$ and $E_T^{(i)}[e^m t_2^n]$, are, respectively, the total many-electron energies of multiplets $|j\rangle$ and $|i\rangle$. (Only the multiplet representation indices *i* and *j* are the appropriate quantum numbers for these many-electron states. I also include the predominant one-electron configurations $e^{m'} t_2^{n'}$ and $e^m t_2^n$ here only as a reminder that different multiplets can correspond to different dominant one-electron configurations.)

Since both the excited electron and the hole left behind remain, in most cases, partially bound, the excitation energy of Eq. (6.2) contains an electron–hole excitonic contribution, much like that of the 3*d* core excitons in

[48] B. D. Dunlap and G. M. Kalvius, *in* "Mössbauer Isomer Shifts." (G. K. Shenoy and F. E. Wagner, eds.), p. 15. North-Holland Publ., Amsterdam, 1978.
[49] G. K. Shenoy and B. D. Dunlap, *in* "Mössbauer Isomer Shifts." (G. K. Shenoy and F. E. Wagner, eds.), p. 869. North-Holland Publ., Amsterdam, 1978.
[50] P. C. Norem and G. K. Wertheim, *J. Phys. Chem. Solids* **23**, 1111 (1962).
[51] G. Weyer, A Kettschau, G. Grebe, W. Schröter, and W. Bergholz, *Phys. Stat. Sol.* (a) **51** 459 (1979); W. Bergholz, S. Damgaard, J. W. Petersen, and G. Weyer, *Phys. Stat. Sol.* **75A**, 789 (1983); **81A**, 239 (1984); G. Bemski, F. Gonzalez, and J. J. Peyre, *Phys. Lett.* **32A**, 231 (1970).
[52] P. P. Seregin, F. S. Nasredinov, and Yu. P. Demakov, *Fiz. Tekh. Polutprovdn.* **10**, 2009 (1976) [*Sov. Phys. Semicond.* **10**, 1200 (1976)]; P. P. Seregin, A. K. Kamolov, and A. I. Blashku, *Fiz. Tverd. Tela* **16**, 2017 (1974) [*Sov. Phys. Solid State* **16**, 1311 (1975)]; P. P. Seregin, F. S. Nasredinov, and Sh. Bakhtiyarov, *Phys. Status Solidi* **91B**, 35 (1979); B. J. Boltaks, A. A. Efimov, P. P. Seregin, and V. T. Shipatov, *Fiz. Tverd. Tela* **12**, 2004 (1970) [*Sov. Phys. Solid State* **12**, 1594 (1971)]; see also a recent review by A. R. Regel and P. P. Seregin, *Sov. Phys. Semicond.* **18**, 723 (1984); G. N. Belozerskii, Yu. A. Shvedchikov, S. B. Tomilov, and A. V. Schvedchikov, *Fiz. Tverd. Tela* **7**, 2908 (1965) [*Sov. Phys. Solid State* **7**, 2908 (1960)].
[53] C. Garcin, P. Imbert, and G. Jehanno, *Solid State Commun.* **21**, 545 (1977); C. Garcin, P. Imbert, G. Jehanno, A. Gerard, and J. Danon, *J. Phys. Chem. Solids* **41**, 969 (1980); P. Bonville, C. Garcin, A. Gerard, P. Imbert, and G. Jehanno, *Phys. Rev. B* **23**, 4293 (1981).
[54] V. Singh and A. Zunger, *Phys. Rev. B* **31**, 3729 (1985).

semiconductors.[55] Internal transitions can be spin-allowed ($S = S'$) or spin-forbidden ($S \neq S'$), orbitally allowed (e.g., $E \leftrightarrow T$) or orbitally forbidden (e.g., $A \leftrightarrow A'$). The occurrence of $l = 1$ character in t_2 states of T_d (but not O_h) symmetry [cf. Eq. (2.14)] renders $e \leftrightarrow t_2$ transitions (having an $l = 1 \leftrightarrow l = 2$ component in their oscillator strength) far more intense than in O_h symmetry.[3,5] Internal transitions have been observed in absorption (usually below a wavelength of 4 μm) and luminescence for many $3d$ impurities. In some cases zero-phonon lines (ZPL) are resolved, aiding in the identification of the defect. When ZPL lines are resolved, strain or magnetic fields can be applied to split these lines. Luminescence can, however, be inhibited if: (1) the relevant level is shallow enough to be depopulated thermally, (2) the relevant level is resonant in the conduction band so it can be observed in absorption but not in luminescence (e.g., the ^5E excited state of Cr^{2+} in GaAs and InP), (3) there is an efficient energy transfer to a different center, (4) another level is lower in energy and depopulates the relevant level, or (5) strong electron–phonon coupling at the deep center leads to efficient radiationless recombination.

Figure 5 depicts the observed internal $d \rightarrow d^*$ transitions for the Co^{2+} impurity in a number of host systems. They are seen to differ substantially from the hydrogenic internal transitions observed for sp-electron impurities in semiconductors (e.g., those of substitutional sulfur, $[S^{4+}, a_1^2, {}^1A_1]$ or other chalcogens in silicon[56]): They exhibit a multiplet structure (Fig. 5) rather than hydrogenic Rydberg-like characteristics. Table V summarizes the best-established internal transition energies of the T^{2+} $3d$ impurities in a number of semiconductors (using the multiplet designation to be clarified in Part IV,12–14). The radiative lifetime of the lowest d^* excited state[57] ranges in the microsecond (3 μsec and 10 μsec for $^5E \rightarrow {}^5T_2$ of GaAs:Cr^{2+} and GaAs:Fe^{2+}, respectively) or millisecond (0.12 msec for $^4T_2 \rightarrow {}^4A_2$ of InP:Co^{2+}) regime. Table V and Fig. 5 highlight the significance of the phenomenological assignment of a number of "active" electrons to each impurity state: Despite variation in the formal charge state A^q, we see that transitions associated with a *fixed oxidation state* (hence, also a fixed number of active electrons, e.g., Co^{2+} d^7 in Fig. 5) resemble each other.

Usually one observes intracenter transitions of only one oxidation state (e.g., T^{2+}) in each crystal. There are, however, a few exceptions to this rule. In some cases, $d \rightarrow d^*$ internal transitions of oxidation states other than T^{2+} were observed. These relatively rare cases include: (1) the Ni^+ d^9 system, showing

[55] A. Zunger, *Phys. Rev. Lett.* **50,** 1215 (1983).

[56] H. Grimmeiss and E. Janzen, *in* "Defects in Semiconductors II." (S. Mahajan and J. W. Corbett, eds.), p. 33. North-Holland Publ., New York, 1983; E. Janzen, R. Stedman, and H. Grimmeiss, *Physica* **117B,** 125 (1983).

[57] G. Guillot, C. Benjeddou, P. Leyral, and A. Nouailhat, *J. Lumin.* **31/32,** 439 (1984).

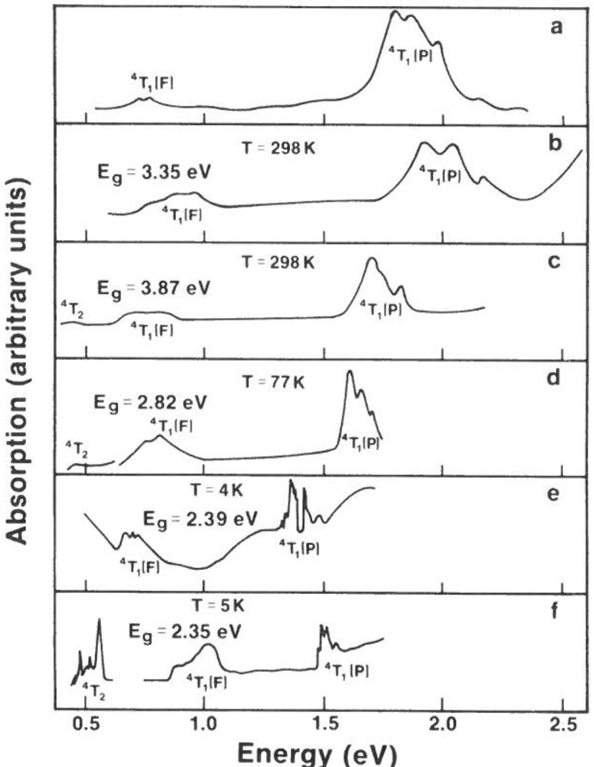

FIG. 5. Internal $d \rightarrow d^*$ transitions of Co^{2+} observed spectroscopically in various host systems at sub-band-gap photon energies. The band gap E_g is denoted for each system. (a) $(CoCl_4)^{2-}$ [B. N. Figgis, "Introduction to Ligand Field", p. 224 Wiley, New York, 1967; (b) ZnO:Co and (c) ZnS:Co [H. A. Weakliem, *J. Chem. Phys.* **36,** 2117 (1962)]; (d) ZnSe:Co and (e) ZnTe:Co [J. M. Baranowski, J. W. Allen, and G. L. Pearson, *Phys. Rev.* **160,** 627 (1967)]; (f) GaP:Co [S. G. Bishop, P. J. Dean, P. Porteous, and D. J. Robbins, *J. Phys. C* **13,** 1331 (1980)].

the $^2T_2 \rightarrow {}^2E$ transition in GaP[58a] (ZPL at 0.66 eV, center at 0.705 eV), in GaAs (ZPL at 0.57 V[58b]) in ZnSe and ZnS (ZPLs at 0.404 and 0.438 eV, respectively[59]), in ZnTe (ZPL at 0.383 eV[60]), and in CdTe (ZPL at 0.362 eV[61]); (2) the 0.57-eV luminescence band in GaAs:Cr, with ZPL at

[58a] U. Kaufmann, W. H. Koschel, J. Schneider, and J. Weber, *Phys. Rev. B* **19,** 3343 (1979); H. Ennen and U. Kaufmann, *J. Appl. Phys.* **51,** 1615 (1980).

[58b] W. Drozdzewicz, A. M. Hennel, Z. Wasilewski, B. Clerjaud, P. Gendron,C. Porte, and R. Germer, *Phys. Rev. B* **29,** 2438 (1984).

[59] G. Roussos, J. Nagel, and H. J. Schulz, *Z. Phys. B* **53,** 95 (1983); B. Clerjaud, A. Gelineau, F. Gendron, C. Porte, J. M. Baranowski, and Z. Liro, *Physica* **116B,** 500 (1982).

[60] B. Clerjaud, A. Gelineau, F. Gendron, C. Naud, and C. Porte, *J. Cryst. Growth* **72,** 351 (1985).

[61] U. Kaufmann, J. Windscheif, and G. Brunthaler, *J. Phys. C.* **17,** 6169 (1984).

TABLE V. OBSERVED INTERNAL $d \rightarrow d^*$ EXCITATION ENERGIES (IN eV) IN CATION SUBSTITUTIONAL T^{2+} TRANSITION-ATOM-DOPED SEMICONDUCTORS*

Host \ Ground-state impurity	$^3A_2$ Ti^{2+}	$^4T_1$ V^{2+}	$^5T_2$ Cr^{2+}	$^6A_1$ Mn^{2+}	^5E Fe^{2+}	$^4A_2$ Co^{2+}	$^3T_1$ Ni^{2+}
ZnS	1.21[a] ($^3T_1$)	0.53[b] ($^4T_2$) 1.14[b] ($^4A_2$) 1.39[b] ($^4T_1$)	0.64[c] (^5E) 1.36[c] ($^3T_2$) 1.75[c] ($^3T_1$)	2.34[d] ($^4T_1$) 2.53[d] ($^4T_2$) 2.67[d] (^4E)	0.44[e] ($^5T_2$) 2.07[e] ($^3A_2$) 2.14[e] ($^3A_1$)	0.46[f] ($^4T_2$) 0.77[f] ($^4T_1$) 1.76[f,g] ($^4T_1$)	0.54[h] ($^3T_2$) 1.13[h] ($^3A_2$) 1.52[h] ($^3T_1$)
ZnSe	0.74[i] ($^3T_1$) 1.22[i] ($^3T_1$)	0.50[i] ($^4T_2$) 1.08[b,i] ($^4A_2$) 1.24[b,i] ($^4T_1$)	0.68[j] (^5E) 1.61[j] ($^3T_2$) 1.85[j] ($^3T_1$)	2.31[j] ($^4T_1$) 2.47[k] ($^4T_2$) 2.67[k] (^4E)	0.34[l] ($^5T_2$) 1.26[m] ($^3T_1$)	0.43[g,l,f] ($^4T_2$) 0.78[g,l] ($^4T_1$) 1.67[g,l] ($^4T_1$)	0.50[i] ($^3T_2$) 1.10[i] ($^3A_2$) 1.46[i] ($^3T_1$)
ZnTe	—	—	0.68[n] (^5E)	2.3[o] ($^4T_1$) 2.4[o] ($^4T_2$) 2.6[o] (^4E)	0.31[l] ($^5T_2$)	0.72[l] ($^4T_1$) 1.44[l,p] ($^4T_1$)	—
CdS	0.40[q] ($^3T_2$) 0.71[q] ($^3T_1$) 1.22[q] ($^3T_1$)	0.61[r] 1.08[r] 1.80[r] ($^4T_1$)	0.66[s] (^5E)	—	0.32[s] ($^5T_2$, ?)	0.68[s] ($^4T_1$) 1.73[s] ($^4T_1$)	0.51[s] ($^3T_2$) 1.01[s] ($^3A_2$) 1.58[s] ($^3T_1$)
CdSe	0.38[u] ($^3T_2$) 0.62[u] ($^3T_1$) 1.18[u] ($^3T_1$)	0.43[u] ($^4T_2$) 0.86[u] ($^4A_2$) 1.31[u] ($^4T_1$)	0.62[u] (^5E)	—	0.37[u] ($^5T_2$) 0.29[t] (ZPL)	0.37[u] ($^4T_2$) (0.35[t], ZPL) 0.68[u] ($^4T_1$) 1.61[u] ($^4T_1$)	0.52[u] ($^3T_2$) (0.45[t], ZPL) 0.99[u] ($^3A_2$) 1.42[u] ($^3T_1$) (1.35[t], ZPL)
CdTe	0.35[v] ($^3T_2$) 0.62[v] ($^3T_1$) 1.14[v] ($^3T_1$)	0.82[v] ($^4A_2$) 1.11[v] ($^4T_1$)	0.63[v] (^5E)	2.2[w] ($^4T_1$?) 2.5[w] ($^4T_2$?)	0.28[e,l] ($^5T_2$)	0.37[l] ($^4T_2$) 0.72[l] ($^4T_1$) 1.44[l] ($^4T_1$)	—
GaP	0.60[ee] ($^3T_2$) —	1.07[x] (max)	0.87[y] (^5E)	1.34[z] (max) ($^4T_1$) 1.53 (ZPL)	0.41[aa,l] ($^5T_2$)	0.56[bb] ($^4T_2$) 0.87–1.24[l] ($^4T_1$) (max at 1.05) 1.50[l,bb] ($^4T_1$)	0.82[cc] ($^3T_2$) 1.24[dd] ($^3T_1$) 1.43[dd] ($^3A_2$)
GaAs	0.565[ee] ($^3T_1$, ?) 0.66[ee] ($^3T_1$, $^3T_2$) 1.04[ee] ($^3T_1$)	1.03[x] (max) 0.69 (weak)	0.9[ff] (max) 0.84 (ZPL, ^5E)	—	0.37[l,gg] ($^5T_2$)	0.5[hh], (ZPL, $^4T_2$) 0.87–1.05[hh] ($^4T_1$) (0.97 max) 1.40[hh] (ZPL, $^4T_1$)	1.15[ii] (max, $^3T_1$)
InP	—	—	0.76[jj], (ZPL, ^5E)	—	0.35[kk] ($^5T_2$) (Lumin max)	0.47[ll], (ZPL, $^4T_2$) 0.92, max ($^4T_1$) 0.79 (ZPL) 0.78–0.92 (resonance)	— —

* The initial state is indicated next to the chemical symbol; final states, indicated in parentheses, are from the analysis of A. Fazzio, M. Caldas, and A. Zunger Phys. Rev. B **30,** 3430 (1984), and unpublished results. No data are available for Si.

[a] J. M. Baranowski, J. M. Noras, and J. W. Allen, *Proc. Int. Conf. Semicond., 12th, Stuttgart* p. 416 (1974).

[b] Le. M. Hoang and J. M. Baranowski, *Phys. Status Solidi B* **84,** 361 (1977).

[c] G. Grebe and H. J. Schulz, *Phys. Status Solidi B* **54,** K69 (1972); and *Z. Naturforsch.* **29A,** 1803 (1974).

[d] H. E. Gumlich, R. L. Pfrogner, J. C. Schaffer, and F. E. Williams, *J. Chem. Phys.* **44,** 3929 (1966); see also W. Busse, H. E. Gumlich, B. Meissner, and T. Theis, *J. Lumin.* **12/13,** 693 (1976).

[e] M. Skowronski and Z. Liro, *J. Phys. C* **15,** 137 (1982); F. F. Kodzhespirov, M. Bulanyi, and J. A. Tereb, *Sov. Phys. Solid State* **16,** 2052 (1975); G. A. Slack, F. S. Ham, and R. M. Chrenko, *Phys. Rev.* **152,** 376 (1964); F. S. Ham and G. A. Slack, *Phys. Rev. B* **4,** 477 (1971).

[f] H. A. Weakliem, *J. Chem. Phys.* **36,** 2117 (1962); A. P. Radlinski, *J. Lumin.* **18/19,** 147 (1979) gives luminescence results.

[g] J. M. Noras, H. R. Szawelska, and J. W. Allen, *J. Phys. C* **14,** 3255 (1981).

[h] G. Roussos and H. J. Schulz, *Phys. Status Solidi B* **100,** 577 (1980); G. Roussos and H. J. Schulz, *J. Lumin.* **31/32,** 427 (1984). G. Roussos, J. Nagel, and H. J. Schulz, *Z. Phys. B* **53,** 95 (1983) have also observed the $^2T_2 \rightarrow {}^2E$ transitions of Ni^+ in ZnS and ZnSe. See also the emission and absorption data for ZnS:Ni^{2+} of I. Broser, R. Broser, and E. Birkicht, *J. Lumin.* **31/32,** 424 (1984), showing variations due to different ZnS polytypes.

[i] E. M. Wray and J. W. Allen, *J. Phys. C* **4,** 512 (1971), and unpublished results.

[j] G. Grebe, G. Roussos, and H. J. Schulz, *J. Phys. C* **9,** 4511 (1976).

[k] D. W. Langer and H. J. Richter, *Phys. Rev.* **146,** 554 (1966).

[l] J. M. Baranowski, J. M. Allen, and G. L. Pearson, *Phys. Rev.* **160,** 627 (1967).

[m] K. P. O'Donnell, K. M. Lee, and G. D. Watkins, *J. Phys. C* **16,** 728 (1983).

[n] H. Komura and M. Sekinobu, *J. Phys. Soc. Jpn,* **29,** 1100 (1970).

[o] Alloy data: M. Skowronski, J. M. Baranowski, and J. J. Ludwicki, *Pol. Akad Nauk* **75,** 127 (1978); J. E. Morales-Toro, W. M. Becker, B. I. Wang, U. Debska, and J. W. Richardson, *Solid State Commun.* **52,** 41 (1984).

Table V. footnotes (*Continued*)

[p] Yu. P. Gnatenko, A. I. Zhmurko, I. V. Potykevich, and I. A. Farina, *Sov. Phys. Semicond.* **18,** 689 (1984).

[q] R. Boyn, J. Dziesiaty, and D. Wruck, *Phys. Status Solidi* **42B,** K197 (1970); R. Boyn and G. Ruszczynski, *Phys. Status Solidi* **48B,** 643 (1971).

[r] D. Buhmann, H. J. Schulz, and M. Thiede, *Phys. Rev. B* **19,** 5360 (1979) have interpreted the three transitions in CdS:V as ${}^3A_2 \rightarrow {}^3T_1$ and ${}^3T_1$ excitations of V^{3+} (not V^{2+}).

[s] R. Pappalardo and R. E. Dietz, *Phys. Rev.* **123,** 1188 (1961).

[t] D. Buhmann, H. J. Schulz, and M. Thiede, *Phys. Rev. B* **24,** 6221 (1981); G. Roussos, H. J. Schulz, and M. Thiede, *J. Lumin,* **31/32,** 409 (1984).

[u] J. M. Baranowski and J. M. Langer, *Phys. Status Solidi* **48B,** 963 (1971); J. M. Langer and J. M. Baranowski, *Phys. Status Solidi* **44B,** 155 (1971).

[v] J. M. Baranowski, J. M. Langer, and S. Stefanova, *Int. Conf. Phys. Semicond., 11th, Warsaw* p. 1001 (1972) observed the ${}^3A_2 \rightarrow {}^3T_1$ transition in CdTe:Ti at ~0.1 eV above the CBM. See also P. A. Sladowy and J. M. Baranowski, *Phys. Status Solidi* **49B,** 499 (1972); J. Gardavsky, I. Barvik, and M. Zvara, *Phys. Status Solidi* **84B,** 691 (1977); and L. M. Hoang and J. M. Baranowski, *Phys. Status Solidi* **84B,** 361 (1977).

[w] Alloy data: E. Müller, G. Webhardt, and W. Rehwald, *J. Phys. C* **16,** L1141 (1983); M. El Amrani, J. Lascaray, and J. Diouri, *Solid State Commun.* **45,** 351 (1983); R. Y. Tao, M. M. Moriwaki, W. M. Becker, and R. R. Galazka, *J. Appl. Phys.* **53,** 3772 (1982).

[x] B. Clerjaud, B. Naud, B. Deveaud, B. Lambert, B. Plot-Chan, G. Bremond, C. Benjeddou, G. Guillot, and A. Nouailhat, *J. Appl. Phys.* **58,** 4027 (1985). Similar results were also reported recently by W. Ulrici, K. Friedland, L. Eaves, and D. P. Halliday, *Phys. Status Solidi* **131B,** 719 (1985); and by A. M. Hennel, unpublished (1985). It is not clear that the ground state for V^{2+} in III-Vs is ${}^4T_1$, as is the case for V^{2+} in II-VIs. Calculations by the author (see text and Ref. 217) suggests a ${}^2E$ low-spin ground state.

[y] U. Kaufmann, M. Ennen, and J. Weber, unpublished results quoted in Ref. 11, p. 218, and Ref. 12, p. 109.

[z] A. T. Vink and G. G. P. Van Gorkom, *J. Lumin.* **5,** 379 (1972).

[aa] D. G. Andrianov, P. M. Grinshtein, G. K. Ippolitova, E. M. Omel'yanovskii, N. I. Suchkova, and V. I. Fistul, *Fiz. Tekh. Poluprovodn.* **10,** 1173 (1976) [*Sov. Phys. Semicond.* **10,** 696 (1976)].

[bb] S. G. Bishop, P. J. Dean, P. Porteous, and D. J. Robbins, *J. Phys. C* **13,** 1331 (1980).

[cc] U. Kaufmann, W. H. Koschel, J. Schneider, and J. Weber, *Phys. Rev. B* **19,** 3343 (1979) proposed a value of 0.58 eV for the ${}^3T_2$ state of GaP:Ni^{2+}, but this corresponds most probably to a complex. The older value of 0.705 eV proposed by Baranowski *et al.* [Ref. (dd)] is not due to Ni^{2+} but due to Ni^{+}. The recent value of Z. Liro (unpublished) of 0.82 eV for the ${}^3T_2$ state is the most reliable.

[dd] J. M. Baranowski, J. W. Allen, and G. L. Pearson, *Phys. Rev.* **167,** 758 (1968).

[ee] The results on Ti^{2+} are contradictory and still inconclusive. See W. Ulrici, L. Eaves, K. Friedland, and D. P. Halliday, *Lund Int. Conf. Deep Level Impurities Semicond. 5th, St. Andrews, Scotland, and J. Phys. C* (in press) (1985) who suggest a luminescence ZPL line for GaAs:Ti^{2+} at 0.565 eV due to ${}^3T_1 \rightarrow {}^3A_2$ and ${}^3T_1(p) \rightarrow {}^3A_2$ at 1.04 eV; V. V. Ushakov and A. A. Gippius, *Sov. Phys. Semicond.* **16,** 1042 (1982) suggest the 0.66 eV luminescence to be due to ${}^3T_2 \rightarrow {}^3A_2$. In the author's opinion these data need reexamination.

[ff] D. Bois and P. Pinard, *Phys. Rev. B* **9,** 4171 (1974); A. M. Hennel, W. Szuszkiewicz, M. Balkanski, G. Martinez, and B. Clerjaud, *Phys. Rev. B* **23,** 3933 (1981); B. Clerjaud, A. M. Hennel, and G. Martinez, *Solid State Commun.* **33,** 983 (1980); W. Ulrici, *Phys. Status Solidi* **84A,** 243 (1984); B. Deveaud, B. Lambert, H. L'Haridon, and G. Picoli, *J. Lumin.* **24/25,** 273 (1982); B. Deveaud, G. Picoli, B. Lambert, and G. Martinez, *Phys. Rev. B* **29,** 5749 (1984); A. S. Abhvani, S. P. Austen, C. A. Bates, L. W. Parker, and D. R. Pooler, *J. Phys. C* **15,** 2217 (1982). Y. Fujiwara, A. Kojima, T. Nishino, and Y. Hamakawa, *J. Lumin.* **31/32,** 451 (1984) have observed that As vacancies contribute to the ~0.84 eV luminescence line of GaAs:Cr^{2+} previously attributed to ${}^5T_2 \leftrightarrow {}^5E$ transitions.

[gg] F. Litty, P. Leyral, S. Loualiche, A. Nouailhat, G. Guillot, and M. Lannoo, *Physica* **117/118,** 182 (1983).

[hh] (a) H. Ennen, U. Kaufmann, and J. Schneider, *Solid State Commun.* **34,** 603 (1980); (b) A. M. Hennel and S. M. Uba, *J. Phys. C* **11,** 4565 (1978); J. M. Baranowski, J. W. Allen, and G. L. Pearson, *Phys. Rev.* **160,** 627 (1967). See also earlier results by D. G. Andrianov, N. I. Suchkova, A. S. Savelev, E. P. Rashevskaya, and M. A. Filippov, *Sov. Phys. Semicond.* **11,** 426 (1977) [*Fiz. Tekh. Polup.* **11,** 730 (1977)] on the absorption spectra of GaAs:Co^{2+}.

[ii] N. I. Suchkova, D. G. Andrianov, E. M. Omel'yanovskii, E. P. Rashevskaya, A. S. Savel'ev, V. I. Fistul, and M. A. Filipov, *Fiz. Tekh. Popuprovodn.* **11,** 1742 (1977) [*Sov. Phys. Semicond.* **11,** 1022 (1977)].

[jj] B. Clerjaud, C. Naud, G. Picoli, and Y. Toudic, *J. Phys. C.* **17,** 6469 (1984).

[kk] W. H. Koschel and U. Kaufmann, *Solid State Commun.* **21,** 1069 (1977); S. G. Bishop, P. B. Klein, R. L. Henry, and B. D. McCombe, *in* "Semi-Insulating III-V Materials" (G. J. Rees, ed.), p. 161. Shiva, Orpington, England, 1980; P. Leyral, G. Bremond, A. Nouailhat, and G. Guillot, *J. Lumin.* **24/25,** 245 (1981).

[ll] M. S. Skolnick, P. R. Tapster, P. J. Dean, R. G. Humphreys, B. Cockayne, W. R. MacEwan, and J. M. Noras, *J. Phys. C* **15,** 3333 (1982); M. S. Skolnick, R. G. Humphreys, P. R. Tapster, B. Cockayne, and W. R. MacEwan, *J. Phys. C* **16,** 7003 (1983); M. J. Kane, Ch. Uihlein, M. S. Skolnick, P. J. Dean, W. Hayes, and B. Cockayne, *J. Phys. C* **16,** 5277 (1983).

0.666 eV, has been interpreted[62a] to be due to a spin-forbidden $^2E \to {}^4T_1$ transition of Cr^{3+}; similarly, the 1.03 eV line of GaP:Cr has been tentatively assigned[62b] to the $^4A_2$ (or $^4T_2$)$\leftrightarrow {}^4T_1$ system of Cr^{3+}. (3) in GaAs:V^{3+}, the $^3A_2 \to {}^3T_2$ (ZPL at 0.739 eV), and $^3A_2 \to {}^3T_1(F)$ (1.008 eV), transitions have been observed.[63] In addition, two weak transitions at 0.909 and 1.336 eV have been seen. A similar $^3A_2 \to {}^3T_2$ transition has been observed[64] in InP:V^{3+} (ZPL at 0.707 eV) and in GaP (ZPL at 0.793 eV). These transitions disappear when the sample is doped n-type and V^{3+} is converted into V^{2+}; (4) internal transitions of Ni^{3+} in ZnO were recently observed in luminescence[65] at 0.75 eV and attributed to the $^4T_2 \to {}^4A_2$ transition.

The number of internal transitions that can be observed is limited by the size of the host crystal band gap (cf. Table V): Usually more are observed in the wider-gap II-VI systems than in III-Vs. No $d \to d^*$ transitions were observed so far for Si:3d (presumably because of their very low solubility and the fact that the "near O_h" interstitial site symmetry couples $l = 1$ and 2 wave-function components only weakly, hence the oscillator strength for $d \to d^*$ transitions is smaller than in "strong" T_d-like impurities).

It is interesting to contrast the type of internal transitions observed for 3d impurities in ionic crystals[2,3,5,66] with those in semiconductors (Table V). Ionic crystals have sufficiently large band gaps to accommodate both the 3d as well as the 4s and 4p levels of the 3d impurity[66]; their valence band is, however, often too narrow to accommodate any broad transition-atom-induced resonances. This is illustrated in Fig. 6a by results of a cluster calculation[67] for $[Cu^+, d^{10}, t_2^6e^4, {}^1A_{1g}]$ in NaCl, showing the highly localized Cu 3d-derived one-electron e_g and t_{2g} levels, as well as the 4s-derived a_{1g} state, all inside the NaCl band gap. Transitions from e_g to a_{1g} (^1E_g and ^3E_g in Fig. 6b), as well as from t_{2g} to a_{1g} ($^1T_{2g}$ and $^3T_{2g}$ in Fig. 6b), have been observed[66] and calculated,[67,68] and mimic the trends in the atomic $3d \to 4s$ excitations. Likewise, in the large-band-gap oxides, numerous $d \to d^*$ transitions were found in the band gap; e.g., for NiO, final states of the type $[Ni^{3+}, d^7, A^+, t^4e^3, {}^4T_2]$ and $[Ni^{3+}, d^7, A^+, t_2^5e^2, {}^4T_1]$ were observed[69] and calculated.[70,71] A few pertinent differences relative to the analogous transitions in semiconductors exist: (1) No $d \to s$ or $d \to p$ internal transitions have been observed in semiconductors; the impurity 4s and 4p states are itinerant within the conduction band. Higher excited states of the d^N system may lie above the

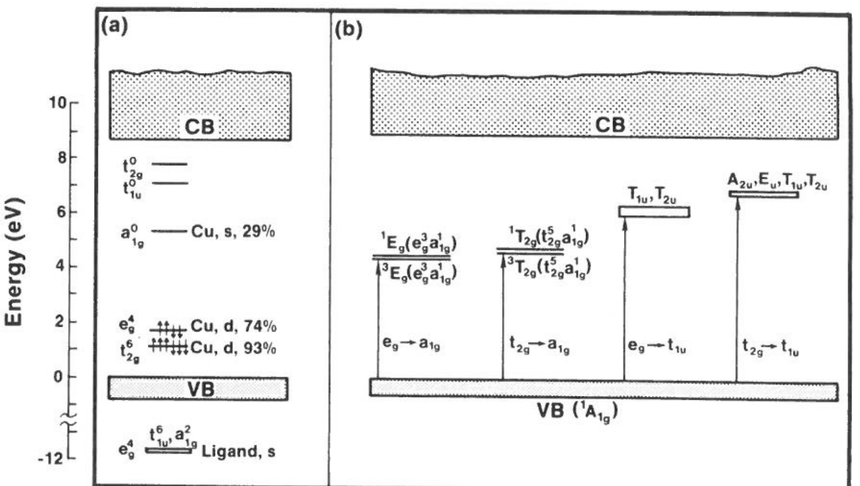

FIG. 6. (a) Calculated [H. Chermette and C. Pedrini, *J. Chem. Phys.* **75**, 1869 (1981)] and (b) observed [D. B. Chase and D. S. McClure, *J. Chem. Phys.* **64**, 74 (1976)] levels of Cu^+ in NaCl. The shaded areas denote the valence band (VB) and conduction band (CB). The calculated one-electron level structure in (a) shows two fully occupied levels in the band gap: t_{2g} and e_g, with 93% and 74%, respectively, Cu d character. The $t_{2g}^6e_{2g}^4$ configuration leads to the ground-state multiplet $^1A_1$. Above t_{2g} and e_{2g} we have the empty a_{1g} level (29% Cu s character) and the empty t_{1u} and t_{2g} levels. Transitions shown in (b) from e_g to a_{1g} give rise to a singlet (^1E_g) and a triplet (^3E_g) final multiplet states. Similarly, transitions from t_{2g} to a_{1g} give rise to the final multiplets $^1T_{2g}$ and $^3T_{2g}$, etc. Observe that, due to the existence of a wide band gap and a narrow valence band, all states are inside the band gap. The opposite situation encountered in semiconductors (small band gaps, wide valence bands) leads to the occurrence of numerous states in resonance with the valence and conduction bands.

[62a] B. Deveaud, G. Picoli, B. Lambert, and G. Martinez, *Phys. Rev. B* **29**, 5749 (1984).

[62b] L. Eaves, D. P. Halliday, and Ch. Vihlein, *J. Phys. C* **18**, L449 (1985).

[63] W. Ulrici, K. Friedland, L. Eaves, and D. P. Halliday, *Phys. Status Solidi* **131B**, 719 (1985); G. Armelles, J. Barrau, and D. Thebault, *J. Phys. C* **17**, 6883 (1984). The transitions of GaAs:V^{3+} and their assignments are currently under investigation.

[64] M. S. Skolnick, P. J. Dean, M. J. Kane, C. Uihlein, D. J. Robbins, W. Hayes, B. Cockayne, and W. R. MacEwan, *J. Phys. C* **16**, L767 (1983); M. J. Kane, M. S. Skolnick, P. J. Dean, W. Hayes, B. Cockayne, and W. R. MacEwan, *J. Phys. C* **17**, 6455 (1984).

[65] H. J. Schulz and M. Thiede, *Gen. Conf. Condensed Matter Div., Eur. Phys. Soc., 5th* Abstr. PTU-3-064 (1985).

[66] D. B. Chase and D. S. McClure, *J. Chem. Phys.* **64**, 74 (1976); J. F. Sabatini, A. E. Salwin, and D. S. McClure, *Phys. Rev. B* **11**, 2832 (1975); A. B. Goldberg, S. A. Payne, and D. S. McClure, *J. Chem. Phys.* **81**, 1523 (1984).

[67] H. Chermette and C. Pedrini, *J. Chem. Phys.* **75**, 1869 (1981).

[68] J. G. Harrison and C. C. Lin, *Phys. Rev. B* **23**, 3894 (1981).

[69] G. W. Pratt and R. Coelho, *Phys. Rev.* **116**, 281 (1959); R. Newman and R. M. Cherenko, *Phys. Rev.* **114**, 1507 (1959).

[70] P. S. Bagus and U. Wahlgren, *Mol. Phys.* **33**, 641 (1977).

[71] A. Fazzio and A. Zunger, *Solid State Commun.* **52**, 265 (1984).

conduction-band minima; transitions to such resonances have been observed.[72] (2) Whereas in ionic solids internal transitions involve only the $N = N_I - N_H - q$ "active" electrons in the gap levels, the occurrence of valence-band resonances in semiconductors suggests[54] that additional internal transitions between these levels and gap (or host) levels are possible. (3) Whereas in octahedral ionic solids internal $e \leftrightarrow t_2$ transitions do not significantly redistribute the charge around the impurity (i.e., both the initial and the final one-electron wave functions are almost equally localized around the impurity, hence the term "internal" transitions), in covalent tetrahedral solids such excitations can redistribute the charge[19,54] from impurity-centered orbitals (i.e., the essentially pure d-like e states) to ligand-centered orbitals (i.e., the p-d hybridized t_2 states). They are, therefore, not really "internal" excitations.

Using the data of Table V and the definitions of Eqs. (2.19)–(2.21), I present in Table VI the observed many-electron crystal-field splittings Δ_{ME} in a number of semiconductors. [Note that the classical expression of Eqs. (2.19)–(2.21) for Δ_{ME} neglect configuration mixing between multiplets of the same symmetry (e.g., the two excited $^4T_1$ states of Co^{2+} in Table V) and hence could be used only as a rough guide to estimate environmental effects on the states of the free ions.] They are larger by an order of magnitude than the splittings between the effective-mass-like transitions of sp-electron impurities in semiconductors (e.g., GaAs:Se); they are seen to constitute a sizeable fraction of the band gap and increase with the covalency of the host crystal.[73]

Absorption, luminescence, and photo-EPR experiments reveal also the spin-orbit splitting of various transitions. The observed values[12,14] are reduced substantially (by ~30–80%) relative to the free-ion values. The free-ion one-electron spin-orbit coupling ξ_{nl} of the T^{2+} ion states are,[74] in cm^{-1}, Ti, ^3F (121); V, ^4F (168); Cr, ^5D (236); Fe, ^5D (404); Co, ^4F (528); Ni, ^3F (644), and Cu, ^2D (829). A similar observation on the reduction of spin-orbit effects transpires from the trends in the g values (Table II): It is found that the free-ion spin-orbit parameter λ [which for maximum S and L is related to the one-electron spin-orbit coupling ξ_{nl} by $\lambda = \pm(1/2S)\xi_{nl}$, where the plus sign applies to d^1–d^5 and the minus spin applies to d^6–d^9] needs to be reduced to account

[72] For a few examples, see K. Kocot and J. M. Baranowski, *Phys. Status Solidi* **59B**, K11 (1973); **81B**, 629 (1977); A. P. Radlinski, *Phys. Status Solidi* **84B**, 503 (1977); M. D. Sturge, H. J. Guggenheim, and M. H. L. Pryce, *Phys. Rev. B* **2**, 2459 (1970); R. Boyn and G. Ruszczynski, *Phys. Status Solidi* **48B**, 643 (1971); J. M. Baranowski and J. Langer, *Phys. Status Solidi* **48B**, 863 (1971).

[73] A. M. Hennel, *Phys. Status Solidi* **72B**, K9 (1975).

[74] C. E. Moore, "Atomic Energy Levels," Natl. Bur. Standards, Washington, D. C. Circ. 467, Vol. I, 1949, Vol. II, 1952.

TABLE VI. VALUES (IN eV) OF THE MANY-ELECTRON CRYSTAL-FIELD SPLITTINGS Δ_{ME}

	ZnS $E_g = 3.85$ eV $a = 5.41$ Å $f = 0.623$	ZnSe $E_g = 2.80$ eV $a = 5.67$ Å $f = 0.63$	InP $E_g = 1.42$ eV $a = 5.87$ Å $f = 0.421$	GaP $E_g = 2.35$ eV $a = 5.45$ Å $f = 0.327$	GaAs $E_g = 1.52$ eV $a = 5.65$ Å $f = 0.31$
D Terms					
Cr^{2+}, d^4, Δ_{ME}	0.645, 0.595[a]	0.685, 0.57[a]	≥0.76	0.873	0.75–0.82
Fe^{2+}, d^6, Δ_{ME}	0.442	0.365[b]	0.35	0.413	0.37
F Terms					
V^{3+}, d^2, $\Delta_{ME}^{(1)}$	—	—	0.71	0.79	0.74
V^{2+}, d^3, $\Delta_{ME}^{(1)}$	0.608	0.585	—	—	—
$\Delta_{ME}^{(2)}$	0.666	0.625	—	—	—
Mn^{2+}, d^{5*}, $\Delta_{ME}^{(2)}$	0.239	0.197	—	—	—
Co^{2+}, d^7, $\Delta_{ME}^{(1)}$	0.459	0.434	≥0.47	0.559	~0.5
$\Delta_{ME}^{(2)}$	0.388	0.434	≥0.56	0.615	≥0.58
Ni^{2+}, d^8, $\Delta_{ME}^{(1)}$	0.587	0.607	—	~0.61	—
$\Delta_{ME}^{(2)}$	0.679	0.627	—	~1.02	—

* From Table V and Eqs. (2.19)–(2.21). We also give the host lattice constants and Phillips electronegativities. (J. C. Phillips, "Bonds and Bands in Semiconductors," p. 42. Academic Press, New York, 1973.)

[a] Extracted by M. Kaminska, J. M. Baranowski, S. M. Uba, and J. T. Vallin, *J. Phys. C.* **12**, 2197 (1979) from a fit to the spectra. These authors also give $\Delta_{ME} = 0.57$, 0.51 eV for ZnTe:Cr^{2+} and CdTe:Cr^{2+}, respectively.

[b] D. Buhmann, H. J. Schulz, and M. Thiede, *Phys. Rev. B* **24**, 6221 (1981) give $\Delta_{ME} = 0.24$ eV for CdSe:Fe^{2+}.

for the observed g values of impurities in silicon.[39] This has also been noted in ionic systems.[75] Interestingly, the spin-orbit splitting of the top of the valence band in $A^IB^{III}C_2^{VI}$ chalcopyrites (e.g., $CuGaSe_2$) was also observed[76] to be reduced relative to its $A^{II}C^{VI}$ binary analogs (e.g., ZnSe). All of these observations share a common physical orgin[77]: hybridization of p states of the anion with the d states of the transition atom (this hybridization is smaller in ZnSe than in $CuGaSe_2$ since the Zn $3d$ states are deeper than the Cu $3d$ states). This is discussed theoretically in Part VI,18.

[75] J. Owen, *Proc. R. Soc. (London) Ser. A* **227**, 183 (1955).

[76] J. L. Shay, B. Tell, H. M. Kasper, and L. M. Schiavone, *Phys. Rev. B* **5**, 5003 (1972).

[77] J. E. Jaffe and A. Zunger, *Phys. Rev. B* **28**, 5822 (1983); **29**, 1982 (1984); **30**, 741 (1984).

b. Ionizations

Whereas internal excitations conserve the oxidation state, the second type ("charge transfer") of electronic transitions, i.e., thermal ionizations or photoionizations, change the formal charge state of the center. I refer to these as ionizations, although the removed electron or added hole remains in the crystal, and its wave function can have a finite amplitude on the excited atom.[55] They are analogous to the charge-transfer spectra optically observed for $3d$ impurities in large-band-gap ionic solids.[2,3,66,69] In semiconductors these ionizations can be observed both optically and thermally. A few such ionization processes are pertinent here.

(1) *The single-acceptor ionizations* correspond to a process in which, for example, a valence-band (VB) electron is transferred to an impurity level α of type e or t_2, thereby changing the charge state from A^0 to A^-. If the fully occupied valence band has M electrons, such a single-acceptor ionization (a reduction reaction) can be described as

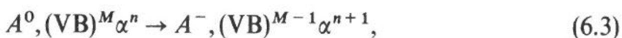

$$A^0, (\mathrm{VB})^M \alpha^n \rightarrow A^-, (\mathrm{VB})^{M-1} \alpha^{n+1}, \qquad (6.3)$$

where $\alpha = t_2$ or e. This type of single-acceptor process is often referred to as "hole emission to the valence band," and the associated change in the total many-electron energy E_{T} of the system is denoted $E^{(\alpha)}(-/0)$

$$E^{(\alpha)}(-/0) = E_{\mathrm{T}}^{(j)}[A^-, (\mathrm{VB})^{M-1} \alpha^{n+1}] - E_{\mathrm{T}}^{(i)}[A^0, (\mathrm{VB})^M \alpha^n]. \qquad (6.4)$$

Each total-energy term corresponds to the lowest multiplet (i or j) of the corresponding charge state. A complementary acceptor ionization process can occur when a conduction-band (CB) electron is captured by an impurity center. This can be described as an "electron capture" process

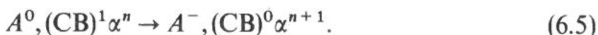

$$A^0, (\mathrm{CB})^1 \alpha^n \rightarrow A^-, (\mathrm{CB})^0 \alpha^{n+1}. \qquad (6.5)$$

(2) *Double-acceptor ionizations* correspond to a process in which a second valence-band electron is transferred to the impurity levels, thereby changing the charge state from A^- to A^{2-}. This can be described as a "second hole-emission" process

$$A^-, (\mathrm{VB})^{M-1} \alpha^{n+1} \rightarrow A^{2-}, (\mathrm{VB})^{M-2} \alpha^{n+2}. \qquad (6.6)$$

The change in total (free) energy in this process can be denoted as $E^{(\alpha)}(-/2-)$, or

$$E^{(\alpha)}(-/2-) = E_{\mathrm{T}}^{(j)}[A^{2-}, (\mathrm{VB})^{M-2} \alpha^{n+2}] - E_{\mathrm{T}}^{(i)}[A^-, (\mathrm{VB})^{M-1} \alpha^{n+1}]. \qquad (6.7)$$

Again, the complementary process of capture of a second electron from the conduction band is possible.

(3) *Single-donor ionization* (an oxidation reaction) corresponds to a process in which the impurity level emits an electron to the conduction band, changing the formal charge state from A^0 to A^+. This can be described as

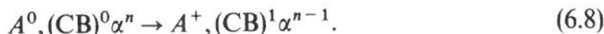

$$A^0, (\mathrm{CB})^0 \alpha^n \rightarrow A^+, (\mathrm{CB})^1 \alpha^{n-1}. \qquad (6.8)$$

The change in the total energy in this electron emission process is denoted as $E^{(\alpha)}(0/+)$ and is given by

$$E^{(\alpha)}(0/+) = E_{\mathrm{T}}^{(j)}[A^+, (\mathrm{CB})^1 \alpha^{n-1}] - E_{\mathrm{T}}^{(i)}[A^0, (\mathrm{CB})^0 \alpha^n]. \qquad (6.9)$$

The complementary process of a single-donor transition through hole capture from the valence band is possible and can be described as

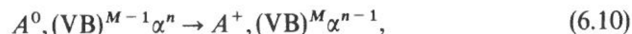

$$A^0, (\mathrm{VB})^{M-1} \alpha^n \rightarrow A^+, (\mathrm{VB})^M \alpha^{n-1}, \qquad (6.10)$$

Double-donor transitions can be constructed in analogy with the single-donor electron-emission process.

Observation of the ionization energies enables one to determine the level position $E(q/q')$ within the gap, i.e., the position of the Fermi energy below which the center has the charge state A^q and above which it is in the $A^{q'}$ charge state. Since ionic crystals cannot be doped continuously, one can produce different charge states of an impurity only by irradiation (γ rays, electron beams, etc.) or by photoionization. Conventional semiconductor characterization techniques, e.g., temperature dependence of resistivity and Hall effect, have played a central role in establishing the sign of the carriers and the activation energies for charge-transfer excitations. These techniques are somewhat more difficult to apply to deep $3d$ centers than to shallow impurities because of the lower solubility of the 3d centers and masking effects caused by shallow levels. Other techniques include thermally stimulated currents (TSC), thermally stimulated capacitance, and photoconductivity. Conventional capacitance techniques, however, do not clearly separate the different charge states of the same center (unless one is dominant), whereas photocapacitance methods clearly detect changes in the charge states of a center. Different centers, occurring simultaneously, are more easily separated than in conventional capacitance methods. Modern junction techniques have enabled significant progress in this direction to be made; thin p–n junctions or rectifying metal–semiconductor layers used under bias (direct or reversed), shift the Fermi energy through the band gap and deplete carriers from the junction region. Such junction techniques, most notably DLTS,[78] can separate different charge states of the same center (providing the center's "signature")

[78] D. V. Lang, *J. Appl. Phys.* **45**, 3023 (1974).

and prevent masking by shallow levels. They provide ionization energies as well as cross sections and concentrations of different charge states of the same impurity. In a typical experiment one injects carriers into a junction depleted by a reverse bias, then, following their nonequilibrium trapping by the center A, these carriers are released thermally, either to the VB or to the CB, and swept away by the electric field at the barrier. Measuring the difference in capacitances at two different times (the capacitance transient) as a function of temperature T, one isolates the different transitions as a function of T. Combined with applied stress,[79] DLTS experiments can also provide information on the symmetry of the defect. A number of other, related techniques have also been developed, in which the trap-filling pulse is optical rather than electrical (optical deep level transient spectroscopy, ODLTS[80]), enabling minority carrier traps to be observed, or in which current rather than capacitance is measured. Such techniques are charge-state specific (observing different A^q's before and after carrier emission), but they are obviously not chemically specific (different T's before and after carrier emission). Furthermore, DLTS is limited to conducting samples.

All of these thermal techniques provide information on the transition between two *equilibrated* centers A^q and A^{q+1}, i.e., when each is at its respective equilibrium lattice configuration. Optical techniques, on the other hand, yield vertical (Franck–Condon) transitions, in which both the initial and final state share the same lattice configuration. Thermal ionization energies can be lower by as much as 0.2–0.4 eV than optical ionization energies.[81] Photoionization experiments do not clearly separate the different charge states or VB from CB transitions.

Techniques that can combine measurements of interelectronic excitation with characterization of the impurity itself are of special value. Such is the photo-EPR technique,[82] in which the EPR signal is created or destroyed by light, and the appearance or disappearance of the EPR signal is observed as a function of wavelength. So also are optically detected magnetic resonance (ODMR) technique, and a combination[83,84] of EPR and DLTS, e.g., the spin-dependent DLTS[83] and the depletion-width modulated EPR methods.[84]

[79] J. M. Meese, J. W. Farmer, and C. D. Lamp, *Phys. Rev. Lett.* **51,** 1286 (1983).

[80] A. Mitonneau, G. M. Martin, and A. Mircea, *Inst. Phys. Conf. Ser.* **33A,** 73 (1977).

[81] M. Godlewski and M. Kaminska, *J. Phys. C* **13,** 6537 (1980).

[82] For example, see H. J. Von Bardeleben, A. Goltzene, C. Schwab, and R. S. Feigelson, *J. Appl. Phys.* **52,** 5037 (1981), and references therein. A recent review on photo EPR was published by M. Godlewski, *Phys. Status Solidi* **90a,** 11 (1985).

[83] M. C. Chen and D. V. Lang, *Phys. Rev. Lett.* **51,** 427 (1983).

[84] J. D. Cohen, J. P. Harbison, and K. W. Wecht, *Phys. Rev. Lett.* **48,** 109 (1982).

A number of excitation techniques have been applied recently to $3d$ impurities in semiconductor *alloys*.[85–92] They provide information on level positions and intracenter excitations as a function of alloy composition. For example, measurement[92] of the transition $[Fe^{2+}, d^6, A^-, e^3t_2^3, {}^5E] \rightarrow [Fe^{2+}, d^6, A^-, e^2t_2^4, {}^5T_2]$ in Fe-doped $Al_xGa_{1-x}As$ shows that the excitation energy $\Delta^{(ij)}(x)$ depends linearly on the composition x

$$\Delta^{(ij)}(x) \cong \Delta^{(ij)}(0) + \bar{\alpha}x. \tag{6.11}$$

Remarkably, the slope $\bar{\alpha}$ appears to depend on the host crystal but not on the impurity. For example,

$$\bar{\alpha}[Al_xGa_{1-x}As{:}Fe] = 0.46\ \text{eV},^{92} \qquad \bar{\alpha}[Al_xGa_{1-x}As{:}Cu] = 0.45\ \text{eV},^{90}$$

and all different photoluminescence lines in $GaAs_{1-x}P_x$:Cu show a common $\bar{\alpha} = 0.43$ eV.[89] This phenomenon is discussed theoretically in Part VI,28.

Table VII collects the values of the best-established ionization transition energies for $3d$ impurities in ZnS, ZnSe, ZnTe, CdS, CdSe, CdTe, GaP, GaAs, InP, and Si. The observed trends are addressed by theoretical calculations in Part VI,26.

c. *Combined Ionization-Excitation Diagrams*

Using the ionization energies of Table VII and the $d \rightarrow d^*$ transition energies of Table V, we can now construct combined ionization and internal excitation diagrams for each impurity, illustrated in Fig. 7 for the substitutional Cr impurity in a number of semiconductors. The thick horizontal lines denote the donor or acceptor ionization energies delineating the charge state $q + 1$ which resides below the line from the charge state q residing above these lines. For example, the Cr^{2+} charge state in ZnSe exists above $E_v + E(0/+) \cong E_v + 0.46$ eV but below $E_v + E(-/0) = E_v + 2.25$ eV; in GaP it

[85] K. H. Goetz, D. Bimberg, K. A. Brauchll, H. Jurgensen, J. Selders, M. Razeghi, and E. Kuphal, *Appl. Phys. Lett.* **46,** 277 (1985).

[86] M. Zafar-Iqbal, H. G. Grimmeiss, and L. Samuelson, *J. Phys. C* **18,** 1017 (1985).

[87] L. Samuelson, *J. Electron. Mater.* **14a,** 101 (1984).

[88] M. Grimmeiss, E. Meijer, R. Mach, and G. O. Müller, *J. Appl. Phys.* **56,** 2768 (1984).

[89] L. Samuelson, S. Nilsson, Z. G. Wang, and H. G. Grimmeiss, *Phys. Rev. Lett.* **53,** 1501 (1984); recent results on $In_{1-x}Ga_xP$:Mn were reported by A. A. Reeder and J. M. Chamberlain, *Solid State Commun.* **54,** 705 (1985).

[90] L. Janssen, Z. G. Wang, L. Å, Ledebo, and H. G. Grimmeiss, *Nuovo Cim.* **2D,** 1718 (1983).

[91] S. Nilsson and L. Samuelson, presented at the *Fifth Lund Conf. Deep Level Impurities Semicond., St. Andrews, Scotland, 1985* unpublished.

[92] Z. G. Wang, L. Å, Ledebo, and H. G. Grimmeiss, *J. Appl. Phys.* **56,** 2762 (1984); see also an order value given by D. V. Lang, R. A. Logan, and L. C. Kimerling, *Phys. Semicond. Proc. Int. Conf., 13th, Rome* p. 516 (1976).

TABLE VII. IONIZATION ENERGIES OF SUBSTITUTIONAL 3*d* IMPURITIES IN HETEROPOLAR SEMICONDUCTORS AND FOR INTERSTITIAL 3*d* IMPURITIES IN Si* (EXCEPT Mn, FOR WHICH VALUES ARE GIVEN FOR BOTH SITES)

Semiconductor	E_g	Ti	V	Cr	Mn	Fe	Co	Ni	Transition Type
ZnS	3.85	(gap)	2.11[a]	1.0[b], 1.74[b]	(VB)	2.01[d]	(gap)	0.75[e]	(0/+)
		—	(gap, ?)	2.78[c], 2.48[c]	—	(gap)	(gap, ?)	2.46[f]	(−/0)
ZnSe	2.82	1.75[g]	(gap)	0.46[h,c]	(VB)	1.1[i], 1.25[i] (?)	~0.3[j] (?)	0.15[k]	(0/+)
		—	(gap, ?)	2.26[c], 2.1[h]	—	(gap, ?)	(gap, ?)	1.85[f]	(−/0)
ZnTe	2.39	(gap)	(gap)	(VB, ?)	(VB)	(gap, ?)	0.86[m] (?)	(VB)	(0/+)
		—	—	1.4[c,l] (?)	—	(gap)	—	~1[n]	(−/0)
CdS (hexagonal)	2.50	~2.21[o]	≳1.8[p] (?)	1.47[q] (?)	(VB)	(gap)[i]	(gap)	≥0.27[r] (?)	(0/+)
CdSe (hexagonal)	1.98	1.69[g]	~1.5[s2]	0.64[s1]	(VB)	0.64[s2]	0.22[t,u]	0.32[s3]	(0/+)
		—	—	(CB, ?)	—	—	—	1.81[s3]	(−/0)
CdTe	1.6 (2 K)	~0.55[u]	0.74[u,v]	(VB, ?)	(VB)[x]	0.13[y]	—	(VB)	(0/+)
	1.48 (300 K)	—	—	1.34[w]	—	—	—	0.92[z]	(−/0)
GaP	2.35	—	—	0.5 ± 0.1[bb] (?)	—	—	—	—	(0/+)
		(gap)	1.55[aa]	1.12[cc] (?)	0.4[ee]	0.86[ff,gg]	0.41[ii]	0.5[kk]	(−/0)
		—	—	1.85[dd] (?)	—	2.09[gg,hh]	2.02[jj] (?)	1.55 ± 0.2[ll]	(−/2−)
GaAs	—	—	—	(0.32–0.45)[oo]; 0.68[oo]	—	—	—	—	(0/+)
	1.52	1.07[mm], 1.29	1.38[nn]	0.74[pp]	0.11[qq]	0.49[ff]	0.16[rr]	0.22[ss], 0.35[ss]	(−/0)
		—	—	1.57[pp] (CB)	—	(CB)	1.67[tt] (CB)	1.13[ss]	(−/2−)
InP	1.42	—	(CB)	(0.94–1.03)[vv]	0.22[xx]	0.8 ± 0.2[ff]	0.24[ww] − 0.32[yy]	—	(−/0)
		—	0.2[uu] (?)	(lower gap?)	—	—	—	—	(0/+)
Si	1.17	0.89[zz,aaa]	0.72[zz,bbb]	0.95[zz,ccc]	0.75[zz,bbb]; 0.38[eee] (s)	0.385[ddd]	—	—	(0/+)
		1.09[zz]	1.01[zz,aaa]	—	1.06[zz,bbb]	—	—	—	(−/0)
		0.25[zz]	0.30[zz,bbb]	—	0.25[zz,bbb]	—	—	—	(+/2+)

* Measured in eV from the valence-band maximum. Ionization energies that are predicted by the vacuum pinning rule (Part VI,28) to reside inside the host bands are denoted by (VB) or (CB). Those that are predicted to be in the band gap, but were not observed yet, are denoted "gap."

[a] L. M. Hoang and J. M. Baranowski, *Phys. Status Solidi* **84B**, 361 (1977) (absorption).

[b] J. Dieleman, R. S. Title, and W. V. Smith, *Phys. Lett.* **1**, 334 (1962); M. Kaminska, J. M. Baranowski, and M. Godlewski *in* "Physics of Semiconductors 1978" (B. L. Wilson, ed.), p. 203. Inst. of Physics, Bristol, 1978.

[c] M. D. Fair, R. D. Ewing, and F. E. Williams, *Phys. Rev.* **144**, 298 (1966); M. Godlewski and M. Kaminska, *J. Phys. C* **13**, 6537 (1980); K. Suto and M. Aoki, *J. Phys. Soc. Jpn.* **22**, 1121 (1967). The thermal value for the ZnS:Cr acceptor is 2.41 eV, whereas for ZnSe and ZnTe it is 1.93 and 1.21 eV, respectively. For the optical value of the ZnS:Cr acceptor at $\sim E_c - 0.9$ eV; see also F. F. Kodzhespirov, M. F. Bulang, and I. A. Tereb., *Sov. Phys. Semicond.* **16**, 205 (1975).

[d] M. Skowronski and Z. Liro, *J. Phys. C* **15**, 137 (1982) (absorption); M. Skowronski and M. Godlewski, *J. Phys. C* **17**, 2901 (1984) [photo-EPR]. Recent thermoluminescence experiments [K. E. Tarkpea and A. Ots, *Phys. Status Solidi* **129B**, 799 (1985)] have also observed the (0/+) transition in ZnS:Fe.

[e] Deduced from W. C. Holton, J. Schneider, and T. L. Estle, *Phys. Rev.* **133**, 1638 (1964).

[f] J. M. Noras and J. W. Allen, *J. Phys. C* **13**, 3511 (1980) (absorption). See also absorption experiment for ZnS:Ni by G. Roussos and H. J. Schulz, *Phys. Status Solidi* **100B**, 577 (1980), and B. Muller, G. Roussos, and H. J. Schulz, *J. Cryst. Growth* **72**, 360 (1985). For photoluminescence of ZnSe:Ni [E(−/0) ≅ 1.8 eV] see S. G. Bishop, D. J. Robbins, and P. J. Dean, *Solid State Comun.* **33**, 119 (1980).

[g] K. Kocot and J. M. Baranowski, *Phys. Status Solidi* **59B**, K11 (1973) [PC] and **81**, 629 (1977).

[h] G. Grebe, G. Roussos, and H. J. Schulz, *J. Phys. C* **9**, 4511 (1976) (absorption).

[i] Estimated from K. P. O'Donnell, K. M. Lee, and G. D. Watkins, *J. Phys. C.* **16**, 728 (1983) [ODMR] as well as from J. H. Haanstra, *in* "II-VI Semiconducting Compounds" (D. G. Thomas, ed.), p. 207. Benjamin, New York, 1967, (absorption); J. Dieleman, J. W. deJong, and T. Meijer, *J. Chem. Phys.* **45**, 3178 (1966) suggest donor energies of ≤1.4, ≤1.1, and ≤1.3 eV, for ZnS:Fe, ZnSe:Fe, and CdS:Fe, respectively (EPR).

[j] Deduced by D. J. Robbins, *J. Lumin.* **24/25**, 137 (1981); and D. J. Robbins, P. J. Dean, J. L. Glasper, and S. G. Bishop, *Solid State Commun.* **36**, 61 (1980); from J. M. Noras, H. R. Szawelska, and J. W. Allen, *J. Phys. C* **14**, 3255 (1981) (photocapacitance), who suggest, however, values of 1.45 and 0.62 eV for the donor states in ZnS:Co and ZnSe:Co, respectively. See also Ref. (t).

[k] V. I. Sokolov, V. V. Chernyaev, M. V. Chukichev, Vu. Zoan M'en, and V. S. Vavilov, *Sov. Phys. Semicond.* **25**, 915 (1983) (absorption and cathodoluminescence); V. I. Sokolov, T. P. Surkova, and V. V. Chernyaev, *Phys. Status Solidi* **114B**, K195 (1982) (absorption).

[l] H. Komura and M. Sekinobu, *J. Phys. Soc. Jpn.* **29**, 1100 (1970) have observed optically in ZnTe:Cr a shoulder at ~0.8 μm, which may be associated with the Cr acceptor photoionization; see also K. Suto and M. Aoki, *J. Phys. Soc. Jpn.* **22**, 149 (1967).

[m] Yu. P. Gnatenko, A. I. Zhmurko, I. V. Poltykevich, and I. A. Farina, *Sov. Phys. Semicond.* **18**, 689 (1984) (absorption). Values of donor levels of Co in II-VI are generally uncertain; see Ref. (t).

[n] B. Clerjaud, A. Gelineau, F. Gendron, C. Naud, and C. Porte, *J. Cryst. Growth* **72**, 351 (1985) (EPR and absorption) have observed the acceptor of ZnTe:Ni at $\sim E_v + 1$ eV; Yu. P. Gnatenko and A. I. Zhmurko, *Ukr. Fiz. Zh.* **29**, 1182 (1984) have observed the acceptor at $E_v + 1.5$ eV; see also U. Kaufmann, J. Windscheif, and G. Brunthaler, *J. Phys. C* **17**, 6169 (1984) for EPR identification.

[o] R. Boydn and G. Ruszczynski, *Phys. Status Solidi* **48B**, 643 (1971); R. Boyn, J. Dziesiaty, and D. Wruck, *Phys. Status Solidi* **42B**, K197 (1970).

TABLE VII. footnotes (*Continued*)

[p] Estimated from the charge-transfer absorption spectra of D. Buhmann, H. J. Schulz, and M. Thiede, *Phys. Rev. B* **19**, 5360 (1979).

[q] Estimated from absorption edge given by R. Pappalardo and R. E. Dietz, *Phys. Rev.* **123**, 1188 (1961).

[r] A. V. Bobyl and M. K. Sheinkman, *Sov. Phys. Semicond.* **13**, 1296 (1979); and *J. Appl. Spectrosc.* **28**, 682 (1978); Y. I. Vertsimakha, Yu, P. Gnatenko, and A. K. Rozhko, *Sov. Phys. Solid State* **16**, 2236 (1975); A. V. Bobyl, G. S. Pekar, and M. K. Sheinkman, *Phys. Status Solidi* **48A**, 249 (1978) (conductivity and PC).

[s1] L. Jastrzebski and J. M. Baranowski, *Phys. Status Solidi* **58B**, 401 (1973) [PC]; [s2] J. M. Baranowski and J. M. Langer, *Phys. Status Solidi* **48B**, 863 (1971); [s3] J. M. Baranowski and Phuong-An, *Phys. Status Solidi* **122B**, 331 (1984) (PC).

[t] D. Buhmann, H. J. Schulz, and M. Thiede, *Phys. Rev. B* **24**, 6221 (1981) have observed the photoionization of CdSe:Co at $\sim E_v + 0.22$ eV. A. R. Radlinski, *J. Phys. C* **12**, 4477 (1979): *Phys. Status Solidi* **84B**, 503 (1977); *J. Lumin.* **18/10**, 147 (1979) has approximated the ionization energy of Co^{2+} in a series of II-VI compounds by adding to the observed ${}^4T_2 \rightarrow {}^4A_2$ excitation energies a thermal activation energy which he deduces from a model-dependent fit to his thermal quenching data. His values for ZnS:Co and CdSe:Co of $E_v + 2.11$ eV and $E_v + 1.62$ eV, respectively, do not agree with those measured directly (this Table); i.e., $E_v + 0.3$ eV and $E_v + 0.15$ eV, respectively. He gives for ZnTe:Co a value of $E_v + 1.95$ eV. I suspect that his assumption that the ${}^4T_2$ level is directly excited thermally into the CB is wrong. This, and the similar controversy discussed in Ref (j) highlight the great uncertainty in the Co levels in II-VIs.

[u] J. M. Baranowski, J. M. Langer, and S. Stevanova, *Proc. Int. Conf. Semicond. 11th, Warsaw* p. 1001 (1972) (absorption and PC). The photocurrent threshold for CdSe:Co was at $\sim E_v + 0.7$ eV, for CdTe:V at $\sim E_v + 0.9$ eV and for CdTe:Ti at $\sim E_v + 0.55$ eV.

[v] P. A. Slodowy and J. M. Baranowski, *Phys. Status Solidi* **49B**, 499 (1972) (absorption); Ref. (a) suggests a donor photoionization of CdTe:V with onset at ~ 1 eV.

[w] M. Godlewski and J. M. Baranowski, *Phys. Status Solidi* **97B**, 281 (1980). The optical value of the acceptor in CdTe:Cr was determined to be 1.50 eV; see also M. Z. Cieplak, M. Godlewski, and J. M. Baranowski, *Phys. Status Solidi* **70B**, 323 (1975); and P. I. Babii, N. P. Gavaleshko, Yu. P. Gnatenko, P. A. Skubenko, and V. I. Oleinik, *Sov. Phys. Semicond.* **12**, 1310 (1978).

[x] M. Popova, *J. Phys. C* **11**, L 43 (1978) suggests that the CdTe:Mn donor level is in the gap at $E_v + 0.6$ eV, but this is doubtful.

[y] K. Lischka, G. Brunthaler, and J. W. Jantsch, *J. Cryst. Growth* **72**, 355 (1985); G. Brunthaler, U. Kaufmann, and J. Schneider, *J. Appl. Phys.* **56**, 2974 (1984) similarly find the CdTe:Fe donor at $\leq E_c - 1$ eV [photo-EPR].

[z] W. Jantsch and G. Brunthaler, *Lund Conf. Deep Impurities Semicond. 5th, St. Andrews, Scotland* unpublished (1985).

[aa] S. A. Abagyan, G. A. Ivanov, Yu. N. Kuznetsov, and Yu. A. Okunev, *Sov. Phys. Semicond.* **8**, 1096 (1975) give a value of 0.85–1.2 eV from absorption data, but B. Clerjaud, C. Naud, B. Deveaud, B. Lambert, B. Plot-Chan, G. Bremond, C. Benjeddou, G. Guillot, and A. Nouailhat (*J. Appl. Phys.* **58**, 4207,1985) suggest a value of 1.55 eV.

[bb] U. Kaufmann and J. Schneider, *Appl. Phys. Lett.* **36**, 748 (1980) [absorption, EPR]; R. Gloriozova and L. I. Kolesnik, *Sov. Phys. Semicond.* **12**, 66 (1978) (photocapacitance).

[cc] D. Engemann and Th. Hornung, unpublished (optical, PL).

[dd] B. Clerjaud, F. Gendron, and C. Porte, *Appl. Phys. Lett.* **38**, 212 (1981); see also U. Kaufmann and W. H. Koschel, *Phys. Rev. B* **17**, 2081 (1978) (EPR photoquenching).

[ee] S. A. Abagyan, G. A. Ivanov, G. A. Kovoleva, Yu. N. Kusnetsov, and Yu. A. Okunev, *Sov. Phys. Semicond.* **9**, 243 (1975) (photoionization); A. O. Evwaray and H. H. Woodbury, *J. Appl. Phys.* **47**, 1595 (1976) (Hall effect); R. F. Brunwin, B. Hamilton, J. Hodgkinson, A. R. Peaker, and P. J. Dean, *Solid State Electron.* **24**, 249 (1981) (DLTS).

[ff] B. V. Shanabrook, P. B. Klein, and S. G. Bishop, *Physica* **116B**, 444 (1983) [PL]; P. R. Tapster, M. S. Skolnick, R. G. Humphreys, P. J. Dean, and B. Cockayne, *J. Phys. C* **14**, 5069 (1981); L. Eaves, A. W. Smith, P. J. Williams, B. Cockayne, and W. R. MacEwan, *J. Phys. C* **14**, 5063 (1981); M. Kleverman, P. Omling, L. A. Ledebo, H. G. Grimmeis, *J. Appl. Phys.* **54**, 814 (1983). Assuming a ${}^5E$–${}^5T_2$ excitation energy of 0.35 eV (Table V), the 1.13 eV edge observed by S. Fung and R. J. Nicholas [*J. Phys. C* **18**, 259 (1985)] in InP:Fe suggests an acceptor of $1.13 - 0.35 = 0.78$ eV, in good agreement with other data in Table VII.

[gg] S. Brehme, *J. Phys. C* **18**, L319 (1985).

[hh] K. Suto and J. Nishizawa, *J. Appl. Phys.* **43**, 2247 (1972) (EPR, Hall).

[ii] D. M. Loescher, J. W. Allen, and G. L. Pearson, *J. Phys. Soc. Jpn.* **21** (Suppl), 239 (1966) (Hall effect).

[jj] M. Jezewski and J. Baranowski, *Lund Conf. 4th* (1983) unpublished (optical).

[kk] (Hall effect and absorption) S. A. Abagyan, G. A. Ivanov, and G. A. Kovoleva, *Sov. Phys. Semicond.* **10**, 1056 (1976). A. R. Peaker, U. Kaufmann, Z. G. Wang, R. Wörner, B. Hamilton, and H. Grimmeiss, *J. Phys. C* **17**, 6161 (1984).

[ll] S. G. Bishop, P. J. Dean, P. Porteous, and D. J. Robbins, *J. Phys. C* **13**, 1331 (1980) [Luminesc]; X. Z. Yang, L. Samuelson, and H. G. Grimmeiss, *J. Phys. C* **17**, 6521 (1984) (DLTS).

[mm] M. F. Berkmuratov and V. I. Murygin, *Sov. Phys. Semicond.* **7**, 55 (1973) (Hall effect); see, however, D. A. Stevenson, P. I. Ketrush, S. C. Chang, and A. Borchewsky, *Appl. Phys. Lett.* **37**, 823 (1980), who found no acceptor action (Hall effect). Recent optical experiments (W. Ulrici, L. Eaves, K. Friedland, and D. P. Halliday, unpublished (1985) observe the Ti^{2+}/Ti^{3+} acceptor (through excitation into the CB) at $E_c - 0.61$ eV $\cong E_v + 0.91$ eV, below the thermal value of $E_c - 0.45$ eV $\cong E_v + 1.07$ eV, suggesting a Franck-Condon shift of -0.16 eV. The most recent [A. M. Hennel, C. D. Brandt, Y. T. Wu, T. Bryskiewicz, K. Ko, J. Lagowski, and H. C. Gator, unpublished] DLTS value of the Ti acceptor is $E_c - 0.23$ eV $\simeq E_g + 1.29$ eV.

[nn] R. W. Haisty and G. R. Cronin, *in* "Physics of Semiconductors" (M. Hulin, ed.), p. 1161. Donod, Paris, 1964 [Hall]; A. Mircea-Roussel, G. M. Martin, and J. E. Lowther, *Solid State Commun.* **36**, 171 (1980) [DLTS]; E. Litty, P. Leyral, S. Loualiche, A. Nouailhat, G. Guillot, and M. Lannoo, *Physica* **117/118B**, 182 (1983) (DLTS, DLOS); B. Clerjaud, C. Naud, B. Deveaud, B. Lambert, B. Plot-Chan, G. Bremond, C. Benjeddou, G. Guillot, and A. Novalihat, *J. Appl. Phys.* **58**, 4207 (1985) (absorption, luminescence, DLTS); C. D. Brandt, A. M. Hennel, L. M. Pawloicz, F. P. Dabkowski, J. Lagowski, and M. C. Gatos, *Appl. Phys. Lett.* **47**, 607 (1985) (DLTS); W. Ulrici, K. Friedland, L. Eaves, and D. P. Halliday, *Phys. Status Solidi* **131B**, 719 (1985) (absorption, luminescence, TDH).

[oo] D. C. Look, S. Chaudhuri, and L. Eaves, *Phys. Rev. Lett.* **49**, 1728 (1982) suggest 0.324 eV from the Hall effect; and J. S. Blakemore, S. G. Johnson, and S. Rahimi, *in* "Semi Insulating III-V Materials (S. Makram-Ebeid and B. Tuck, eds.), p. 172. Shiva, Nantwick, UK, 1981, suggest 0.45 eV from photoconductivity. A recent *optical* experiment by W. Ulrici and P. Kleinert, *Phys. Status Solidi* **129B**, 339 (1985), shows a value of ~ 0.68 eV.

[pp] A. M. Hennel, W. Szuszkiewicz, M. Balkanski, G. Martinez, and B. Clerjaud, *Phys. Rev. B* **23**, 3933 (1981) (absorption and resistivity; pressure); G. Martinez, A. M. Hennel, W. Szuszkiewicz, M. Balkanski, and B. Clerjaud, *Phys. Rev. B* **23**, 3920 (1981) (photoionization under pressure); A. M. Hennel and G. Martinez, *Phys. Rev. B* **25**, 1039 (1972) (Hall effect under pressure); P. S. S. Guimaraes, K. R. Duncan, L. Eaves, K. W. H. Stevens, R. M. Bowley, J. C. Portal, J. Cisowski, M. S. Skolnick, and D. J. Stirland, *J. Phys. C* **18**, 1431 (1985) (absorption).

TABLE VII. footnotes (*Continued*)

[qq] R. A. Chapman and W. Hutchinson, *Phys. Rev. Lett.* **18**, 443 (1967) (photoionization); W. Schairer and M. Schmidt, *Phys. Rev. B* **10**, 2501 (1974) (luminescence); R. W. Haisty and G. R. Cronin, *in* "Physics of Semiconductors" (M. Hulin, ed.), p. 1161. Dunod, Paris, 1964 (Hall effect). K. Lassmann and Hp. Schad, *Solid State Commun.* **18**, 449 (1976) [Hall effect].

[rr] J. M. Baranowski, M. Grynberg, and E. M. Magerramov, *Phys. Status Solidi* **50B**, 433 (1972) (absorption); H. Ennen and U. Kaufmann, *J. Appl. Phys.* **51**, K15 (1980) (luminescence); R. W. Haisty and G. R. Cronin, *in* "Physics of Semiconductors" (M. Hulin, ed.), p. 1161. Dunod, Paris, 1964, (Hall effect).

[ss] W. J. Brown and J. Blakemore, *J. Appl. Phys.* **43**, 2242 (1972) (Hall effect); A. A. Gutkin, D. N. Nasledov, and F. E. Faradzhev, *Sov. Phys. Semicond.* **8**, 298, (1974) (absorption); W. Drozdzewicz, A. M. Hennel, Z. Wasilewski, B. Clerjaud, F. Gendron, C. Porte, and R. Germer, *Phys. Rev. B* **29**, 2438 (1984) (absorption, stress); D. L. Partin, J. W. Chen, A. G. Milnes, and Vassamillet, *J. Appl. Phys.* **50**, 6845 (1979). D. G. Andrianov, N. I. Suchkova, A. S. Savelev, E. P. Rashevskaya, and M. A. Filippov, *Sov. Phys. Semicond.* **11**, 426 (1977), report $E(0/-) \simeq E_v + 0.35$ eV for GaAs:Ni from absorption data.

[tt] D. Wasik, A. M. Hennel, and M. Baj, *Acta Phys. Pol.* **67A**, 129 (1985) (Hall effect under pressure).

[uu] No acceptor level has been found by B. Lambert, B. Deveaud, Y. Toudic, G. Pelous, J. C. Paris, and G. Grandpierre, *Solid State Commun.* **47**, 337 (1983) (luminescence); or M. S. Skolnick, R. G. Humphreys, P. R. Tapster, B. Cockayne, and W. R. MacEwan, *J. Phys. C* **16**, 7003 (1983). However, B. Deveaud, B. Plot, B. Lambert, G. Bremond, G. Guillot, A. Nouailhat, B. Clerjaud, and C. Naud, *J. Appl. Phys.*, in press (1985) find evidence for a donor level at $E_v + 0.21$ eV in DLTS.

[vv] G. W. Iseler, *Inst. Phys. Conf. Ser.* **45**, 144 (Hall effect). S. Fung and R. Nicholas, *J. Phys. C* **14**, 2135 (1981) (PC); *ibid.*, **18**, 259 (1985) (PC); J. K. Rhee and P. K. Battacharga, *J. Appl. Phys.* **53**, 4247 (1982) (photoinduced currents).

[ww] L-Å. Ledebo and B. K. Ridley, *J. Phys. C* **15**, L961 (1982); P. Rojo, P. Leyral, A. Nouailhat, and G. Guillot, *J. Appl. Phys.* **55**, 395 (1984) (luminescence, DLTS); M. S. Skolnick, E. J. Foulkes, and B. Tuck, *J. Appl. Phys.* **55**, 2951 (1984).

[xx] L. Eaves, A. W. Smith, M. Skolnick, and B. Cockayne, *J. Appl. Phys.* **53**, 4955 (1982) (luminescence); V. P. Kuznetsov, M. A. Messmer, and A. Omelyanovski, *Sov. Phys. Semicond.* **18**, 278 (1984) (Hall effect); B. Lambert, B. Clerjaud, C. Naud, B. Deveaud, G. Picoli, and Y. Toudic, *J. Electron. Mater.* **14a**, 1141 (1985) (photoionization).

[yy] M. S. Skolnick, R. G. Humphreys, P. R. Tapster, B. Cockayne, and W. R. MacEwan, *J. Phys. C* **16**, 7003 (1983) (Hall effect and DLTS).

[zz] K. Graff and H. Pieper, *in* "Semiconducting Silicon 1981" (H. R. Huff, R. J. Krieger, and Y. Takeishi, eds.), p. 331. Electrochemical Soc., Pennington, New Jersey, 1981 (DLTS).

[aaa] A. M. Salama and L. J. Cheng, *J. Electrochem. Soc.* **127**, 1164 (1980).

[bbb] H. Lemke, *Phys. Status Solidi* **64A**, 549 (1981) (TSC).

[ccc] H. Feichtinger and R. Czaputa, *Appl. Phys. Lett.* **39**, 706 (1981).

[ddd] (DLTS, Hall effect): H. Lemke, *Phys. Status Solidi* **64A**, 215 (1981); K. Wünstel and P. Wagner, *Appl. Phys.* **27A**, 207 (1982); H. Feichtinger, J. Waltl, and A. Gschwandtner, *Solid State Commun.* **27**, 867 (1978).

[eee] The first confirmed substitutional 3*d* impurity in Si for which an electrical level was observed is Si:Mn. R. Czaputa, H. Feichtinger, J. Oswald, H. Sitter, and M. Haider, *Phys. Rev. Lett.* **55**, 758 (1985), found $E(0/+) = E_v + 0.38$ eV by DLTS.

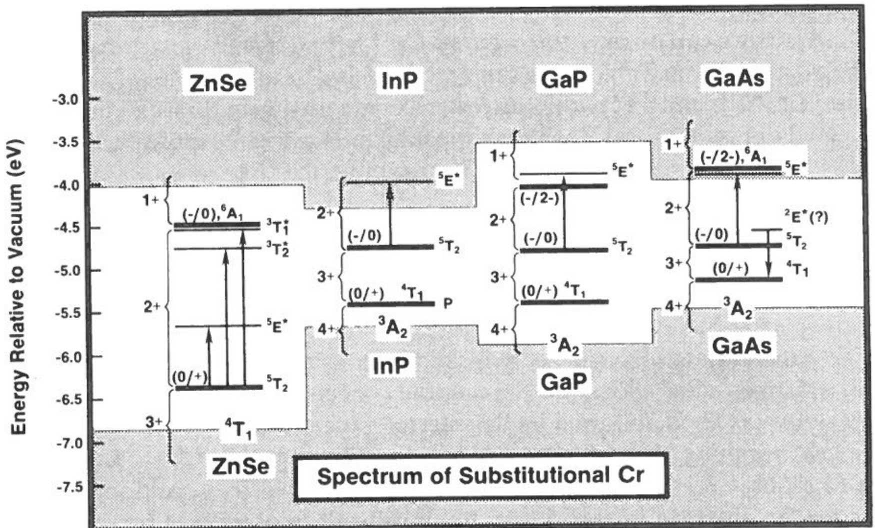

FIG. 7. A combined energy-level diagram showing $d \rightarrow d^*$ internal transitions and ionization levels of the substitutional Cr impurity in semiconductors. Data from Tables V and VII except for the $(0/+)$ donor level of InP:Cr which is predicted (P). The shaded areas denote the valence and conduction bands. Thick horizontal lines denote ionization levels; e.g., $(0/+)$ [or $(-/0)$] denotes the position of the Fermi level below which the system is in the A^+(or A^0) charge state and above which it is in the A^0 (or A^-) charge state. The energy range between $(0/+)$ and $(-/0)$ is the existence domain of A^0; that between $(-/0)$ and $(-/2-)$ is the existence domain of A^-, etc. Thin horizontal lines denote internally excited d states of a fixed charge state; e.g., between $(0/+)$ and $(-/0)$ we have the ground state of A^0 ($^5T_2$ in II-VIs, $^4T_1$ in III-Vs), as well as its internally excited states (^5E, $^3T_2$ and $^3T_1$ in II-VIs). Note that some of these excited states overlap with the conduction band (e.g., ^5E in InP and GaAs).

exists above $E_v + E(-/0) = E_v + 1.12$ eV, but below $E_v + E(-/2-) = E_v + 1.85$ eV, etc. These ionization energies take up different positions for thermal and optical processes (only one is shown in Fig. 7 for lack of space). This construct shows which oxidation states exist inside the band gap (e.g., Cr^{2+}) and which are resonant in part (e.g., Cr^+ in II-VIs) or entirely (Cr^+ in GaAs) with the host bands. Using Fig. 4 we can assign the various cubic *ground*-state multiplets to each oxidation state: $^3A_2$, $^4T_1$, $^5T_2$ and $^6A_1$ for Cr^{4+}, Cr^{3+}, Cr^{2+}, and Cr^{1+}, respectively. From the EPR data of Tables III and IV we observe Cr^{3+} and Cr^{2+} to be orthorhombically and tetragonally distorted centers, respectively. The $^3A_2$ ground state of Cr^{4+} in III-Vs can be anywhere from inside the VB to below $(0/+)$; similarly, the $^4T_1$ ground states of Cr^{3+} in II-VIs can be anywhere from inside the VB up to below $(0/+)$. In p-type samples we expect to have the Cr^{3+} charge state in II-VIs but the Cr^{4+} charge state in III-Vs. In n-type GaAs, we will find Cr^{2+}; in semi-insulating

GaAs:Cr both Cr^{2+} and Cr^{3+} will be present. As we illuminate p-type GaAs:Cr we can observe the reaction $Cr^{4+} \xrightarrow{h\nu} Cr^{3+} + \text{hole}_{VB} \xrightarrow{h\nu} Cr^{2+} + \text{hole}_{VB}$, etc. From Table V we can find the $d \to d^*$ excited states of Cr^{2+}, i.e., the $^5E^*$, $^4T_2^*$, and $^3T_1^*$multiplets (asterisks are used here to distinguish them from the ground states). The thin horizontal lines in Fig. 7 denote these excited d^* states of a given oxidation state. For example, the $^5E^*$ excited state of Cr^{2+} in ZnSe is located at $E_v + E(0/+) + \Delta(^5T_2 \to {}^5E) = E_v + 0.46 + 0.65$ eV $= E_v + 1.145$ eV, whereas in GaP this excited state is located at $E_v + E(-/0) + \Delta(^5T_2 \to {}^5E) = E_v + 1.12 + 0.873 = E_v + 1.99$ eV. This shows that the $^5E^*$ state in ZnSe and GaP are below the conduction-band minima (since the host crystal band gaps are 2.82 and 2.35 eV, respectively). In contrast, the $^5E^*$ excited state in GaAs (as well as in InP) is inside the conduction band: It is formed after providing the neutral systems with the acceptor energy $E(-/0) = 0.73$ eV, followed by the internal excitation energy $\Delta(^5T_2 \to {}^5E) = 0.9$ eV, resulting in an energy position $E_v + E(-/0) + \Delta(^5T_2 \to {}^5E) = E_v + 1.63$ eV or $\approx E_c + 0.1$ eV. This explains why the $^5E^* \leftrightarrow {}^5T_2$ transition in GaAs is readily observed in absorption, but is difficult to observe in luminescence due to thermalization into the conduction-band minimum. If the band gap of the GaAs host crystal is increased slightly (e.g., by applying pressure or by alloying with Al), the $^5E^*$ excited state can be exposed inside the gap. This figure also illustrates possible overlaps of the $d \to d^*$ spectra with photoionization spectra: Only three excited states of Cr^{2+} are observed in II-VIs ($^5E^*$, $^3T_2^*$, and $^3T_1^*$), since, as one supplies photons with higher energies, the system undergoes photoionization, which masks the $d \to d^*$ spectra. In contrast, in III-Vs, only a single excited state of Cr^{2+} is observed since it already is near (or inside) the conduction band. A possible excited state ($^2E^*$) of Cr^{3+} in GaAs is shown too.

Similar considerations show that at least some of the excited states of Ti^{2+} in II-VIs are in the conduction band. For example, the excitation energies in CdTe:Ti from the $^3A_2$ ground state to the $^3T_2^*$, $^3T_1^*$, and $^3T_1^*$ excited states are 0.35, 0.62, and 1.14 eV, respectively (Table V). Using $E(0/+) = E_v + 0.55$ (Table VII), these excited states are at 0.9, 1.17, and 1.76 eV, respectively; i.e., for $E_g = 1.62$ eV, the third excited state is inside the conduction band. In this case, the $^3A_2 \to {}^3T_1^*$ absorption gives rise to photoconductivity which can be observed to follow the $d \to d^*$ excitation spectra. A similar argument, applied to CdSe:Ti, shows all three excited states to be inside the CB, because of the large donor energy of this system; in this case the photocurrent spectrum parallels the $d \to d^*$ absorption spectrum.

Using the data of Tables V and VII, one can construct diagrams like that shown in Fig. 7 for all other impurities. These serve to clarify which excited states are in the band gap and which are resonant within the host bands, what are the regions of band-gap energies where a given oxidation state is stable,

why impurities in II-VI materials often show more $d \to d^*$ transitions than in III-V materials, and why it is difficult to observe $d \to d^*$ transitions of several different oxidation states in a given crystal (Cr^{3+} in GaAs being the only well-established exception shown in Fig. 7; see, however, Ref. 62b).

While Tables V and VII highlight the tremendous progress made over the years in measuring the excitation and ionization spectra of 3d impurities in semiconductors, they also indicate numerous systems for which data are unavailable. Until recently, no guides were available to indicate whether the missing ionization levels exist at all in the band gaps (so the failure to observe them is accidental) or not (in which case they are unobservable by current techniques). Furthermore, no material-dependent chemical trends are apparent in Tables V and VII to aid systematization and provide guides for searching for "missing levels." This situation has changed in recent years—theoretical advances going beyond the classical phenomenological models (discussed in Part VI) have made it possible to unravel the chemical trends which underly the data and predict, with useful accuracy, the positions of hitherto unobserved levels.

d. Mott–Hubbard Coulomb Energies

The donor and acceptor energies of Eqs. (6.3)–(6.10) can further define the apparent Mott–Hubbard Coulomb repulsion energy $U^{(\alpha\beta)}$ as the energy required to transfer an electron from orbital α on an impurity site to orbital β on a distant impurity site. If we carry out this process for the neutral center A^0, we first ionize an electron from orbital α to form A^+, investing an energy $E^{(\alpha)}(0/+)$ [Eq. (6.9)], and then we add an electron to orbital β on a distant neutral center A^0, transforming it to an A^- center by investing the energy $E^{(\beta)}(-/0)$ [Eq. (6.4)]. If all three species A^0, A^+, and A^- involve the same space orbital $\alpha = \beta$ in the electron-transfer processes, we then have the *diagonal Mott–Hubbard energy* $U^{(\alpha\alpha)}(A^0)$ for the intermediate species A^0, given by the difference in single-donor and single-acceptor energies (referred to the same VB edge) as

$$U^{(\alpha\alpha)}(A^0) = E^{(\alpha)}(-/0) - E^{(\alpha)}(0/+). \tag{6.12}$$

For most impurities $U^{\alpha\alpha}(A^0)$ is positive; i.e., the donor level is lower in the band gap than the acceptor level if the two transitions are associated with the same center. A different apparent Mott–Hubbard energy can be obtained for the A^- center by first ionizing an electron from orbital α on A^-, transforming the center to A^0 through an energy change $E^{(\alpha)}(-/0)$ [Eq. (6.4)] and then adding an electron to orbital β at a distant center A^-, transforming it to an A^{2-} center through an energy change $E^{(\alpha)}(-/2-)$ [Eq. (6.7)]. The diagonal Mott–Hubbard energy $U^{(\alpha\alpha)}(A^-)$ for the intermediate species A^- is given by the

difference in double-acceptor and single-acceptor energy as

$$U^{(\alpha\alpha)}(A^-) = E^{(\alpha)}(-/2) - E^{(\alpha)}(0/-), \tag{6.13}$$

where we have referred both acceptor energies to the valence-band edge. For most impurities, $U^{(\alpha\alpha)}(A^-)$ is also positive; i.e., the single-acceptor level is lower in the gap than the double-acceptor level if both belong to the same center. In general, $U^{(\alpha\alpha)}(A^0) \neq U^{(\alpha\alpha)}(A^-)$.

The Mott–Hubbard energy $U^{(\alpha\alpha)}(A^q)$ as we have defined it corresponds to the difference between two ionization energies: that of $A^q(N)$ with N electrons, $A^q(N) \rightarrow A^{q+1}(N-1)$, and that of $A^{q-1}(N+1)$ with $N+1$ electrons, $A^{q-1}(N+1) \rightarrow A^q(N)$. Using the definitions of the corresponding transition energies of Eqs. (6.4) and (6.9), the general expression for $U^{(\alpha\alpha)}(A^q)$ is hence

$$U^{(\alpha\alpha)}(A^q) = E^{(\alpha)}(q-1/q) - E^{(\alpha)}(q/q+1),$$

$$= E_T^{(i)}[A^{q-1}, N+1] + E_T^{(k)}[A^{q+1}, N-1] - 2E_T^{(i)}[A^q, N]. \tag{6.14}$$

We see from Eq. (6.14) that $U^{(\alpha\alpha)}(A^q)$ is the energy of the formal chemical reaction

$$2A^q(N) \leftrightarrows A^{q+1}(N-1) + A^{q-1}(N+1), \tag{6.15}$$

where two identical but isolated centers $A^q(N)$ disproportionate into their (isolated) asymmetric products $A^{q+1}(N-1)$ and $A^{q-1}(N+1)$. Consider next the two possibilities: $U > 0$ and $U < 0$.

If $U(A^q) > 0$, then the reaction of Eq. (6.15) proceeds from right to left; i.e., $2A^q$ is more stable than the disproportionated product and its concentration dominates that of the other two species. This means that ionization of the second electron from orbital α requires more energy than the ionization from the same orbital of the first electron. (Clearly, it is less useful to consider the sign of the *off-diagonal* term $U^{(\alpha\beta)}$, since in that case we are comparing ionizations of different orbitals. A limiting case illustrates this point: If the first ionization is from a deep core level α and the second from a shallow valence level β, then $U^{(\alpha\beta)} < 0$, trivially.) If $U^{(\alpha\alpha)}(A^q)$ is positive, all three charge states can be stable; i.e., A^{q+1} is the ground state if the Fermi energy E_F satisfies $E_F < \Delta E(q/q+1)$, followed by A^q as the ground state if $\Delta E(q-1/q) > E_F > \Delta E(q/q+1)$, and, finally, A^{q-1} is the ground state if $E_F > \Delta E(q-1/q)$.

On the other hand, if $U^{(\alpha\alpha)}(A^q)$ is negative, the reaction in Eq. (6.15) proceeds from left to right; i.e., the disproportionation products are more stable than $2A^q(N)$. This corresponds to the unusual situation where the ionization of the second electron from α requires *less energy* than the ionization of the first electron.[93] In this case, $A^q(N)$ is never the ground state for any value of E_F (but can be observed as a transient metastable species): For $E_F < \Delta E(q/q+1)$,

[93] G. D. Watkins, *Festkörperprobleme* **24,** 163 (1984).

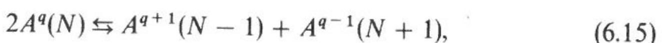

A^{q+1} is the ground state, whereas above this energy $A^{q+1}(N-1)$ acquires two electrons simultaneously to become $A^{q-1}(N+1)$. Hence, simple Hall-effect experiments will detect a single "electrical level" in the band gap. The implications of a negative $U^{(\alpha\alpha)}(A^q)$ on the transport and paramagnetic properties of these systems are discussed in Refs. 93–95, and in Part VI,27.

Experimental values for diagonal Mott–Hubbard Coulomb energies[96–98] for 3*d* impurities in a number of semiconductors are collected in Table VIII. Note that a theoretical analysis is necessary to establish whether both the donor and the acceptor transitions commence from the same type of one-electron orbital α (in which case their difference provides the *diagonal* U) or not (in which case their difference gives an *off-diagonal* U). The theoretical analysis leading to the assignments given in Table VIII will be discussed in Part IV,14.

7. Observations of the Lattice Symmetry around the Impurity

Possible deviations from cubic lattice symmetry around an impurity in a cubic crystal are often inferred from a combination of a number of experiments, such as EPR under stress and illumination, Zeeman spectra, and vibronic interactions in luminescence, absorption, and EPR. These are often used to identify symmetry lowering around the impurity, e.g., Jahn–Teller (JT) distortions. (If the effect of internal strains exceeds that of the tunneling splitting a symmetry lowering can be observed; otherwise, one observes undistorted cubic symmetry.) Figure 4 reveals a number of nonsinglet configurations, subject in principle to a JT distortion. However, not all charge and oxidation states indicated in this figure have ionization levels in the gap (cf. Table VII). The states that have orbital nonsinglet ground states in cubic symmetry and have been found to have the corresponding oxidation states in

[94] D. Adler, *Semicond. Semimetals* **21A,** 291 (1984).

[95] D. Adler, *in* "Handbook of Semiconductors" (W. Paul, ed.), p. 805. North-Holland Publ., Amsterdam, 1982.

[96] The reader should be aware that thare are numerous different definitions of Hubbard U in the literature [for example, the classical Coulomb energy of a charge distribution $\rho(\mathbf{r})$, or various screened versions of it].[97] In this article I use strictly the phenomenological definition[98] of Eq. (6.14) as the difference of two successive ionization energies. Equation (6.14) then emphasizes that any physical effect that contributes to the total energy $E_T^{(i)}[A, N]$ a term of order N^λ, with $\lambda \geq 2$, will also contribute to $U^{(\alpha\alpha)}(A^q)$. This includes the classical Coulomb energy of the electrons (a positive-definite quantity with $\lambda = 2$), differences in the kinetic energies and crystal-field energies caused by ionization (i.e., orbital relaxation effects), differences in elastic energies (i.e., lattice relaxation effects) and differences in many-electron correlation energies. All latter terms could be either positive or negative.

[97] B. H. Brandow, *Adv. Phys.* **26,** 651 (1977).

[98] N. Mott, "Metal-Insulator Transition." Taylor & Francis, New York, 1974).

TABLE VIII. OBSERVED IONIZATION ENERGIES (FROM TABLE VII) AND DIAGONAL MOTT–HUBBARD COULOMB ENERGIES $U^{(\alpha\alpha)}(A^q)$ FOR GAP LEVEL α AND CHARGE STATE* A^q

Host	Impurity	Single donor (0/+)	Single acceptor (−/0)	Double acceptor (−/2−)	Hubbard energy $U^{\alpha\alpha}(A^q)$ (expt)	Multiplet correction $\Delta U_{MC}^{(ijk)}$ (calc)	Mean-field $U_{MF}^{\alpha\alpha}(A^q)$ (calc)
ZnS	Cr	$E_v + 1.0$ (?)	$E_v + 2.78$ (?)	—	~1.78, (tt), A^0	−0.67	~2.45 (t)
	Ni	$E_v + 0.75$	$E_v + 2.46$	—	1.71, (tt), A^0	−0.31	2.02 (t)
ZnSe	Cr	$E_v + 0.46$ (?)	$E_v + 2.26$ (?)	—	~1.80, (tt), A^0	−0.72	~2.52 (t)
	Ni	$E_v + 0.15$	$E_v + 1.85$	—	1.70, (tt), A^0	−0.29	1.99 (t)
CdSe	Ni	$E_v + 0.32$	$E_v + 1.81$	—	1.49, (tt), A^0	—	—
GaP	Cr	$E_v + 0.5$	$E_v + 1.12$	$E_v + 1.85$	0.73, (tt), A^- 0.62, (tt), A^0	−0.31	1.04 (t)
	Fe	—	$E_v + 0.86$	$E_v + 2.09$	1.23, (ee), A^-	−0.21	1.44 (e)
	Co	—	$E_v + 0.41$	$E_v + 2.02$	1.61, (ee), A^-	—	—
	Ni	—	$E_v + 0.5$	$E_v + 1.55$	1.05, (tt), A^-	−0.10	1.15 (t)
GaAs	Cr	$E_v + 0.32$	$E_v + 0.74$	$E_v + 1.57$	0.83, (tt), A^- 0.42, (tt), A^0		
	Co	—	$E_v + 0.16$	$E_v + 1.67$	1.49, (ee), A^-		
	Ni	—	$E_v + 0.22$	$E_v + 1.13$	0.91, (tt), A^-		
Si	Ti	$E_v + 0.89$	$E_v + 1.09$	—	0.20, (tt), A^0		
	V	$E_v + 0.72$	$E_v + 1.01$	—	0.29, (tt), A^0		
	Mn	$E_v + 0.75$	$E_v + 1.06$	—	0.31, (t/e), A^0		

* Calculated many-electron corrections are from A. Fazzio, M. Caldas, and A. Zunger, *Phys. Rev. B* **30**, 3430 (1984) except for GaP:Ni, for which the new experimental result of Liro, unpublished (1985) for the $^3T_1 \rightarrow {}^3T_2$ transition energy was used. e or t denote the type of one-electron orbital α involved in the ionization process. Results for heteropolar semiconductors pertain to substitutional impurities; those for Si pertain to interstitial impurities. More results on InP and GaAs can be found in M. Caldas, A. Fazzio, and A. Zunger, *J. Elect. Mat.* **14a**, 1035 (1984).

the band gap include, for *substitutional* impurities, the following classes

(1) The $[d^9, e^4t^5, {}^2T_2]$ series, e.g., Ni^+ and Cu^{2+}.
(2) The $[d^8, e^4t^4, {}^3T_1]$ series, e.g., Ni^{2+}.
(3) The $[d^4, e^2t^2, {}^5T_2]$ series, e.g., Cr^{2+}.
(4) The $[d^3, e^2t^1, {}^4T_1]$ series, e.g., high-spin V^{2+} and Cr^{3+}.
(5) The $[d^1, e^1t^0, {}^2E]$ series, e.g., Ti^{3+}.

For *interstitial* impurities, the candidate series for JT distortions include

(1) The $[d^9, t^6e^3, {}^2E]$ series, e.g., Si:Co^0.
(2) The $[d^7, t^5e^2, {}^4T_1]$ series, e.g., Si:Mn^0 and Si:Fe^+.
(3) The $[d^6, t^4e^2, {}^5T_2]$ series, e.g., Si:V^-, Si:Cr^0, and Si:Mn^+.

Not all of the centers that are expected by symmetry to have a JT coupling and that are known to have stable oxidation states in the band gap have been shown to actually have such a distortion. For the *substitutional* series, following the five classes (1)–(5), the experimental findings are

(1) EPR was not detected for Ni^+ in GaAs,[58] although Zeeman experiments suggest coupling of $^2T_2$ to E-mode vibrations. EPR experiments[99] for GaP:Ni^+ (Table III) show an isotropic g value. No Zeeman experiments have been reported on InP:Ni^+ (in fact, even internal transitions were not observed; cf. Table V). The reduction in the g values of Ni^+ (see Table III) relative to the free-electron value $g = 2$ has been interpreted[57,58] in terms of dynamic Jahn–Teller coupling. In II-VIs, analysis[100] of the $^2T_2 \leftrightarrow {}^2E$ internal transitions of Ni^+ in ZnS and ZnSe (using the results of Ref. 101) revealed moderate JT energies of ~0.07 eV, but only an isotropic g value was observed (Table IV). However, the results of Ref. 101 are applicable only when JT energies are larger than spin-orbit energies, a situation not met for Ni^+ in ZnS and ZnSe. A more exact analysis[102] reveals smaller JT energies: 0.026 and 0.022 eV in ZnS:Ni^+ and ZnSe:Ni^+, respectively. Yamaguchi and Kamimura[103] have convincingly demonstrated theoretically a dynamic Jahn–Teller effect for Cu^{2+} in II-VI compounds.

(2) EPR of Ni^{2+}, d^8 is not expected to be detected (the ground state is a nondegenerate spin-orbit level). In II-VIs, a $^3T_1(P) \rightarrow {}^3T_1(F)$ emission of Ni^{2+} has been observed (cf. Table V); both a tetragonal and a trigonal JT distortion

[99] U. Kaufmann, W. H. Koschel, J. Schneider, and J. Weber, *Phys. Rev. B* **19**, 3343 (1979).
[100] G. Roussos, J. Nagel, and H. J. Schulz, *Z. Phys. B* **53**, 95 (1983).
[101] B. Clerjaud and A. Gelineau, *Phys. Rev. B* **9**, 2832 (1974).
[102] B. Clerjaud, A. Gelineau, F. Gendron, G. Porte, J. M. Baranowski, and Z. Liro, *J. Phys. C.* **17**, 3837 (1984).
[103] T. Yamaguchi and H. Kamimura, *J. Phys. Soc. Jpn.* **33**, 953 (1972).

were assumed[104] to explain the intensity ratios and splitting pattern. A dynamic JT effect has been suggested to explain the absorption spectra[105] of Ni^{2+} in ZnS with a moderate JT energy of 0.052 eV.

(3) Cr^{2+} has been observed to be JT coupled in III-Vs[106] (Table III). This center in GaAs has been studied by Krebs and Stauss[107] under uniaxial stress, showing that trigonal stress has no effect on the EPR spectra, whereas tetragonal stress leads to the alignment of all Cr^{2+} ions along the stress axis. This suggests a ground-state tetragonal JT coupling to the E-mode vibrations. Absorption studies[108] of GaAs:Cr^{2+} were likewise explained in terms of a tetragonal distortion of the $^5T_2$ ground state and a very weak dynamic coupling in the ^5E excited state. The JT energy in the ground state was determined to be $E_{JT} = 0.074$ eV, but an attempt to directly observe a transition at $3E_{JT}$ failed.[108] Cr^{2+} has also been shown to have a tetragonal distortion in InP,[109] and in GaP[110] (although in the latter case the rather unusual spin Hamiltonian parameters observed cast some doubt on whether this corresponds to isolated GaP:Cr^{2+}; observation of a characteristic Cr^{2+} internal absorption[12] will be needed to establish that isolated Cr^{2+} is present in the experiment of Ref. 110). Mn^{3+} belongs to this series too, but was not identified unambiguously in III-Vs. The magnetic susceptibility data of Andrianov *et al.*[30,111] on GaAs:Mn have been interpreted to indicate the presence of $[Mn^{3+}, d^4, A^0, {}^5T_2]$ with JT distortion, but its EPR signature has not been observed.[30,111] In II-VIs, the Cr^{2+} has been studied intensively. Rather small JT E-mode energies of 0.037, 0.042, 0.04, and 0.046 eV have been deduced by Kaminska *et al.*[112] from absorption and luminescence data for the Cr^{2+}, $^5T_2$ state in ZnS, ZnSe, ZnTe, and CdTe, respectively. The E-mode JT distortion has been observed directly in EPR studies,[113] from which distortion energies of $E_{JT} \cong 0.06$ and 0.02 eV have been deduced for ZnSe:Cr and ZnTe:Cr, respectively.

[104] G. Roussos and H. J. Schulz, *J. Lumin.* **31/32,** 427 (1984); D. Buhmann, H. J. Schulz, and M. Thiede, *Phys. Rev. B* **24,** 6221 (1981).
[105] U. G. Kaufmann and P. Koidl, *J. Phys. C* **7** 791 (1974); U. Kaufmann, P. Koidl, and O. F. Schirmer, *J. Phys. C* **6,** 310 (1983).
[106] J. J. Krebs and G. H. Stauss, *Phys. Rev. B* **16,** 971 (1977).
[107] J. J. Krebs and G. H. Stauss, *Phys. Rev. B* **20,** 795 (1979).
[108] A. M. Hennel, W. Szuszkiewicz, M. Balkanski, G. Martinez, and B. Clerjaud, *Phys. Rev. B* **23,** 3933 (1981).
[109] G. H. Stauss, J. J. Krebs, and R. L. Henry, *Phys. Rev. B* **16,** 974 (1977).
[110] C. A. Bates, J. Handley, A. Vasson, and A. M. Vasson, *J. Phys. C* **17,** L603 (1984).
[111] D. G. Andrianov, Yu. A. Grigorev, S. O. Klimonskii, A. S. Savelev, and S. M. Yakubenya, *Fiz. Tekh. Poluprovdn.* **18,** 262 (1984) [*Sov. Phys. Semicond.* **18,** 162 (1984)].
[112] M. Kaminska, J. M. Baranowski, S. M. Uba, and J. T. Vallin, *J. Phys. C* **12,** 2197 (1979).
[113] J. T. Vallin and G. D. Watkins, *Phys. Rev. B* **9,** 2051 (1974).

(4) Cr^{3+}, belonging to the fourth series, has been shown to have a JT distortion in III-Vs (Table III). Krebs and Stauss[114] showed an orthorhombic site symmetry in GaAs and a coupling to $E + T_2$ vibration modes.[115] Uniaxial-stress experiments by Ramdane *et al.*[116a] for GaAs:Cr^{3+} showed a decrease in phonon scattering attributed to $E + T_2$ phonon couplings. An apparent orthorhombic center has been suggested to occur in GaP:Cr^{3+} by Kaufmann and Ennen[117] and by Kaufmann and Schneider[12] (although it may be due to a complex since it does not exhibit a temperature dependence expected of normal JT systems), but was not observed in InP:Cr^{3+}, although this state exists in the band gap. V^{2+} also belongs to this series, but, although this level exists in the band gap of GaAs and GaP, its EPR has not been observed. Recent stress-dependent thermal conductivity experiments[116b] on GaP:Cr^{3+} and InP:Cr^{3+} also suggest orthorhombic JT coupling.

(5) No JT coupled centers of the $[d^1, {}^2E]$ type have been proven for $3d$ impurities in II-VIs or III-Vs (Sc^{2+} in ZnS may, however, be a likely case). The analogous $[d^9, {}^2E]$ state is a common JT center for $3d$ impurities in O_h-like ionic crystals.[35]

In some cases, JT couplings have been observed in *excited d* states; e.g., whereas the ground state of d^2 in substitutial symmetry is a singlet $^3A_2$ (see Fig. 4), the excited $^3T_2$ and $^3T_1$ are subject to a JT coupling. This has been observed for V^{3+} in InP.[118]

A similar survey of the centers that are supposed to be JT coupled in interstitial symmetry [classes (1)–(3) above, under interstitial impurities] reveals that none show unambiguously a static JT coupling in silicon. The only possible candidate is Si:Ni^+ [class (1) above], which Ludwig and Woodbury[1] associated with a distorted site. Its EPR signal shows motional narrowing between 10 and 20 K, and below 2 K the g value is anisotropic. It is possible[1] that this is associated with a dynamic JT effect above ~ 10 K and a static one below 2 K, with exceedingly small JT energies. However, since Ni is a very fast diffuser in Si (like Cu and Co), it has been suggested[10] that it might be stabilized by some nearby lattice defects, leading to a distortion. A new[119] EPR spectrum of Si:Ni with $S = \frac{1}{2}$ is thought to originate similarly from a coupling to a lattice defect.

[114] J. J. Krebs and G. M. Stauss, *Phys. Rev. B* **15,** 17 (1977).
[115] G. M. Stauss, J. J. Krebs, S. H. Lee, and E. M. Swiggard, *Phys. Rev. B* **22,** 3141 (1980).
[116a] A. Ramdane, B. Salce, and L. T. Challis, *Phys. Rev. B* **27,** 2554 (1983).
[116b] N. Butler, J. Jouglar, B. Salce, L. J. Challis, and P. L. Vuillermoz, *J. Phys. C* **18,** L725 (1985).
[117] U. Kaufmann and M. Ennen, unpublished (1978).
[118] M. S. Skolnick, R. G. Humphreys, P. R. Tapster, B. Cockayne, and W. R. MacEwan, *J. Phys. C* **16,** 7003 (1983).
[119] E. Weber and N. Wiehl, *Verhandl. Dtsch. Phys. Ges,* (*VI*) **15,** 223 (1980); quoted also in ref. 10.

The types of data with which we can characterize different states of a given impurity are illustrated in Fig. 8a for GaP:Fe. Similar diagrams for ZnS:Fe and Si:Fe appear in Fig. 8c. They show ionization transitions and internal transitions, as well as the electronic configurations deduced from single-state experiments such as EPR. These illustrate the basic types of data that electronic-structure theory needs to address. This is discussed in Part V.

8. Trends in the Data

a. *The Identification Problem*

Inspection of the data surveyed in Tables II–VIII shows that impurities observed by one technique can escape detection by other techniques. For example, Mn^{2+} is well characterized by EPR in Si (Tables II, III), GaAs, GaP, InP (Table III), and ZnS, ZnSe (Table IV), but its $d \rightarrow d^*$ excitations have not been seen in Si, GaAs, or InP (Table V), and its electrical levels have been not observed in ZnS, ZnSe, CdSe, or CdTe (Table VII). Similarly, no EPR of Ni^{2+} has been observed in III-Vs (its lowest A_1 ground state is not paramagnetic), although its electrical levels have been observed in GaAs. Many more such examples are apparent in Tables II–VIII. This reflects both the limiting factors of the different experimental techniques and the fact that different techniques exhibit sensitivities to different aspects of the impurity's properties. For example, while nonmagnetic impurity states are ENDOR- and EPR-invisible, they can control optical and thermal excitations; impurities with no (or very shallow) gap levels are DLTS-invisible, but could give rise to strong EPR signals if paramagnetic (ZnS:Mn); impurities with strong radiationless decay channels are luminescence-invisible but could give distinct absorption and DLTS signals, etc. This emphasizes the need to combine a number of experimental techniques and highlights the potential danger that exists in this field of erroneous conclusions based on either limited experimental observations or narrowly selected theoretical emphasis. Considering the fact that the equilibrium concentration of most 3*d* impurities in semiconductors is below the threshold needed for unambiguous chemical identification, yet profoundly control the optical, magnetic, and electrical response of the system, one is faced with the challenge (common in high-energy elementary particle physics) of identifying and characterizing "ghost particles" from their *indirect* imprints.

b. *Energy Scales in the System*

Our survey of the experimental situation in this field suggests the following characteristic energy scales

(1) The spread in the atomic valence-orbital ionization energies of the 3*d* ions and the atoms constituting the host crystals is around 10–60 eV (see also Part III,8,c).

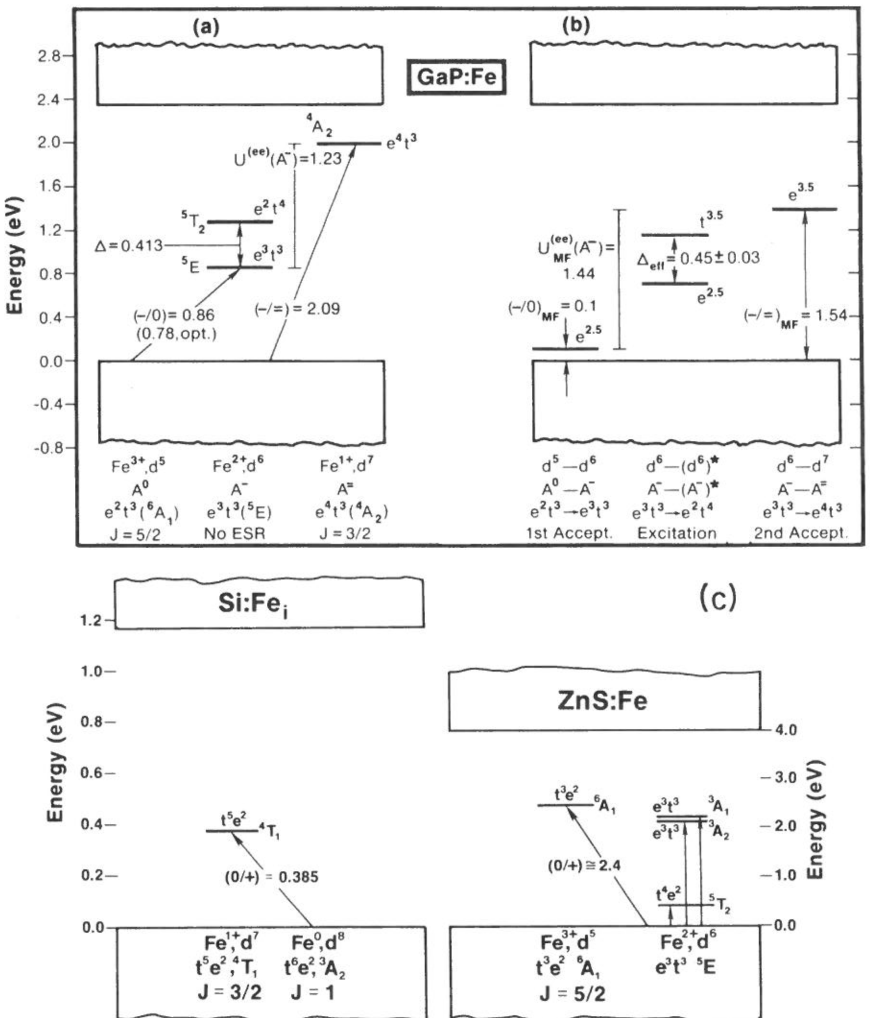

Fig. 8. (a) Observed (Tables V and VII) levels of GaP:Fe (see also Ref. 259 below). (b) The one-electron mean-field analog expressed in terms of transition-state levels in the local-density formalism; (c) Observed (Tables V and VII) levels of Si:Fe and ZnS:Fe. These figures show the internal states of a given charge state (e.g., $^5T_2$ and ^5E of Fe^{2+} in GaP, $^4T_1$ of Fe^{+} in Si), the ionization transitions between the ground states of two different charge states [e.g., $(-/0)$ for $Fe^{3+} \leftrightarrow Fe^{2+}$ in GaP], and the spin states observed in EPR. Figure 8b shows that the mean-field analog of the $Fe^{3+} \leftrightarrow Fe^{2+}$ acceptor energy in GaP is the energy separation between the *e*-like gap level and the valence-band maximum when the former is occupied by 2.5 electrons. If occupied by 3.5 electrons, the energy separation gives the mean-field part of the *second* acceptor energy. The mean-field component of the internal $(e^3t^3, {}^5E) \rightarrow (e^2t^4, {}^5T_2)$ transition is given by the energy that separates the *t* level from the *e* level at the intermediate occupation $e^{2.5}t^{3.5}$. The effective Mott–Hubbard energy $U^{(ee)}(A^-)$ is the difference between the second and first acceptor energies. Its mean-field component is the energy separation between the *e* level with 3.5 electrons and the *e* level with 2.5 electrons.

(2) Characteristic host-crystal band gaps (Table VII) range around 1–4 eV; the lowest ionization energies of the pure host crystals (photothresholds) are around 5–8 eV (see Part III,8,c).

(3) The donor and acceptor ionization energies of $3d$ impurities (Table VII) range around 0.1–2.5 eV relative to the valence-band maximum, or $\sim$5–7 eV relative to vacuum (see Part III,8,c).

(4) Mott–Hubbard Coulomb energies (Table VIII) range around 0.2–2 eV (i.e., are equal or larger than exchange energies).

(5) The internal ($d \rightarrow d^*$) transition energies (Table V) range around 0.3–2 eV.

(6) Crystal-field splittings (Table VI) are around 0.4–1 eV (and so are the exchange and many-electron energies of these systems; see Part IV,13).

(7) Spin-orbit energies are around 0.03–0.1 eV.

(8) Jahn–Teller energies are around 0.03–0.08 eV, i.e., of the order of optical phonon energies in semiconductors. [For comparison, note that for shallow *sp*-electron impurities, items (3)–(8) above have characteristic energies in the meV region.]

Clearly, the large spread in characteristic energies presents a difficult challenge to theory in describing the impurity's electronic structure [(3)–(8)] in terms of atomic [(1)] and band-structure [(2)] theories. The "strong interactions" of this problem ($\sim$0.3–60 eV) set up the electronic excitation, ionizations, and splittings; "intermediate-energy interactions" ($\sim$0.1–0.3 eV) are responsible for global lattice distortion effects, whereas the "weak interactions" of this problem ($\leq$0.1 eV) involve spin-orbit, lattice phonons, and Jahn–Teller effects. I will concentrate in this article on the role of the strong and intermediate interactions.

c. Basic Regularities in the data

In this subsection I point to a number of trends suggested by the experimental data surveyed in Part III,3–7 and use these observations to formulate some of the issues that need to be resolved by an electronic-structure theory.[19,39,54]

Figure 9 graphically depicts the ionization energies observed (relative to the host valence-band maximum) in $3d$ impurities in a number of semiconductors (cf. Table VII) arranged as isoelectronic transitions, i.e., $d^N/d^{N\pm1}$. Figure 9a and Table IX contain the same information for the free transition-metal ions.[120] Table IX also provides the experimental Mott–Hubbard Coulomb energies of the free ions in the three oxidation states T^{2+}, T^{3+}, and

[120] C. E. Moore, "Ionization Potentials and Ionization Limits Derived from the Analysis of Optical Spectra." NSRDS-NBS 34, National Bureau of Standards, Washington, D. C., 1971.

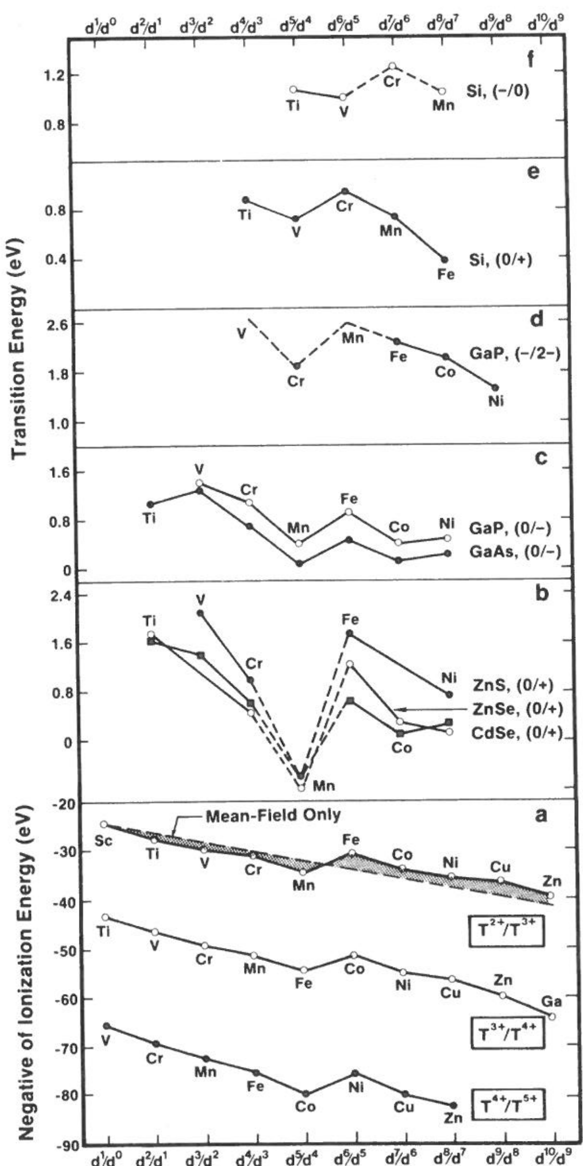

FIG. 9. (a) Observed (Table IX) ionization energies of free $3d$ ions. Note the local minimum at the d^5/d^4 "Hund's point." The dashed line for the T^{2+}/T^{3+} ionization energies represents the mean-field component; the shaded area represents multiplet corrections. Note that Hund's point is created by the different signs of multiplet corrections for the d^5/d^4 and d^6/d^5 transitions. Parts (b)–(f) show the ionization energies of the $3d$ ions as impurities in various semiconductors (Table VII). Dashed lines indicate interpolated values. Data are arranged in an isoelectronic sequence. Hund's point exists in all $3d$ impurities except in Si, where the d^5/d^4 transition (for Ti) is *higher* in the gap then the d^5/d^5 transition (for V). (b) T^{2+}/T^{3+} in II-V; (c) T^{2+}/T^{3+} in III-V; (d) T^{+}/T^{2+} in III-V; (e) T^{0}/T^{+} in Si; (f) T^{0}/T^{-} in Si.

TABLE IX. OBSERVED FREE-ION IONIZATION ENERGIES[a]

Ion	$E(T^{1+}/T^{2+})$		$E(T^{2+}/T^{3+})$		$E(T^{3+}/T^{4+})$		$E(T^{4+}/T^{5+})$		$U(T^{2+})$		$U(T^{3+})$		$U(T^{4+})$	
d^1s^2 Sc	d^2/d^1	—	d^1/d^0	24.76	—	—	—	—	$(d^0/d^1/d^2)$	—	—	—	—	—
d^2s^2 Ti	d^3/d^2	—	d^2/d^1	27.49	d^1/d^0	43.27	—	—	$(d^1/d^2/d^3)$	—	$(d^0/d^1/d^2)$	15.8	—	—
d^3s^2 V	d^4/d^3	—	d^3/d^2	29.31	d^2/d^1	46.71	d^1/d^0	65.23	$(d^2/d^3/d^4)$	—	$(d^1/d^2/d^3)$	17.4	$(d^0/d^1/d^2)$	18.5
d^5s^1 Cr	d^5/d^4	16.50	d^4/d^3	30.96	d^3/d^2	49.1	d^2/d^1	69.3	$(d^3/d^4/d^5)$	14.5	$(d^2/d^3/d^4)$	18.1	$(d^1/d^2/d^3)$	20.2
d^5s^2 Mn	d^6/d^5	—	d^5/d^4	33.67	d^4/d^3	51.2	d^3/d^2	72.4	$(d^4/d^5/d^6)$	—	$(d^3/d^4/d^5)$	17.5	$(d^2/d^3/d^4)$	21.2
d^6s^2 Fe	d^7/d^6	—	d^6/d^5	30.65	d^5/d^4	54.8	d^4/d^3	75.0	$(d^5/d^6/d^7)$	—	$(d^4/d^5/d^6)$	24.2	$(d^3/d^4/d^5)$	20.2
d^7s^2 Co	d^8/d^7	—	d^7/d^6	33.50	d^6/d^5	51.3	d^5/d^4	79.5	$(d^6/d^7/d^8)$	—	$(d^5/d^6/d^7)$	17.8	$(d^4/d^5/d^6)$	28.2
d^8s^2 Ni	d^9/d^8	—	d^8/d^7	35.17	d^7/d^6	54.9	d^6/d^5	75.5	$(d^7/d^8/d^9)$	—	$(d^6/d^7/d^8)$	19.7	$(d^5/d^6/d^7)$	20.6
$d^{10}s^1$ Cu	d^{10}/d^9	20.29	d^9/d^8	36.83	d^8/d^7	55.2	d^7/d^6	79.9	$(d^8/d^9/d^{10})$	16.5	$(d^7/d^8/d^9)$	18.4	$(d^6/d^7/d^8)$	24.7
$d^{10}s^2$ Zn	—	—	d^{10}/d^9	39.72	d^9/d^8	59.4	d^8/d^7	82.6	—	—	$(d^8/d^9/d^{10})$	19.7	$(d^7/d^8/d^9)$	23.2
$d^{10}s^2p^1$ Ga	—	—	—	—	d^{10}/d^9	64	d^9/d^8	—	—	—	—	—	$(d^8/d^9/d^{10})$	—

[a] (C. E. Moore, "Ionization Potentials and Ionization Limits Derived from the Analysis of Optical Spectra" NSRDS-NBS 34, National Bureau of Standards, Washington, D. C., 1971) and the corresponding Coulomb energies $U^{(dd)}(T)$ [Eq. (6.14)], all in eV.

T^{4+} for which sufficient experimental data exist.[120] A cursory look at Fig. 9 reveals significant general similarities between the trends in the free-ion ionization energies and those for the same ions as impurities. All show an overall increase in ionization energy (with respect to the vacuum level) as we proceed from the low-atomic-number (Z) end of the series (Sc, Ti) to the high-Z end (Cu, Zn), and almost all show a local minimum at the d^5/d^4 point (to be referred to as "Hund's point"). This universality highlights once again the usefulness of the phenomenological classification of various impurities in terms of their "d^N" configurations.

Zunger,[16] Katayama-Yoshida and Zunger,[39] and Singh and Zunger[54] have pointed out that the experimental data concerning $3d$ impurities in semiconductors suggest apparently contradictory conclusions on the strength and nature of the impurity–host interactions. I illustrate this by assuming, as a thought experiment, that the crystal environment is only a weak perturbation on the states of the free ion, and I examine the consequences of this assumption *vis à vis* the experimental data.

First, observe that the free-ion ionization energies become larger as Z increases (primarily an electron–nucleus Coulomb attraction effect) at a rate of about 1–3 eV per unit increment in Z. A similar trend is observed in the calculated free-ion orbital energies (Fig. 10a). Since this is also the order of magnitude of typical semiconductor band gaps (Table VII), at this rate no more than a single impurity from anywhere in the $3d$ series can have an ionization level inside the band gap. In fact, Table VII and Fig. 9 show that almost all $3d$ impurities have ionization levels inside the band gaps of most semiconductors. For this to be the case, the rate of change of ionization energies with Z must be reduced in the solid by about an order of magnitude relative to the free-ion values. This implies substantial electronic interaction with the lattice ("bonding"), a phenomenon to be explained by theory (Part VI,18).

Second, observe that the free-ion Mott–Hubbard energies (15–30 eV, Table IX) are far larger than typical semiconducting band gaps. If a given oxidation state of an impurity has an ionization transition inside the band gap of a semiconductor, when ionized further, the level will shift by U, hence, using this range of values, it will be removed from the band gap. Similarly, if an ionization level of a given transition atom exists in the band gap of GaP (T^{3+}, when neutral), it would most likely not exist in the band gap of ZnS (T^{2+}, when neutral). In fact, Table VII shows that most impurities exist in a number of stable oxidation states inside the band gap of the semiconductors (e.g., Cr shows three ionizing transitions, and hence four different oxidation states, inside the band gap of GaP). Furthermore, a given impurity can exhibit ionization levels in the band gaps of various semiconductors having different valences. It is indeed remarkable that, whereas the first four d ionization energies of free transition-metal ions span about 60 eV (Table IX), the

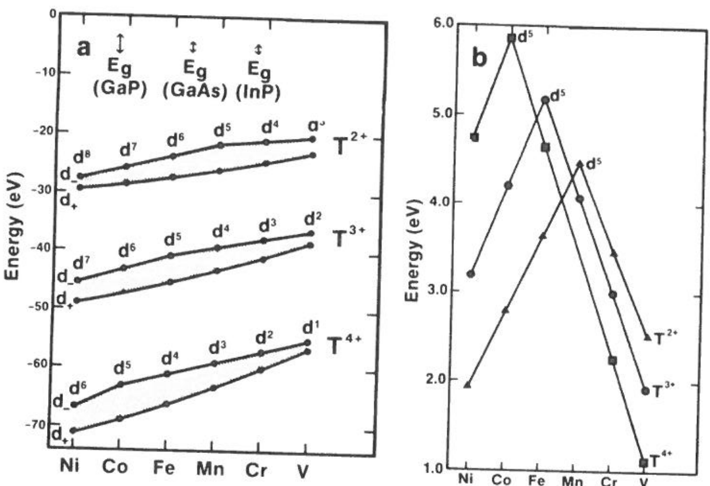

FIG. 10. (a) Calculated one-electron energy levels of free $3d$ ions in the local spin-density (LSD) formalism for spin-up (d_+) and spin-down (d_-); (b) the exchange splitting between spin-up and spin-down $3d$ levels (A. Zunger, unpublished, 1983) (▲, T^{2+}; ●, T^{3+}; ■, T^{4+}). Note in (a) that the one-electron levels rise rapidly as one moves from the Ni end to the V end, and that the levels of a given atom become rapidly deeper as it is ionized. The shaded areas in (a) denote the d_+–d_- exchange splitting. At the top of the figure, typical scales of semiconducting band gaps are shown. Part (b) shows that the exchange splitting has a maximum for the d^5 configurations (Co^{4+}, Fe^{3+}, Mn^{2+}) and that the order of these splitting switches from the Ni end $[\Delta_x(T^{4+}) > \Delta_x(T^{3+}) > \Delta_x(T^{2+})]$ to the V end $[\Delta_x(T^{2+}) > \Delta_x(T^{3+}) > \Delta_x(T^{4+})]$.

corresponding ionization transitions inside a semiconductor are compressed to a range of about 1 eV (Table VII). This implies that some sort of efficient screening mechanism is operative, reducing the effective Mott–Hubbard U of the free ions by up to two orders of magnitude (Table VIII), a striking phenomenon to be dealt with by theory (Part VI,20). (While small effective U's also exist for *sp*-electron impurities, e.g., Si:P,[18] this phenomenon is understandable in light of the very extended nature of these effective-mass-like orbitals. In contrast, $3d$ impurities have small U's even though ENDOR and EPR data suggest their having rather localized orbitals.)

Third, compare the order of magnitude of the absolute ionization energies of impurities in semiconductors to those for the same ions in different media and in free space. For this purpose we need to refer the impurity ionization energy to the vacuum level, rather than to the valence-band maximum (VBM), as done in Fig. 9b–f. This can be done by subtracting the impurity ionization energy relative to the VBM from the separation of the VBM from the vacuum level, i.e., the *intrinsic* semiconductor work function Φ (the intrinsic photo-threshold). Although measured[121–124] values of Φ combine the intrinsic bulk

[121] R. K. Swank, *Phys. Rev.* **153,** 844 (1967); T. E. Fisher, *Phys. Rev.* **142,** 519 (1966); G. W. Gobeli and F. G. Allen, *Phys. Rev.* **137,** 245 (1965).

value with surface contributions, the latter is sufficiently small to be neglected in this rough estimate (see, however, Parts VI,28 and 29). We use the observed[121,122,124] and extrapolated[123] values (in eV)

$$\Phi_{ZnS} = 7.5,^{121} \quad \Phi_{ZnSe} = 6.82,^{121} \quad \Phi_{ZnTe} = 5.76,^{121}$$
$$\Phi_{CdS} = 7.26,^{121} \quad \Phi_{CdSe} = 6.62,^{121} \quad \Phi_{CdTe} = 5.78,^{121}$$
$$\Phi_{InP} = 5.69 - 5.85^{123}\,[(110)\text{ surface}] \tag{8.1}$$
$$\Phi_{GaP} \cong 5.9^{123} - 6.01^{122}\,[(110)\text{ surface}]$$
$$\Phi_{GaAs} = 5.49 - 5.56^{122}\,[(110)\text{ surface}]$$

and

$$\Phi_{Si} = 5.2.^{124}$$

Using these values, and the host-referred binding energies (HRBE) of Table VII, we can find the approximate vacuum-related binding energies (VRBE) as $E_{VRBE} \cong \Phi - E_{HRBE}$. We can then compare these "absolute" ionization energies E_{VRBE} to those in free space (Table IX), or, in the opposite extreme, to ionization energies in a highly polarizable medium like water. For the latter purpose we can use the standard oxidation/reduction ("redox") potentials[125] determined electrochemically relative to a hydrogen reference electrode, and then apply the correction of $\sim 4.2 \pm 0.2$ eV necessary to refer these redox potentials to vacuum.[125,126] Using, for example, the T^{2+}/T^{3+} ionization transition, we find from Eqs. (8.1) and the data of Table VII that the absolute ionization energies of Fe^{2+}/Fe^{3+} are 5.75, 5.6, 5.0, and 5.0 eV, respectively, in ZnS, ZnSe, GaP, and GaAs. The same ionization process in acidic aqueous solution[125] occurs at a very similar energy, 5.3 eV, whereas in free space it occurs at a far higher energy, 30.65 eV (Table IX). For V^{2+}/V^{3+} we find absolute ionization energies of 5.4, 4.3, and 4.2 eV, respectively, in ZnS, GaP, and GaAs; the ionization in aqueous solution[125] is similar—4.2 eV—whereas the free-space ionization energy is again far larger: 29.3 eV. These results are striking: The similarity of the ionization energies in aqueous solution and in semiconductors, and their disparity from the free-space ionization energies indicate that, despite a much larger nominal dielectric constant of water (i.e., *ionic* polarization), a semiconductor medium can screen

[122] J. Van Laar, A. Huijser, and T. L. Van Rooy, *J. Vac. Sci. Technol.* **14,** 894 (1977).

[123] Extrapolated from Figs. 10–13 in W. A. Harrison, "Electronic Structure and Properties of Solids," p. 254. Freeman, San Francisco, 1980.

[124] A. Tharailakis, *Inst. Phys. Conf. Ser. 1974*, p. 59; F. G. Allen and G. W. Gobeli, *J. Appl. Phys.* **35,** 597 (1964).

[125] K. E. Heusler, *in* "Encyclopedia of Electrochemistry of the Elements" (A. J. Bard, ed.). Dekker, New York, 1982.

[126] H. Gerischer and W. Ekart, *Appl. Phys. Lett.* **43,** 393 (1983); H. Reiss, *J. Electrochem. Soc. Solid State Technol. Sci.* **125,** 937 (1978).

(*electronically*) the 3*d* ion as well as water! It is also interesting to observe that Fe^{2+}/Fe^{3+} ionization energies in covalent semiconductors (~ 5.0 eV in III-Vs) are typical of the same ionization process in biological Fe-containing molecules, e.g., cytochrome *C* and heme proteins (~ 5 eV).[127] This effect of strong attenuation in the Coulomb energies is addressed by theory in Parts VI,20, 26, and 27. [Interestingly, the T^{2+}/T^{3+} ionization energies in aqueous solution[125] follow the general structure of Fig. 9a, with a local minimum (i.e., Hund's point) at Mn, e.g., 4.2, 4.1, 6.02, 5.28, and 6.33 eV for V^{2+}/V^{3+}, Cr^{2+}/Cr^{3+}, Mn^{2+}/Mn^{3+}, Fe^{2+}/Fe^{3+}, and Co^{2+}/Co^{3+}, respectively.]

Fourth, the observed effective Mott–Hubbard Coulomb energies for 3*d* impurities in semiconductors (Table VIII) show a progressive decrease from ZnS to Si (i.e., as the covalency of the host crystal increases), implying *chemically specific* screening effects (for the most ionic members of this series, i.e., for NiO, MnO, and CoO, effective Coulomb energies ranging from 2 up to 15 eV have been proposed in the literature,[97,128,129] but no definitive values exist).

Fifth, whereas all free ions and (almost) all 3*d* impurities exhibit a characteristic Hund's point in their d^5/d^4 ionization energies[130] (i.e., relative to vacuum, d^5 is more difficult to ionize than its neighboring configurations due to the extra stability of maxium spin pairing in d^5), the magnitude of this effect can be significantly attenuated for impurities in covalent crystals. This is illustrated in Table X, which depicts the difference in ionization energies $E(d^6/d^5) - E(d^5/d^4)$. 3*d* impurities in semiconductors exhibit the entire range of stabilization, from strong Hund's-rule stabilization (e.g., in ZnS) to none at all (e.g., in Si). This is discussed in Parts VI,20 and 26.

The extra stability of the d^5 state is likewise highlighted by the existence of a maximum in the Mott–Hubbard Coulomb energies involving the d^4-d^5-d^6

[127] E. Margoliash and A. Schejter, *Adv. Protein. Chem.* **21,** 113 (1966); *in* "Haematin Enzymes" (J. E. Falk, R. Lemberg, and R. K. Horton, eds.). Pergamon, Oxford, 1961.

[128] P. W. Anderson, *Phys. Rev.* **79,** 350 (1950); S. Van Houghton, *J. Phys. Chem. Solids* **17,** 7 (1960).

[129] K. Terakura, A. R. Williams, and J. Kübler, *Phys. Rev. B* **30,** 4734 (1984). These authors find a very small Mott-Hubbard U of 1-2 eV in NiO, in contrast with all other determinations (e.g., review in Ref. 96) and recent analysis by R. Merlin, *Phys. Rev. Lett.* **54,** 2727 (1985), where considerably larger (6–10 eV) values are deduced.

[130] It is interesting to observe that this Hund's rule stabilization effect exists also for *p*-orbitals, but it is far weaker than for *d* orbitals. For example, using ionization energies[120] observed for the first row elements, we find:

$E[p^3/p^2, N^{1+}] - E[p^4/p^3, O^{1+}] = 0.9$ eV,

$E[p^3/p^2, O^{2+}] - E[p^4/p^3, F^{2+}] \cong 0.1$ eV,

$E[p^3/p^2, F^{3+}] - E[p^4/p^3, Ne^{3+}] = -0.7$ eV.

Compared with the Hund's rule half-shell stabilization effects in the 3d series (Table X), these effects are considerably reduced. The local maximum in the observed impurity binding energies at the half-shell point is indeed characteristic of d-electron impurities and not sp-electron impurities.

TABLE X. OBSERVED DIFFERENCES IN d^6/d^5 AND d^5/d^4 IONIZATION ENERGIES[a]

Oxidation states	Elements	Host crystal	Type of transition	$E(d^6/d^5) - E(d^5/d^4)$ (eV)
T^{4+}/T^{5+}	Co–Ni	Free-ion	—	4.0
T^{3+}/T^{4+}	Fe–Co	Free-ion	—	3.5
T^{2+}/T^{3+}	Mn–Fe	Free-ion	—	3.0
T^{2+}/T^{3+}	Mn–Fe	ZnS	(0/+)	>1.75
T^{2+}/T^{3+}	Mn–Fe	ZnSe	(0/+)	>1.25
T^{2+}/T^{3+}	Mn–Fe	CdSe	(0/+)	>0.64
T^{2+}/T^{3+}	Mn–Fe	GaP	(−/0)	0.46
T^{2+}/T^{3+}	Mn–Fe	GaAs	(−/0)	0.38
T^{2+}/T^{3+}	Mn–Fe	InP	(−/0)	0.58
T^0/T^+	V–Cr	Si	(0/+)	0.23
T^0/T^-	Ti–V	Si	(−/0)	−0.08

[a] Hund's-rule stabilization energies. Note that Hund's rule is not satisfied for the acceptor series in Si.

configurations of free ions; i.e., at $U(T^{3+}) = 24.2$ eV for Fe and at $U(T^{4+}) = 28.2$ eV for Co (Table IX). According to Eqs. (6.14) and (6.15), this suggests that the reaction $d^4 + d^6 \rightarrow 2d^5$ is particularly exothermic (e.g., by 7–8 eV more than the reaction $d^3 + d^5 \rightarrow 2d^4$). This reduction in U for the d^3-d^4-d^5 system relative to d^4-d^5-d^6 reflects the gain in (negative) exchange energy in the d^5 configuration. Table IX shows this effect to be particularly strong in the Cr^{2+} ion ($U = 14.5$ eV) relative to the Mn^{2+} ion ($U = 17.5$ eV) and Fe^{2+}($U = 20.2$ eV). The implications of this exchange reduction of U on impurity physics will be addressed in Part VI,27.

Sixth, despite the fact that the first few *ionization* transitions of the impurity are compressed into a far narrower energy range than the corresponding free-ion ionization transitions, *internal* $d \rightarrow d^*$ *excitations* of the free ion and the impurity span roughly the same energy range. Furthermore, clear trends towards reduction of the $d \rightarrow d^*$ transition energies with increasing covalency of the host crystal (Table V) are apparent; e.g., the second ${}^4A_2 \rightarrow {}^4T_1$ transition of Co^{2+} occurs at 2.04, 1.76, 1.67, and 1.50 eV, in ZnO, ZnS, ZnSe, and GaP, respectively. These chemical trends and the far smaller "spectral compression" of the $d \rightarrow d^*$ *excitation* energies (which conserve charge) relative to *ionizing* transitions (which carry a net charge and are hence screened) provide another issue to be dealt by electronic-structure theory (Parts IV,14 and VI,20).

Seventh, an examination of the many-electron crystal-field splittings of Table VI reveals that they constitute a significant fraction of the band gap

TABLE XI. OBSERVED HYPERFINE CONSTANTS A IN A SERIES OF MATERIALS[a]

Impurity	CaO[b]	ZnS	InP	GaP	GaAs	Si
V^{2+}	76.1	40–49	—	—	—	42.1
Mn^{2+}	80.7	64.5	52.0	53.5	52.4	53.5
Fe^{+}	33.9	—	—	—	—	3.0

[a] In 10^{-4} cm^{-1}. Data from Tables I–IV. Results for Si pertain to interstitial T_d impurities, those for CaO pertain to substitutional O_h impurities; all others are substitutional T_d impurities.
[b] Values given by B. Henderson and J. E. Wertz.

(~15–17% in ZnS, up to 37% in GaP) and increase as the covalency of the host crystal increases. Such sizeable effects of the crystalline environment on the free-ion states are indicative of substantial host–impurity interactions.

Eighth, an examination of the spin values deduced from EPR (e.g., results for 3*d* impurities in Si given in Table II) shows that for all impurities measured to date which can be distinguished according to high and low spin values, a high-spin (Hund's-rule) value has been found. (Notice, however, that in some cases low-spin configurations can be more difficult to detect by EPR; e.g., for d^5, the high-spin $^6A_1$ is readily observed, but the low-spin $^2T_2$ is less commonly observed; cf. Tables III and IV.) For these impurities, then, the exchange splitting Δ_x [Eq. (2.17)] must dominate over crystal-field energies Δ_{CF} [Eq. (2.16)]. Hence, despite the fact that Coulomb interelectronic repulsions are reduced substantially in the solid, exchange interactions (2–5 eV in free 3*d* ions, depicted in Fig. 10b) must necessarily remain reasonably high to prefer the Hund's-rule high-spin ground state.

Ninth, a comparison of the observed central hyperfine coupling constants of 3*d* impurities in semiconductors and in ionic crystals (Table XI) reveals a substantial reduction of the former values with respect to the latter (which are, in turn, close to the calculated[131] *free-ion* values). For example, the reduction factors η for GaAs:$^{61}V^{3+}$ and ZnS:$^{51}V^{3+}$ (obtained from calculated atomic values[131] and observed solid-state values) are $\eta = 0.6$ and 0.7, respectively. For $^{55}Mn^{2+}$ in GaAs, GaP, and InP we have $\eta \cong 0.6$. For $^{53}Cr^{+}$, $^{55}Mn^{2+}$, and $^{57}Fe^{3+}$ in ZnS, we have, respectively, $\eta = 0.8, 0.7$, and 0.7, and for Si:$^{57}Fe^{0}$, we have $\eta \cong 0.4$. This suggests that, despite the occurrence of a maximum-spin ground state, the spin *density* of 3*d* impurities in semiconductors must be partially delocalized throughout the crystal. This is also suggested by ENDOR experiments.[40–46] Such reductions in hyperfine coupling constants correlate well with the covalency of the host crystal. For example, Fig. 11a

[131] A. J. Freeman and R. E. Watson, *Phys. Rev. Lett.* **5**, 498 (1960).

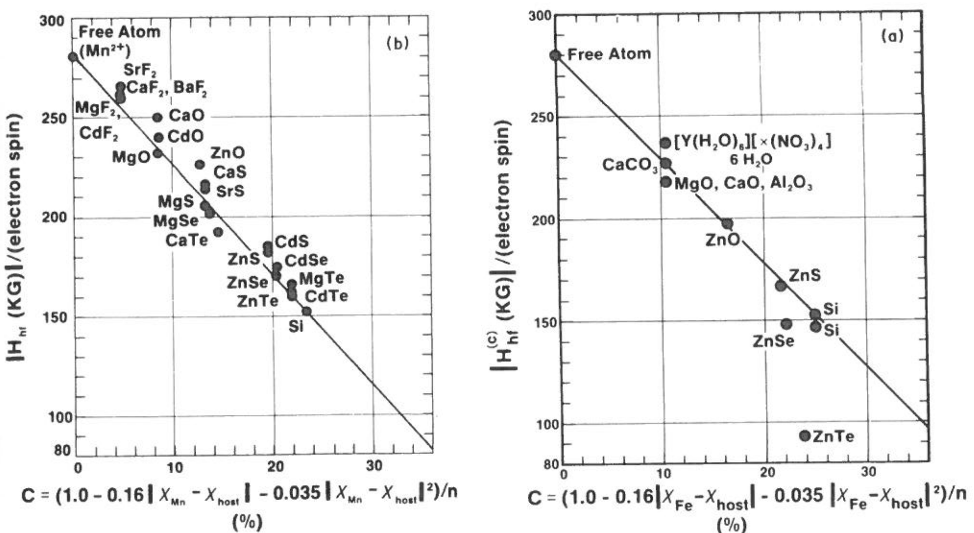

FIG. 11. Chemical trends in the observed hyperfine field of (a) Fe and (b) Mn impurities in various host crystals, as a function of an empirical electronegativity scale. See J. C. Henning, *Phys. Lett.* **24A**, 40 (1967); and E. Simanek and K. A. Müller, *J. Phys. Chem. Solids* **31**, 1027 (1970) for data.

shows the experimentally observed[132] hyperfine field of Fe impurity nuclei per electron spin S in various systems, and Fig. 11b shows similar trends for the Mn impurity. The horizontal axis depicts covalency evaluated from Gordy's and Thomas's electronegativity[132] using empirical equations.[132,133] From these results, we can conclude that the absolute value of the hyperfine field decreases as covalency increases. The hyperfine field H_{hf} of the Fe impurity in an ionic crystal (e.g., Fe in $CaCO_3$, MgO, CaO, and Al_2O_3 in Fig. 11) is very close to the H_{hf} of the free atom obtained in Hartree–Fock calculations.[131] Likewise, spin–orbit interactions manifested both in the g values and in the splittings observed in absorption and luminescence appear to be reduced significantly in the solid (Part III,6), again suggesting a strong impurity–host coupling.

Tenth, a survey of the Jahn–Teller energies deduced experimentally for 3*d* impurities in semiconductors (Part III,7) shows them to be generally small compared with JT energies of non-*d* impurities and defects in semiconductors,[17,134] e.g., the neutral vacancy (V^0_{ac}) in diamond ($E_{JT} = 0.6$ eV for the E mode and >0.7 eV for the T mode) or in silicon ($E_{JT} = 0.4$ eV for the E mode

[132] J. C. Henning, *Phys. Lett.* **24A**, 40 (1967).
[133] W. Gordy and W. J. O. Thomas, *J. Chem. Phys.* **24**, 439 (1956).
[134] G. D. Watkins, *in* "Deep Levels in Semiconductors" (S. Pantelides, ed). in press.

of Si:V_{ac}^{+}, E_{JT} = 1.5 eV for the same mode in Si:V_{ac}^{0}, and E_{JT} = 2.1 eV for the combined $E + T$ mode in the negatively charged vacancy.) Particularly striking is the fact that for Si:$3d_i$ there is apparently no static JT distortion of any of the "Jahn–Teller ions," which suggests vanishingly small JT energies. This suggests that in the competition between exchange effects (stabilizing the undistorted configuration with the maximum number of parallel spins possible) and JT distortion effects, the former overwhelm the latter.

Eleventh, Tables II–IV, depicting observed g values (g_{expt}) and their spin-only part g_S (Table II), suggest a quenching of the angular-momentum contribution g_L (nonzero only for $L = 1$), i.e., that $g_{expt} \approx g_S$. Since this appears to be a universal feature of all $L \neq 0$ centers, Ham[35] suggested that the origin of this effect must also be universal. Since covalency effects were not considered at that time to be shared universally by all impurities, an additional mechanism for quenching g_L was proposed—the dynamic Jahn–Teller effect. However, a quantitative calculation of g such as that reported by Yamaguchi and Kamimura[103] (see also Clerjaud and Gelineau[101]) for Cu^{2+} in II-VI's has not been attempted to support this point of view. [Typically,[98–99] the quenching of g, e.g., for the d^9, $^2T_2$ system (Tables III and IV), or the d^4, $^3T_1$ system (Table II) is attributed to a combination of covalent reduction and dynamic effects, but no first-principles calculations of covalency effects have been attempted to substantiate its relative importance.] Explaining the chemical trends apparent in g_{exp} and the quenching of g_L is therefore another challenge to be addressed by electronic-structure theory (Part VI,25).

9. Puzzles and the Dual Characteristics of 3d Impurities in Semiconductors

The foregoing observations of the trends in the physical and chemical properties of $3d$ impurities in semiconductors have suggested[16,19,39,54] a paradoxical situation: both a picture of a covalently delocalized impurity, interacting strongly with the crystal, and its opposite: that of an atomically localized impurity, perturbed only weakly by the lattice. This should be contrasted with the classical viewpoint, which[1,12] described $3d$ impurities in semiconductors using the concepts that were developed for *localized* $3d$ impurities in ionic crystals.

Arguing for the covalently delocalized model, I note the following:

(1) The substantial reduction in the slope of the ionization energies with atomic number relative to free ions suggests the formation of chemical bonds.

(2) The one-to-two-orders-of-magnitude reduction in the Mott–Hubbard Coulomb energies suggests very efficient screening.

(3) The similarity of the absolute ionization energy in the solid to those observed in strongly polarizable (e.g., aqueous) media also suggests strong screening and impurity–host coupling.

(4) The relatively large crystal-field energies indicate substantial impurity–host interactions.

(5) The significant reduction in central hyperfine-coupling constants relative to free ions or $3d$ impurities in highly ionic crystals suggests covalency.

(6) The observation by ENDOR of a delocalization in the spin densities up to the fifth shell of neighbors (up to 40% of the spin density can be outside the impurity cell) suggests impurity–host (exchange) coupling.

(7) The quenching of the angular-momentum parts of the g values suggests covalency as a possible mechanism.

(8) The strong reduction of spin-orbit effects in the solid suggests covalency, in addition to dynamic coupling effects.

(9) The near constancy of the Mössbauer isomer shift in different charge states suggests that the host crystal resupplies the impurity with s electrons when the latter are ionized, i.e., again a manifestation of impurity–host interaction.

Arguing for the opposite, the atomically localized model, I note the following:

(1) The atomiclike multiplet structure (indicative of localized states) is largely retained in the solid, with similar ranges of $d \rightarrow d^*$ excitation energies as in free ions.

(2) The existence of atomiclike high-spin (Hund's-rule) ground states, suggesting that, as large as crystal-field effects may be, exchange effects usually outweigh them.

(3) The existence of only small (or vanishing) JT energies suggests the dominance of (localization-induced) exchange interactions over symmetry-lowering elastic deformation.

(4) The appearance of most of the spin density near the impurity site suggests that, at least inside the central cell, the spin density is atomically localized.

(5) The occurrence of a strong half-shell d^5/d^4 stabilization, like that in the free $3d$ ions, suggests that much of the atomic characteristics are preserved in the solid.

(6) The occurrence of different thermal and optical ionization energies suggests that sufficient localization must exist to induce occupation-dependent lattice-relaxation effects.

(7) The great similarity between $d \rightarrow d^*$ excitation energies of $3d$ impurities in zincblende and wurtzite II-VI semiconductors[15] (which differ in their coordination structure only beyond the second shell of neighbors) suggests that the impurity wave functions may be localized.

Electronic-structure theory is faced with the task of resolving this apparent paradoxical behavior (Part VI).

IV. Theoretical Content of Excitation and Ionization Energies

10. Mean-Field, Many-Electron, and Relaxation Contributions

Considerable ambiguity exists in the literature regarding the interpretation of the observed excitation and ionization energies of impurities in terms of electronic-structure models. I describe here the physical content of these observables in terms of calculable quantities. Comparisons of theory and the relevant observed quantities are given in Part VI,26.

The excitation and ionization energies of Eqs. (6.2), (6.4), (6.7), and (6.9) correspond to differences in the total many-electron energies $E_T^{(i)}$ of the initial and final states. Many of the currently available electronic-structure models calculate only a piece of $E_T^{(i)}$, i.e., its mean-field component. Moreover, such calculations are often restricted to a fixed lattice geometry. Spin- and space-restricted electronic-structure calculations for both bulk solids and point impurities have traditionally made strong commitments to the one-electron viewpoint of such systems. This commitment is rooted in the fundamental computational strategy chosen: Largely because of computational ease, the spin- and space-restricted (hereafter referred to as mean-field, or MF) calculations of systems with incomplete one-electron levels restrict the one-particle charge density to the symmetry of the underlying nuclear framework [i.e., to the totally symmetric a_1 representation of the physical symmetry group; cf., Eqs. (2.1)–(2.8) for T_d symmetry]. This means that, if N electrons are available to occupy a degenerate level that can accommodate a larger number $\bar{N}$ of electrons, one constructs the one-particle charge density using a procedure equivalent to assigning $N/\bar{N}$ electrons to each of the $\bar{N}$ partners. By Unsöld's theorem the charge density constructed in this way is totally symmetric. This procedure, common to many contemporary calculations of atoms,[135] bulk metals,[136] and impurities,[13,17,19,137] constitutes an enormous computational simplification, since all different arrangements of electrons

[135] F. Herman and S. Skillman, Atomic Structure Calculations." Prentice-Hall, New York, 1963; C. Frose-Fisher, "Hartree–Fock Method for Atoms." Wiley (Interscience), New York, 1977.

[136] V. L. Moruzzi, J. F. Janak, and A. R. Williams, "Calculated Electronic Properties of Metals." Pergamon, New York, 1978.

[137] (a) G. A. Baraff and M. Schlüter, *Phys. Rev. B* **19**, 4965 (1979); G. A. Baraff, E. O. Kane, and M. Schlüter, *Phys. Rev. B* **21**, 5662 (1980); (b) J. Bernholc, N. Lipari, and S. T. Pantelides, *Phys. Rev. B* **21**, 3545 (1980).

being explored share the same simplest form of a highly symmetric one-particle density and potential. Since the a_1-symmetric density *is* incorporated in the total energy, *average* multiplet effects (analogous to the Racah parameter A in atoms[8]) are included. However, this a_1 symmetrization of the charge density deprives the system of much of the stabilization effects of spatial correlation energy since it does not allow different electron orbits to get out of each other's way by occupying spatially distinct and variationally independent orbitals (e.g., t_x or t_y or t_z rather than their average). The spin part of this correlation energy can be represented approximately by spin-polarized calculations, e.g., as in Fig. 10. The piece of the charge density that is omitted from mean-field calculations (e.g., the non-totally-symmetric density) is responsible for two (generally competing) effects in impurity physics: Jahn–Teller (JT) distortion and multiplet splitting. Mean-field calculations, however, do not provide direct information on the magnitude or importance of many-electron effects, except in an *a posteriori* fashion when success or failure in reproducing experimental data is analyzed. This suggests that it is useful to attempt a separation of the total many-electron energy $E_T^{(i)}$ of Eqs. (6.3), (6.4), (6.7), and (6.9) into MF and multiplet correction (MC) components[138]; i.e.,

$$E_T^{(i)} = E_{MF}^{(N)}[d^N, A^q, e^m t_2^n, (VB)^M, (CB)^P] + E_{MC}^{(N,i)}[d^N, A^q, e^m t_2^n, (VB)^M, (CB)^P, {}^{2S+1}\Gamma]. \quad (10.1)$$

Here the first term denotes the total *mean-field* energy of the N-electron system ($N = m + n + M + P$) in the formal charge state q with the configuration $e^m t_2^n$ of the gap levels, M electrons in the valence band (VB) and P electrons in the conduction band (CB). Contemporary electronic-structure models are able to calculate this quantity at different levels of computational sophistication (to be reviewed in Part V). The second term denotes the *correction* due to explicit *many-electron* (*multiplet*) effects with respect to their *average* (which is included in $E_{MF}^{(N)}$). This quantity is rarely calculated. In Part IV,12, I describe a new formalism due to Fazzio *et al.*[138] (FCZ) that can be used either to calculate this quantity from first principles or to extract it from the experimental data; the relative magnitude of the two terms in Eq. (10.1) will then be discussed. (Since I will conclude that multiplet effects are significant, I will retain this term here.) I next describe the type of physical effects included in contemporary calculations of the mean-field energy $E_{MF}^{(N)}$.

The basic structure of contemporary mean-field theories of localized impurities (Part V) involves a bare Hamiltonian of the type

$$\hat{H}_0 = -\tfrac{1}{2}\nabla^2 + V_{ext}^{H}(\mathbf{r}) + \Delta V_{ext}(\mathbf{r}), \quad (10.2)$$

[138] A. Fazzio, M. J. Caldas, and A. Zunger, *Phys. Rev. B* **30**, 3430 (1984); **29**, 5999 (1984), and unpublished results.

and an a_1-averaged interelectronic Hamiltonian of the type

$$\langle \hat{H}_1 \rangle = V^{\mathrm{H}}_{\mathrm{scr}}(\mathbf{r}) + \Delta V_{\mathrm{scr}}(\mathbf{r}). \tag{10.3}$$

Here, $V^{\mathrm{H}}_{\mathrm{ext}}(\mathbf{r})$ is the host (H) crystal external potential (e.g., electron–ion interaction or host pseudopotential) and $\Delta V_{\mathrm{ext}}(\mathbf{r})$ is the external *perturbation* caused by the impurity (e.g., the difference in electron–ion interactions, or pseudopotentials of the impurity atom and the host atom being replaced, including possible changes in lattice coordinates). Green's-function models use a periodic $V^{\mathrm{H}}_{\mathrm{ext}}(\mathbf{r})$, whereas cluster models employ only a truncated piece of it. $V^{\mathrm{H}}_{\mathrm{scr}}(\mathbf{r})$ represents the screening (scr) response of the host electrons to the host external potential $V^{\mathrm{H}}_{\mathrm{ext}}(\mathbf{r})$, and is usually obtained from self-consistent-cluster or band-structure calculations as a functional of the host-crystal electronic charge density $\rho^{\mathrm{H}}(\mathbf{r})$. $\Delta V_{\mathrm{scr}}(\mathbf{r})$ represents the impurity-induced *perturbation* in the *screening* potential (including Coulomb and exchange-correlation effects) and is associated with the corresponding impurity-induced change in the charge density $\Delta\rho(\mathbf{r})$. Given a total external potential of the form

$$V_{\mathrm{ext}}(\mathbf{r}) = V^{\mathrm{H}}_{\mathrm{ext}}(\mathbf{r}) + \Delta V_{\mathrm{ext}}(\mathbf{r}), \tag{10.4}$$

different one-electron models seek MF solutions for the total electronic charge density

$$\rho(\mathbf{r}) = \rho^{\mathrm{H}}(\mathbf{r}) + \Delta\rho(\mathbf{r}) \tag{10.5}$$

(for a particular one-electron configuration) and for the corresponding total screening potential

$$V_{\mathrm{scr}}(\mathbf{r}) = V^{\mathrm{H}}_{\mathrm{scr}}(\mathbf{r}) + \Delta V_{\mathrm{scr}}(\mathbf{r}). \tag{10.6}$$

Both $\rho(\mathbf{r})$ and $V_{\mathrm{scr}}(\mathbf{r})$ include contributions from band-gap levels as well as valence-band resonances. These define the total mean-field energy $E^{(N)}_{\mathrm{MF}}$ for the particular electronic configuration $[d^N, A^q, e^m t_2^n, (\mathrm{VB})^M, (\mathrm{CB})^P]$ assumed in constructing $\langle H_1 \rangle$ and for the particular atomic positions assumed in constructing $V_{\mathrm{ext}}(\mathbf{r})$. For example, in the local-density formalism[139]

$$E^{(N)}_{\mathrm{MF}} = \sum_{\alpha}^{\mathrm{occ}} N_\alpha \epsilon_\alpha(N) + \int \rho(\mathbf{r})[V_{\mathrm{xc}}(\mathbf{r}) - \tfrac{1}{2}V_{ee}(\mathbf{r})]\,d\mathbf{r} + E_{\mathrm{xc}}[\rho(\mathbf{r})] + \frac{1}{2}\sum_{a\neq b}\frac{Z_a Z_b}{|\mathbf{R}_a - \mathbf{R}_b|}, \tag{10.7}$$

where N_α are the occupation numbers; $\epsilon_\alpha(N)$ are the one-electron orbital energies of Eq. (2.15), V_{xc} and V_{ee} are, respectively, the exchange-correlation (xc) and interelectronic (*ee*) Coulomb screening potentials, and E_{xc} is the total exchange-correlation energy.[139] $E^{(N)}_{\mathrm{MF}}$ constitutes a solution to the $\hat{H}_0 + \langle \hat{H}_1 \rangle$

[139] W. Kohn and L. J. Sham, *Phys. Rev.* **140** A1133 (1965); P. Hohenberg and W. Kohn, *Phys. Rev.* **136,** 864 (1964).

problem and leaves out the multiplet correction which corresponds to the deviations of the actual interelectronic interactions from their average, i.e., $\hat{H}_1 - \langle \hat{H}_1 \rangle$. (The popular Tanabe–Sugano approach,[9] on the other hand, seeks directly parametrized solutions to the $\hat{H}_0 + \hat{H}_1$ problem, and hence makes no contact with the results of mean-field calculations which address the $\hat{H}_0 + \langle \hat{H}_1 \rangle$ problem.) In MF calculations, the total energy $E^{(N)}_{\mathrm{MF}}$ and the orbital energies $\epsilon_\alpha(N)$ depend on the occupation numbers, and hence on the formal charge (non-self-consistent models, e.g., the standard empirical tight-binding method, neglect this dependence). $E^{(N)}_{\mathrm{MF}}$ also depends on the displacements $\mathbf{Q}$ of the atoms in the system; i.e.,

$$E^{(N)}_{\mathrm{MF}} = E^{(N)}_{\mathrm{MF}}[\rho(\mathbf{r}, \mathbf{Q}), \mathbf{Q}]. \tag{10.8}$$

The multiplet correction $E^{(N,i)}_{\mathrm{MC}}$ depends as well on the displacements. However, I will treat this dependence explicitly only for the mean-field energy, since multiplet corrections will subsequently be (Part IV,12) determined from optical data, where the initial and final states occur at the same (Franck–Condon) configuration. A second-order expansion of $E^{(N)}_{\mathrm{MF}}$ in the displacements $\{Q_\gamma\}$ away from some reference configuration $Q_\gamma = 0$ yields

$$E^{(N)}_{\mathrm{MF}}(\{Q_\gamma\}) = E^{(N)}_{\mathrm{ver}} - \sum_{\gamma} Q_\gamma(N) f_\gamma(N) + \frac{1}{2}\sum_{\gamma}\sum_{\varepsilon} Q_\gamma(N) Q_\varepsilon(N) k_{\gamma\varepsilon}(N), \tag{10.9}$$

where $f_\gamma(N)$ is the linear force along γ for the N-electron system and $k_{\gamma\varepsilon}(N)$ is the force-constant matrix for this state. The first term, $E^{(N)}_{\mathrm{ver}} = E^{(N)}_{\mathrm{ver}}[A^q, e^m t_2^n, (\mathrm{VB})^M, (\mathrm{CB})^P]$, is the vertical (ver) mean-field total energy, corresponding to the *undistorted* system with the one-electron configuration denoted in Eq. (10.1). The displacement $Q_\gamma(N)$ depends on the occupation numbers N (hence, formal charge) and can represent both symmetric breathing-mode (b) distortions and symmetry-lowering Jahn–Teller (JT) deformations. The deformations Q need not be restricted to small amplitudes, since the total force $\mathbf{F}_\gamma(Q, N)$ can be calculated in practice[140] as a gradient of the total energy

$$\mathbf{F}_\gamma(Q, N) = -\nabla_\gamma E^{(N)}_{\mathrm{MF}}[\rho(\mathbf{r}, \mathbf{Q}), \mathbf{Q}]. \tag{10.10}$$

The solutions of $\mathbf{F}_\gamma(Q, N) = 0$ provide the equilibrium geometry $\{Q^{\mathrm{eq}}_\gamma(N)\}$ of the N-electron mean-field system in a given one-electron configuration. Practical methods for solving this problem are discussed in Ref. 140; results are given in Part VI,23. From Eq. (10.9) we then have the equilibrium (eq) geometry, in a diagonal, normal-mode representation of the force-constant matrix, as

$$Q^{\mathrm{eq}}_\gamma(N) = f_\gamma(N)/k_{\gamma\gamma}(N), \tag{10.11}$$

[140] U. Lindefelt and A. Zunger, *Phys. Rev. B* **30,** 1102 (1984); ibid *J. Phys. C* **17,** 6047 (1984); U. Lindefelt, *Phys. Rev. B* **28,** 4510 (1983).

and the equilibrium mean-field energy of the N-electron system,

$$E_{\mathrm{MF,eq}}^{(N)} = E_{\mathrm{ver}}^{(N)} - \sum_{\gamma} \frac{f_{\gamma}^{2}(N)}{2k_{\gamma\gamma}(N)} \equiv E_{\mathrm{ver}}^{(N)} + E_{\mathrm{rel}}^{(N)} \tag{10.12}$$

where $E_{\mathrm{rel}}^{(N)}$ represents the relaxation (rel) energy of the N-electron system. The total equilibrium many-electron energy of the state $(N,i) = [T^{N_{\mathrm{H}}+q}, d^{N}, A^{q}, e^{m}t_{2}^{n}, (\mathrm{VB})^{M}, (\mathrm{CB})^{P}, {}^{2S+1}\Gamma]$ can now be expressed as

$$E_{\mathrm{T}}^{(i)} = E_{\mathrm{ver}}^{(N)} + E_{\mathrm{rel}}^{(N)} + E_{\mathrm{MC}}^{(N)}. \tag{10.13}$$

Differences of $E_{\mathrm{T}}^{(i)}$ for various states i constitute the excitation and ionization energies compiled in Tables V and VII. This is illustrated next.

(1) The excitation energy of internal transitions in a frozen (Franck–Condon) lattice, pertinent to absorption experiments, is given as

$$\Delta^{(ij)} = \Delta_{\mathrm{eff}}^{(N)}[mn, m'n'] + \Delta E_{\mathrm{MC}}^{(N,N)}(i, j), \tag{10.14}$$

where the "effective crystal-field splitting" for the N-electron system is the total mean-field energy that separates the two configurations $e^{m}t_{2}^{n}$ and $e^{m'}t_{2}^{n'}$ in a fixed geometry and charge state; i.e.,

$$\Delta_{\mathrm{eff}}^{(N)}[mn; m'n'] = E_{\mathrm{ver}}^{(N)}[d^{N}, A^{q}, e^{m}t_{2}^{n}] - E_{\mathrm{ver}}^{(N)}[d^{N}, A^{q}, e^{m'}t_{2}^{n'}]. \tag{10.15}$$

$\Delta E_{\mathrm{MC}}^{(N,N)}(i, j)$ represents the change in many-electron corrections for a charge-conserving excitation between multiplets i and j (with the dominant one-electron configurations $e^{m}t_{2}^{n}$ and $e^{m'}t_{2}^{n'}$, respectively); i.e.,

$$\Delta E_{\mathrm{MC}}^{(N,N)}(i, j) = E_{\mathrm{MC}}^{(N,i)}[d^{N}, A^{q}, e^{m}t_{2}^{n}, {}^{2S+1}\Gamma] - E^{(N,j)}[d^{N}, A^{q}, e^{m'}t_{2}^{n'}, {}^{2S'+1}\Gamma']. \tag{10.16}$$

Notice that Δ_{eff} is different from the one-electron crystal-field splitting Δ_{CF} of Eq. (2.16) and from the many-electron crystal-field splitting Δ_{ME} of Eqs. (2.10)–(2.21) [the latter is simply $\Delta^{(ij)}$ of Eq. (10.14) for specific i and j values given in Eqs. (2.14)–(2.21)]. Since Koopmans' theorem is not used in its evaluation, Δ_{eff} does not correspond to a difference in orbital energies. Furthermore, Δ_{eff} is expressed as a difference of two independently calculated *total* energies; hence, it incorporates the change in one-electron energies as well as Coulomb and exchange-correlation energies of *all orbitals in the system*: gap levels as well as valence-band resonances.

(2) The energy of a donor ionization transition between multiplets i and j corresponding to $A^{q}(N)$ and $A^{q+1}(N-1)$ is given as

$$E^{(\alpha)}(q/q+1) = \Delta E_{\mathrm{ver}}^{(N,N-1)}(\alpha) + \Delta E_{\mathrm{rel}}^{(N,N-1)}(\alpha) + \Delta E_{\mathrm{MC}}^{(N,N-1)}(i, j), \tag{10.17}$$

where orbital α is ionized. Here, the change in the vertical mean-field energy (e.g., for a donor-electron emission to the conduction band) is

$$\Delta E_{\mathrm{ver}}^{(N,N-1)}(\alpha) = E_{\mathrm{ver}}^{(N)}[d^{N-1}, A^{q}, \alpha^{N-1}, (\mathrm{CB})^{1}] - E_{\mathrm{ver}}^{(N-1)}[d^{N}, A^{q+1}, \alpha^{N}, (\mathrm{CB})^{0}]. \tag{10.18}$$

$\Delta E_{\mathrm{rel}}^{(N,N-1)}(\alpha)$ and $\Delta E_{\mathrm{MC}}^{(N,N-1)}(i, j)$ are the corresponding differences in relaxation and multiplet correction energies, respectively.

(3) The energy of an acceptor ionization transition between multiplets i and k corresponding to $A^{q}(N)$ and $A^{q-1}(N+1)$ is likewise

$$E^{(\beta)}(q - 1/q) = \Delta E_{\mathrm{ver}}^{(N+1,N)}(\beta) + \Delta E_{\mathrm{rel}}^{(N+1,N)}(\beta) + \Delta E_{\mathrm{MC}}^{(N+1,N)}(k, i), \tag{10.19}$$

where the vertical mean-field component (e.g., for an acceptor electron capture from the conduction band) is

$$\Delta E_{\mathrm{ver}}^{(N+1,N)}(\beta) = E_{\mathrm{ver}}^{(N+1)}[d^{N+1}, A^{q-1}, \beta^{N+1}, (\mathrm{CB})^{0}] - E_{\mathrm{ver}}^{(N)}[d^{N}, A^{q}, \beta^{N}, (\mathrm{CB})^{1}]. \tag{10.20}$$

(4) The diagonal Mott–Hubbard energy of Eq. (6.15) is hence

$$U^{(\alpha\alpha)}(A^{q}) = [\Delta E_{\mathrm{ver}}^{(N+1,N)}(\alpha) - \Delta E_{\mathrm{ver}}^{(N,N-1)}(\alpha)] + [\Delta E_{\mathrm{rel}}^{(N+1,N)}(\alpha) - \Delta E_{\mathrm{rel}}^{(N,N-1)}(\alpha)] + [\Delta E_{\mathrm{MC}}^{(N+1,N)}(k,i) - \Delta E_{\mathrm{MC}}^{(N,N-1)}(i, j)], \tag{10.21}$$

or

$$U^{(\alpha\alpha)}(A^{q}) = U_{\mathrm{ver}}^{(\alpha\alpha)}(A^{q}) + \Delta U_{\mathrm{rel}}^{(\alpha\alpha)}(A^{q}) + \Delta U_{\mathrm{MC}}^{(ijk)}(A^{q}). \tag{10.22}$$

In a useful approximation,[141] the force $f_{\gamma}(N)$ of Eq. (10.9) is assumed to depend linearly on the number of electrons that provide coupling to the lattice. Assuming that $n(N)$ out of N "active" electrons can couple to the lattice mode γ, then[141]

$$f_{\gamma}(n(N)) = f_{\gamma}(0) + n(N)V_{\gamma}, \tag{10.23}$$

where V_{γ} is the electron–lattice coupling coefficient for the γth mode. It is, further, customary to assume[137a,141] that $k_{\gamma\gamma}(N)$ does not depend on N. Defining the occupation-induced and zero-occupation γ-mode elastic deformation energies per electron as

$$\hat{E}_{\gamma} \equiv V_{\gamma}^{2}/2k_{\gamma\gamma} \quad \text{and} \quad E_{\gamma}(0) = f_{\gamma}^{2}(0)/2k_{\gamma\gamma}, \tag{10.24}$$

respectively, and the equilibrium γ-mode displacement at zero occupation [Eq. (10.11)] as

$$Q_{\gamma}^{\mathrm{eq}}(0) = f_{\gamma}(0)/k_{\gamma\gamma}, \tag{10.25}$$

[141] R. Englman, "The Jahn Teller Effect In Molecules and Crystals" Wiley (Interscience), London, 1972.

the various relaxation energies of Eqs. (10.13), (10.17), (10.19), and (10.22) are

$$E_{\rm rel}^{(N)} = -\sum_{\gamma} [n^2(N)\hat{E}_{\gamma} + E_{\gamma}(0) + n(N)V_{\gamma}Q_{\gamma}^{\rm eq}(0)], \quad (10.26)$$

$$\Delta E_{\rm rel}^{(N,N')} = -\sum_{\gamma} \{(n^2(N) - n^2(N')]\hat{E}_{\gamma} + [n(N) - n(N')]V_{\gamma}Q_{\gamma}^{\rm eq}(0)\}, \quad (10.27)$$

$$\Delta U_{\rm rel} = -\sum_{\gamma} \hat{E}_{\gamma}[n^2(N+1) + n^2(N-1) - 2n^2(N)] \equiv -\sum_{\gamma} \hat{E}_{\gamma}N_{\rm eff}, \quad (10.28)$$

where the sum on γ extends over JT and breathing-mode distortions. Notice that $\Delta U_{\rm rel}$ is determined by the *occupation-induced* deformation energy $\hat{E}_{\gamma}$, whereas the relaxation energy $E_{\rm rel}^{(N)}$ of a given state and the relaxation energy $\Delta E_{\rm rel}^{(N,N')}$ of an ionizing transition is determined both by $\hat{E}_{\gamma}$ and by the zero-occupation elastic energies $E_{\gamma}(0)$. Baraff *et al.*[137a] have emphasized (in the context of the Si vacancy) that the latter terms can contribute to the relaxation energies as much as does $\hat{E}_{\gamma}$. Equation (10.28) highlights the fact that only energy terms which scale as N^{λ} with $\lambda > 2$ affect $\Delta U_{\rm rel}$. For example, whereas $\Delta E_{\rm rel}^{(N,N')}$ can contain a large contribution from the change in Madelung energy upon relaxation, most of this effect is cancelled in $\Delta U_{\rm rel}$, since Madelung energies are linear in N. Large relaxation energies $\Delta E_{\rm rel}^{(N,N')}$ for ionizations lower many ionization transitions into the host valence band, where they escape detection.

A few observations are in order.

(1) Optical ionization energies differ from thermal ionization energies by $\Delta E_{\rm rel}^{(N,N-1)}(\alpha)$ or $\Delta E_{\rm rel}^{(N+1,N)}(\alpha)$. Comparison of the two ionizations for the transition $[{\rm Cr}^{2+}, d^4, A^0, e^2t_2^2, {}^5T_2] \rightarrow [{\rm Cr}^{+}, d^5, A^-, e^2t_2^3, {}^6A_1]$ of Cr in ZnS and ZnSe yielded[81,112] $\Delta E_{\rm rel}^{(N+1,N)}(t_2) = -0.2$ to -0.4 eV. A similar comparison for $[{\rm Ti}^{2+}, d^2, A^-, e^2, {}^3A_2] \rightarrow [{\rm Ti}^{3+}, d^1, A^0, e^1, {}^2E]$ in GaAs[142a] shows $\Delta E_{\rm rel}^{(N+1,N)}(e) = -0.16$ eV, whereas for GaAs:Cr, $\Delta E_{\rm rel}^{(N+1,N)} = -0.16$ eV, too.[142b]

(2) $\hat{E}_{\rm JT}$ for most $3d$ impurities in semiconductors is $\lesssim 0.1$ eV. Breathing-mode lattice distortions are around ~ 0.1 Å[28,140] (Part VI,23), and the corresponding relaxation energies $\hat{E}_b$ can be a few tenths of an eV.

(3) The sum of the energy for the (acceptor) hole emission [Eq. (6.3)] and (acceptor) electron capture [Eq. (6.5)] need not equal the band gap, since different relaxation energies may be involved. The sum of the energy for the (donor) electron emission [Eq. (6.8)] and (donor) hole capture [Eq. (6.10)] need not equal the band gap either, for the same reason. The correction is of the order of 0.1–0.3 eV in III-Vs (cf. GaAs:Ti in Table VII). However, in II-VI and I-VI materials[143a] and in glasses[143b] this "band-gap excess" can be as large as 1 eV.

[142] (a) W. Ulrici, L. Eaves, K. Friedland, and D. P. Halliday, unpublished, 1985; (b) G. Martinez, A. M. Hennel, W. Szuszkiewicz, M. Balkanski and B. Clerjaud, *Phys. Rev. B* **23**, 3920 (1981).

[143] J. H. Harding and A. M. Stoneham, *J. Phys. C* **15**, 4649 (1982); Z. Vardeny and J. Tauc, *Phys. Rev. Lett.* **54**, 1844 (1985).

(4) The sign of the diagonal effective Mott–Hubbard energy $U^{(\alpha\alpha)}(A^q)$ depends on the balance between the three terms in Eq. (10.22). An "Anderson negative U"[144] pertains to the situation where the negative $\Delta U_{\rm rel}^{(\alpha\alpha)}(A^q)$ outweighs the positive $U_{\rm ver}^{(\alpha\alpha)}(A^q)$. Another type of "negative U" can exist if $\Delta U_{\rm MC}(A^q)$ outweighs $U_{\rm ver}^{(\alpha\alpha)}(A^q)$ (in optical experiments) or $U_{\rm ver}^{(\alpha\alpha)}(A^q) + \Delta U_{\rm rel}^{(\alpha\alpha)}(A^q)$ (in thermal experiments). This is discussed in Part VI,27.

(5) Non-self-consistent electronic-structure calculations (i.e., empirical tight binding[145]) provide no coupling between the orbital energies and the charge distribution; hence they all assume $U_{\rm ver} \equiv 0$. Furthermore, they neglect the portion of $\Delta E_{\rm ver}^{(N,N-1)}$ or $\Delta E_{\rm ver}^{(N+1,N)}$ which results from the dependence of the electronic structure on N (orbital-relaxation effects). As discussed in Part V, these are rather drastic assumptions.

(6) Empirical force-field models[143,146,147] which describe excitation energies in terms of charge-dependent atom–atom and shell interaction potentials approximate $\Delta E_{\rm ver}^{(N,N-1)}$ or $\Delta E_{\rm ver}^{(N+1,N)}$ by the corresponding $(N/N-1)$ or $(N+1/N)$ *free-ion* ionization potentials and electron afinities, corrected by lattice-polarization effects of the unrelaxed lattice. As discussed in Part V, the free-ion ionization energies grossly *overestimate* the (screened) ionization energies and Hubbard energies in the semiconductor (this approximation is better suited for ionic crystals). Force-field models further represent $\Delta E_{\rm rel}^{(N,N-1)}$, $\Delta E_{\rm rel}^{(N+1,N)}$, and $\Delta U_{\rm rel}^{(\alpha\alpha)}$ by changes in the polarization energies accompanying lattic relaxation. Such non-self-consistent estimates result in very large negative corrections [e.g.,[143a,147] $\Delta U_{\rm rel}(Ni^{2+}) = -9.9$ and -11.9 eV in ZnSe and MgO, respectively, where the free-ion value of $U_{\rm ver}({\rm Ni}^{2+})$ is 18.15 eV]. These large negative polarization-relaxation corrections compensate in part the overly positive vertical terms used in these methods. While the resulting U values are still overestimated (e.g.,[122a] 8.2 eV for ZnSe:Ni, compared with the observed value of 1.73 eV; see Table VIII), they are substantially smaller than $U_{\rm ver}$. This reduction in U was used[147] to explain the existence of many stable charge states of $3d$ impurities in ionic crystals.

(7) Self-consistent mean-field electronic-structure calculations can provide the quantities $\Delta_{\rm eff}^{(N)}[mn; m'n']$, $\Delta E_{\rm ver}^{(N,N-1)}(\alpha)$, $\Delta E_{\rm ver}^{(N+1,N)}(\alpha)$, and $U_{\rm ver}^{(\alpha\alpha)}(A^q)$ as differences in the corresponding total MF energies. The relaxation corrections $\Delta E_{\rm rel}^{(N,N-1)}(\alpha)$, $\Delta E_{\rm rel}^{(N+1,N)}(\alpha)$, and $\Delta U_{\rm rel}^{(\alpha\alpha)}(A^q)$, as well as the many-electron corrections $\Delta E_{\rm MC}^{(N,N)}$, $\Delta E_{\rm MC}^{(N,N-1)}$, $\Delta E_{\rm MC}^{(N+1,N)}$, and $\Delta U_{\rm MC}^{(ijk)}$ need to be included

[144] P. W. Anderson, *Phys. Rev. Lett.* **37**, 953 (1975).

[145] P. Vogl, *Adv. Electron. Electron Phys.* **62,** 101 (1984); H. P. Hjalmarson, P. Vogl, D. J. Woolford, and J. D. Dow, *Phys. Rev. Lett.* **44**, 810 (1980).

[146] A. M. Stoneham, *in Radiation Effects in Semiconductors* (J. W. Corbett and G. D. Watkins eds.), p. 7. Gordon & Breach, New York, 1971.

[147] A. M. Stoneham and M. J. L. Sangster, *Philos. Mag.* **43B**, 609 (1981).

before comparison with experiment is made. This has been done in the modern calculations discussed in Part VI,26.

(8) Spin-*unrestricted* calculations[39] provide approximations to $\Delta E_{MC}^{(N,N)}$, $\Delta E_{MC}^{(N,N-1)}$, $\Delta E_{MC}^{(N+1,N)}$, and ΔU_{MC} by including spin correlations but neglecting orbital space correlations (i.e., broken symmetries).

The relative importance of relaxation effects has been discussed in Part III,7 (see also Part VI,23 below). I consider next the relative magnitudes of MF and MC contributions to the spectra of 3*d* impurities.

11. Contemporary Approaches to Separation of MF and MC Effects

The relative importance of MF and MC effects has been a subject of controversy in the context of band theory of perfect solids,[97,129] as well as in the theory of point defects.[146,148,149] This situation is well known in the physics of Mott insulators[97] (e.g., MnO, CoO, and NiO), where one-electron band theory[150,151] usually predicts such systems to be partially filled *d*-band metals at least above the Néel temperature[150] (e.g., CoO), or to be narrow-gap semiconductors[151] (e.g., NiO and MnO). In fact (with the exception of VO and TiO), all 3*d* monoxides are wide-gap (Mott) insulators both above and below the Néel temperature.[97] This failure of mean-field theory is ascribed in Mott's picture[98] to the neglect of space and spin-correlation effects that lead to site-localized states. Indeed, when a 3*d* element is surrounded by highly electronegative narrow-band ligands such as oxygen, Mott's picture[98] suggests that the ground state involves "broken-symmetry" configurations in which the metal states are atomically localized, retaining large Coulomb energies and local magnetic moments and sustaining atomiclike multiplet excitations. At the opposite limit, when a 3*d* element is surrounded by ligands capable of sustaining itinerant covalent bonds such as silicon (e.g., 3*d* silicides[152]), the ground state of the system is often described successfully by itinerant band theory,[153,154] showing, in agreement with experiment, covalent metallic bonding, weak or no magnetism, and a normal band-to-band excitation spectrum. Between these limits we find the transition-metal

[148] G. T. Surrat and W. A. Goddard, *Phys. Rev. B* **18**, 2831 (1978).
[149] G. D. Watkins and R. P. Messmer, *Phys. Rev. Lett.* **32**, 1244 (1974).
[150] T. M. Wilson, *Int. J. Quantum Chem. Symp.* **3**, 757 (1970): L. F. Mattheiss, *Phys. Rev. B* **5**, 290, 306 (1972).
[151] K. Terakura, A. R. Williams, T. Oguchi, and J. Kübler, *Phys. Rev. Lett.* **52**, 1830 (1984).
[152] G. W. Rubloff, *Surf. Sci.* **132**, 268 (1983).
[153] O. Bisi and C. Calandra, *Phys. Rev. B* **22**, 4784 (1980).
[154] P. S. Ho, G. W. Rubloff, J. E. Lewis, V. L. Moruzzi, and A. R. Williams, *Phys. Rev. B* **22**, 4784 (1980).

phosphides and arsenides (3*d* pnictides[155]), which exhibit mixed characteristics, appearing both as insulators and as metals having local magnetic moments. Transition-atom impurities in phosphides (InP, GaP) or arsenides (GaAs) constitute the "dilute limit" of such bulk pnictides. The extent of many-electron multiplet effects in such systems is not obvious *a priori*. A similar transition from the prevalence of one-electron effects to the dominance of localization with its attendant many-electron interactions, is familiar in the spectroscopy of covalent semiconductors and insulators. Whereas the general features of the optical band-to-band spectra can be described reasonably well by itinerant band-structure theory, the x-ray excitations that involve core holes and core excitons are often dominated by many-electron multiplet phenomena.[55] Again, 3*d* impurities in semiconductor systems form an intermediate case, as their spectra involve excitations of localized "semi-core-like" 3*d* orbitals in a semiconducting matrix. Most electronic-structure calculations of solids have not confronted directly the problem of quantitative evaluation of such many-electron multiplet effects. Small-cluster models[148,149] may overestimate $E_{MC}^{(N,i)}$, since they deprive the electrons of the ability to freely delocalize, and hence loses some of the localization-induced many-electron effects. On the other hand, both the band theory of wide-valence-band solids and the effective-mass theory of shallow impurities owe much of their success to the smallness of MC effects in such systems.

Multiplet effects are significant, however, in free 3*d* ions and can be simply separated from MF effects.[8] Considering 3*d* ions with only *d* but no outer *s* electrons (e.g., T^{2+}, T^{3+}), the spherically averaged Coulomb energy of the *d* electrons $A(d^N)$ is linear[8] with N. In this case, the ionization energy $E^{(d)}[N/N-1]$ can be expressed[8] as

$$E^{(d)}[N/N-1] = [\bar{\phi} - (N-1)A] + (a_1 B + a_2 C), \qquad (11.1)$$

where $\bar{\phi}$ is the change in the electrostatic energy of the nucleus plus all non-*d* electrons upon ionization, B and C are the anisotropic Coulomb energies (Racah's parameters), and $a_1(N)$ and $a_2(N)$ are numerical coefficients known from Racah's theory. The first term in Eq. (11.1) is $E_{MF}^{(N,N-1)}(d)$, and it includes all *average* multiplet effects, whereas the second term, $\Delta E_{MC}^{(N,N-1)}(i,j)$, includes multiplet corrections and does not depend on A. Using the observed $E^{(d)}[N/N-1]$ (Fig. 9a) and the parameters B, C obtained from fitting the $d \to d^*$ spectra,[8] one can deduce $E_{MF}^{(N,N-1)}(d)$ from Eq. (11.1). It is represented by the dashed line in Fig. 9a for the $T^{2+} \to T^{3+}$ ionization. The shaded area then represents the multiplet correction $\Delta E_{MC}^{(N,N-1)}(i,j)$. Notice that (1) $E_{MF}^{(N,N-1)}(d)$ varies smoothly (almost linearly) across the 3*d* series, (2) $E_{MC}^{(N,N-1)}$ can be as large as ~4–5 eV, and (3) the nonmonotonicity at the Hund's point (Fig. 9a) is

[155] B. F. Stein and R. H. Walmsley, *Phys. Rev.* **148**, 993 (1966); K. Motizuki and K. Katoh, *J. Phys. Soc. Jpn.* **53**, 735 (1984); R. Podloucky, *J. Phys. F* **14**, L145 (1984).

caused mostly by these multiplet corrections[156] $\Delta E_{MC}^{(N,N-1)}(i, j)$. Notice further that free ions with both s and d outer electrons do not have a simple MF term like Eq. (11.1), since $A(d^n s^m)$ depends on the manner in which the $N = n + m$ electrons are distributed among the s and d orbitals. Consequently, $E_{MF}^{N,N-1}(d)$ is not linear in $N\bar{A}$, and a simple separation into MF and MC is not possible.

In a pioneering work, Allen[157] attempted a similar separation into MF and MC for $3d$ impurities in semiconductors. His central approximation was to assume that the isotropic interelectronic energy $A(e^n t_2^m)$ for an impurity does not depend on the manner in which these electrons are distributed among the e and t_2 orbitals (i.e., on the configuration $e^n t_2^m$), much like the situation for free ions with d electrons only. If $A(e^n t^m)$ were configuration independent and equal to some $\bar{A}$, one could express the ionization energy in the solid in close analogy with the free-ion expression of Eq. (11.1); i.e.,

$$E^{(t,e)}[N/N-1] = [\bar{\phi} - (N-1)\bar{A} + k_N \Delta_{CF}] + [a_1 B + a_2 C]$$
$$\equiv E_{MF}^{(N,N-1)}(t,e) + E_{MC}^{(N,N-1)}(i,j), \tag{11.2}$$

or, specifically for the $[T^{2+}, d^7, e^4 t_2^3, {}^4A_2] \to [T^{3+}, d^6, e^3 t_2^3, {}^5E]$ donor transition of Co in II-VI semiconductors[157] as $E^{(e)}[7/6] = [\bar{\phi} - 6\bar{A} + \frac{3}{5}\Delta_{CF}] + (8B - 7C)$. This is similar to Eq. (11.1) (where k_N accounts for the change in Δ_{CF} in ionization). Allen further assumed that B, C, and Δ_{CF} (approximated as the empirical $10Dq$ value[5-9]) are the same for all d^N configurations in a given semiconductor and used two observed ionization levels $E^{(t,e)}[N/N-1]$ in ZnS to evaluate $E_{MF}^{(N,N-1)}$, assuming its linearity with N. From this and the known B and C values, he could evaluate $E^{(t,e)}[N/N-1]$ for intermediate impurities, observing again Hund's point for the d^5/d^4 ionization. In a subsequent work,[158] the same procedure was applied to $3d$ impurities in GaAs. This approach provided an approximate separation of MF and MC effects in the impurity spectra. However, the approximation of the configuration independence of $A(e^n t_2^m)$ may be problematic—in T_d symmetry, t_2 states are p-d hybridized, whereas e states are not [see Eqs. (2.12) and (2.14)]; hence, different configurations will have different radial charge distributions

[156] L. H. Ahrens, "Ionization Potentials," p. 18, (Pergamon, Oxford, 1983), has observed a remarkable property of the T^{2+}/T^{3+} ionization energies of the 3d and 4d series: he noted that if the following pairs of ionization energies in Fig. 9a are joined by straight lines [Zn – Sc, Cu – Ti, Ni – V and Co – Cr, i.e., successive end-point], all lines intersect at a common point (the "Mendeleyv Point") midway between Mn and Fe (or Tc and Ru) at an ionization energy of 32.2 eV (or 29.0 eV). I noticed that the mean-field ionization energy $E_{MF}^{N,N-1}(d)$ of Eq. (11.1) almost coincides with this point. I suspect therefore that Ahrens's construction acts to cancel the various multiplet corrections of the different elements, revealing approximately the point where $E_{MC}^{(N,N-1)} = 0$, i.e., $N \cong 5.3 \pm 0.2$

[157] J. W. Allen, *Proc. Int. Conf. Phys. Semicond., 7th*, p. 781 (1964).

[158] J. W. Allen, *in* "Semi-Insulating III-V Materials" (G. J. Rees, ed.), p. 80. Shiva, Orpington, 1980.

and thus different As. Since A is larger than B and C by about two orders of magnitude,[8] even small errors in A might overwhelm B and C. Furthermore, no simple contact can be made with the results of mean-field calculations since such theories do not use an average A nor do they employ an empirical $10Dq$ value for Δ_{CF}.

Alternative approaches[159,160] have allowed for the possibility that e and t_2 wave functions may contribute differently to the Coulomb energies by introducing the orbital-deformation parameters λ_e and λ_t

$$\lambda_e^4 = \frac{\langle ee \| ee \rangle_s}{\langle dd \| dd \rangle_I}; \qquad \lambda_t^4 = \frac{\langle tt \| tt \rangle_s}{\langle dd \| dd \rangle_I} \tag{11.3}$$

which reflect the ratio between interelectronic repulsion energies in the solid (s) and the free ion (I). The mixed deformation parameter λ_{et} can be evaluated in analogy with Eq. (11.3), or estimated as $\lambda_{et} = \sqrt{\lambda_e \lambda_t}$. However, these "orbital-deformation parameters" were used to scale B and C alone, neglecting once again the important configuration dependence of $A(e^m t_2^n)$. In the classical Tanabe–Sugano–Kamimura[9] treatment for ions in solids, differential hybridization is neglected (hence, one assumes $\lambda_e = \lambda_t$). The multiplet energies should still depend on $A(m, n)$. Nevertheless, *in analogy with the free-ion case, the configuration dependence of A has been neglected in this approach*, resulting in a common A in all diagonal elements. The observed transitions are hence fitted to B, C, and Δ_{CF} (hence the term the "B, C, and Δ_{CF} approach"). Fazzio *et al.*[71,138] showed that this commonly accepted approximation $A(m,n) = A(m',n')$ can lead to substantial errors in the calculated multiplet spectra, including erroneous assignments of various transitions. It is more suited to impurities in O_h symmetry, where the e and t_2 states are nearly pure d [inversion symmetry in O_h excludes $l = 1$ contributions to the t_2 states; cf. Eq. (2.14)].

In the Hemstreet–Dimmock (HD) approach,[161] an attempt is made to bridge the classical "B, C, Δ_{CF} approach" with the content of electronic-structure calculations. First, differential hybridization is acknowledged, but the orbital-deformation parameters λ (e.g., the ratio between two interelectronic repulsion integrals) are replaced by the square of the fraction of $l = 2$ charge enclosed in a sphere of radius R_{MT},

$$\tilde{\lambda}_e^4 = \left(\int_0^{R_{MT}} \phi_e(r)\phi_e^*(r) r^2 \, dr \bigg/ \int_0^{\infty} \phi_d(r)\phi_d^*(r) r^2 \, dr \right)^2, \tag{11.4}$$

[159] S. Koide and M. L. M. Pryce, *Philos. Mag.* **3**, 607 (1967); L. L. Lohr, *J. Chem. Phys.* **45**, 364 (1966).

[160] A. G. O'Neill and J. W. Allen, *Solid State Commun.* **46**, 833 (1983). See also S. W. Biernacki, *Phys. Status Solidi* **130b**, K59 (1985); *ibid.*, **131b**, 349 (1985).

[161] L. A. Hemstreet and J. P. Dimmock, *Phys. Rev. B* **20**, 1527 (1979).

where R_{MT} is the muffin-tin (MT) radius (usually half of the bond length of the host crystal). While intuitively appealing, there is no reason to believe that Eq. (11.4) constitutes a reasonable approximation to Eq. (11.3), since the interelectronic operator (sensitive to small r_1-r_2 regions) is replaced by unity (weighing all space equally). Second and more important, the configuration dependence of $A(m, n)$ is neglected once again, and a common A is calculated by assuming that a MF calculation for a *fixed* configuration $e^m t_2^n$ incorporates the average multiplet effects of *all* configurations $\{e^{m+n}t_2^0, e^{m+n-1}t_2^1, \ldots, e^0 t_2^{m+n}\}$. In the limit $\lambda_e = \lambda_t = 1$, this assumption gives $\bar{A} = (14B_0 - 7C_0)/9$. This approximation has been criticized by Fazzio *et al.*,[138] who noted that, while a MF calculation for $e^m t_2^n$ indeed includes average multiplet effects, it does so only for the configuration $e^m t_2^n$ and not for others. Using this expression for $\bar{A}$ and the free-ion integrals B_0 and C_0, the HD model expresses the multiplet energies in terms of $\tilde{\lambda}_e$, $\tilde{\lambda}_t$, and Δ_{CF}. DeLeo *et al.*[162] have applied this multiplet approach extensively in their calculations on Si:$3d_i$, deducing multiplet corrections to donor and acceptor energies which were then used to augment their MF cluster results. Fazzio *et al.*[138] demonstrated that a significantly different multiplet structure is obtained in this approach if the configuration dependence of $A(m, n)$ is not neglected.

While it has been previously appreciated[159–163] that the configuration dependence of $A(m, n)$ greatly affects the multiplet spectra (see, in particular, an early and nearly forgotten account on the problem by Jørgensen[163]) and that Δ_{CF} is not interpretable in terms of MF energies alone, it has not been recognized that *the problem can be simply transformed to a form where the explicit calculation of* $A(m, n)$ *becomes unnecessary* and, at the same time, the free parameter Δ_{CF} is replaced by a well-defined mean-field energy Δ_{eff} that *implicitly contains* $A(m, n)$. This will be demonstrated in the next section.

12. Effective-Crystal-Field Approach

The approach of Fazzio *et al.*[138] (FCZ) is based on Slater's ansatz that a mean-field electronic-structure calculation for a fixed configuration $e^m t_2^n$ includes in its total energy $E_{MF}^{(N)}$ the average effect of all single-configuration energies that originate from the configuration (m, n). There is no place in such mean-field calculations for configuration mixing, or for single-configuration energies that do not belong[161] to the configuration $e^m t_2^n$ for which a self-consistent MF solution is sought.

Define the *single-configuration average energy* $\hat{E}(m, n)$ as the weighted average of all single-configuration (SC) energies $E_{SC}^{(i)}(m, n)$ for multiplets i that

[162] G. G. DeLeo, G. W. Watkins, and W. B. Fowler, *Phys. Rev. B* **25**, 4962 (1982).

[163] C. K. Jørgensen, *Acta Chem. Scand.* **12**, 903 (1958).

evolve from the configuration $e^m t_2^n$; i.e.,

$$\hat{E}(m, n) = \sum_i \omega_i E_{SC}^{(i)}(m, n). \qquad (12.1)$$

Here $E_{SC}^{(i)}(m, n)$ is the matrix element of $\hat{H}_1$ within the (m, n) single-configuration determinant, and the weights are taken over spin (S) and space (g_Γ) degeneracies

$$\omega_i = (2S + 1)g_\Gamma \Big/ \sum_{S,\Gamma} (2S - 1)g_\Gamma. \qquad (12.2)$$

FCZ noted that $\hat{E}(m, n)$ has the same universal form for all d^N arrangements; i.e.,

$$\hat{E}(m, n) = f_{m,n}(\lambda_e, \lambda_t)A(m, n) + g_{m,n}(\lambda_e, \lambda_t)(2B - C), \qquad (12.3)$$

where $f_{m,n}(\lambda_e, \lambda_t)$ and $g_{m,n}(\lambda_e, \lambda_t)$ are fixed coefficients given in Ref. 138. One can now express the single-configuration energy $E_{SC}^{\alpha}(m, n)$ relative to the average $\hat{E}(m, n)$, defining thereby the single-configuration *shift* $\Delta E_{SC}^{\alpha}(m, n)$ by writing the diagonal element of $\hat{H}_0 + \hat{H}_1$ in a determinantal basis for the Γth representation as

$$^\Gamma D_{\alpha\alpha}(m, n) = \hat{E}(m, n) + \Delta E_{SC}^{\alpha}(m, n) + k_{\alpha\alpha}\Delta_{CF}. \qquad (12.4)$$

Here, the numerical coefficient $k_{\alpha\alpha}$ reflects the fact that the diagonal element $D_{\alpha\alpha}$ is taken with respect to a fixed reference configuration. The usefulness of this partitioning lies in the fact that all of the dependence on the a_1-symmetric contribution $A(m, n)$ is absorbed into $\hat{E}(m, n)$ of Eq. (12.3) and the single-configuration *shift* $\Delta E_{SC}^{\alpha}(m, n)$ depends only on λ_e, λ_t, B_0, and C_0, but not on A, similar to the situation for the free-ion example of Eq. (11.1) (except that $\lambda_e = \lambda_t = 1$ in free ions). Referring the average single-configuration energies $\hat{E}(m, n)$ to some reference configuration $\hat{E}(m^0, n^0)$

$$\hat{E}(m, n) \equiv \hat{E}(m^0, n^0) + \Delta(m, n; m^0, n^0), \qquad (12.5)$$

the diagonal element of the interaction matrix is

$$\begin{aligned} ^\Gamma D_{\alpha\alpha}(m, n) - \hat{E}(m^0, n^0) &= \Delta E_{SC}^{\alpha}(m, n) + [\Delta(m, n; m^0, n^0) + k_{\alpha\alpha}\Delta_{CF}] \\ &\equiv \Delta E_{SC}^{\alpha}(m, n) + \Delta_{eff}[m, n; m^0, n^0], \end{aligned} \qquad (12.6)$$

where $\hat{E}(m^0, n^0)$ *is common to all diagonal elements and hence does not affect the multiplet splitting*. The term in square brackets in Eq. (12.6) is denoted the "effective crystal-field splitting" $\Delta_{eff}(m, n; m^0, n^0)$ and represents as in Eq. (10.13) the average energy separation between the configurations (m, n) and (m^0, n^0), including both bare-ion ($\hat{H}_0$) and mean-field ($\langle \hat{H}_1 \rangle$) effects. The

diagonal and off-diagonal elements are therefore given (up to a constant) as

$$\begin{aligned} {}^{\Gamma}D_{\alpha\alpha}(m,n) &= \Delta E^{\alpha}_{SC}(m,n) + \Delta_{eff}(m,n;m^0,n^0), \\ {}^{\Gamma}D_{\alpha\beta} &= E^{\alpha,\beta}_{CM}(m,n;m',n'). \end{aligned} \tag{12.7}$$

The off-diagonal elements ${}^{\Gamma}D_{\alpha\beta}$ of the interaction matrix represent configuration mixing (CM) between (m,n) and (m',n') that belong to the same multiplet and do not depend on A. The solution to the multiplet problem provides therefore the multiplet correction $E^{(N,i)}_{MC}$ to the MF total energy relative to the reference configuration (m^0, m^0). This multiplet correction energy has, in general, a contribution from the anisotropic interelectronic interactions within a single configuration $e^m t_2^n$ [i.e., due to the diagonal elements in Eq. (12.7)] as well as a contribution due to interaction between configurations $e^m t_2^n$ and $e^{m'} t_2^{n'}$ [i.e., the nondiagonal terms in Eq. (12.7)].

Using the ${}^3T_1$ multiplet of d^2 as an example, and choosing the e^2 configuration as reference, the complete matrix is

$$\begin{pmatrix} -\lambda_t^4(3B_0 - C_0) + [\Delta(0,2;2,0) + 2\Delta_{CF}] & -6\lambda_e\lambda_t^3 B_0 \\ -6\lambda_e\lambda_t^3 B_0 & \lambda_e^2\lambda_t^2(5B - \tfrac{1}{2}C) + [\Delta(1,1;2,0) + \Delta_{CF}] \end{pmatrix}. \tag{12.8}$$

This result is completely different from either the Tanabe–Sugano–Kamimura results[9]

$$\begin{pmatrix} -5B + 2\Delta_{CF} & -6B \\ -6B & 4B + \Delta_{CF} \end{pmatrix}, \tag{12.9}$$

or the results of the Hemstreet–Dimmock approach[161]

$$\begin{pmatrix} -\tfrac{1}{9}\tilde{\lambda}_t^4(31B_0 + 7C_0) + 2\Delta_{CF} & -6\tilde{\lambda}_e\tilde{\lambda}_t^3 B_0 \\ -6\tilde{\lambda}_e\tilde{\lambda}_t^3 B_0 & \tfrac{1}{9}\tilde{\lambda}_e^2\tilde{\lambda}_t^2(50B_0 - 7C_0) + \Delta_{CF} \end{pmatrix}. \tag{12.10}$$

The striking difference is that in the Tanabe–Sugano–Kamimura formalism (where B is fitted from the impurity spectra) the separation between these multiplets does not depend on C at all, while in the fomalism of FCZ (where B_0, C_0 are atomic values), it always has a contribution from C_0. There can be no doubt that the treatments that neglect the configuration dependence of $A(m,n)$ [Eqs. (12.9) and (12.10)] yield solutions different from the one that does not [Eq. (12.8)]. (Another example is the fact that the Tanabe–Sugano approach predicts the degeneracy of the ${}^4E$ and ${}^4T_1$ excited states of d^5, unlike the more general method.) The central point here is that the transformation suggested by FCZ identifies both bare-ion (Δ_{CF}) as well as average multiplet effects (Δ) in the effective crystal-field splitting Δ_{eff} of Eq. (12.6) and that the configuration dependence in $A(m,n)$ is renormalized in Δ in a way which permits direct comparison with electronic-structure calculations.

The three central quantities in this approach—λ_e, λ_t, and Δ_{eff}—can be computed from electronic-structure calculations directly from their definitions (e.g., from the wave functions obtained in Green's function calculations). Together with the free-ion values[8] of B_0 and C_0, these can be used to obtain the multiplet structure. Alternatively, it is possible to reverse the process and determine λ_e, λ_t, and Δ_{eff} from experiment by fitting the $d \rightarrow d^*$ spectra. In the following section I discuss the results of the latter approach, in which FCZ have analyzed the spectra of $3d$ impurities in ZnO, ZnS, ZnSe, GaAs, InP, and GaP for which sufficient data exist as well as for bulk $3d$ oxides. This will establish the extent of multiplet corrections underlying the data, display the chemical trends in the mean-field parameters and in multiplet effects, and isolate from the experimental data those mean-field quantities which are directly comparable with one-electron theory. In view of the availability of only a small number of observed transitions per ion (Table V), FCZ have used a single, average Δ_{eff} parameter so that the theory has only three independent quantities: Δ_{eff}, λ_e, and λ_t. In cases where the number of observed transitions is smaller than the number of parameters in the model (e.g., GaAs:Ni^{2+}) (Table V), a range of the parameters consistent with the data and with the results for the same impurity in the closest semiconductor (e.g., GaP) was found. Figure 12 illustrates the observed, fitted, and predicted multiplet structure[138] of ZnSe:T^{2+}.

13. Chemical Trends in the Mean-Field Parameters

a. *Trends in λ_e, λ_t, and Δ_{eff}*

Table XII and Fig. 13 display a simple chemical regularity in the effective crystal-field splitting Δ_{eff}: a minimum at Mn and a maximum at the high-Z end of the series. Interestingly, the existence of a minimum Δ_{CF} at Mn was also observed in tetrahedrally coordinated $3d$ complexes in solution[6] in comparing the series $(\phi_3AsO)_2NiCl_2$, $(CoCl_4)^{2-}$, and Cs_2MnCl_4, yielding $\Delta_{CF} = 0.52$, 0.4, and 0.25 eV, respectively. The simple trend of Δ_{eff} observed in Fig. 13 is to be contrasted with the complex S-shaped trend obtained previously[164] with B, C, Δ_{CF} fits, a trend that is unmatched by any calculation (cf. Part V). The trend of Δ_{eff} with the $3d$ element (often referred to as the "spectrochemical series") shows an increase in Δ_{eff} with increasing covalency (GaP > ZnSe > ZnS). It conflicts, however, with the expectation from the point-ion crystal-field theory (see Part VI,18), which predicts a scaling of the splitting $10Dq$ with the fourth

[164] J. M. Baranowski, J. W. Allen, and G. L. Pearson, *Phys. Rev.* **160**, 627 (1967).

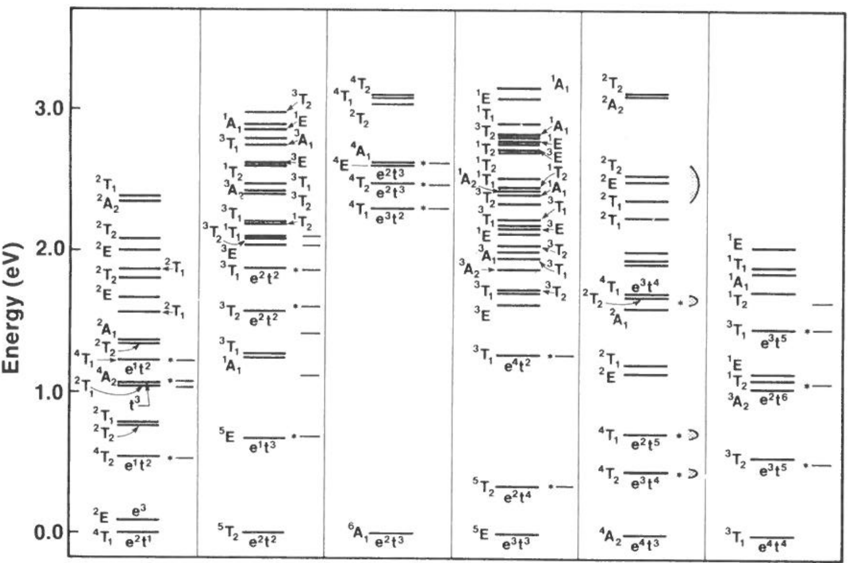

FIG. 12. Internal $d \rightarrow d^*$ spectra of divalent substitutional 3d impurities in ZnSe. Levels denoted by an asterisk are observed (Table V); the others are obtained by A. Fazzio, M. Caldas, and A. Zunger, *Phys. Rev. B* **30**, 3430 (1984) from their multiplet theory by fitting the observed lines. The predicted doublets $^2T_2$, ^2E, $^2T_1$, and $^2T_1$ for ZnSe:Co^{2+} around 2.3–2.6 eV agree with recent measurements [V. I. Sokolov, T. P. Surkova, M. Kulakov, and A. V. Fadeev, *Phys. Status Solidi* **130b**, 267 (1985)].

moment $\langle 3d|r^4|3d\rangle$ of the bare-ion 3d orbital (hence, a monotonic decrease with atomic number) and a rapid (d^{-5}) decrease of $10Dq$ with the impurity–ligand bond distance d [hence $\Delta(\text{ZnO}) > \Delta(\text{ZnS})$].

The trends in the orbital-deformation parameters λ_e and λ_t in Fig. 13b,c (often referred to as the "nephelauxetic series") are likewise very simple: a maximum at Mn (except ZnSe:Cr which is slightly higher than ZnSe:Mn) and a decrease with increasing covalency of the host crystal (i.e., increased hybridization). In all cases except ZnSe:Ti, ZnSe:Ni, and ZnS:Ni, FCZ found $\lambda_e > \lambda_t$, suggesting a stronger hybridization of the t_2 orbitals (which in tetrahedral coordination form σ bonds with the nearest-neighbor ligands) than for the e orbitals (which form σ bonds only with the next-nearest ligands and weaker, π bonds with the nearest neighbors). The orbital-deformation parameters obtained here [cf. the definition in Eq. (11.3)] are substantially larger than those approximated by the d-orbital charge enclosed in a sphere[161,162] [the charge localization of Eq. (11.4)].

In the past, much emphasis has been placed on the decisive role of d orbitals[5–9] (as opposed to p-d hybridization) on the spectra of 3d ions in

TABLE XII. INTERNAL MF PARAMETERS, OBTAINED BY FITTING ABSORPTION DATA[a]

Impurity	Host	λ_e	λ_t	Δ_{eff}
Ni	ZnS	0.806	0.870	0.520
	ZnSe	0.800	0.854	0.510
	GaAs	0.815 ± 0.001	0.589 ± 0.006	0.91 ± 0.01
	GaP	0.815	0.608	0.97 ± 0.01
Co	ZnS	0.883	0.852	0.453
	ZnSe	0.890	0.849	0.459
	InP	0.825 ± 0.04	0.745 ± 0.04	0.575 ± 0.02
	GaAs	0.825	0.748	0.590
	GaP	0.831	0.759	0.608
Fe	ZnS	0.930	0.913	0.430
	ZnSe	0.93 ± 0.04	0.91 ± 0.04	0.41 ± 0.03
	InP	0.848 ± 0.08	0.822 ± 0.08	0.43 ± 0.03
	GaAs	0.847 ± 0.08	0.823 ± 0.08	0.44 ± 0.03
	GaP	0.843 ± 0.08	0.828 ± 0.08	0.45 ± 0.03
Mn	ZnS	0.967	0.938	0.402
	ZnSe	0.970	0.926	0.400
	GaP	0.86 ± 0.08	0.858 ± 0.08	0.52 ± 0.03
Cr	ZnS	0.950	0.923	0.540
	ZnSe	0.975	0.940	0.540
	InP	0.863 ± 0.08	0.790 ± 0.08	0.64 ± 0.03
	GaAs	0.872 ± 0.08	0.778 ± 0.008	0.65 ± 0.03
	GaP	0.872 ± 0.08	0.774 ± 0.08	0.67 ± 0.03

[a] Where fewer than three transitions are available, a range is indicated. From A. Fazzio, M. Caldas, and A. Zunger, *Phys. Rev. B* **30**, 3430 (1984); *J. Elect. Mat.* **14a**, 1035 (1984); and unpublished results (1984).

complexes and in solids. The calculation of FCZ highlights the importance of the small but highly significant hybridization with ligand orbitals. They found that the position of the multiplets can be extremely sensitive to small reductions of λ_e and λ_t from unity. Hence, even a small radial expansion of the e orbital or a p-d hybridization in the t_2 orbital sensitively controls the spectra of the system and can even convert a high-spin ground state (e.g., Cr^{2+}, $^5T_2$) into a low-spin ground state (e.g., Cr^{2+}, $^1A_1$). Such changes may be effected by pressure.[165]

[165] M. Zigone, P. Galtier, G. Martinez, and B. Deveaud *J. Electron. Mater.* **14a**, 1059 (1985).

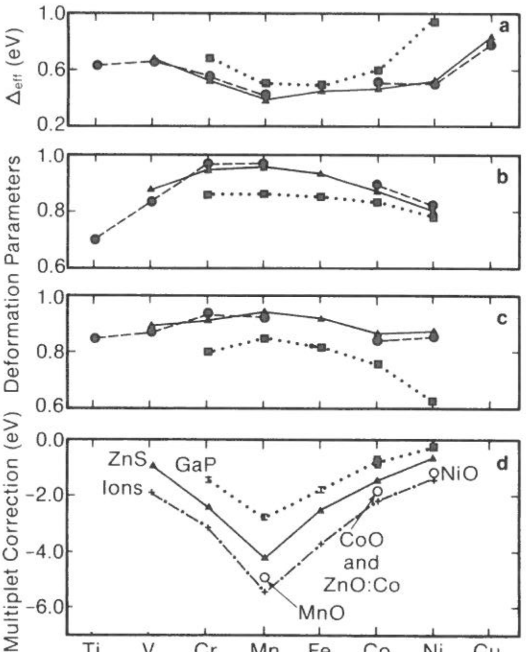

FIG. 13. Chemical trends in (a) the effective crystal field energy Δ_{eff}; (b) and (c) the orbital deformation parameters λ_e and λ_t; and (d) the ground-state multiplet correction energy of divalent $3d$ impurities in semiconductors (▲, ZnS; ●, ZnSe; ■, GaP). Results are also shown in (d) for free ions (+) and bulk oxides (○). After A. Fazzio, M. Caldas, and A. Zunger, *Phys. Rev. B* **30**, 3430 (1984). (See also Ref. 259 below.) The deformation parameters measure the relative delocalization of the $3d$ orbitals in the solid and free ion ($\lambda_e = \lambda_t = 1$ in the free ion). Δ_{eff} measures the average energy that separates two configurations, $e^n t^m$ and $e^{n'} t^{m'}$, in a mean-field sense.

b. *Trends in Ground-State Multiplet Corrections*

Figure 13d[138] depicts the multiplet correction $E_{MC}^{(N,i)}[T^{N_H+q}, d^N, A^q, {}^{2S+1}\Gamma]$ [Eq. (10.1)] to the ground state of the T^{2+} impurities. It also includes results for the bulk Mott insulators[71] NiO, CoO, and MnO, as well as for free $3d$ ions in their 2+ charge state obtained by fitting their spectra. While $E_{MC}^{(N,i)}$ is small on the scale of the total energy $E_T^{(i)}$, in all cases shown it is sufficient to stabilize the high-spin (Hund's-rule) ground state. Chemical trends are again transparent:

(1) The largest multiplet stabilization occurs for Mn with its highest spin ($S = \frac{5}{2}$), and it decreases monotonically (but not symmetrically) as one moves to either side of Mn in the $3d$ series. This parallels the trend in the free-ion exchange energies (Fig. 10b).

(2) The multiplet correction decreases rapidly with covalency in going from the free ions to oxides, sulfides, and phosphides (presumably for Si:$3d$, for which no absorption spectra have yet been recorded, the corrections are yet smaller). Introduction of a $3d$ impurity into a covalent crystal results, therefore, in a larger loss of multiplet stabilization energy than for an impurity in a more ionic system. The implication of this fact on impurity solubilities will be discussed further in Part IV,13.

(3) The correction for the impurity system ZnO:Co is virtually identical to that obtained for bulk CoO, suggesting that much of the multiplet effect is confined to the nearest-neighbor ligang cage.

(4) The octahedrally coordinated bulk Mott insulators NiO, CoO, and MnO fit the general trend observed for the dilute impurities.

Since the spectra of Co^{2+} were observed in a number of host crystals (Fig. 5), they offer the opportunity to inspect the chemical trends in λ_e, λ_t, and Δ_{eff} with the host crystal. Figure 14 depicts this information (solid circles) for ZnO, ZnS, ZnSe, and GaP. It is evident that Δ_{eff} is small in a highly ionic system like ZnO (0.340 eV, although it has the smallest lattice parameter), is similar in ZnS (0.453 eV) and ZnSe (0.459 eV) (which have nearly identical electronegativities), and increases in going to the covalent GaP (0.61 eV). The deformation parameter λ_e varies slowly with the covalency of the host crystal, whereas the deformation parameter λ_t distinguishes one host crystal from the other. Notice that the trends obtained with the method of O'Neill and Allen[160] (open circles in Fig. 14) showing $\Delta_{eff}(ZnO) < \Delta_{eff}(ZnS)$ and

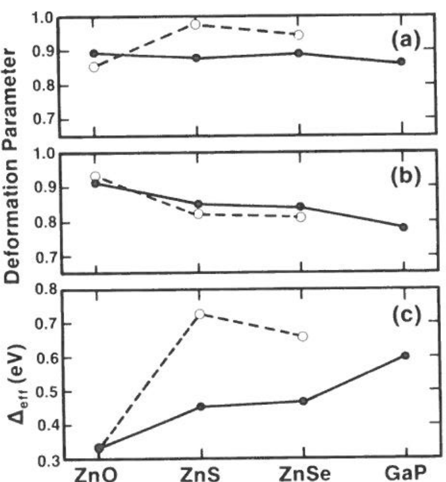

FIG. 14. Chemical trends in the mean-field parameters of the Co^{2+} impurity in various host crystals. (a) λ_e; (b) λ_t; (c) Δ_{eff}. (●), from the theory of A. Fazzio, M. Caldas, and A. Zunger, *Phys. Rev. B* **30**, 3430 (1984); (○), from the theory of A. G. O'Neill and J. W. Allen, *Solid State Commun.* **46**, 833 (1983). Note that the crystal-field energy Δ_{eff} increases as the host crystal becomes more covalent (in the ZnO → ZnS → ZnSe → GaP sequence), whereas the deformation parameters λ_e and λ_t decrease with increasing covalency.

λ_e(ZnO) < λ_e(ZnS) appear at odds with the simpler chemical trends obtained in Ref. 138.

c. The Possibility of Low-Spin Ground States

The foregoing findings on the trends in Δ_{eff}, λ_e, and λ_t and in the ground-state multiplet corrections (Fig. 13) suggest the possibility of formation of a *low-spin ground state*. Such a ground state is formed if $\Delta_{eff} > \Delta_x$. Figure 13a shows that Δ_{eff} is large at the high-Z end of the 3d series, and that at the low-Z end of the series the localization parameters λ_e and λ_t (Fig. 13b,c) tend to be small; i.e., the orbits are extended. Figure 13d shows correspondingly that the multiplet corrections (reflecting largely Δ_x) are small at the low-Z and high-Z end of the series. This suggests that at both ends of the 3d series it is possible that $\Delta_{eff} < \Delta_x$. This possibility has been rejected by classical models, which were inspired by the data on 3d impurities in *ionic* solids (where $\Delta_{eff} \ll \Delta_x$ in all cases). Using the fitted λ_e and λ_t values, we find for GaAs:V^{2+} a likely low-spin ground state[54,138] of $^2E(e^3)$, not the $^4T_1(e^2t^1)$ high-spin state. Similarly, for ZnSe:V^+ such a calculation suggests the system to be very near the $^1A_1(e^4)$ low-spin ground state. Similar considerations suggest low-spin ground states for impurities in Si. In Part VI,24,b, detailed calculations on Si:3d reveal indeed low-spin ground states both at the low-Z limit (V^0, $^2T_2$; Ti, $^3T_1$ and V^+, $^3T_1$) and at the high-Z limit (Co^{2+}, ^2E). In 4d and 5d impurities we expect larger Δ_{eff} and smaller Δ_x values, hence even a greater prevalence of low-spin ground states. Experimental search for such possible low-spin ground states will be very desirable.

d. Crystal-Field Stabilization Energy

The energy E_b that binds an impurity to the lattice (the heat of solution) consists both of MF and MC effects; i.e.,

$$E_b = [E_{MF}^{(N)}(\text{solid}) - E_{MF}^{(N)}(\text{atoms})] + [E_{MC}^{(N,i)}(\text{solid}) - E_{MC}^{(N,j)}(\text{atoms})]. \quad (13.1)$$

The first term contains both closed-shell and open-shell effects. When the e and t_2 gap levels are empty (e.g., Ca^{2+}, Zn^{2+}, Sc^{3+}, Ga^{3+}, etc.), this term includes only closed-shell effects E_b^0 represented by the electronic interactions of a closed-shell ion with the lattice. This contribution varies almost linearly with the atomic number[6] and leads to a simple monotonic trend in the bond lengths and cohesive energies of such compounds. When the e and t_2 gap levels are partially occupied ($e^m t_2^n$), an additional contribution to E_b exists[5,6]; i.e., the excess energy gained in the solid by occupying the e and t_2 levels whose barycenter lies below the free-ion 3d level by the amount $[(2n - 3m)/5]\Delta_{CF}$ (or the negative of this quantity in octahedral fields). This is termed[5–7] the "crystal-field stabilization energy" (CFSE) and is denoted E_b^{CFSE}. The heat of solution depends on the impurity charge state since E_b^{CFSE} (more properly, the

change in position of the electrical level in the band gap) varies with occupation. E_b^{CFSE} is depicted by the dashed lines in Fig. 15, where the experimentally deduced effective crystal-field splittings Δ_{eff} for the various impurities (Table XII) have been used. This crystal-field stabilization energy vanishes for Mn^{2+} (where the barycenter of the half-filled shell coincides with the energy of the free-ion 3d level) and increases as one moves away from Mn to either side of the 3d series. These types of variation in the CFSE (except that less reliable values of Δ_{eff} have been used) have been widely used[5–7] in the past to explain a large body of chemical data pertaining to excess stability of compounds with open-shell ions relative to compounds with closed-shell ions, or the relative stability of octahedral *vs* tetrahedral coordination compounds. For example, the anomalously small lattice energy of Mn chalcogenides and halides and the attendant anomalously long metal–nonmetal bond distance were rationalized[6] in terms of the vanishing CFSE (dashed lines in Fig. 15) for these half-filled d^5 ions. *These arguments usually ignore the last term of Eq. (13.1), i.e., the multiplet contribution* E_b^{MC} *to the binding energy*. This term reflects the loss in many-electron stabilization energy in going from the more localized free ion to the more extended states in the solid (compare difference between the free-ion and impurity multiplet corrections in Fig. 13d). The dot-dashed lines in Fig. 15 depict this loss of multiplet energy in the solid relative to the free ion. This E_b^{MC} constitutes a repulsive contribution to the binding energy and is seen to be large for covalent host crystals such as GaP (since much of the multiplet stabilization is lost in the solid because of delocalization of the orbitals; see Fig. 13d) and substantially less repulsive in the more ionic host crystals such as ZnS. Hence this analysis predicts that the solubility of a 3d ion would increase as the covalency of the host crystal is reduced in going from Si to III-V and II-VI semiconductors, in agreement with the data surveyed in Part III,4. Note that the multiplet destabilization E_b^{MC} is larger than the crystal-field stabilization energy E_b^{CFSE}, so that the sum of the two contributions (solid line in Fig. 15) is *positive*, having, hence, a net destabilizing effect. Open-shell contributions are thus more properly termed "crystal-field *destabilization*" effects. (The reason that Mn coordination compounds have anomalously small cohesive energies and anomalously large bond lengths lies, therefore, in their large *destabilizing* multiplet correction rather than their vanishing *stabilizing* CFSE. Since E_b^{MC} depends sensitively on *sp* hybridization of the d orbitals (covalency), it is this effect (not the pure d-electron effect underlying CFSE) that controls much of the stability of the system. This has been pointed out recently[166–168] from a pseudopotential point of view. It

[166] A. Zunger, *in* "Structure and Bonding in Crystals" (M. O'Keefe and A. Navrotsky, eds.) p. 73. Academic Press. New York, 1980.
[167] A. Zunger, *Phys. Rev. Lett.* **44**, 582 (1980).
[168] J. K. Burdett, G. D. Price, and S. L. Price, *J. Am. Chem. Soc.* **104**, 92 (1982); *Phys. Rev. B* **24**, 2903 (1981).

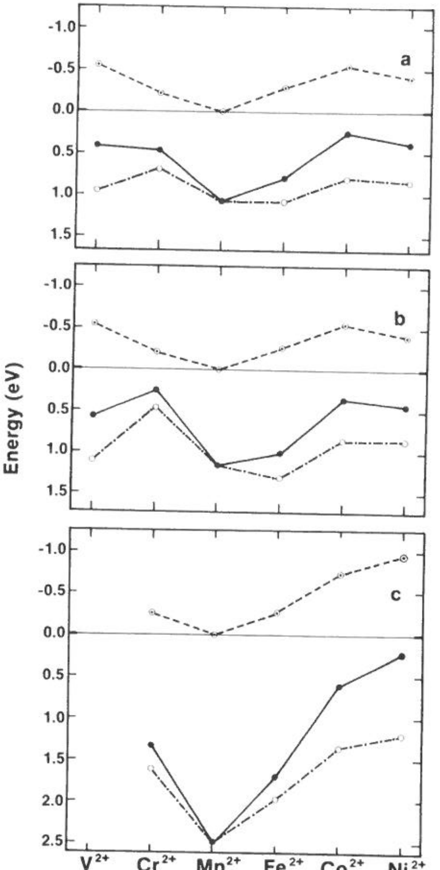

FIG. 15. Variations in the crystal-field stabilization energies ("CF binding energy," ---), ground-state multiplet corrections in the solid relative to the free ions (-·-·-), and their sum (total open-shell contribution to the binding energy, ———) for divalent $3d$ impurities in (a) ZnS, (b) ZnSe, and (c) GaP. After A. Fazzio, M. Caldas, and A. Zunger, *Phys. Rev. B* **30**, 3430 (1984). (See also Ref. 259 below.) The CF binding energy vanishes for a half-filled shell (Mn^{2+}, d^5) and is negative otherwise; the multiplet binding energy is positive and represents the loss of many-electron stabilization energy when a localized free ion enters the solid and acquires some delocalization through covalent interactions. The sum of the two contribution constitutes the open-shell contribution to the enthalpy of solution.

seems that the widely held misconception of the predominance of d-electron CFSE effects is largely based on the remarkable (but superficial) resemblance of the trends in CFSE (dashed lines in Fig. 15) to the trends in the total open-shell contribution (solid lines in Fig. 15). The physical origin (e.g., sign) of both effects is, however, quite different.

Using the concept of the open-shell contribution to the cohesive energy, one can further analyze[138] the data for bulk oxides and compare different limits of crystal-field configurations. Figure 16[138] shows the sum of E_b^{CFSE} and E_b^{MC} for the Mott insulators MnO, CoO, and NiO (connected by a dotted line to guide the eye). For MnO, the vanishing CFSE and the positive multiplet correction add up to produce a destabilizing term (0.55 eV) in the cohesive energy. In contrast, the larger negative CFSE and the smaller positive multiplet correction in CoO and NiO add up to produce a total *stabilizing* contribution to the cohesive energy (−0.30 and −0.74 eV, respectively). As we move to $3d$ impurities in a less ionic host crystal (e.g., in ZnSe, see in Fig. 16 the curve labeled "weak field") the impurity states become more delocalized relative to oxides, resulting in a larger loss of multiplet stabilization energy in going from free ions to the solid. The attractive CFSE is now overwhelmed by the repulsive multiplet energy, producing a net destabilizing effect. Bulk oxides (or impurities in ZnO) are hence unique in that open-shell effects may stabilize the system. In contrast, impurities in covalent semiconductors have a large *destabilizing* open-shell contribution resulting in an overall small substitutional solubility that, nevertheless, will increase as the host crystal becomes more ionic. This highlights the reason for the stability of the bulk $3d$ oxides relative to $3d$ impurities, which show only limited solubilities. Note also that if one assumes a low-spin configuration ("strong field" in Fig. 16), the destabilizing multiplet effect is far larger; the difference between the two curves in Fig. 16 reflects the spin preference driving force for solubilities. Further, if

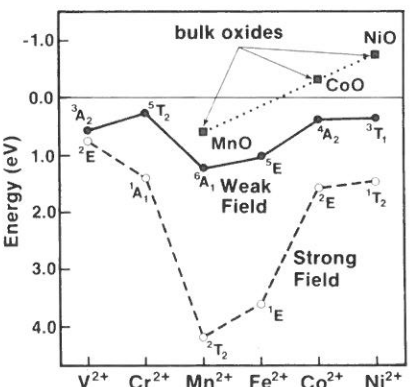

FIG. 16. Total open-shell contribution to the cohesive energy (see also caption to Fig. 15). (■) represent results for bulk oxides, whereas (●), (○) represent results for divalent $3d$ impurities in ZnSe. Ground-state multiplets are denoted for the weak- and strong-field cases. Note that the weak-field (high-spin) configurations (———) are stabler than the strong-field (low-spin) configurations (---). [After A. Fazzio, M. Caldas, and A. Zunger, *Phys. Rev. B* **30**, 3430 (1984).]

E_b^{MC} is ignored and only E_b^{CFSE} is used, the low-spin states of d^3-d^6 are predicted to be the ground state, in contrast with experiments.

14. Chemical Trends in Excitation and Ionization Energies

a. *Internal Transitions*

Having obtained the mean-field parameters λ_e, λ_t, and Δ_{eff} from the absorption spectra, we are in a position to evaluate the multiplet correction for excitation energies $\Delta E_{MC}^{(N,N)}(i, j)$ [Eq. (10.14)]. Figure 17a[138] displays this correction for the three lowest excited states of ZnS:3*d*, ZnSe:3*d*, and GaP:3*d*. The symmetries of the final states are indicated in each case. The simple chemical trends in the MF parameters λ_e, λ_t, and Δ_{eff} (Fig. 13) are now transformed to more complex, nonmonotonic trends in the many-electron energies. We note the following salient features. *First*, the lowest excited state has a very small multiplet correction in all crystals for all impurities but Mn, for which the multiplet correction in the ground state ($^6A_1$ with spin $\frac{5}{2}$) far exceeds that in the excited state ($^4T_1$ with spin $\frac{3}{2}$) because of the decrease in total spin. In contrast, the corrections for the second and third excited state are substantial on the physically relevant scale of the band gap (up to 80% of the gap even in GaP). *Second*, the multiplet corrections have a maximum at Mn for all three excited states, and they decrease monotonically on both sides of the 3*d* series. These corrections can be substantial even if the spin is conserved in the excitation process. *Third*, multiplet corrections for excitations can be either positive (increasing the energy relative to the MF results) or negative (producing a lower excitation energy relative to the MF results, e.g., the second excited state of Co). *Fourth*, the corrections are reduced with the covalency of the host crystal. I conclude that, with the exception of the first excited state in all impurities but Mn, a correct mean-field electronic-structure calculation cannot reproduce the observed excitation energies of 3*d* impurities.

Table XIII gives the multiplet corrections for the ground state and first three excited states of the ZnS:3*d* system.[138] It shows separately the configuration-mixing contribution to the multiplet correction. We see that in the ground state the multiplet correction for all impurities but V^{2+} and Ni^{2+} arises purely from anisotropic interelectronic interactions within a *single configuration*. On the other hand, *configuration mixing* becomes progressively more dominant in the excited states; for the $^1A_1$ excited state of Cr^{2+} and the ^2E excited state of Co^{2+}, configuration mixing constitutes all of the multiplet correction. In such cases where interconfigurational many-electron interactions dominate, one-electron mean-field theory is clearly inapplicable.

The variation in multiplet correction energies with the host crystal lead to different ordering in the excited states. This is illustrated in Fig. 18 for the

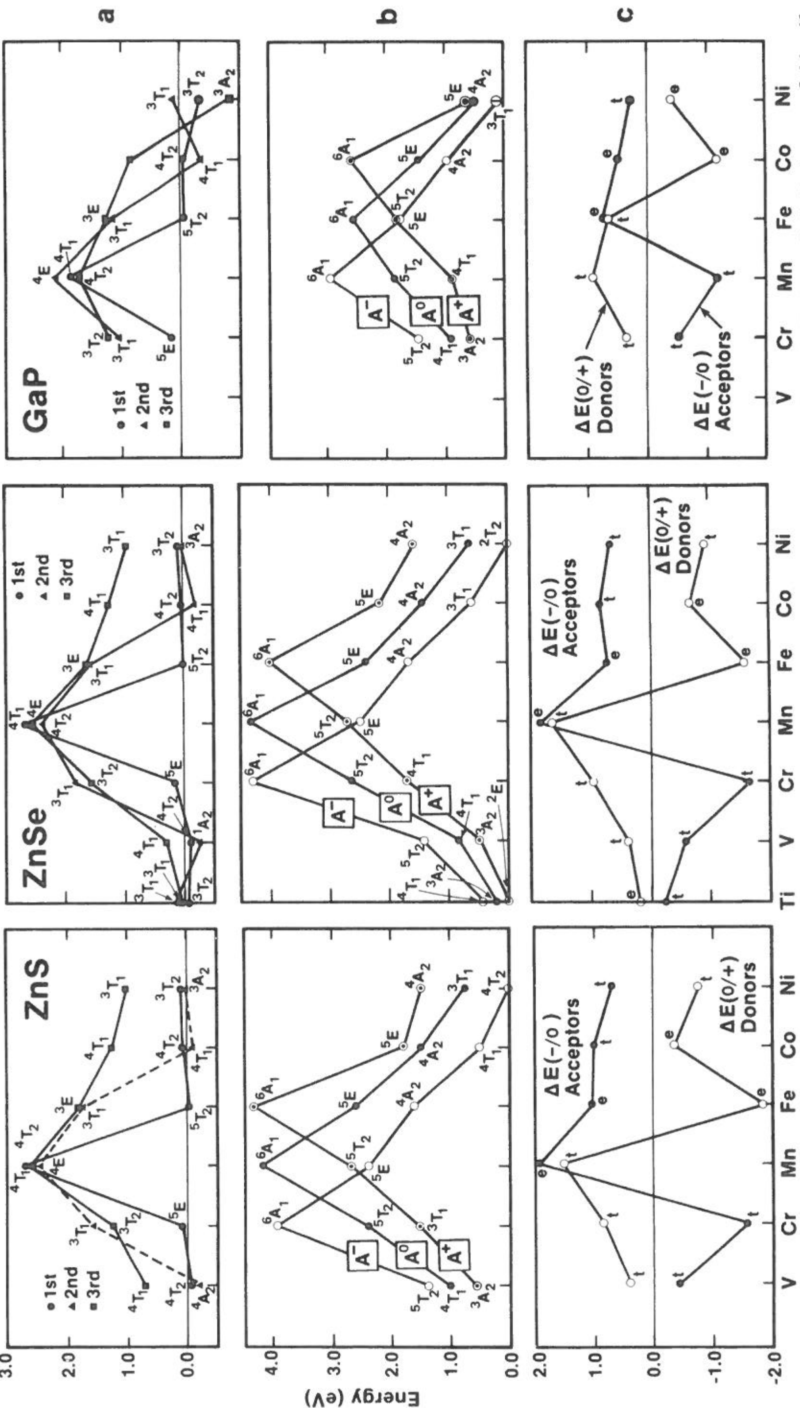

Fig. 17. Many-electron multiplet corrections (MC) for excitation and ionization energies of 3*d* impurities in ZnS, ZnSe, and GaP. A mean-field self-consistent calculation neglects all quantities shown in this figure. (a) MC for the lowest three $d \rightarrow d^*$ transitions of divalent impurities. The multiplets shown are the final states in each transition; the initial states are given in Table V. Note the large positive multiplet effects for the internal transitions in Mn^{2+}. (b) The negative of the MC to the ground states of three different charge states. The multiplet notation refers to the ground state of each charge state; note the maxima in the $^6A_1$ state, similar to that observed in the exchange energy of free ions (Fig. 10b). (c) The MC to the donor and acceptor energies. These are differences between the MC for A^0 to A^+ (for donors), or A^- and A^0 (for acceptors). In each case the one-electron orbital (*e* or *t*) being ionized is indicated. [After A. Fazzio, M. Caldas, and A. Zunger, *Phys. Rev. B* **30**, 3430 (1984); see also Ref. 259 below.]

TABLE XIII. MULTIPLET CORRECTION ENERGY FOR THE GROUND AND THE THREE LOWEST EXCITED STATES OF DIVALENT IMPURITIES IN ZnS[a]

Impurity	Multiplet	Predominant configuration	Total multiplet correction (eV)	Configuration mixing energy (eV)	Multiplet	Predominant configuration	Total multiplet correction (eV)	Configuration mixing energy (eV)
	Ground state				*Second excited state*			
V^{2+}	$^4T_1$	e^2t^1	−1.012	−0.101	$^4T_2$	e^1t^2	−1.100	0.0
Cr^{2+}	$^5T_2$	e^2t^2	−2.414	0.0	$^1A_1$	e^4	−0.295	−0.295
Mn^{2+}	$^6A_1$	e^2t^3	−4.43	0.0	$^4T_2$	t^3e^2	−1.490	−0.320
Fe^{2+}	^5E	e^3t^3	−2.636	0.0	$^3T_1$	e^4t^2	−0.827	−0.266
Co^{2+}	$^4A_2$	e^4t^3	−1.511	0.0	$^4T_1$	e^2t^5	−1.646	−0.295
Ni^{2+}	$^3T_1$	e^4t^4	−0.701	−0.130	$^3A_2$	e^2t^6	−0.640	0.0
	First excited state				*Third excited state*			
V^{2+}	^2E	e^3	−0.119	−0.119	$^2T_2$	e^2t^1	−0.071	−0.359
Cr^{2+}	^5E	e^1t^3	−2.330	−0.0	$^3T_1$	e^3t^1	−0.762	−0.203
Mn^{2+}	$^4T_1$	e^3t^2	−1.684	−0.170	^4E	e^2t^3	−1.791	−0.219
Fe^{2+}	$^5T_2$	e^2t^4	−2.410	0.0	^3E	e^3t^3	−0.783	−0.307
Co^{2+}	$^4T_2$	e^3t^4	−1.436	0.0	^2E	e^4t^3	−0.202	−0.202
Ni^{2+}	$^3T_2$	e^3t^5	−0.609	0.0	$^1T_2$	e^4t^4	0.464	−0.108

[a] Some of the multiplets involve a single one-electron configuration (e.g., ground state of Cr, Mn, Fe, and Co). Others involve configuration mixing. We give separately the contribution to the total multiplet energy from such interconfigurational interactions. This effect accounts for all of the multiplet correction in some cases (e.g., second excited state of Cr^{2+}). From A. Fazzio, M. Caldas, and A. Zunger, *Phys. Rev. B* **30**, 3430 (1984).

FIG. 18. Trends in the $d \rightarrow d^*$ internal transition energies of the Co^{2+} impurity in various host crystals. Asterisks denote observed transitions (Table V and Fig. 5); others are obtained from the effective crystal-field multiplet theory (M. Caldas, A. Fazzio and A. Zunger, unpublished, 1984). The ground state is $^4A_2(e^4t^3)$; the excited-state multiplet is shown in each case, as well as its dominant one-electron configuration. P denotes predicted. Dashed lines connect the same excited state in different host crystals, to guide the eye.

Co^{2+} impurity in a number of semiconductors. Note that many hitherto unobserved transitions are predicted here. Despite the global similarities in the observed spectra of Co^{2+} in various host crystals (showing only spin-allowed transition; see Fig. 5), *spin-forbidden* transitions are predicted to be distinctly different in various materials.

b. Donor and Acceptor Ionization Energies

Since the observed $d \rightarrow d^*$ transitions for $3d$ impurities pertain to the A^0 charge state in II-VI semiconductors and the A^- charge state in III-V semiconductors, the fit to the excitation spectra[138] produces just the mean-field parameters for these charge states. In what follows I will estimate the chemical trends in the other charged state by assuming, for a lack of better information, that the orbital-deformation parameters λ_e and λ_t that pertain to the 2+ oxidation state are also approximately valid for the neighboring oxidation states 3+ and 1+. The "self-regulating response" of the charge density to ionization (Part VI,20) provides a justification for this approximation. No such approximation is needed for Δ_{eff} because the multiplet *correction* does not depend on Δ_{eff}.

Figure 17b[138] depicts the negative of the multiplet corrections $[E_{\text{MC}}^{(N,i)}$ of Eq. (10.1)] to the ground states of A^0, A^+, and A^- $3d$ impurities in ZnS, ZnSe, and

GaP, respectively, calculated from the FCZ formalism, using the spectroscopically determined MF parameters. In all cases the largest correction occurs for the highest spin state $^6A_1$, i.e., in II-VI semiconductors for $Cr^+(A^-)$, $Mn^{2+}(A^0)$, and $Fe^{3+}(A^+)$ and in III-V semiconductors for $Mn^{2+}(A^-)$, $Fe^{3+}(A^0)$, and $Co^{4+}(A^+)$. The ordering of the corrections reverses in the low-Z limit ($A^- > A^0 > A^+$) relative to the high-Z limit ($A^+ > A^0 > A^-$). This parallels the trends in the spin-only contributions (Fig. 10b) and suggests that much of the MC results from spin effects. Notice the overall reduction in MC in going from ionic (ZnS) to more covalent (GaP) semiconductors.

Using the multiplet corrections to the ground states of A^0, A^+, and A^-, we can further calculate their differences, i.e., the multiplet correction $\Delta E_{MC}^{(N+1,N)}$ for the $A^0 \to A^-$ acceptor transitions [Eq. (10.16)] and the correction $\Delta E_{MC}^{(N,N-1)}$ for the $A^0 \to A^+$ donor transitions [Eq. (10.18)]. These corrections to the mean-field predictions for donor and acceptor activation energies are displayed in Fig. 17c. I have labeled each point with the symbol e or t, which denotes the orbital being ionized in the transition. Figure 19 shows on a block diagram the MC part (clear areas), the MF parts (shaded areas), and their sum (the experimental transition energy, depicted as a solid dot) for the ionization transitions in GaP:3d. The multiplet corrections to the ionization energies are seen to be substantial on the scale of the band gap. For the V and Cr acceptors, the correction is negative in II-VI materials and III-V materials (pushing the acceptor level of MF calculations toward the VBM). The opposite is true for Ni and Co, having positive acceptor corrections. The largest corrections occur for the Mn states in II-VI semiconductors and the Mn acceptor in III-V semiconductors, reflecting the combination of large deformation parameters (Fig. 13b,c) with small effective crystal-field splitting (Fig. 13a). DeLeo *et al.*[162] drew similar conclusions for interstitial 3d impurities in Si.

By subtracting the multiplet corrections $\Delta E_{MC}^{(N+1,N)}$ and $\Delta E_{MC}^{(N,N-1)}$ (Fig. 17c) from the observed acceptor and donor energies, respectively (Table VII), we can obtain the corresponding ionization energy expected from MF theory [first two terms in Eqs. (10.17) and (10.19)]. [Having obtained the e or t_2 level position in this way, we can apply the experimentally deduced crystal-field energy Δ_{eff} (Table XII) and find the approximate position of the partner level.] Figure 20 displays the observed (thick horizontal lines) single-donor (in II-VI materials) and single-acceptor (in III-Vs) transition energies, along with the positions of the mean-field levels e and t_2 deduced in this analysis. I indicate in each case the one-electron configurations which correspond to each transition in the FCZ analysis of the data. Since no donor levels are observed with certainty for ZnS:Mn and ZnSe:Mn, we can predict these levels by the reverse process of extrapolating the transition-state t_2 levels of the adjacent elements and applying the experimentally deduced multiplet correction of Figs. 17 and 19.

FIG. 19. Deconvolution of the experimental transition energies for (a) first acceptors, (b) second acceptors, and (c) the lowest intracenter $d \to d^*$ excitation energies of divalent 3d impurities in GaP into a mean-field contribution (shaded area) and many-electron multiplet corrections (clear area). (●) denote their sum (i.e., the experimentally observed energies). [After V. Singh and A. Zunger, *Phys. Rev. B* **31**, 3729 (1985); see also Ref. 259 below.] Note that many-electron effects can have an opposite sign to that of the mean-field effects. The nonmonotonic trends in the observed energies often result from the nonmonotonicity in many-electron effects; mean-field effects are usually monotonic, showing simple chemical trends.

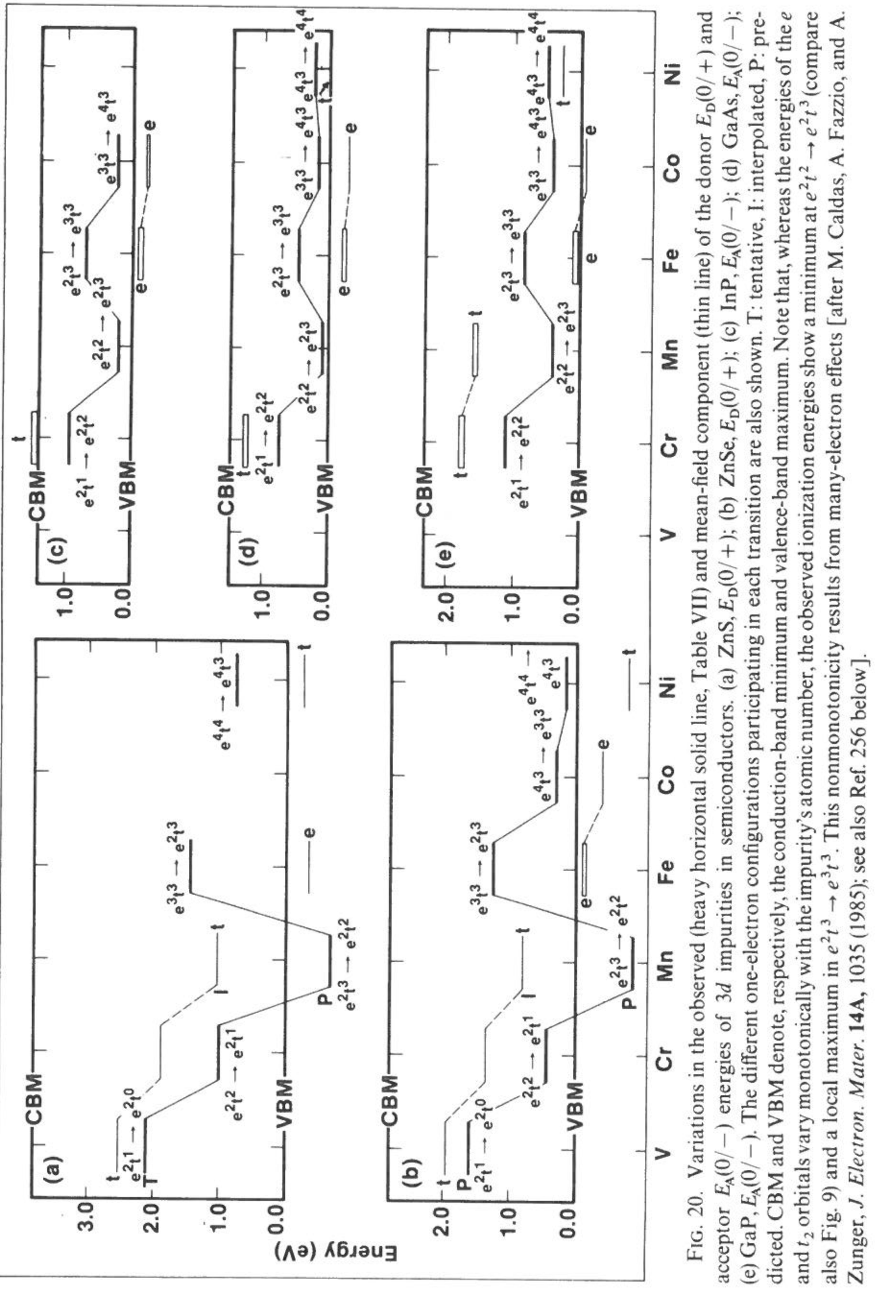

FIG. 20. Variations in the observed (heavy horizontal solid line, Table VII) and mean-field component (thin line) of the donor $E_D(0/+)$ and acceptor $E_A(0/-)$ energies of $3d$ impurities in semiconductors. (a) ZnS, $E_D(0/+)$; (b) ZnSe, $E_D(0/+)$; (c) InP, $E_A(0/-)$; (d) GaAs, $E_A(0/-)$; (e) GaP, $E_A(0/-)$. The different one-electron configurations participating in each transition are also shown. T: tentative, I: interpolated, P: predicted. CBM and VBM denote, respectively, the conduction-band minimum and valence-band maximum. Note that, whereas the energies of the e and t_2 orbitals vary monotonically with the impurity's atomic number, the observed ionization energies show a minimum at $e^2t^2 \to e^2t^3$ (compare also Fig. 9) and a local maximum in $e^2t^3 \to e^3t^3$. This nonmonotonicity results from many-electron effects [after M. Caldas, A. Fazzio, and A. Zunger, *J. Electron. Mater.* **14A**, 1035 (1985); see also Ref. 256 below].

The trends observed in Fig. 20 are revealing. *First*, we see that the strong nonmonotonicity exhibited by the experimental donor and acceptor energies (see also Fig. 9) results from similar nonmonotonicity in the multiplet corrections $\Delta E_{MC}^{(N+1,N)}$ and $E_{MC}^{(N,N-1)}$. Hence, mean-field theory should exhibit a simple monotonic trend of the e and t_2 levels. The trend in the one-electron levels for a fixed impurity and changing host crystal is an increase in the binding energy as the ligand (anion) orbital becomes more tightly bound ($E_{ZnS} > E_{ZnSe} > E_{ZnTe} > E_{GaP}$). *Second*, this analysis predicts that the Mn donor levels in II-VI materials are inside the valence band, explaining the fact that, despite persistent attempts, its determination still remains elusive. *Third*, the analysis explains why Mn forms a shallow acceptor in III-V materials (E_v + 0.4 eV in GaP, E_v + 0.22 eV in InP, and E_v + 0.11 eV in GaAs) in terms of its large multiplet correction (Fig. 19a), associated with its large orbital-deformation parameters (Figs. 13b,c). *Fourth*, the theory predicts that the e level will disappear from the gap into the valence band in going from Fe to Co impurities in GaP and for the Fe impurity in ZnSe. It also predicts the position of the yet-unobserved donor level in ZnSe:V at $E_v + (1.6 \pm 0.3)$ eV.

c. *The Mott–Hubbard Coulomb Energies*

The analysis we have used makes it possible to calculate the multiplet correction $\Delta U_{MC}^{(ijk)}(A^q)$ to the mean-field approximation for the Coulomb repulsion energy [Eqs. (10.21)] from the corresponding MC corrections to the donor and acceptor energies. Table VIII[138] depicts the results for those systems that have a common one-electron level in both donor and acceptor transitions. It is seen that these *multiplet corrections are negative, hence tend to reduce Coulomb energies*, in particular at the center of the $3d$ series. Hence, the stability of many charged states of transition-atom impurities in semiconductors results both from the reduction of U by *nonlinear screening effects* (to be discussed in Part VI,20) and from its reduction by *many-electron multiplet effects*. If $\Delta U_{MC}^{(ijk)}(A^q)$ [Eq. (10.21)] is sufficiently negative, it could outweigh the relaxed U_{MF}, leading to the possibility of an "exchange-correlation negative effective U." This is further discussed in Part VI,27.

Having separated MF from MC effects in the observed spectra of $3d$ impurities in semiconductors, we now review the MF calculations performed on $3d$ impurities in semiconductors.

V. Electronic-Structure Calculations in the Mean-Field Approach

In this section I review the electronic structure calculations on $3d$ impurities in semiconductors performed within the MF approach, i.e., using an a_1-symmetric charge density, where a_1 is the totally symmetric representation of

the symmetry group formed by the nuclei of the ligands and the impurity. Such calculations can, at best, reproduce that portion of the experimental observable that is non-many-electron in nature, as discussed in Part IV,10–12. Many-electron corrections obtained in Part IV,14 have to be added; these will be discussed in Part VI,26.

15. The Point-Ion Crystal-Field Model

Perhaps the simplest and earliest approach[169] to the problem (see also Refs. 4,5) has been the point-ion crystal-field approach. In essence, this approach takes into consideration the correct symmetry of the problem, as manifested in Eqs. (2.1)–(2.13) and (2.18) and in Table I, but it represents the radial integrals (which obviously are not symmetry determined) by adjustable parameters. Since this approach has been discussed extensively in the literature,[4–9] I formulate here only its essential points as applied to T_d symmetry.

The main approximations made by the point-ion crystal-field method for T_d symmetry are as follows: (1) The correct symmetry of the potential $V(\mathbf{r})$ of Eq. (2.1) is formally implied; only its first two or three l components are retained, however. (2) The actual radial dependence of the crystal potential $V_l(|\mathbf{r}|)$ is not calculated from the electronic structure (as in Fig. 3). Instead, these coefficients are evaluated by assuming that each of the four nearest-neighbor ligands, at distance d from the impurity, carries a point charge $\bar{q}$ (usually, its nominal valence) and by expanding this electrostatic field with respect to the impurity site as origin. More distant ligand sites are ignored and the existence of a *spatially distributed* bond charge density is represented by *point* charges. This leads to simple expressions for the coefficients of Eq. (2.1), e.g., $V_0(|\mathbf{r}|) = (4\bar{q}/d)\sqrt{4\pi}$; $V_3(|\mathbf{r}|) = 20(2\pi/315)^{1/2}(\bar{q}e/d^4)r^3$, etc. (3) It is assumed that the N "active" electrons occupy a single one-electron level i for each representation e and t_2. Other representations [Eqs. (2.10)–(2.13)], or the existence of more than one e and t_2 state (i.e., valence-band resonances) are omitted. (4) In first order, only the $l = 2$ component of $\psi_\sigma^{t_2,\lambda}(\mathbf{r})$ is retained; p-like contributions may be added as a perturbation. Because $l = 1$ is omitted, as shown below, the $V_3(|\mathbf{r}|)$ component of the potential does not enter the problem. (5) The general radial functions $\mathbf{G}_{i,l}^{\alpha,\sigma}(|\mathbf{r}|)$ are represented in this approach by atomic (or ionic) radial orbitals $R_{nl}(|\mathbf{r}|)$. Radial expansion or contraction of these orbitals relative to the free ions (resulting from impurity–host interactions) are neglected. (6) It is assumed that the e and t_2 representations have *the same* radial orbitals; i.e., $G_2^{t_2,\sigma}(|\mathbf{r}|) = G_2^{e,\sigma}(|\mathbf{r}|)$ in Eqs. (2.12) and (2.14).

[169] H. Bethe, *Ann. Phys.* **3**, 133 (1929).

(7) It is assumed (with no proof) that the impurity radial orbitals $G_l^{\alpha,\sigma}(|\mathbf{r}|) = R_{nl}(|\mathbf{r}|)$ are eigenfunctions of $T_R + V_{l=0}(|\mathbf{r}|)$, where $\hat{T}_R$ is the radial Laplacian, and $V_{l=0}(|\mathbf{r}|)$ is the spherically symmetric component of the a_1-symmetric potential.

Using these assumptions, it is straightforward to evaluate the one-electron orbital energies $\varepsilon_\sigma^\alpha$ of Eq. (2.15) and their difference, i.e., the one-electron crystal-field splitting Δ_{CF} of Eq. (2.16). The result is

$$\Delta_{CF} = -\frac{20}{27}\frac{\bar{q}e^2}{d^5}\langle R_{nl}|r^4|R_{nl}\rangle \equiv \text{"}10Dq\text{"}. \qquad (15.1)$$

In these approximations, Δ_{CF} is decided by $V_{l=4}(|\mathbf{r}|)$ and not by $V_{l=3}(|\mathbf{r}|)$ (since an angular integral of the three Kubic harmonics $K_2^{t_2} \times K_3^{a_1} \times K_2^{t_2}$ is zero). Equation (15.1) implies that (1) Δ_{CF} decreases rapidly ($\sim d^{-5}$) as the impurity–ligand distance increases (for ZnS, GaP, ZnSe, and InP, d = 4.43, 4.46, 4.62, 4.64, and 4.80 a.u., respectively). (2) Δ_{CF} increases rapidly ($\sim\langle r^4\rangle$) as the impurity d orbital becomes more expanded. Hartree–Fock radial integrals $\langle r^4\rangle$ for the T^{2+} oxidation state[170] are: Sc (19.13), Ti (12.51), V (9.07), Cr (6.89), Mn (5.29), Fe (4.50), Co (3.76), Ni (3.16), and Cu (2.67), all in atomic units. (3) Δ_{CF} increases linearly with the nominal ionicity of the ligands[73] $\bar{q}$; i.e., for sulphides, phosphides, and silicides we have $\bar{q}_S > \bar{q}_P > \bar{q}_{Si}$. (4) Δ_{CF} is negative; i.e., the e orbital is lower in energy than the t_2 orbital. (5) Δ_{CF} for tetrahedral T_d symmetry is $\frac{4}{9}$ as small as Δ_{CF} for octahedral symmetry (having 6 nearest neighbors) and has the opposite sign.

Except for giving the correct sign of Δ_{CF}, none of the other implications of Eq. (15.1) survives *quantitative* scrutiny for 3d impurities in semiconductors (using the values of d and $\bar{q}$ given above and comparing the resulting Δ_{CF} with that obtained in self-consistent Green's-function calculations; see Part VI). The strength of this approach lies in the interpretation of the quantity "10Dq" as a completely adjustable parameter, to be fit to the observed spectra through the Tanabe–Sugano diagrams, but its microscopic analysis through Eq. (15.1) is often off by 100–200%. [Regrettably, since the application of the Tanabe–Sugano diagrams to T_d symmetry pertinent to cubic semiconductors is by itself a crude approximation (see Part IV,11), the 10Dq values obtained in such fits are of little significance; in fact, they *decrease* as $\langle r^4\rangle$ increases.] The situation is somewhat better for 3d impurities in highly ionic octahedrally coordinated compounds, since in these: (1) $V_{l=3}(|\mathbf{r}|) \equiv 0$, (2) $G_1^{t_2,\sigma}(|\mathbf{r}|) \equiv 0$, (3) the ligands are indeed close to having a highly localized, pointlike charge distribution, and (4) the impurity radial orbitals $G_l^{\alpha,\sigma}(|\mathbf{r}|)$ show smaller distortion

[170] S. Fraga, J. Karwowski, and K. M. S. Saxena, "Handbook of Atomic Data," p. 481. Elsevier, Amsterdam, 1976.

relative to the free ions. It is now recognized[171,172] that Δ_{CF} does not arise solely from the electrostatic effect of the negatively charged ligands, since the impurity orbitals can penetrate the ligands sufficiently to experience the opposing shield of their nuclei (see also Part VI,18,c). Furthermore, Δ_{CF} also receives sizable contributions from *kinetic*, rather than *potential* effects [cf. Eq. (2.15)], because of the orthogonality nodes at the ligand sites as well as from covalency effects.

A number of refinements of the point-ion crystal-field model have been attempted, most notably incorporation of different radial functions for e and t_2 representations by empirical adjustments[4,173] [yet, retaining the point-ion version of $V(\mathbf{r})$ and simple atomic R_{nl} orbitals] and an empirical covalency factor.[174] In the author's opinion, the point-ion crystal-field model remains as a useful interpolation scheme for known data but lacks any quantitative predictive ability.

16. Ligand-Field and Cluster Models

In this approach, a few of the atoms surrounding the impurity are characterized not only by the *potential* $V(\mathbf{r})$ they experience (as is the case in crystal-field models), but also by the *orbitals* which they span. The potential $V(\mathbf{r})$ is usually calculated quantum mechanically from the wave functions, and no simple electrostatic form is assumed. In essence, this approach provides the first step towards a more complete incorporation of environmental effects, recognizing that host states may be strongly coupled to the orbitals of the free ions. Different calculations are distinguished by the type of MF Hamiltonian used (Hartree–Fock, local density, or semiempirical), the number of ligand atoms included (cluster size), the way that the dangling bonds at the surface of the cluster are handled, and the type of results sought (one-electron orbital energies, crystal-field splittings, excited states, ionization energies, etc.).

Earlier applications (e.g., Roitsin and Firshtein,[175] Walter and Birman,[176] and Kogan and Tolpygo[177]) have utilized linear-combination-of-atomic-

[171] A. J. H. Wachters and W. C. Nieuwpoort, *Phys. Rev. B* **15,** 4291 (1972).
[172] T. F. Soules, J. W. Richardson, and D. M. Vaught, *Phys. Rev. B* **3** 2186 (1971).
[173] E. F. Kustov and L. I. Uskova, *Phys. Status Solidi* **102B,** 209 (1980).
[174] S. W. Biernacki and H. J. Schulz, *Phys. Status Solidi* **103B,** K163 (1981); S. W. Biernacki, *Phys. Status Solidi* **118B,** 525 (1983).
[175] A. B. Roitsin and L. A. Firshtein, *Fiz. Tverd. Tela* **13,** 63 (1971) [*Sov. Phys. Solid State* **13,** 50 (1971)].
[176] W. Walter and J. L. Birman, *in* "II-VI Semiconducting Compounds" (D. G. Thomas, ed.), p. 89. Benjamin, New York, 1967.
[177] L. S. Kogan and K. B. Tolpygo, *Fiz. Tverd. Tela* **15,** 1544 (1973) [*Sov. Phys. Solid State* **15,** 1033 (1973)]; **16,** 3176 (1974) [*Sov. Phys. Solid State* **16,** 2067 (1975)].

orbital (LCAO) methods, and have not treated the surface dangling bonds, an approach which has proved useful in previous studies[171,172,178] of $3d$ impurities in ionic crystals. Minimal basis sets, non-self-consistent solutions, and the neglect[176] or approximation[175] of the Hartree–Fock many-center integrals characterized these pioneering calculations. Despite such simplifications, these early calculations already captured many essential aspects of the problem: the significance of covalency and the delocalization of the t_2 states relative to e states.

Subsequent applications were based on self-consistent approaches. These included primarily the multiple-scattering X_α method[179] (MSX_α) and semiempirical complete neglect of differential overlap (CNDO)[180] or intermediate neglect of differential overlap (INDO) methods. In the MSX_α approach[179] the potential $V(\mathbf{r})$ is approximated by spherically symmetric potentials around each atomic site (within spheres of typically half a bond length, $d/2$) and constant potentials between the spheres. Since a *numerical* solution to the Schrödinger equation is involved, no basis-set convergence difficulties exist. The local-density approach[139] is used, with an adjustable coefficient α multiplying the $\rho^{1/3}$ exchange term. The CNDO and INDO methods[180] represent semiempirical simplifications of the Hartree–Fock Hamiltonian within a minimal, valence-only basis set.

Three types of boundary conditions have been explored in these approaches: saturation of the dangling bonds with hydrogen atoms,[181–186] or Watson-sphere saturation,[187,188] and embedding schemes.[189] These approaches

[178] W. H. Kleiner, *J. Chem. Phys.* **20,** 1784 (1952); J. W. Richardson, T. F. Soules, D. M. Vaught, and R. R. Powell, *Phys. Rev. B* **4,** 1721 (1971).
[179] K. H. Johnson and F. C. Smith, *Phys. Rev. B* **5,** 831 (1972).
[180] J. A. Pople and G. A. Segal, *J. Chem. Phys.* **44,** 3289 (1966); D. P. Santry and G. A. Segal, *J. Chem. Phys.* **47,** 158 (1967).
[181] Bo. G. Cartling, *J. Phys. C* **8,** 3183 (1975).
[182] L. A. Hemstreet, *Phys. Rev. B* **15,** 834 (1977).
[183] G. G. DeLeo, G. D. Watkins, and W. B. Fowler, *Phys. Rev. B* **23,** 1851 (1981); **25,** 4972 (1982); G. D. Watkins, G. G. DeLeo, and W. B. Fowler, *Physica* **116B,** 28 (1983).
[184] L. A. Hemstreet and J. O. Dimmock, *Solid State Commun.* **31,** 461 (1979); *Phys. Rev. B* **20,** 1527 (1979).
[185] L. A. Hemstreet, *Phys. Rev. B* **22,** 4590 (1980).
[186a] L. Hemstreet, *J. Electron. Mater.* **14a,** 1043 (1985).
[186b] P. K. Khowash, D. C. Khan, and V. A. Singh, *J. Phys. C* **18,** 6177 (1985). This cluster calculation on InP:$3d$ has assumed excited rather than ground state occupation numbers [for neutral Cr, Mn, Fe, and Co they used e^3t^0, e^4t^0, e^4t^1, and e^4t^2, while the correct occupations (see Fig. 48) are e^2t^1, e^2t^2, e^2t^3, and e^3t^3, respectively].
[187] (a) A. Fazzio and J. R. Leite, *Phys. Rev. B* **21,** 4710 (1980); (b) A. Fazzio, J. R. Leite, and M. L. De Siqueira, *J. Phys. C* **12,** 3469 (1979); (c) A. Dal Pino, A. Fazzio, and J. R. Leite, *Solid State Commun.* **44,** 369 (1982).
[188] M. L. De Siqueira and S. Larsson, *Chem. Phys. Lett.* **32,** 359 (1975).
[189] C. M. Müller and U. Scherz, *Phys. Rev. B* **21,** 5717 (1980).

attempt to circumvent the occurrence of molecular orbitals which represent surface states of the cluster (rather than legitimate impurity or bulk states), since a significant surface-to-volume ratio persists for most computationally manageable clusters. The hydrogen saturation approach[181–186] utilizes the fact that the hydrogen–host bonds created at the cluster's surface are often stronger than the host–host bonds. This pushes the spurious bonding (antibonding) surface states into the valence (conduction) bands, "cleaning up" the band-gap region from such surface states, at the risk of having them reappear in the valence band and interact with impurity-induced valence-band resonances. This bonding–antibonding repulsion enlarges artificially the band gap, and creates a sensitive dependence of the results on the assumed hydrogen–ligand bond length. In an alternative approach,[187,188] an external potential (in the form of a "Watson sphere"[179]) is applied to the cluster with the intention that it raise the energy of the spurious surface orbitals, rendering them high-energy scattering states, unable to couple to the impurity-induced states. This expulsion of electrons from the cluster lowers, however, the overall Coulomb repulsion potential there, leading sometimes to an exaggerated binding of localized impurity states. Gemma[190] proposed to eliminate surface states by removing all basis orbitals which would span such states, thereby depriving the system of the variational flexibility necessary to describe the spurious surface states. However, this reduces also the *overall* variational flexibility of the method since a subminimal basis set is used to describe even the physically relevant impurity states. The method is not amenable to a systematic improvement of the basis set, as a larger basis will reintroduce the unwanted surface states. (Sferco and Passeggi[191] have recently pointed out that Gemma[190] used incomplete shells of ligands around the central impurity, leading to an incorrect field at the impurity site.) Müller and Scherz[189] proposed to embed their 17-atom cluster in an external potential set up by the point-ion (Madelung) field of the atoms outside the cluster. Since the *repulsive* interaction of the electrons of the cluster (which are retained) with those outside the cluster (which are excluded) was omitted, a spurious charge imbalance on the surface was obtained. This required adding constant terms to the diagonal matrix elements of the Hamiltonian to reverse the flow of charge towards neutrality. It is then unclear how these manipulations of cluster states affect the physically relevant impurity states.

The sensitivity of the results of cluster models to different treatments of the cluster's surface states can be partially assessed from the data available in the literature by comparing results using the same Hamiltonian and method of solution, but different boundary conditions. Figure 21a and b compares the

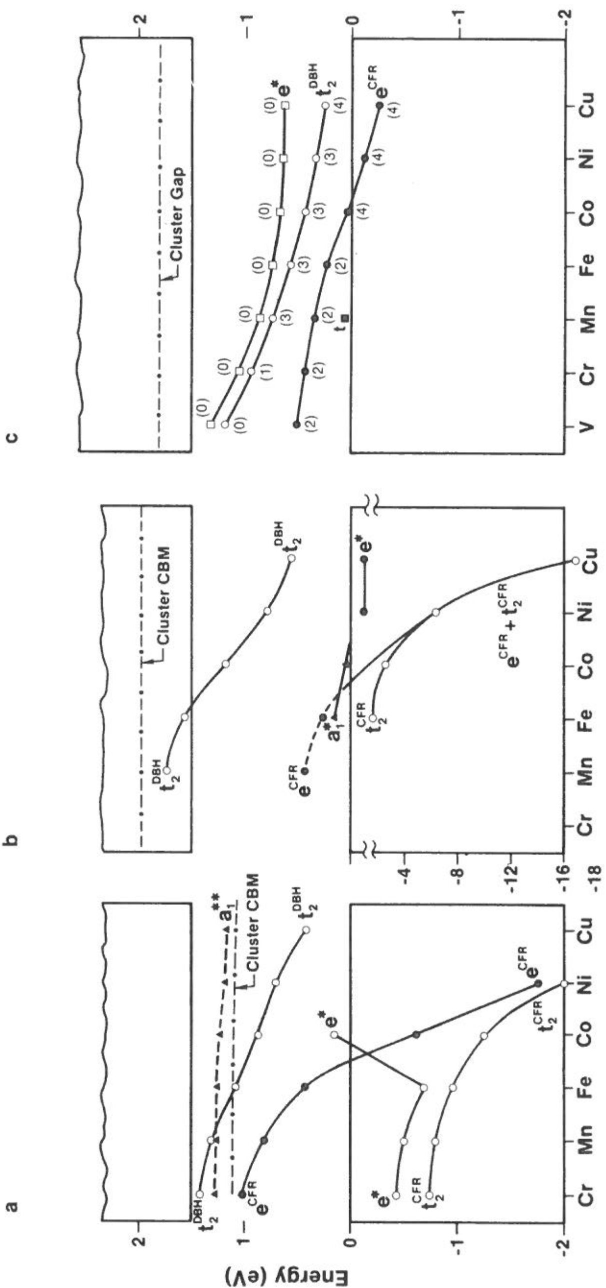

FIG. 21. Calculated one-electron energy levels of 3*d* impurities in GaAs. (a) MSX_α cluster calculation of L. A. Hemstreet, *Phys. Rev. B* **22**, 4590 (1980) using hydrogen saturation, $H_{12}As_4{:}T^{3+}$; (b) MSX_α cluster calculation of A. Fazzio and J. R. Leite, *Phys. Rev. B* **21**, 4710 (1980), using Watson-sphere saturation, $Ga_{12}As_4{:}T^{3+}$; (c) continued-fraction Green's-function calculation of M. P. Lin and V. F. Masterov, *Sov. Phys. Semicond.* **11**, 864 (1976), using the extended Hückel approximation. Numbers in parentheses give level occupations. t_2^{CFR}, e^{CFR}, and t_2^{DBH} denote, respectively, the t_2 and e "crystal-field resonances" (CFR) and the t_2 "dangling-bond hybrids." These levels are found also in self-consistent Green's-function calculations (e.g., Fig. 25b below). The other levels—e^*, a_1^*, a_1^{**}—are not. The figure shows the experimental band gap of GaAs, along with the band gap obtained in the respective cluster calculation (–·–·– denote "cluster gap"). The two MSX_α calculations give similar positions of the t_2^{DBH} levels, but differ substantially in the predicted positions of the e^{CFR} levels of the heavy 3*d* impurities. These two calculations produce localized e^* levels which have no counterparts in calculations using periodic boundary conditions. The results in (c) show an empty e^* level in the gap missing both from other cluster and from self-consistent Green's-function calculations.

[190] N. Gemma, *J. Phys. C* **17**, 2333 (1984).

[191] S. J. Sferco and M. C. G. Passeggi, *J. Phys. C* **18**, 3717 (1985).

results for two MSX_α cluster calculations for neutral substitutional $3d$ impurities in GaAs: that of Fazzio and Leite[187a] (Fig. 21b), using Watson sphere saturation, and that of Hemstreet[185] (Fig. 21a), using hydrogen saturators. Both methods show a t_2 gap level, labeled "dangling-bond hybrid" (DBH, for reasons to become apparent below), as well as t_2 and e levels, labeled "crystal-field resonance" (CFR). The t_2^{DBH} gap-level positions differ by ≤ 0.6 eV in these two calculations, but the e^{CFR} levels differ by as much as 13 eV for Cu (the Watson-sphere saturation[187] pulls this localized level to very negative energies, as discussed above). In addition, Hemstreet[185] found an a_1-type gap level near the conduction band (labeled a_1^{**}) which Fazzio *et al.*[187a] did not find. Instead, they found an occupied a_1 level near the valence-band maximum for Fe and Co (labeled a_1^*). Both authors found an e level just below the valence-band maximum (labeled e^*). [Recent first-principles self-consistent Green's-function calculations[54] for $3d$ impurities in GaP (Fig. 25b below) do not find any of the a_1^{**}, a_1^*, or e^* levels.] The one-electron crystal-field splitting in the calculation with the Watson-sphere saturation is 2–5 times larger than that obtained with hydrogen saturators. Similarly, a MSX_α cluster calculation of Khowash *et al.*[186b] for InP: $3d$, utilizing a simple Watson sphere outside the cluster, shows significant quantitative discrepancies relative to an earlier MSX_α calculation[186a] with hydrogen saturators. In a different system, DeLeo *et al.*[183] observed a fourfold increase in the band gap of the $Si_{10}H_{16}$ cluster as the Si–H distance was reduced by 25%. Δ_{CF} and the degree of localization of the impurity gap levels changed significantly, too. Figure 22 compares the energy levels of neutral interstitial $3d$ impurities as obtained in an MSX_α cluster calculation[162,183] with those obtained in a first-principles self-consistent Green's-function approach[192] (the quasi-band crystal-field approach, to be described in Part V,17). Compared with the extended crystal Green's-function results, the MSX_α cluster model reveals an upward shift of the energy levels and a dramatic reduction in Δ_{CF} (with Fe, Co, and Ni having $\Delta_{CF} \approx 0$). This has been attributed[20] to the neglect of nonspherical potential components inside the muffin-tin sphere in the MSX_α model,[183] which underestimates the covalency in favor of an atomically localized description.

The application of self-consistent cluster models to d-electron impurities in semiconductors[175–177,181–189,193,194] revealed a number of important features in the electronic structure: (1) The impurity-atom $3d$ orbitals distribute their amplitude both in e and t_2 gap levels as well as in valence-band resonances. (2) The impurity orbital energies move as a function of the impurity's atomic number Z (Figs. 21, 22) from deep inside the host valence

[192] A. Zunger and U. Lindefelt, *Phys. Rev. B* **26,** 5989 (1982).
[193] R. L. Kleinhenz, V. A. Singh, and J. A. Corbett, unpublished results, 1981.
[194] J. E. Lowther, *Phys. Lett.* **104A,** 273 (1984); see details on method in J. E. Lowther *J. Phys. C* **13,** 3665 (1980).

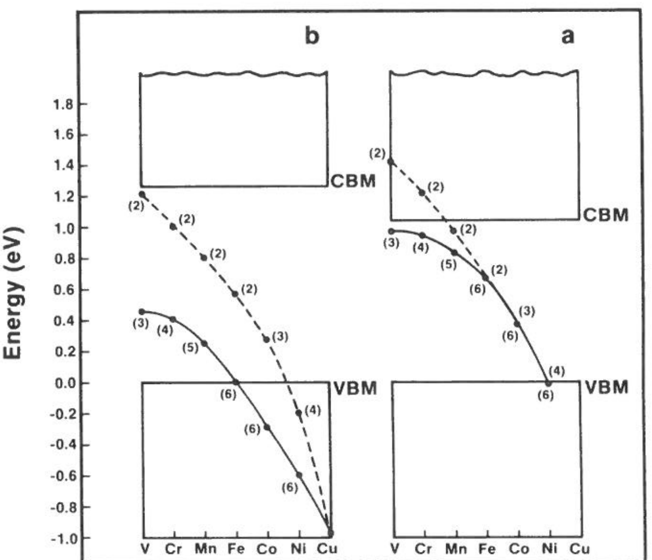

FIG. 22. Comparison of the calculated one-electron gap levels of neutral interstitial $3d$ impurities in Si as calculated by (a) the MSX_α cluster method of G. G. DeLeo, G. D. Watkins, and W. B. Fowler, *Phys. Rev. B* **23,** 1851 (1981) using hydrogen saturators and muffin-tin potentials, and (b) the QBCF Green's-function method of A. Zunger and U. Lindefelt, *Phys. Rev. B* **26,** 5989 (1982). Occupation numbers are denoted in parentheses. (———) show the t_2 levels, (– – –) show the e levels. Relative to the Green's-function calculations, the cluster model shows an overall shift of the spectra towards higher energies, and far smaller e-t_2 crystal-field splittings.

band (high Z) to the band-gap region (low Z). (3) As the t_2 impurity level approaches the band-gap region it becomes more delocalized and acquires a hostlike character. (4) Interstitial impurities have their t_2 gap level below the e gap level (Fig. 22), whereas for substitutional impurities the order is reversed (Fig. 21). (5) The one-electron crystal-field splitting Δ_{CF} increases with the covalency of the host crystal.

Picoli *et al.*[195] presented a two-level ligand-field model for $3d$ impurities in sp-bonded tetrahedral solids. This model is similar to that used previously[19,196] (discussed also in Part VI,18c) to analyze the results of the detailed Green's-function calculations. However, the model of Picoli *et al.* describes the impurity energies in terms of eight free parameters for each impurity and each charge state. The eight parameters of the model are not calculated, but are partially guessed and partially used to fit known data and other calculations.

[195] G. Picoli, A. Chomette, and M. Lannoo, *Phys. Rev. B* **30,** 7138 (1984).
[196] A. Zunger and U. Lindefelt, *Solid State Commun.* **45,** 343 (1983); *Physica* **117B,** 185 (1983).

This eight-parameter ligand-field model has been used to calculate $d \rightarrow d^*$ excitation energies for GaAs:Cr^{2+}, predicting 7.9 eV for the $^5E \rightarrow {}^5T_2$ excitation energy, an order of magnitude larger than the observed value (see Table V). In a subsequent calculation, Picoli *et al.*[195] fitted their result to this experimental value. The corrected orbital energies compare poorly, however, with the nonempirical spin-polarized cluster calculation of Hemstreet and Dimmock[184] for GaAs:Cr^{3+}: the orbital energies for the gap levels, e_+, e_-, t_+, and t_- are (relative to the valence-band maximum) 0.3, 0.65, 0.65, and 0.78 eV, respectively, in the cluster calculation,[184] and −0.3, 1.14, 0.59, and 1.5 eV in the calculation of Picoli *et al.*[195] It appears that this eight-parameter model has sufficient flexibility to be fitted judiciously to the data and other calculations (and hence can be used as a useful interpolation scheme); however, its success depends strongly on the *availability* of better calculations and experimental data to fit this model.

Cluster models for impurities have often been criticized[13,17] for their inability to obtain the correct host-crystal band edges, treat surface effects adequately, or demonstrate convincingly the convergence of the calculated properties with the cluster's size. The underlying premise of such applications is that it is practical to handle cluster sizes that equal or exceed the range of localization of deep impurity states, and that there exists a natural hierarchy of coordination shells around the impurity such that more distant shells can be safely neglected. There are, however, two hitherto unrecognized potential difficulties with these assumptions. *First*, the occurrence of impurity states in bonding–antibonding pairs suggests that, as the bonding state becomes more *localized*, so does the antibonding state become more *delocalized* (being expelled by the orthogonality condition from the volume occupied by the lower bonding state). This suggests that it is not always reasonable to expect that cluster models will better suit more localized impurities, since their physically interesting *antibonding* (gap) levels may then have wave functions that extend beyond the cluster. *Second*, while it is true that each distant shell of ligand atoms interacts more weakly with the central impurity atom than closer shells do, the density of states set up by distant shells increases rapidly with distance. In other words, since cluster models neglect the continuous *energy dependence* of the distribution of the various host levels, physically significant states associated with distant ligands may be omitted, too. An ideal cluster model should include all states of the pure host crystal that are energetically close to the impurity level (and spatially overlap with it), whether these host states are associated with nearby ligand shells or with distant ones. To illustrate this I present in Fig. 23[197] the local density of states (LDOS) of a *pure Si crystal* (obtained from band-structure calculations[197]), projected on

[197] H. Katayama-Yoshida and A. Zunger, unpublished, 1985.

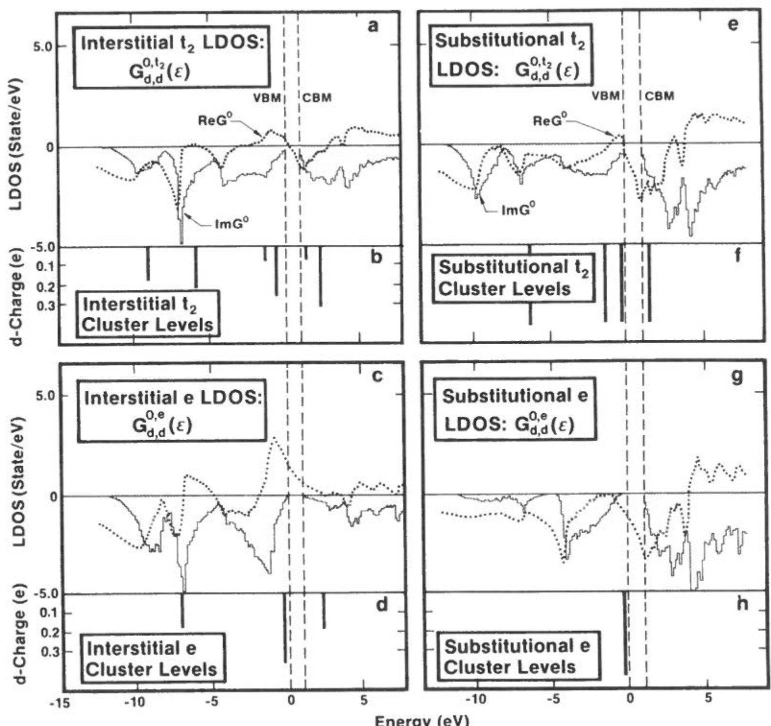

FIG. 23. Local density of states of a pure Si crystal (Im, G^0, shaded areas) calculated from a pseudopotential band structure, projected at the interstitial site (a, c) or the substitutional site (e, g). Results are given for the *d*-orbital components of the t_2 and *e* representations. (···) show the real part of the Green's function. Vertical lines (---) denote the valence-band maximum and conduction-band minimum. The solid vertical lines in parts (b), (d), (f), and (h) show the discrete levels obtained in cluster calculations. [(f) and (h) are from Bo. G. Cartling, *J. Phys. C* **8**, 3183 (1975); and L. A. Hemstreet, *Phys. Rev. B* **15**, 834 (1977), using the Si_5H_{12} cluster. (b) and (d) are band *d* from G. G. DeLeo, G. D. Watkins, and W. B. Fowler, *Phys. Rev. B* **23** 1851 (1981), using the $Si_{10}H_{16}$ cluster.] The figure shows that, whereas some of the peaks in the continuous LDOS are mimicked correctly by cluster models [e.g., in parts (c) and (d), the *e*-type peak −8 eV], most are not [e.g., in parts (c), (d), (g), and (h) the cluster model shows spurious *e* states near the VBM and CBM.] Since one-electron impurity levels are formed through the interaction of the impurity atomic orbitals with the host states of the appropriate symmetry, the misrepresentation by cluster models of the correct energy dependence of the host crystal levels may lead to errors in the impurity levels (e.g., e^* levels in Fig. 21a,b). [LDOS calculated by H. Katayama-Yoshida and A. Zunger (unpublished, 1985), from their Green's function method, using a local pseudopotential band structure of Si.]

the (empty) interstitial site (a and c) or the substitutional site (e and g). In each case I show separately t_2-like states (Fig. 23a,e) and *e*-like states (Fig. 23c,g). For comparison, I show the discrete levels obtained in (pure) *cluster* calculations (Fig. 23b, d, f, and h). Ideally, there should be a match between the

cluster levels and the peaks of the local density of states (Im G^0 in Fig. 23). Unfortunately, this is not the case. For the interstitial case, cluster models position correctly the deep host e states (Fig. 23c and d) but show a spurious e state near the VBM and misrepresent the distribution of the t_2 states (Fig. 23a, b) near the top of the VB. For the substitutional case, small-cluster models miss altogether the conduction band e states and show a spurious e state near the VBM (Fig. 23g, h). I suspect that this spurious *pure cluster* level is responsible for the equally spurious e^* level obtained in impurity calculations (see Fig. 21a, b). This analysis suggests that better cluster calculations can be made if the cluster's geometry and parameters are chosen to mimic the peaks in the LDOS of the extended host crystal.

17. Green's-Function Methods

These approaches utilize the decomposition of $V(\mathbf{r})$ [and $\rho(\mathbf{r})$] into an extended periodic piece and a perturbation $\Delta V(\mathbf{r})$ [and $\Delta\rho(\mathbf{r})$] which is localized around the impurity.[198,199] The former is described by the host-crystal Green's function, permitting concentration of one's computational sophistication (i.e., self-consistency, variationally flexible basis sets, realistic Hamiltonians) on a relatively small volume spanned by the perturbation $\Delta V(\mathbf{r})$. None of the difficulties faced by small-cluster approaches occur. The main disadvantages, however, of such approaches are: (1) Green's-function models are considerably more difficult to construct than cluster models (only in the past few years have self-consistent impurity Green's-function models[21,137,200] been set up, although the basic formalism[198,199] existed for over thirty years); (2) information outside the range of $\Delta V(\mathbf{r})$ (e.g., spin densities to be compared with ENDOR data) is not easily obtained (usually a solution to the Lippman–Schwinger equation is necessary for this[21]); and (3) when the impurity orbitals cannot be described by a small number of host crystal states (e.g., if the lattice is severely distorted, or the impurity atom introduces a fundamentally new orbital type into the spectrum), special techniques[21,201] which go beyond the Koster–Slater formalism[198] are needed. Details of the formalism are described elsewhere.[21] Calculations for $3d$ impurities can be separated into: (1) empirical and (2) first-principles self consistent approaches. They differ in the type of Hamiltonian and basis sets used, as well as in the computational strategy used to solve the equations. These are reviewed next.

[198] G. F. Koster and J. C. Slater, *Phys. Rev. B* **96,** 120 8 (1954).

[199] J. Callaway and A. J. Hughes, *Phys. Rev.* **156** 860 (1967); F. Bassani, G. Iadonisi, and B. Preziosi, *Phys. Rev.* **186,** 735 (1969).

[200] R. Podloucky, R. Zeller, and P. H. Dederichs, *Phys. Rev. B* **22,** 5777 (1980).

[201] A. R. Williams, P. J. Feibelman, and N. D. Lang, *Phys. Rev. B* **26,** 5433 (1982).

a. *Empirical Green's-Function Approaches*

These approaches[202–209] parametrize the host-crystal band structure and the impurity potential to achieve agreement with certain experimental data. They are distinguished by the type of parametrization used [e.g., extended Hückel,[202–205] (see Ref. 210 for details of this semiempirical Hamiltonian), empirical tight-binding,[206,207] pseudopotential[208]], the method used to solve the Green's-function equations (e.g., continued-fraction,[202–206] Slater–Koster approach[207]), the spatial extent of the perturbation treated (e.g., impurity site only,[202,207,209] impurity plus nearest neighbors[206]), and the degree of self-consistency attempted (none,[202,209] impurity site only,[207,208] etc.). The early applications of single-particle Green's-function approaches to $3d$ impurities in semiconductors include the work of Ermakov,[202] who used a non-self- consistent extended Hückel (EXH) approach within a 17-atom continued-fraction method. Results on substitutional $3d$ impurities in Si have shown a nonmonotonic trend in the gap levels with atomic number, a trend not matched by modern calculations. Masterov *et al.*[13,203–205] extended this work to substitutional $3d$ impurities in GaAs,[203] GaP,[205] and InP,[204] using a charge-dependent EXH within a 29-atom continued-fraction model. This iterative EXH method used a minimal, valence-only atomic basis set, represented the diagonal matrix elements as a function of the charge q_d, and approximated the off-diagonal matrix elements through the Wolfsberg–Helmholtz[210] approximation [i.e., $H_{ij} = \lambda(H_{ii} + H_{jj})S_{ij}$, where S_{ij} is the off-diagonal overlap matrix element and λ is a free parameter]. Variations of λ were found[203] to change the energy of the impurity levels by more than half the band gap (a rather unconventional value of $\lambda = 0.5$ has been chosen as a canonical value). The results for GaAs:T^{2+} (Fig. 21c) exhibit reasonable trends for the t_2^{DBH} and e^{CFR} gap levels but indicate an additional gap level (e^* in Fig. 21c) which is missing in all other (including recent) calculations. Similar results were obtained for GaP[205] and InP.[204] No data were presented on the band structure of the host crystals as produced by this parametrization.

[202] L. K. Ermakov, *Fiz. Tekh Poluprovodn.* **12,** 1230 (1978) [*Sov. Phys. Semicond.* **12,** 732 (1978)].

[203] V. F. Masterov, *Fiz. Tekh. Poluprovodn.* **18,** 3 (1984) [*Sov. Phys. Semicond.* **18,** 1 (1984)]; M. P. Ilin and V. F. Masterov, *Fiz. Tekh. Poluprovodn.* **11,** 1470 (1977) [*Sov. Phys. Semicond.* **11,** 864 (1976)].

[204] L. K. Ermakov, V. F. Masterov, and B. E. Samorukov, *Fiz. Tekh. Popuprovodn.* **18,** 2092 (1984) [*Sov. Phys. Semicond.* **18,** 1304 (1984)].

[205] V. F. Masterov, *Fiz. Tekh. Popuprovodn.* **12,** 625 (1978) [*Sov. Phys. Semicond.* **12,** 363 (1978)].

[206] P. Pecheur and G. Toussaint, *Physica* **116B,** 112 (1983).

[207] P. Vogl and J. Baranowski, *Int. Conf. Phys. Semicond. 17th*, p. 623 (1985).

[208] T. Hoshindo and K. Suzuki, *J. Phys. Soc. Jpn.* **46,** 341 (1979); **47,** 1141, 2031 (1980).

[209] J. A. Majewski, *Solid State Commun.* **40,** 407 (1981); *Phys. Status Solidi* **108b,** 663 (1981).

[210] R. Hoffman, *J. Chem. Phys.* **39,** 1392 (1963).

Hoshindo and Suzuki[208] used a minimal (pseudized) LCAO basis set, represented the potential $V(\mathbf{r})$ as a superposition of free-atom potentials, and utilized a 29-atom Bethe-lattice description of their Green's function. Application to interstitial $3d$ impurities in Si (Fig. 24a) revealed an unusual level ordering (e below t_2) and a partially occupied a_1 level in the lower part of the gap. These results are at odds with all other results on this system (compare recent QBCF results[140,192] in Fig. 24b). Majewski[209] has applied a non-self-consistent Green's-function approach to $3d$ impurities in ZnS and ZnSe, in which the impurity-atom potential is taken to be spherical and the host lattice is described by a collection of "muffin-tin" potentials; the perturbation was limited to the impurity atom alone. Despite these simplifications, very reasonable trends were observed in the gap levels.

In contrast to LCAO methods, tight-binding approaches[206,207] do not specify a basis set but parametrize instead the Hamiltonian *matrix elements* (hence, only the expansion coefficients of the wave functions in an unspecified basis are obtained). Two groups have applied tight-binding Green's-function methods to this problem. Pecheur and Toussaint[206] (see details of the method in Ref. 211) used a 4-orbital/atom ($s + 3p$) description of Si, included matrix elements H_{ij} up to second-nearest neighbors, allowed the perturbation to extend over the impurity and its first shell of neighbors, and solved the Green's

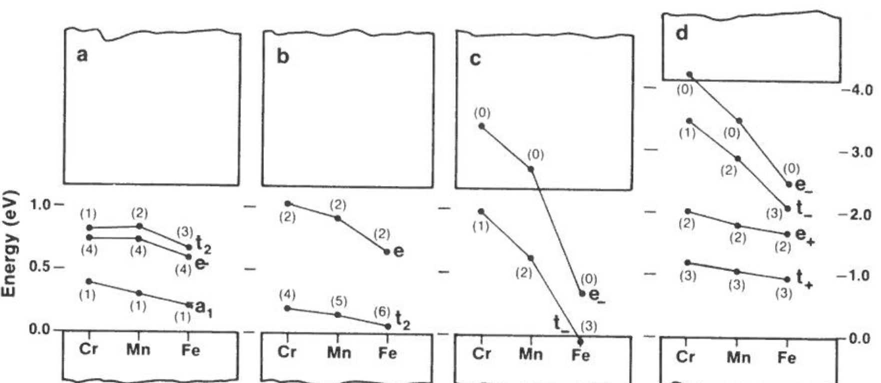

FIG. 24. Calculated one-electron energy levels of interstitial Cr, Mn, and Fe impurities in Si. (a) Bethe lattice LCAO model of T. Hoshindo and K. Suzuki, *J. Phys. Soc. Jpn.* **46**, 341 (1979) (partially occupied a_1 levels in gap and reversed ordering of e and t_2 levels are particular to this model alone); (b) QBCF first-principles Green's function model of A. Zunger and U. Lindefelt, *Phys. Rev. B* **26**, 5989 (1982); (c) empirical tight-binding model of P. Pecheur and G. Toussaint, *Physica* **116B**, 112 (1983); and (d) muffin-tin cluster model of G. G. DeLeo, G. D. Watkins, and W. B. Fowler, *Phys. Rev. B* **25**, 4962, 4972 (1982). (a) and (b) are spin restricted; (c) and (d) are spin unrestricted. Compare also Fig. 43 below for self-consistent spin-unrestricted Green's-function results. Numbers in parentheses show occupations.

function problem by a continued-fraction approach, achieving self-consistency by the heuristic ansatz that the first shell of atoms should be neutral. Vogl and Baranowski[207] used a 5-orbital/atom ($2s + 3p$) description of the host crystal, included matrix elements only up to the first shell of neighbors, restricted the perturbation to the impurity site alone ("diagonal perturbation"), and used a Koster–Slater solution to the Green's function. The approximation of "diagonal perturbation" was criticized by Singh *et al.*[212] and by Van der Rest and Pecheur[211c] as being insufficient, resulting in a great uncertainty in the position of the gap levels and leading to the phenomenon of "vacancy pinning," not observed in more complete treatments (a different type of pinning is observed[19,21]). The approach of Vogl and Baranowski[207] uses a large number of adjustable parameters to represent the band structure, the Coulomb and exchange energies of the impurity ion, and the impurity–host coupling; its success depends on a (delicate) balance of judiciously chosen parameters and data. Their published results for $3d$ impurities in II-VI semiconductors[207] agree with the known donor and acceptor ionization energies. They emphasize, however, the ligand p character of the t_2 gap levels, a result contradicted by first-principles Green's-function calculations (Part VI,18 below). The results of Pecheur and Toussaint[206] for interstitial impurities in Si (Fig. 24c) show that the spin-up states t_+ and e_+ are fully occupied and occur inside the valence band, whereas the minority-spin states t_- and e_- carry the "active electrons." Their results are qualitatively similar to those obtained in first-principles Green's-function calculations (see Fig. 43 below), but differ greatly from spin-unrestricted cluster calculations[183] (Fig. 24d).

The basic findings of the empirical Green's-function calculations on $3d$ impurities in semiconductors include the following: (1) Gap levels occur at higher energies as the impurity's atomic number decreases; (2) the dominant gap states for substitutional impurities are the t_2^{DBH} and e^{CFR}; (3) exchange splittings usually exceed one-electron crystal-field splittings; (4) the t_2 gap levels show p-d hybridization, but the e gap levels do not; (5) impurity-induced valence-band resonances exist for all impurities; and (6) multiple charge states can exist even in narrow-gap materials. These calculations differ in the number and type of levels found in the gap (Figs. 21c and 24), show a large scatter in the calculated Δ_x and Δ_{CF} values, and emphasize orbital energies rather than wave-function-related observables (e.g., g values, spin densities, and hyperfine coupling constants).

[211] (a) P. Pecheur, G. Toussaint, and M. Lannoo, *Inst. Phys. Conf. Ser.* **59**, 147 (1981); (b) P. Pecheur, E. Kauffer, and M. Gerl, *Inst. Phys. Conf. Ser.* **46**, 174 (1979); (c) J. Van der Rest and P. Pecheur, *J. Phys.* **44**, 1297 (1983).

[212] V. Singh, U. Lindefelt, and A. Zunger, *Phys. Rev. B* **25**, 2781 (1982).

b. First-Principles Green's-Function Calculations

First-principles Green's-function calculations for impurities attempt to describe quantitatively the electronic structure of the system in terms of a nonempirical and well-defined (but imperfect) *microscopic theory of interelectronic interactions.* The numerical aspects of the solution and its convergence (basis sets, self-consistency, multiband coupling, anisotropic potentials, etc.) are pushed to an extreme limit of internal precision so that *both our ability and our failure* to explain the data can be analyzed in terms of the underlying microscopic theory of interelectronic interactions used (rather than in terms of computational approximations or incorrect empirical fitting). This aspect constitutes both the weakness (i.e., imperfect agreement with experiment can be expected) and the strength of such an approach. Two closely related variants of such an approach were developed by Zunger and Lindefelt[21] and by Katayama-Yoshida and Shindo[213] and Katayama-Yoshida and Zunger.[39,47] In what follows I describe the salient features of this approach. More details are found in Refs. 21, 39, and 47.

The first method of this sort to be developed was the quasi-band crystal-field (QBCF) Green's-function approach.[21] Its basis features are:

(1) The impurity potential $V(\mathbf{r})$ and density $\rho(\mathbf{r})$ are described by Eqs. (2.1) and (2.2) as having a periodic host crystal part $V_H(\mathbf{r})$ and $\rho_H(\mathbf{r})$ and short-range impurity-induced perturbations $\Delta V(\mathbf{r})$ and $\Delta\rho(\mathbf{r})$. Each is expanded around the impurity in a Kubic harmonic series [Eqs. (2.1)–(2.3)], retaining all components up to $l \leq 8$.

(2) $\rho_H(\mathbf{r})$ and $V_H(\mathbf{r})$ are calculated from a self-consistent pseudopotential band structure of the host crystal[19] (cf. Fig. 3), which also provides the crystalline one-electron states $\epsilon_{n\mathbf{k}}$ and orbitals $\phi_{n\mathbf{k}}(\mathbf{r})$.

(3) A dual description is used of the impurity wave functions $\psi_i^{\alpha,\lambda}(\mathbf{r})$ [within the range of $\Delta V(\mathbf{r})$]: one in terms of an expansion in the host-crystal quasi-bands $\phi_{n\mathbf{k}}^{\mathrm{QB}}(\mathbf{r})$ with band index n and wave vectors $\mathbf{k}$,

$$\psi_i^{\alpha,\lambda}(\mathbf{r}) = \sum_n \sum_{\mathbf{k}} A_{in}^{\alpha\lambda}(\mathbf{k})\phi_{n,\mathbf{k}}^{QB}(\mathbf{r}), \tag{17.1}$$

and the other in terms of impurity-centered orbitals of principal quantum number μ; i.e., in Eq. (2.9) we have

$$G_{il}^{\alpha}(|\mathbf{r}|) = \sum_{\mu}^{M} C_{\mu l i}^{\alpha} F_{\mu l}(|\mathbf{r}|). \tag{17.2}$$

Both expansions are kept equally complete within the range of $\Delta V(\mathbf{r})$. This choice of a (crystal-field-like) expansion of the wavefunctions [Eq. (17.2)] and

[213] H. Katayama-Yoshida and K. Shindo, *Phys. Rev. Lett.* **51,** 207 (1983); *J. Phys. Soc. Japan* **53,** 1114 (1984); *Solid State Commun.* **44,** 989 (1982).

potential [Eq. (2.1)] simplifies the problem immensely (all the integrals are one dimensional, analogous to the situation in atomic physics) without sacrificing any generality.

(4) The local orbitals $\{F_{\mu l}(|\mathbf{r}|)\}$ are taken as a set of Coulomb functions, augmented by the numerical solutions of the free-ion orbitals. The effective nuclear charge Z^* of these Coulomb functions as well as their number M (typically up to 10*s*, 10*p*, 10*d*, 10*f*, and 10*g* orbitals, i.e., a total of 250–300 orbitals per impurity) are optimized to achieve a variational error smaller than a prescribed tolerance. Arbitrary hybridization and covalency are therefore allowed.

(5) A special reformulation of the Koster–Slater Green's-function method[198] is derived,[21] clarifying the fact that the host-crystal states $\phi_{n\mathbf{k}}^{\mathrm{QB}}(\mathbf{r})$ appearing in Green's-function formulations need not be *eigenfunctions* of the host-crystal Hamiltonian but could be any set of functions ("quasi-bands") which merely *diagonalizes* this Hamiltonian. This newly discovered flexibility[21] is then used to achieve a rapidly convergent expansion in Eq. (17.1) in terms of quasi-band wave functions $\{\phi_{n\mathbf{k}}^{\mathrm{QB}}(\mathbf{r})\}$ that include from the outset impurity as well as host orbitals. The large number ($\sim 10^4$) of *pure* host bands $\phi_{n\mathbf{k}}(\mathbf{r})$ that would otherwise have been needed in this expansion[21] are renormalized into a far smaller number (~ 30) of quasi-bands $\phi_{n\mathbf{k}}^{\mathrm{QB}}(\mathbf{r})$.

(6) The electron–electron Coulomb and exchange-correlation interactions [Eq. (10.7)] are described within the local-density formalism[139] using[19,54,192] either a scaled exchange version,[214] a complete exchange-correlation (xc) version[39,47] (the Perdew–Zunger form[215] of the Ceperley–Alder[216] xc), or the self-interaction corrected[215] (SIC) local-density version.[20,39,47,217]

(7) First-principles nonlocal pseudopotentials of Zunger and Cohen[218] are used to describe the impurity's external potential in Eq. (10.4).

(8) Full self-consistently [input and output $\Delta V(r)$ agree to within a few mRy] is achieved efficiently using the Jacobian–Update method.[219]

Special techniques were developed for efficient location of the roots of the Green's-function equations[21] and to calculate various projections of multi-centered orbitals on the impurity site.[21] Convergence with respect to all

[214] J. C. Slater, "The Self-Consistent Field for Molecules and Solids." McGraw Hill, New York, 1974.

[215] A. Zunger, J. P. Perdew, and G. L. Oliver, *Solid State Commun.* **34,** 933 (1980); J. P. Perdew and A. Zunger, *Phys. Rev. B* **23,** 5048 (1981).

[216] D. M. Ceperley and B. J. Alder, *Phys. Rev. Lett.* **45,** 566 (1980).

[217] H. Katayama-Yoshida and A. Zunger, *Int. Conf. Phys. Semicond. 17th*, p. 733 (1985) and results on GaAs: V^{2+} showing a low-spin ground state, *Phys. Rev. B* **33,** 2961 (1986).

[218] A. Zunger and M. L. Cohen, *Phys. Rev. B* **18,** 5449 (1978); **20,** 4082 (1979).

[219] P. Bendt and A. Zunger, *Phys. Rev. B* **26,** 3114 (1982).

internal computational parameters [number of basis functions, number of quasi-bands, self-consistency, or number of angular-momentum terms retained in Eqs. (2.1), (2.2), and (2.9)] was examined[21] to ensure a global precision of $\lesssim 0.1$ eV. The method was developed both in spin-restricted[21] and in spin-polarized versions.[220]

We can use the wave functions obtained from the Green's-function problem to define[19,21] a "population analysis." For example, the degree of localization of a given wave function $\psi_i^{\alpha,\lambda}$ within a sphere of radius R_{cc} (e.g., the central-cell volume of the impurity and its first neighbors, 4.44 a.u. in Si or GaP) can be defined as

$$q_i^\alpha = \sum_l \int_0^{R_{cc}} |G_{li}^\alpha(|\mathbf{r}|)|^2 r^2 \, dr \equiv \sum_l q_{li}^\alpha. \tag{17.3}$$

The contribution to the electronic charge within the central-cell region from the lth component of all occupied states belonging to the αth representation is

$$Q_l^\alpha = \sum_i^{\text{occ}} N_i \int_0^{R_{cc}} [G_{li}^\alpha(r)]^2 r^2 \, dr. \tag{17.4}$$

We refer to Q_l^α as the "orbital-representation charge." This will serve to establish "how p-like all t_2 states are," or "how much f character exists in all a_1 states," etc.

The total charge Q_l below the Fermi energy arising from the various l components in the wave functions will be defined as

$$Q_l = \sum_\alpha Q_l^\alpha. \tag{17.5}$$

We refer to Q_l as the "orbital occupation" and use it to answer questions such as "To what extent is a transition-atom impurity d-like or p-like?"

The distribution of the total central-cell charge among the various allowed representations will be given by the "representation occupation" Q^α,

$$Q^\alpha = \sum_l Q_l^\alpha, \tag{17.6}$$

which measures the contribution to the central-cell charge from occupied states belonging to the irreducible representations a_1, t_2, e, and t_1. Finally, the total electronic charge enclosed in the central-cell region is given by

$$Q^{\text{tot}} = \sum_l Q_l = \sum_\alpha Q^\alpha. \tag{17.7}$$

Q_l^α, Q_l, and Q^α will include contributions both from the impurity atom and from the host-crystal orbitals penetrating the central cell.

[220] U. Lindefelt and A. Zunger, unpublished (1983).

It is instructive to define an "effective impurity atom" that best describes the properties of an "isolated" impurity atom, properly renormalized by its self-consistent interactions with the host. This requires the definition of an arbitrary reference state which represents the host before an impurity is introduced. For substitutional impurities, this reference system is taken as the self-consistent vacancy, whereas for interstitial impurities it is simply the pure host crystal. For the former case we imagine that one first prepares a vacancy and then inserts into it a noninteracting "effective impurity atom" which produces an overall electronic distribution identical to that of the interacting system. The "effective impurity atom" may be different in its electronic structure from the isolated free-space impurity atom; that is, it may have nonspherical components in its charge density (even if the free-space atom is assumed spherical), it may be compressed, it may have a different orbital configuration, etc. We define the representation occupation of the "effective impurity atom" as

$$\Delta Q^\alpha = (Q^\alpha)_{\text{impurity}} - (Q^\alpha)_{\text{vacancy}}, \tag{17.8}$$

its orbital occupation as

$$\Delta Q_l = (Q_l)_{\text{impurity}} - (Q_l)_{\text{vacancy}}, \tag{17.9}$$

its total net electronic charge as

$$\Delta Q^{\text{tot}} = (Q^{\text{tot}})_{\text{impurity}} - (Q^{\text{tot}})_{\text{vacancy}}, \tag{17.10}$$

and its charge-density components as

$$\delta_l(r) = (\Delta\rho_l)_{\text{impurity}} - (\Delta\rho_l)_{\text{vacancy}}, \tag{17.11}$$

etc. Each of the two terms in Eqs. (17.8)–(17.11) is calculated separately in a self-consistent manner. Notice that, since at a large distance from the impurity site the charge densities of both the impurity-containing system and the vacancy are equal (to the unperturbed charge), the effective net charges in Eqs. (17.8)–(17.11) do not depend on the radius R_{cc} used in the integration [cf. Eq. (17.3)], provided R_{cc} is large enough.

In a subsequent development,[140] the QBCF method was generalized to the calculation of the forces $\mathbf{F}_\gamma$ acting on the atoms around the impurity [Eq. (10.10)], permitting the evaluation of breathing-mode distortions. In this approach the short-range forces were obtained from the self-consistent charge perturbation $\Delta\rho(\mathbf{r}, \mathbf{Q}_0)$ of the *unrelaxed* lattice using the Hellmann–Feynman theorem, whereas the restoring forces of the lattice are obtained from an empirical force field fitted to the phonon spectra.

The problems encountered with the QBCF method are: (1) Since the currently known local-density functional for exchange and correlation

interactions[215] is imperfect (leading, for instance, to too-small band gaps[221] and systematic errors in atomic d-s excitation energies[215]), so are the results of its applications to impurities. These problems are partially avoided by adjusting the host-crystal band gap[19,39,54] or using the self-interaction correction[20,39,215] to the local-density formalism. Bounds on errors can be estimated by applying the Green's-function method to free ions (i.e., an impurity in an "empty lattice") and comparing to experiment, and are found to be rather small. (2) Since a pseudopotential is used to represent $V_{ext}(\mathbf{r})$, no information is obtained on core states. This problem was avoided[39,47,217] by replacing the pseudopotential with an all-electron potential in applications in which information on core states (e.g., core polarization) was needed.[39] (3) The method is well suited to single impurities but becomes time consuming when extended defects are considered, since the angular-momentum expansion of Eqs. (2.1), (2.2), and (2.9) converges more slowly.

The QBCF method was first applied to a simple defect—the unrelaxed Si vacancy[21]—to compare its predictions with those of independently developed approaches that are specialized to non-d-electron impurities.[137] Very good agreement with those results was obtained.[21]

In a further work by Katayama-Yoshida and Zunger,[39,47,197,217] a variant of the method was developed to treat spin-polarized core states. In this variant, (1) an all-electron rather than a pseudopotential representation is used for $\Delta V_{ext}(\mathbf{r})$; (2) the extended but fixed basis set $\{F_{\mu l}\}$ of Eq. (17.2) is replaced by a smaller set, but each orbital is optimized nonlinearly, responding to the crystalline potential ("dynamic basis set"); and (3) instead of using the quasi-band transformation[21] to obtain a variationally complete Green's function, the equivalent "adspace representation"[201] is used (for no better reason than experimentation with another approach; the two methods yield the same results).

VI. Results of First-Principles Green's-Function Studies

18. One-Electron Impurity Levels and Wave Functions

Figure 25 depicts the calculated mean-field one-electron orbital energies of substitutional $3d$ impurities in Si[19] and in GaP.[54] Both are obtained from QBCF self-consistent calculations. There are three main impurity-induced states, denoted t_2^{CFR}, e^{CFR}, and t_2^{DBH}. A few more t_2-like and a_1-like resonances are also seen. I next discuss the properties of the main impurity states.

[221] A. Zunger, *J. Vac. Sci. Technol.* **16,** 1337 (1979); A. Zunger and A. J. Freeman, *Phys. Rev. B* **16,** 2901 (1977).

a. *Crystal-Field Resonances*

There is a striking resemblance between the levels of GaP:$3d$ and those of substitutional $3d$ impurities in silicon. To understand the atomic origin of the impurity-induced levels, I place at the origin of Fig. 25b the trivial case of *Ga*P:Ga and proceed to lighter impurities along the abscissa, hence going backward in the $3d$ series. The "impurity-induced" d levels of *Ga*P:Ga are essentially the well known[55,222,223] Ga $3d$ bands of the pure GaP crystal. Clearly, because of the periodicity of the host lattice, these "impurity-induced" states[55] are broadened into bands.[223] Nevertheless, the compactness (on the scale of the lattice constant) of the $3d^{10}$ orbitals of Ga makes this band extremely narrow.[55,222,223] In Fig. 25b the Ga $3d$ orbitals in GaP appear as sharp states below the valence-band minimum. Since this "impurity" has a large (50%) stoichiometric concentration, its ionization energy can be determined experimentally by x-ray photoelectron spectroscopy (XPS). The relation between this energy ($E_v - 18.5$ eV)[222] and the position ($E_v - 13.1$ eV) of the one-electron $3d$ level given in Fig. 25b (involving ~ 5 eV relaxation energy) has been discussed elsewhere.[55] The purpose of choosing *Ga*P:Ga as the impurity at the origin of Fig. 25b and then proceeding to lighter impurities (going backward in the periodic table) is to emphasize that the crystal-field resonances evolve naturally from the cation $3d$ orbitals in the trivial case of *Ga*P:Ga. For *Ga*P:Ga we have the deep t_2 and e spin-unpolarized bands fully occupied by six and four electrons, respectively, with a vanishingly small (crystal-field) splitting between them. As we replace the Ga impurity by Zn, with its weaker atomic Coulomb potential, the e^{CFR} and t_2^{CFR} levels acquire smaller binding energies. As we proceed to Cu, Ni, etc., the $3d$ orbitals become even less bound and their orbitals become more expanded, sampling better the potential exerted by the ligands and therefore acquiring a larger (crystal-field) splitting between e^{CFR} and t_2^{CFR}. Because of their generic evolution from the impurity atomic d orbitals, perturbed by the crystalline field, I refer to these levels as "crystal-field resonances" (CFR).

The e and t_2 crystal-field resonances have the following characteristics:

(1) Much like the situation in free ions (Fig. 10), the binding energies of the CFR levels decrease as the atomic number decreases, reflecting primarily the weakening of the $-Z/r$ Coulomb attraction. However, whereas the slope of this decrease in free ions is large (cf. Figs. 9a, 10a), the slope is considerably reduced for these species as impurities (e.g., ~ 0.5 eV for impurities lighter than Ni). This is a clear manifestation of the formation of new chemical bonds between the impurity and the host atoms.

[222] L. Ley, R. A. Pollak, F. R. McFeely, S. P. Kowalczyk, and D. A. Shirley, *Phys. Rev. B* **9,** 600 (1974).

[223] C. S. Wang and B. Klein, *Phys. Rev. B* **24,** 3393 (1981).

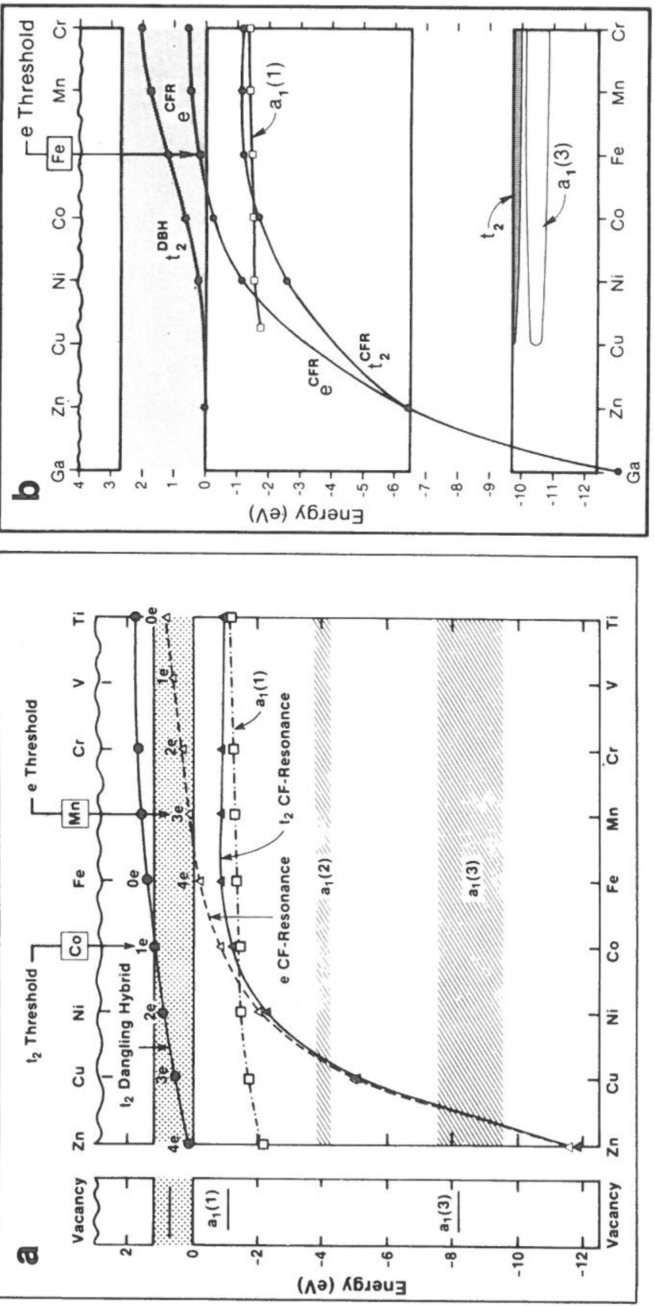

FIG. 25. Calculated one-electron energy levels of substitutional $3d$ impurities in (a) Si [A. Zunger and U. Lindefelt, *Phys. Rev.* **B 27**, 1191 (1983)]; and in (b) GaP [V. Singh and A. Zunger, *Phys. Rev.* **B 31**, 3729 (1985)]. Numbers such as $1e$, $2e$, etc. denote level occupations. The zero of energy is at the valence-band maximum; the shaded area above it denotes the band-gap region. At the left of part (a) are shown for comparison the energy levels of the ideal Si vacancy. Parts (a) and (b) show a global similarity of substitutional $3d$ impurity levels in different semiconductors: a pair of the t_2 levels [the bonding crystal-field resonance (CFR) and its antibonding counterpart—the dangling-bond hybrid (DBH)], as well as a nonbonding e^{CFR} level between them. The two crystal-field resonances, t^{CFR} and e^{CFR}, start at the high-Z limit of Ga, Zn, Cu as deep levels near the bottom of the valence band and go up in energy as the impurity atomic number decreases. The t^{CFR} level is then pinned inside the valence band, whereas the e^{CFR} level penetrates the band-gap region at the point denoted "e threshold." The t_2^{DBH} level starts at the high-Z limit near the top of the valence band, becomes higher in the gap as Z decreases, and penetrates (in Si) the conduction band at the point denoted "t_2 threshold." A few other impurity-induced levels are shown, e.g., $a_1(1)$, $a_1(2)$, and $a_1(3)$.

(2) As we approach the low-Z limit of the series, we see that the energy of the t_2^{CFR} becomes pinned inside the valence band (at about $E_v - 1$ eV, where E_v denotes the valence-band maximum), whereas the e^{CFR} level emerges into the band-gap region, first for GaP:Fe and Si:Mn (the "e threshold" in Fig. 25a and b). It then gives rise to the acceptor states of GaP:Fe and GaP:Co. Hence, the levels which constitute the deep acceptor states of these impurities are generically the same type of levels which give the XPS signal of pure GaP at $E_v - 18.5$ eV. Owing to the low solubility of $3d$ atoms in most semiconductors, their valence-band states e^{CFR} and t_2^{CFR} were not observed in photoemission spectroscopy. As discussed in Part III,4, the exception to this rule is Mn in II-VI compounds, which shows almost continuous solubility. For CdTe:Mn such valence-band resonances were observed in x-ray emission (at $E_v - 2.7$ eV[224]), XPS ($E_v - 3.5$ eV),[225] and ultraviolet photoemission (UPS) (at $E_v -$ 3.5 eV).[226] Similarly, for CdSe:Mn these resonances were observed[227] at $E_v - 3.35$ eV. The predicted position in GaP and Si can be obtained by supplying a downward relaxation correction[55] (2–5 eV for most $3ds$) to the calculated CFR levels of Fig. 25a and b. It is hoped, indeed, that the concentration of $3d$ impurities in III-V semiconductors might eventually be raised, e.g., by ion implantation, to the point where an XPS determination of the e^{CFR} and t_2^{CFR} levels would become possible, too.

(3) Figure 26a,b depicts the wave functions of the e^{CFR} and t^{CFR} levels for a few impurities in Si.[19] Figure 26c,d give plots[54] of the radial e^{CFR} wave-function components $G_{li}^{\alpha}(|\mathbf{r}|)$ for GaP:$3d$. The $l = 2$ (d-orbital) part (Fig. 26c) is dominant, exhibiting an atomiclike behavior in the central cell, with a rapid attenuation in amplitude as we move to lighter impurities. The next-higher symmetry-allowed angular-momentum component ($l = 4$) is small in the central cell and delocalized through the crystal (Fig. 26d). Figure 26 highlights the atomic 3d-like character of t_2^{CFR} and e^{CFR} in both GaP:$3d$ and Si:$3d$. Population analysis [Eq. (17.3)] shows that the localization of e^{CFR} within the nearest-neighbor sphere ranges from 99% for GaP:Zn to 75% for GaP:Cr. The t_2^{CFR} in GaP:$3d$ shows a similar localization in the high-Z limit (97% for GaP:Zn), but a lower localization in the low-Z limit (45% for GaP:Cr), caused by massive hybridization with the t_2-like host states.

I conclude that: (1) the CFR levels represent the perturbed versions of the atomic $3d$ orbitals and that, therefore, their splitting reflects the true "crystal-field splitting" [Eq. (2.16)] of the system; (2) since, for the lighter $3d$ impurities

[224] W. Zahorowski and E. Gilberg, *Solid State Commun.* **52,** 921 (1984).
[225] E. Sobczak and M. Sommer, *Phys. Status Solidi* **112B,** K43 (1982).
[226] C. Webb, M. Kaminska, M. Lichtensteiger, and J. Lagowski, *Solid State Commun.* **40,** 609 (1981).
[227] B. A. Orlowski, K. Kopalko, and C. Chab, *Solid State Commun.* **50,** 749 (1984).

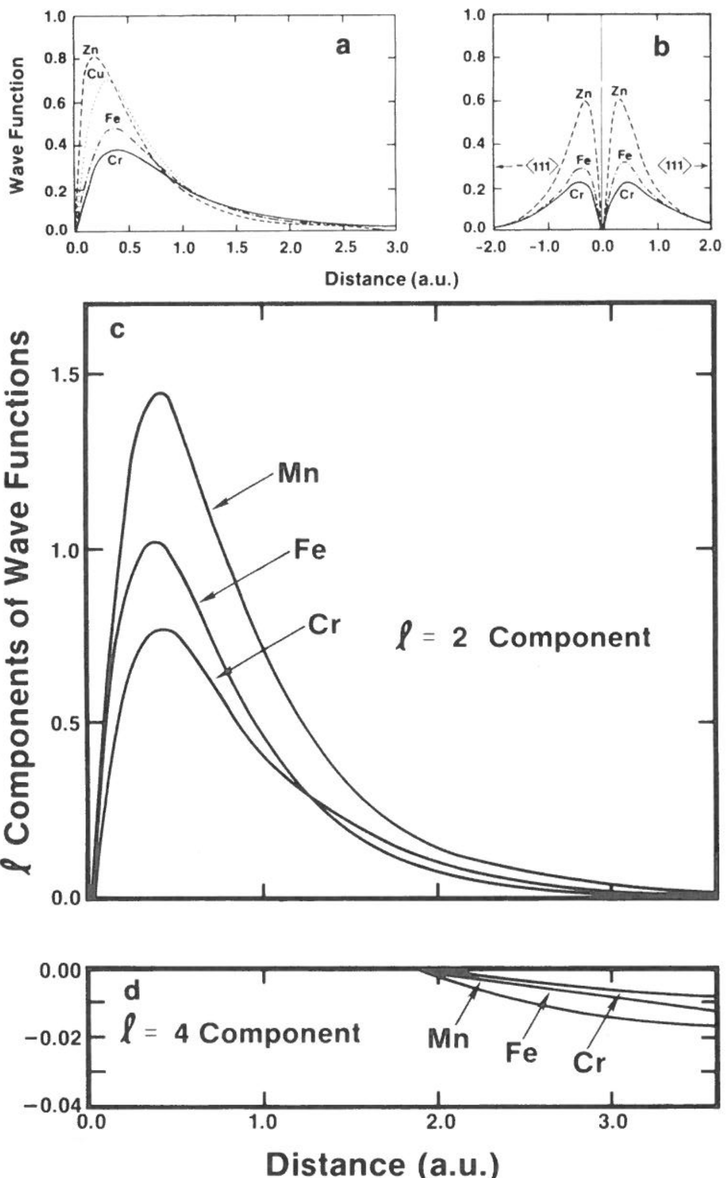

FIG. 26. One-electron wave functions $\psi_{i,\sigma}^{\alpha,\lambda}(\mathbf{r})$ [Eq. (2.9)] of the crystal-field resonances (CFR) of substitutional 3*d* impurities in Si [(a), for *e*, and (b), for t_2, from A. Zunger and U. Lindefelt, *Phys. Rev. B* **27**, 1191 (1983)]; and GaP [(c) and (d), for *e*, from V. Singh and A. Zunger, *Phys. Rev. B* **31**, 3729 (1985)]. In (a) and (b) the wave functions are plotted in the ⟨100⟩ and ±⟨111⟩ crystal directions, respectively. Parts (c) and (d) give the radial components $G_{l,l'}^{\alpha,\sigma}$ [Eq. (2.9)] of the different angular momenta *l*. Note that the CFR wave functions resemble free-ion 3*d* orbitals.

the CFR levels are energetically close to the band gap, they can participate in optical transitions; and (3) since they have a large amplitude on the impurity, they can control its effective charge.

b. The t_2 Dangling-Bond Hybrid

The bonding orbital t_2^{CFR} has an antibonding counterpart in the form of the t_2^{DBH}. In the high-*Z* limit, where the atomic 3*d* orbitals are far deeper than the host t_2 orbitals, there is little interaction between them; hence the *p*-like antibonding t_2^{DBH} orbital is just above the VBM (Fig. 25). As we move to lighter impurities, the orbitals of the impurity atom come closer to those of the host t_2 states, leading to a stronger repulsion and to the appearance of the t_2^{DBH} level in the gap. Because of the larger band gap of GaP compared with Si, the t_2^{DBH} state penetrates the conduction band in Si:Fe, Si:Mn, and Si:Cr, whereas these states are still in the gap of GaP. Since the t_2^{DBH} state evolves generically from the host dangling bonds around the impurity site (hybridized with the impurity *d* states), I refer to it as the "dangling-bond hybrid." The t_2^{DBH}–e^{CFR} splitting has been referred to, following Ludwig and Woodbury,[1] as the "crystal-field splitting." Hence, this conventional, Ludwig–Woodbury crystal-field splitting starts for GaP:Ga at about 13 eV and ends up being ~1.4 eV for GaP:Cr (using acceptor-state occupation numbers). I note, however, that the true atomically derived levels split by the crystalline potential are, in fact, the e^{CFR}–t_2^{CFR} pair.

The lowest $d \to d^*$ excitation involves the e^{CFR}–t_2^{DBH} pair. The results for this separation (Fig. 25b) thus predict an increase in the excitation energy in going from Fe to Mn and Cr, as well as an increase in going from Co to Ni. These trends match the experimental observations.

Figure 27a,b depicts the radial components of the t_2^{DBH} wave functions for a few impurities in GaP.[54] Its $l = 2$ (*d*-orbital) component (Fig. 27a) resembles atomic 3*d* orbitals; however, being antibonding, these wave functions show orthogonality nodes in the central cell (around $r \cong 2$ a.u. in Fig. 27a). The *d* component is strong for GaP:Fe and decays somewhat on both sides of Fe in the periodic table, as the level acquires more *p* character, The *p*-orbital components (Fig. 27b) have maxima that fall in the shaded area of Fig. 27b for most impurities. As shown in this figure, the *p*-orbital components are considerably more delocalized than the *d*-orbital components, peaking around the 3*d*-*p* bond center. Population analysis reveals strong (80%) *p* character at both the Zn and Cr ends of the series and substantial (50%) *d* character at the center of the series (Fe). Notice, therefore, that for impurities with substantial 3*d* character in their t_2^{DBH} state we would predict the VBM $\to t_2^{\mathrm{DBH}}$ transition (an allowed $p \to d$ excitation) to have substantially higher intensity than the $t_2^{\mathrm{DBH}} \to$ CBM transition (a forbidden $d \to s$ excitation). This idea can be illustrated by comparing cross sections of acceptor hole

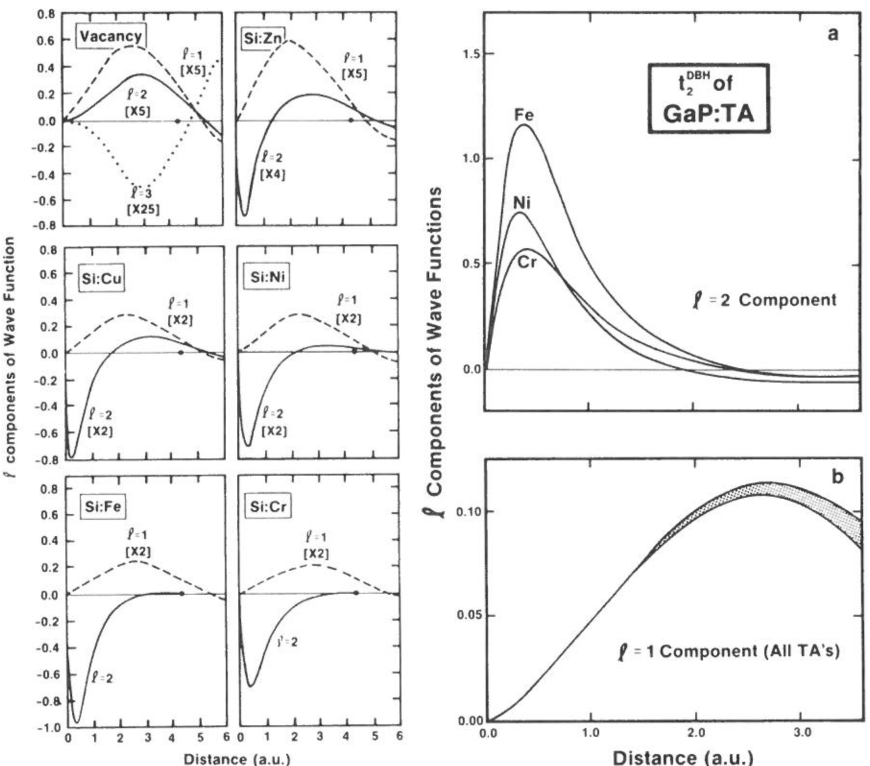

FIG. 27. One-electron wave functions of the t_2 dangling-bond hybrids (DBH) of substitutional $3d$ impurities in silicon [left-hand side, A. Zunger and U. Lindefelt, *Phys. Rev. B* **27**, 1191 (1983)]; and GaP [right-hand side, V. Singh and A. Zunger, *Phys. Rev. B* **31**, 3729 (1985)]. In each case we show the various l components. The t_2^{DBH} orbital has a strong admixture of p and d components and an orthogonality node close to the nearest-neighbor atom (solid dot on the abscissa). The $l = 2$ d character (———) is rather localized, whereas the $l = 1$ p character (---) is more diffused. For comparison, the t_2^{DBH} wave function of the Si vacancy is shown, too. The shaded area in (b) denotes the $l = 1$ component of the wave functions of all three impurities which are closely spaced in this region.

emission $\sigma_v[T^{2+} \rightarrow T^{+}]$, [coupling the *valence band* to the impurity level, e.g., Eqs. (6.3) and (6.6)], with the cross section for acceptor-electron capture $\sigma_c[T^{+} \rightarrow T^{2+}]$ [coupling the impurity level to the *conduction band*, e.g., Eq. (6.5)]. If the gap level contains approximately equal proportions of d and p character (e.g., the t_2^{DBH} level of GaP:Cr in Fig. 26a), then $\sigma_v/\sigma_c \cong 1$, but if the gap level is d-like (e.g., the e^{CFR} level of GaP:Fe in Fig. 26c), we expect to find $\sigma_v[T^{3+} \rightarrow T^{2+}]/\sigma_c[T^{2+} \rightarrow T^{3+}] \gg 1$. This is the opposite of what Vogl and Baranowski[207] have proposed from their tight-binding model. Quantitative measurements of cross sections for such systems could shed light on the wavefunction character presented in Figs. 26 and 27.

The left-hand side of Fig. 27 shows the decomposition of the t_2 wave function in Si:$3d_s$ into its angular-momentum components $G_l^{t_2}(|\mathbf{r}|)$ [Eq. (2.14)] for the first two symmetry-allowed terms $l = 1$ and 2. For comparison, a partial wave resolution is also given for the silicon vacancy (upper left panel). The significant fingerprint feature of the t_2^{DBH} state for all transition-atom impurities is a strongly *localized* atomiclike $l = 2$ component, which has a node in the *inner central-cell* region, and an *opposite sign relative to the* $l = 1$ *wave-function component*. This behavior is distinctly different from that observed in the vacancy dangling-bond wave function, which has a *delocalized* $l = 2$ component with a node only *outside the central-cell* region, and the *same sign as the* $l = 1$ *wave-function component* in the inner region. As one moves backward from the Zn end to the low-Z limit of the $3d$ series, the node moves toward the central-cell boundary.

The amount of p-d hybridization and localization in the DBH of Si:$3d$ is shown[19] in Fig. 28, where the percentage of p and d character [q_{li}^{α} of Eq. (17.3)] is depicted across the $3d$ series. The DBH begins at Si:Zn as a predominantly p-like state (coupling with p-like valence-band states). It reaches a 50%–50% p-d character near the center of the $3d$ series (Fig. 28b) where the level has maximum localization (Fig. 28a), after which the p character increases a little (and the wave-function localization decreases) on account of the renewed availability of nearby p-like host states (this time, from the conduction bands). The large extent of p-d hybridization found near the Fermi energy is not entirely surprising; it is often found in the inorganic chemistry of transition-metal tetrahedral coordinate compounds [e.g.,[228,229] 25% p character in $CuCl_4^{2-}$, 50% in CuI_4^{2-}, 20–30% in the organic complex Cu(α, α′-Br)dipyrromethene[229]]. Note that a t_2 level such as the DBH can by no means be considered simply as "p-like."[207]

c. *A Simple Three-Level Model*

In this section I present a model that qualitatively maps the results of the full calculation for substitutional impurities (Fig. 25) into a simple three-level system.[19,196] This is done by abstracting a small number of "effective states" from the complete LDOS spectrum of host states (cf. Fig. 23). Focusing first on t_2 impurity levels, one identifies those atomic orbitals which can transform like t_2 in the point group T_d and which have orbital energies in the neighborhood

[228] (a) A. Zunger and M. L. Cohen, *Phys. Rev. B* **20**, 1189 (1979); (b) A. Goldmann, *Phys. Status Solidi* **80B**, 475 (1977).

[229] C. A. Bates, W. S. Moore, K. J. Standley, and K. W. H. Stevens, *Proc. Phys. Soc. London* **79**, 73 (1962).

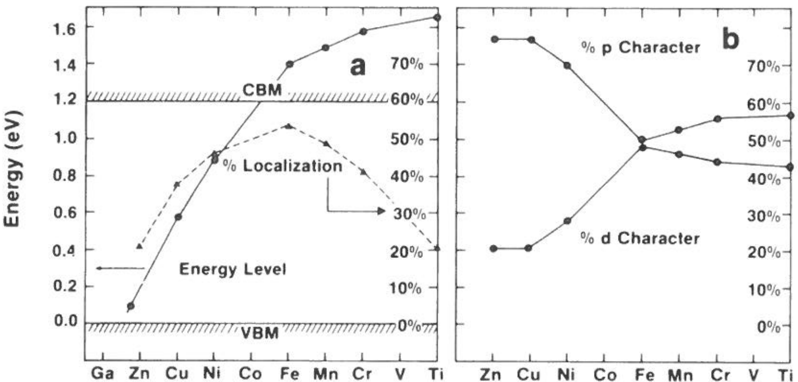

FIG. 28. Percent localization [▲ in (a)] and (b) percent hybridization of the t_2^{DBH} level of substitutional 3*d* impurities in Si [from A. Zunger and U. Lindefelt, *Phys. Rev. B* **27**, 1191 (1983)]. The localization reaches a maximum at the center of the series, where the *d* character is maximal, too. Heavy impurities have a dominant *p* character and small localization in their t_2^{DBH} level, whereas the situation is reversed at the center of the 3*d* series.

of the host effective states. These are the free-ion $3d(t_2^0)$ and $3d(e^0)$ orbitals with unperturbed atomic energies $\epsilon[t_2^0]$ and $\epsilon[e^0]$, respectively (identical to the free-ion orbital energies). These are depicted schematically on the energy scale of the silicon band structure as horizontal lines to the left of Fig. 29. The t_2 atomic levels will interact with the states in the crystal having a high t_2 density of states in the central-cell region, with energies that are sufficiently close to that of $\epsilon[t_2^0]$. An examination of the substitutional t_2 local density of states (Fig. 23) (or the corresponding results[21] for the Si vacancy) reveals two regions where the t_2 LDOS has its maximum intensity. These two peaks comprise our effective "t_2 interaction centers" and correspond to a valence-band peak at $E[t_2^{VB}] \approx E_{VB} - 1$ eV and the (doublet) conduction-band peak around $\epsilon[t_2^{CB}] \approx E_{VB} + 3.8$ eV. The two regions are denoted in Fig. 29 by the cross-hatched areas. (For *heavy* 3*d* impurities, the LDOS peaks at $E_v - 10$ and $E_v - 7$ eV are needed, too.) The energies $\epsilon[t_2^{VB}]$ and $\epsilon[t_2^{CB}]$ define an "effective t_2 band gap," Δ_{t_2} (host) $= \epsilon[t_2^{CB}] - \epsilon[t_2^{VB}] \cong 4.8$ eV, considerably larger than the optical gap $E_g = 1.17$ eV. The latter is irrelevant to our considerations since it does not separate levels which constitute the major t_2 interacting centers. The effective gap Δ_{t_2} is close to the Phillips homopolar band gap[230] E_h (4.77 eV for Si). Hence, the minimum number of levels needed to describe the system in a simple model is *three*: t_2^{VB}, t_2^{CB}, and the atomic level t_2^0. Here I deviate from the tight-binding pinning models,[195] which describe the t_2 levels of a substitutional impurity using a *two*-level system.

[230] J. C. Phillips, "Bonds and Bands in Semiconductors." Academic Press, New York, 1973.

Upon switching on the interaction parameters $\beta_{VB,T}$ and $\beta_{CB,T}$, this three-level system produces an interaction pattern depicted schematically in Fig. 29. It consists of a bonding–antibonding pair t_2^{DBH}–t_2^{CFR} with a nonbonding e^{CFR} state (produced by the interactions with *e* states) between them.

At the high-*Z* limit (Zn, Ga, Ge), the atomic 3*d* energy $\epsilon[t_2^0]$ is highly negative, and the system behaves essentially as a two-level $t_2^0 + t_2^{VB}$ system. The two levels will repel each other, creating a lower energy, nodeless (see Fig. 26b) bonding t_2^{CFR} level and a higher energy, antibonding t_2^{DBH} level with an orthogonality node (see Fig. 27). Their energies are given by

$$\epsilon_{imp} = \bar{\epsilon} \pm (\Delta^2 + \beta^2)^{1/2},$$

where

$$\bar{\epsilon} = \tfrac{1}{2}(\epsilon[t_2^0] + \epsilon[t_2^{VB}]), \tag{18.1}$$

and

$$\Delta = \tfrac{1}{2}(\epsilon[t_2^0] - \epsilon[t_2^{VB}]).$$

The model hence shows that at the high-*Z* limit (Ga, Cu, Zn, and Ni) in the periodic table one will find in a photoemission experiment an atomiclike t_2^{CFR} state at the energy corresponding approximately to the atomic 3*d* energy measured down from the host vacuum level. The higher, antibonding t_2^{DBH} level is predicted in this high-*Z* limit to be pinned at the energy $\epsilon[t_2^{VB}] \approx E_v - 1$ eV, and its wave function will be excluded from the impurity sphere by the orthogonality constraint. As such, this level will be almost exclusively constructed from valence-band states, much like the host vacancy. The long-range effective-mass-like interactions, omitted from this simple model, will then raise the level, making it a shallow acceptor.

As we move backward in the 3*d* series from Zn toward the low-*Z* limit, the atomic energies $\epsilon[t_2^0]$ rapidly approach the hostlike $\epsilon[t_2^{VB}]$ energy. A simple, two-level model will thus predict a pronounced level repulsion because of the proximity of $\epsilon[t_2^0]$ to $\epsilon[t_2^{VB}]$, and therefore a continuing increase in energy of t_2^{DBH}. Nothing like this happens in this system (cf. Fig. 25). In fact, in this limit the t_2^{CB} state becomes important; it constrains the energy of t_2^{DBH} by the "avoided crossing principle" of the two levels $\{t_2^{CB}, t_2^T\}$ (depicted schematically in Fig. 29 by the dashed lines). The model hence shows for the low-*Z* limit that the t_2^{DBH} energy is controlled by the repulsion from t_2^{CB}, not by the conduction-band minimum. The level t_2^{DBH} will thus penetrate the conduction band and acquire more CB character. The t_2^{CFR} level, on the other hand, will be pinned in this limit by the t_2^{VB} energy and hence become more valence-band-like. This model then explains why, in moving from the high-*Z* limit to the low-*Z* limit, the t_2^{CFR} becomes more VB-like and delocalized, whereas the t_2^{DBH} becomes more CB-like and localized. It further shows that the limiting t_2^{DBH}–t_2^{CFR}

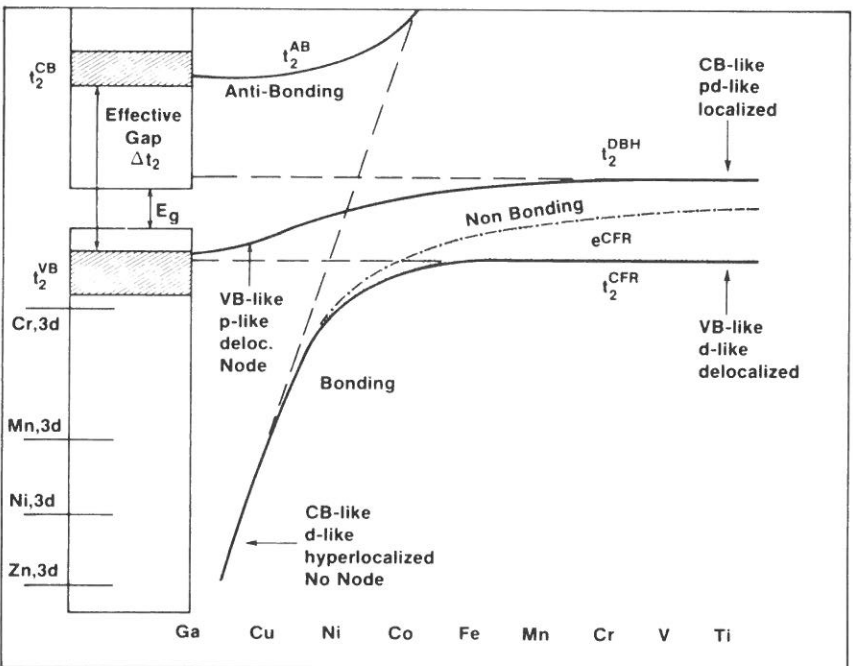

FIG. 29. Schematic three-level model for the one-electron energy levels of substitutional 3d impurities in a semiconductor [numerical values calculated for Si, after A. Zunger, unpublished (1983)]. The model shows the three main unperturbed levels of t_2 symmetry: the maxima in the host LDOS in the upper valence band (t_2^{VB}), the maxima in the conduction band (t_2^{CB}), and the free-ion 3d levels classified in t_2 symmetry (horizontal lines on the left). As the interaction between these three levels is switched on, one gets: (1) the bonding t_2^{CFR} level (d-like and localized at the high-Z limit, delocalized at the low-Z limit), (2) the antibonding (AB) t_2 level t_2^{AB} inside the conduction band, and (3) the dangling-bond hybrid t_2^{DBH} between these two. The t_2^{DBH} starts at the high-Z limit as a p-like delocalized level and becomes at the intermediate- and low-Z limit a localized p-d hybrid. The t_2^{DBH} level shows an avoided crossing relative to t_2^{AB}. This is depicted by (---). The hybridization gap t_2^{CB}–t_2^{VB} (the "effective Δ_{t_2} gap," denoted by the arrow on the left separating the two shaded areas) is the physical gap of the problem, not the optical gap E_g. The nonbonding e^{CFR} level is weakly hybridized and remains a localized d-like level throughout the series.

splitting attainable will saturate in the low-Z limit at a value limited by $|\epsilon[t_2^{CB}] - \epsilon[t_2^{VB}] - \beta_{CB,T}|$, whereas in the high-Z limit it will equal $\epsilon[t_2^{VB}] - \epsilon[t_2^0]$ (about 10–15 eV). Finally, the model explains why the highest localization in the DBH state occurs when the level is well inside the conduction band (cf. Si:Fe in Fig. 28a) and not at midgap or at the vacancy energy, as would be expected if the VBM and CBM levels were the physically relevant confining states: The maximum localization is expected to occur when the impurity level is situated between $\epsilon[t_2^{CB}]$ and $\epsilon[t_2^{VB}]$, and is equally repelled by them.

This simple model explains why a $Z_H^{(S)} - Z_I = 1$ impurity forms *shallow* acceptors in Si and in III-V's (i.e., Si:Ga or GaP:Zn) but in II-VI's (e.g., ZnSe:Cu) it forms a *deep* acceptor. The amount ΔE by which the antibonding t_2^{DBH} level is repelled upwards by the perturbation is inversely proportional to Δ [Eq. (18.1)]. Since the orbital energy $\epsilon[t_2^{VB}]$ of Column-VI anions (S, Se) is considerably deeper (hence, closer to $\epsilon[t_2^0]$) than that of Column-V anions (P, As) or Column-IV (Si, Ge) atoms, *the t_2^{DBH} level of ZnS:Cu or ZnSe:Cu is pushed deeper into the gap, creating a deep acceptor*. Similarly, the reason that the acceptor state in the series ZnX^{VI}:Cu becomes shallower as one proceeds from $X^{VI} = S$ to $X^{VI} = Se$ and Te is that the anion orbital energy $\epsilon[t_2^{VB}]$ becomes progressively less negative in the S → Se → Te series, thereby increasing Δ. If Na instead of Cu is the doping impurity, there are no longer any impurity-atom states that transform like the t_2 representation; hence, no level repulsion occurs. The system shows a *shallow* acceptor (the sample, nevertheless, does not have low resistivity due to compensation effects between substitutional and interstitial Na). Jaffe and Zunger[77] have pointed out that the phenomenon of level repulsion between a transition-atom t_2^0 level and a host-level t_2^{VB} of the same symmetry (e.g., the Γ_{25} VBM in cubic semiconductors) explains both the of *deep* acceptors in ZnX^{VI}:Cu and the anomalously small band gaps of $CuGaX_2^{VI}$ chalcopyrites relative to their ZnX^{VI} binary analogs. These insights are used in Part VI,28 to derive a "universality rule," which states that the antibonding level t_2^{DBH} for cation site impurities will maintain approximately a constant separation from a fixed reference point (e.g., the vacuum level) in different host crystals, since Δ and $\bar{\epsilon}$ have opposing effects on ϵ_{imp}.

d. Comparison of the Three-Level Model with the Classical Ionic Model

It is instructive to contrast the electronic-structure model that emerges from our quantitative calculations on 3d impurities in semiconductors with that used in classical ligand field theories.[3–7] Such models assume that the ligand orbitals are *deeper* in energy than the 3d orbitals of the transition atom (as may be appropriate for highly electronegative ligand atoms such as Cl or O). Consequently, these models predict that the lower t^{CFR} (bonding) state is ligandlike and the higher t_2^{DBH} (antibonding) state is 3d-like, exactly the opposite of our model (Fig. 29). These diverging results have profound consequences for the anticipated optical and magnetic properties of the system, as illustrated below. I first illustrate the appropriateness of the classical ligand field model to *ionic* 3d compounds and then their inappropriateness for 3d impurities in *covalent* semiconductors.

Consider first the tetrahedral structure of CuCl (Fig. 30a). The Cl p orbitals with 5 electrons (L, p in Fig. 30a) are assumed (correctly) in ligand-field models

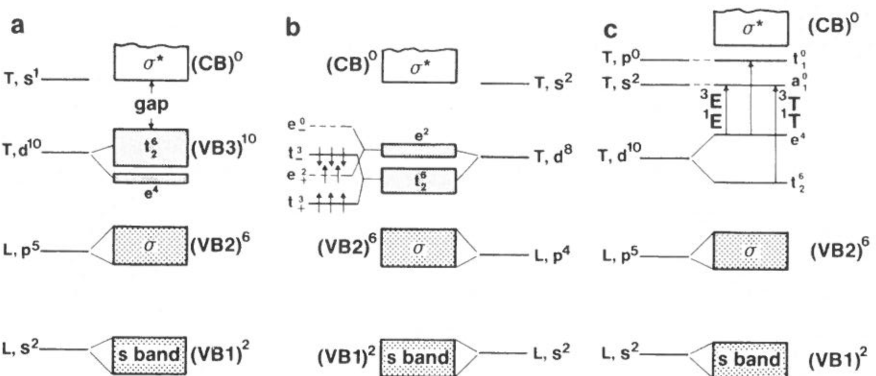

FIG. 30. Schematic ligand-field model depicting the one-electron levels that result from the interaction of ligand (L) orbitals with those of the transition (T) ion [A. Fazzio, M. Caldas, and A. Zunger, *Phys. Rev. B* **32,** 934 (1985)]. The lowest energy bands VB1 and VB2 are formed from the ligand s and p orbitals, respectively, and are fully occupied by 2 and 6 electrons, respectively. Above them we find the metal d orbitals, hybridized with ligand p orbitals (VB3). (a) In CuCl (T_d symmetry, monovalent ligands) and (c) NaCl:Cu (O_h impurity, monovalent ligands) VB3 is fully occupied by 10 electrons. (b) In NiO (O_h symmetry, divalent ligands) they are only partially occupied, giving rise to a magnetic moment. The conduction band (CB or σ^*) is formed from the metal s orbitals. Transitions within VB3 (when partially empty) form the $d \to d^*$ internal excitations; those between VB3 and the CB give rise to charge-transfer bands.

to lie lower in energy than the Cu $3d$ orbital with 10 electrons (T, d in Fig. 30a). As the metal–ligand interaction $\beta_{VB,T}$ is switched on, the Cl level broadens into a bonding state which is fully occupied as one electron is removed from atomic Cu $d^{10}s^1$ to complete the ligand p shell. It forms the occupied Cl p band (VB2), above the Cl s band (VB1). The $N_I - N_H = 10$ electrons left on Cu^+ fill the metal e and t_2 orbitals in a closed-shell $e^4t_2^6$ configuration which in CuCl forms the upper valence band (VB3), below the empty metal s conduction band (CB). Hence the s orbital of the metal atom becomes effectively depopulated in the solid. This picture is substantiated by modern band-structure calculations[228a] and photoemission experiments.[228b] In NiO (Fig. 30b), the O $2p^4$ atomic level (L, p) becomes fully occupied in the solid, forming the O $2p^6$ band (VB2, often referred to as the σ band), as $N_H = 2$ electrons are removed from Ni, leaving $N_I - N_H = 9$ electrons in the Ni^{2+} d states. These nine electrons fill completely the t_2 band but leave the upper e band only half-filled. This open-shell structure gives rise to a series of multiplets,[69,71] as well as to the magnetic properties of NiO.[97] Finally, the same model applies to the Cu and Ag impurities in alkali halides (Fig. 30c; compare also with the cluster calculation of Fig. 6a). After the transfer of one electron from the impurity to the lattice, $N_I - N_H = 10$ remaining electrons form the $t_2^6e^4$ impurity levels.

The empty impurity a_1 and t_1 levels remain unoccupied and higher in the band gap. They constitute the final states in ^3E, ^1E, ^3T, ^1E excitations.

In all cases shown in Fig. 30, the simple ionic model correctly explains numerous experimental observations and is consistent with the result of subsequent accurate electronic-structure calculations.[70,150,151,228a] As can be seen from Fig. 30, the essence of the model is that *the ligand orbitals L are assumed to lie below the d orbitals of the transition* (T) *atom.*

The same model has been applied by Ludwig and Woodbury[1] to Si:$3d$ and subsequently by others[12] to $3d$ impurities in III-Vs. The ligand atomic orbitals are again implied (incorrectly) to be lower in energy than the impurity $3d$ orbitals. Consequently, as the interaction is switched on, the lower-energy bonding state is envisioned, in analogy with the ionic case (Fig. 30), to be *ligand-like*, much like the known VB1 and VB2 valence subbands in $3d$ oxides and halides. Since the valence of the ligand anions is $-N_H$, these models predict then that N_H of the N_I impurity electrons are transferred to the ligand sites, leaving the $3d$ atom (if initially neutral) in the T^{N_H} oxidation state. The remaining $N_I - N_H$ impurity electrons then occupy the antibonding DBH state, which is envisioned to be *impurity like.* This antibonding state can be further split by the exchange interaction and is occupied in accordance with Hund's rule. Since main-row ligand atoms do not have any e-like orbitals available to interact with the transition-atom $3d_e$ orbitals, the latter remain nonbonding in the solid. Their position relative to the antibonding t_2 orbital is determined in such models by the effective crystal field. Ludwig and Woodbury[1] argued that for substitutional impurities only the four nearest ligand atoms interact with the $3d$ orbital, giving rise to the standard *tetrahedral* crystal-field arrangement (e below t_2), whereas for interstitial impurities the effect of the octahedrally coordinated six *next* nearest neighbors outweighs the effect of the tetrahedrally coordinated four *nearest* neighbors, leading to a standard *octahedral* crystal-field arrangement (t_2 below e). Watkins[31,231] suggested, instead, that both in the substitutional and the interstitial cases, the level ordering is determined by the first coordination shell: for interstitial impurities, all the charge is concentrated on the $3d$ ion; hence, the *lack* of electronic charge in the direction of the first neighbors renders them positively charged; the t_2 orbitals (which point toward them) will hence be *lowered* in energy. In contrast, for substitutional impurities the first ligand shell is effectively negatively charged, leading to an *increased* energy of the t_2 orbitals; hence, e is below t_2.

This simple ionic model, leading to the Ludwig–Woodbury (LW) energy-level scheme for $3d$ impurities in semiconductors,[1] has a number of clear implications: (1) The impurity is envisioned to have been stripped of $N_H + q$

[231] G. Watkins, personal communication (1985).

TABLE XIV. CHARGE-DENSITY POPULATION ANALYSIS FOR Si:Mn, Si:Cr, Si:Ti, AND THE SILICON VACANCY[a]

Angular momentum	$Q_l^{a_1}$	Q_l^{e}	$Q_l^{t_1}$	$Q_l^{t_2}$	Q_l	$Q_l^{a_1}$	Q_l^{e}	$Q_l^{t_1}$	$Q_l^{t_2}$	Q_l
	Si:Mn					Si:Cr				
$l = 0$	1.617	0.000	0.000	0.000	1.671	1.603	0.000	0.000	0.000	1.603
1	0.000	0.000	0.000	1.997	1.997	0.000	0.000	0.000	2.113	2.113
2	0.000	3.197	0.000	5.036	8.233	0.000	2.342	0.000	4.922	7.264
3	0.142	0.000	0.452	0.202	0.796	0.146	0.000	0.459	0.173	0.778
4	0.018	0.090	0.072	0.177	0.357	0.018	0.089	0.076	0.060	0.243
Q^α	1.777	3.287	0.524	7.412	$Q^{tot} = 13.00$	1.767	2.431	0.535	7.267	$Q^{tot} = 12.00$
	Si:Ti					Vacancy				
$l = 0$	1.572	0.000	0.000	0.000	1.572	1.516	0.000	0.000	0.000	1.516
1	0.000	0.000	0.000	2.221	2.221	0.000	0.000	0.000	2.136	2.136
2	0.000	0.577	0.000	4.378	4.955	0.000	0.307	0.000	0.978	1.285
3	0.160	0.000	0.500	0.203	0.863	0.167	0.000	0.309	0.147	0.623
4	0.019	0.099	0.079	0.192	0.389	0.024	0.116	0.082	0.228	0.450
Q^α	1.751	0.676	0.579	6.994	$Q^{tot} = 10.00$	1.707	0.423	0.391	3.489	$Q^{tot} = 6.01$

[a] Eqs. (17.4)–(17.7), results in electron units. From A. Zunger and V. Lindefelt, *Phys. Rev. B* **27**, 1191 (1983).

calculated[19] charges Q_l^α, Q^α, and the total charge Q^{tot} for the substitutional Si:3*d* system and the Si vacancy.

Inspection of this table reveals a number of chemical trends. *First*, the total a_1 charge is essentially *s*-like (93% in Zn to 90% in Cr and Ti), the *e* charge is essentially *d*-like (98% in Zn to 85% in Ti), and the t_1 charge is *f*-like (~85%), whereas the t_2 charge is a *p*-*d* hybrid (about 33–66%). *Second*, the t_1 and a_1 representation charges Q^α remain constant throughout the series and are close to the corresponding values for the silicon vacancy. This is consistent with the fact that there are no localized t_1 defect levels for the Si:3*d* system, and that the a_1 resonances have their origin in the host crystal and are similar to the corresponding vacancy resonances. *Third*, the *e* representation charges stay constant from Zn to Fe, but once past Fe they drop linearly with *Z*. This reflects the absence of an *e* gap state from Zn to Fe and the gradual decrease in occupation of the *e* gap level in going from Mn (three e^{CFR} electrons) to Ti (no e^{CFR} electrons). On the other hand, the t_2 representation charges decrease from Zn to Co and remain constant afterwards. This reflects the emptying of the t_2^{DBH} gap states in going from Zn (four t_2^{DBH} electrons) to Co (no t_2^{DBH} electrons) as well as of the unoccupied t_2^{DBH} levels past Co. *Fourth*, the total central-cell charge Q^{tot} [Eq. (17.7)] corresponds to approximately six vacancy electrons (~1.5 per dangling bond, lingering into the central-cell volume) plus all impurity valence electrons (e.g., 6 + 12 for Si:Zn, 6 + 8 for Si:Fe, and 6 + 4 for Si:Ti). *Inside the central-cell region the impurity atom is hence neutral.*

19. Charge Densities

Figure 31a[19] shows the self-consistent impurity charge density $\rho_D(\mathbf{r})$ of a few substitutional transition-atom impurities in silicon along the $\pm\langle 111\rangle$ crystal directions. Figure 31b[19] shows, on an enlarged scale, the tails of $\rho_D(\mathbf{r})$ for $r \geq 2$ a.u.; the results in this range are similar for all impurities. We see that in the inner central-cell region ($r \leq 1.5$ a.u.; Fig. 31a) the charge density resembles an atomic 3*d* charge density and has a very large amplitude (the maximum valence charge density of crystalline silicon is, in the same units, only ≤ 0.1 *e*/cell). In the outer central-cell region ($2 < r < 4.44$ a.u., Fig. 31b), on the other hand, the charge density has dropped by nearly two orders of magnitude and exhibits a strong asymmetric behavior characteristic of the host-crystal charge density. This strong valence-electron density gradient within the central cell distinguishes 3*d* impurities from all *s*-*p* impurities which have a slowly varying central-cell charge density.

Figure 32 depicts the angular-momentum components of $\Delta\rho_l(|\mathbf{r}|)$ [Eq. (2.2)] in substitutional Si:3d[19] (a–c), substitutional GaP:3d[54] (d–e), and interstitial Fe in Si[140] (f–g). *First*, the spherical ($l = 0$) components are shown (Fig. 32a,d),

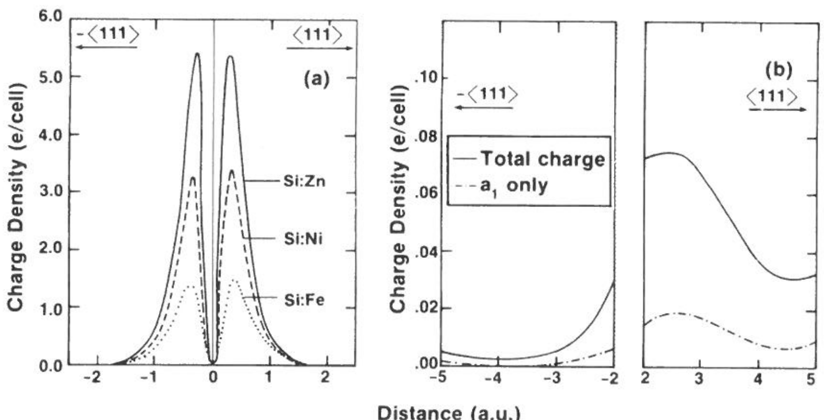

FIG. 31. Electronic pseudo charge density $\rho(\mathbf{r})$ around substitutional $3d$ impurities in Si along the $\pm\langle 111\rangle$ crystal directions. (b) shows, on an enlarged scale, the tails of (a). [From A. Zunger and U. Lindefelt, *Phys. Rev. B* **27,** 1191 (1983).] Note the similarity of $\rho(\mathbf{r})$ at small $\mathbf{r}$ to the atomic pseudo charge densities but its long-range tails at large $\mathbf{r}$ in (b).

indicating a monotonic decrease in the amplitude as the atomic number of the impurity decreases and a very strong localization in the inner central-cell region. Compared with the density fluctuation for a Si host vacancy (Fig. 32c), which has overall dimension of 1–2 host bond lengths, the density fluctuation associated with a $3d$ impurity has a much smaller characteristic radius, i.e., of the order of an atomic core size. This indicates a "healing" of the broken bonds. *Second*, we display in Fig. 32b and e, (on an expanded scale), the different l components of $\Delta\rho(\mathbf{r})$ [Eq. (2.2)]. The spherical ($l = 0$) component dominates, whereas the nonspherical $l = 3$ and 4 terms are ~ 100 times smaller. The charge density $\rho(\mathbf{r})$ of the defect-containing system, as well as $\rho_{\mathrm{H}}(\mathbf{r})$ of the unperturbed host crystal (Fig. 3), are strongly nonspherical and extended in open-structure covalent systems. The density fluctuation $\Delta\rho(\mathbf{r})$, however, is only weakly anisotropic and localized in the central-cell region, due to an effective cancellation. Hence, the $3d$ impurity reduces the anisotropy of the original covalent network. Note further that individual wave functions (c.f. Figs. 26 and 27) can be far more extended than the density fluctuation (Fig. 32). Figure 32f,g shows $\Delta\rho(\mathbf{r})$ for interstitial[140] Si:Fe. The spherical component is similar to that obtained in the substitutional case (Fig. 32a,b), but the characteristic negative part of $\Delta\rho_0(r)$, indicating a depletion in density relative to the pure host crystal, has moved from $r \cong 2.5$ a.u. (Fig. 32b) to $r \cong 4.5$ a.u. (Fig. 32g). Characteristically different charge anisotropies exist in the substitutional and interstitial impurities. These lead to different patterns of lattice relaxation, as discussed in Part VI,23.

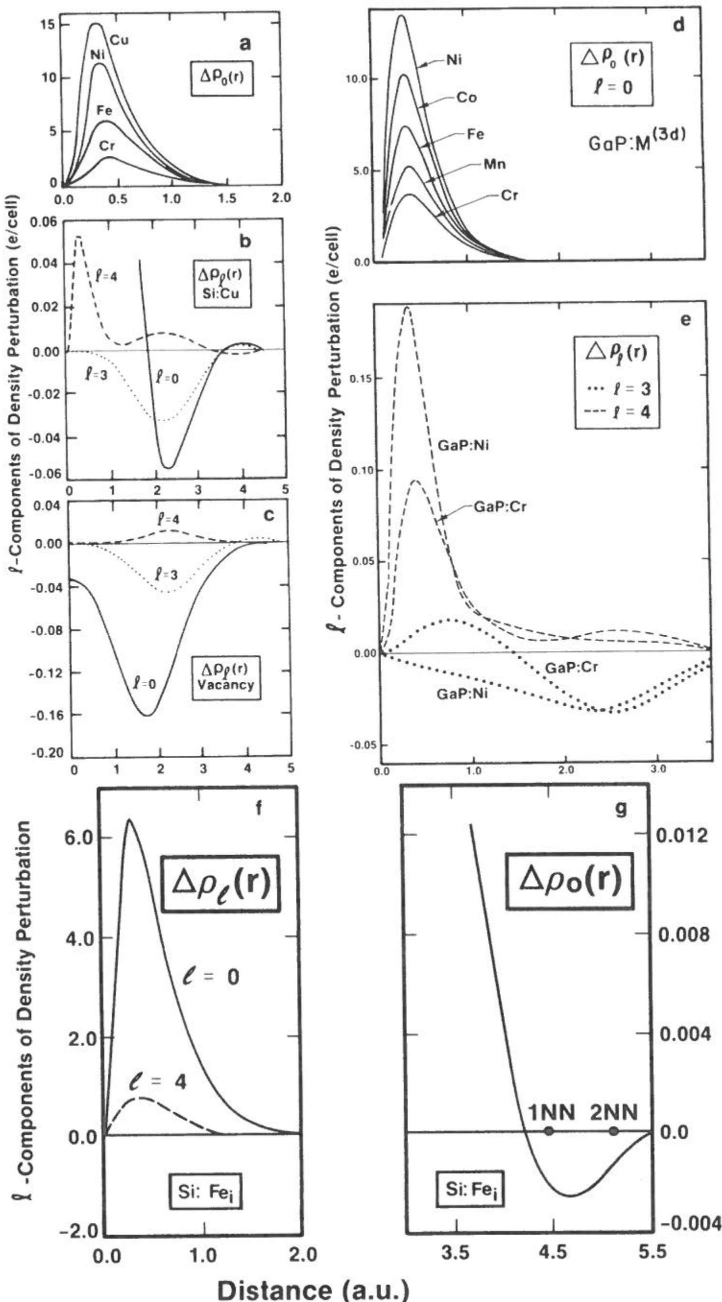

FIG. 32. Change in electronic pseudo charge density $\Delta\rho(\mathbf{r})$, relative to the pure host crystal, around neutral $3d$ impurities. $\Delta\rho_l(r)$ is defined in Eqs. (2.2) and (10.5). (a)–(c) are for substitutional impurities in Si [after A. Zunger and U. Lindefelt, *Phys. Rev. B* **27,** 1191 (1983)]. Note the large spherical ($l = 0$) component in (a) and the smaller anisotropic components ($l = 3, 4$) in (b). In (c) we give $\Delta\rho_l(r)$ for the Si vacancy, for comparison. (d), (e) are for substitutional impurities in GaP [after V. Singh and A. Zunger, *Phys. Rev. B* **31,** 3729 (1985)]. (f), (g) are for neutral interstitial iron in Si [after U. Lindefelt and A. Zunger, *J. Phys. C* **17,** 6047 (1984)]. The solid dots in (g) denote the positions of the first (1NN) and second (2NN) nearest neighbors to the interstitial site.

Figure 33[140] shows for Si:Fe$_i$ the three lowest radial components of the total charge density $\rho(\mathbf{r})$ (solid lines) together with the radial components of the host charge density around the interstitial site (dashed lines). In the direction of the first neighbors (1NN) at $(a/4)$ (1, 1, 1), where a is the lattice constant, the Kubic harmonics are all positive. Therefore, Fig. 33 shows that charge has been displaced toward the impurity, mainly through the spherically symmetric component, but also through the anisotropic components. In the direction of the second nearest neighbor (2NN) at $(a/2)$ (1, 0, 0), $K_3^{a_1}(\hat{r}) = 0$ and $K_4^{a_1}(\hat{r})$ is negative. The spherical $l = 0$ component again describes the largest displacement of charge toward the impurity, whereas there is an anisotropic depletion of charge through the $l = 4$ component close to the nucleus and a minor depletion of charge also at the 2NN. Except for the peaks in $\Delta\rho_0(r)$ and $\Delta\rho_4(r)$, which are both inside the impurity core, the defect-induced charge rearrangement is seen to be small. In this sense interstitial $3d$ impurities interact weakly with the host. We can, therefore, picture an

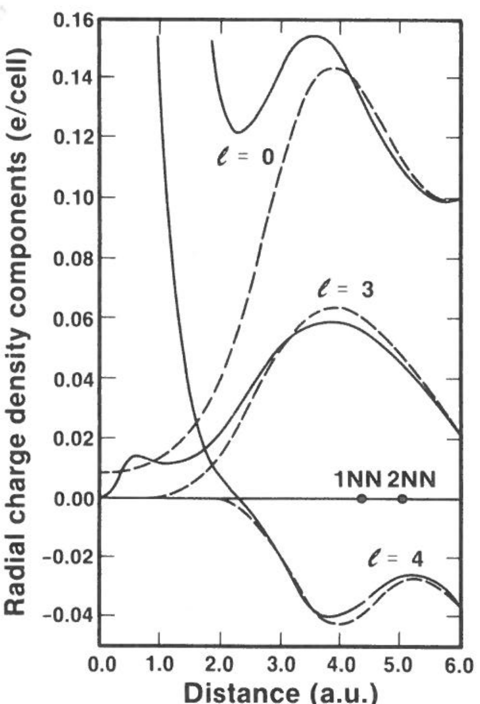

FIG. 33. Radial pseudo charge density around neutral interstitial Fe impurity in Si (———). (– – –) show the corresponding l components of the charge density of pure Si. [After U. Lindefelt and A. Zunger, *J. Phys. C* **17**, 6047 (1984).] 1NN and 2NN denote, respectively, the positions of the first and second nearest neighbors.

interstitial $3d$ impurity as being essentially a spherical cloud of charge, filling the rather empty region around the tetrahedral interstitial position out to the nearest-neighbor atoms without affecting the bonds (or the charge distribution in general) in the rest of the crystal. This is in contrast with substitutional transition-atom impurities and the vacancy (Fig. 32c), for which, again, the impurity-induced charge rearrangement is localized in the central cell but for which there is also a substantial weakening of the bonds due to the deficiency in the number of valence electrons that can repair the broken bonds.

It is interesting to compare the rates of charge accumulation for the same impurity in different host crystals. Figure 34 shows such a comparison[54] for a neutral Fe impurity in Si, GaP, and InP. We show the rate

$$Q_{\mathrm{D}}(R) = \int_0^R \rho_{\mathrm{D}}(r)\,dr \tag{19.1}$$

which the defect (D)-containing system accumulates charge, as well as the rate

$$Q_{\mathrm{H}}(R) = \int_0^R \rho_{\mathrm{H}}(r)\,dr \tag{19.2}$$

at which the pure host crystal accumulates charge. Their difference is denoted $\bar{Q}(r)$. Note that the asymptotic $(R \to \infty)$ limit is $\lim \bar{Q}(r) = Z_{\mathrm{I}} - Z_{\mathrm{H}} = \Delta Z$. The remarkable result is that $\bar{Q}(R)$ *attains its asymptotic limit by the first ligand shell, and that it exceeds this limit ("screening overshoot") around the bond center.* Considering $Q_{\mathrm{D}}(R)$, we may ask, "What is the radius R_{S} of a substitutional impurity which encompasses its nominal valence charge Z_{I} inside R_{S} [i.e., define R_{S} from the condition $Q_{\mathrm{D}}(R_{\mathrm{S}}) \equiv Z_{\mathrm{I}}$]. We find that this effective tetrahedral radius of bonded Fe is similar in the three host crystals, ranging between 2.5 a.u. for GaP:Fe to 2.7 a.u. for InP:Fe. These values are close to the classical host-independent Slater–Bragg[233] radii of a tetrahedral ion (2.65 a.u.; Ref. 233). Radii for other $3d$ impurities in Si were similarly calculated in Ref. 19.

20. THE SELF-REGULATING RESPONSE

The significance of the screening mechanisms that confine the impurity charge $\bar{Q}$ in the central cell (Fig. 34) can be appreciated by breaking down $\bar{Q}$ into contributions from different quantum states. We partition $\bar{Q}(R)$ into

$$\bar{Q}(R) = Q_{\mathrm{gap}}(R) + \Delta Q_{\mathrm{VB}}(R), \tag{20.1}$$

[233] J. C. Slater, "Symmetry and Energy Bands in Crystals," p. 55. Dover, New York, 1972.

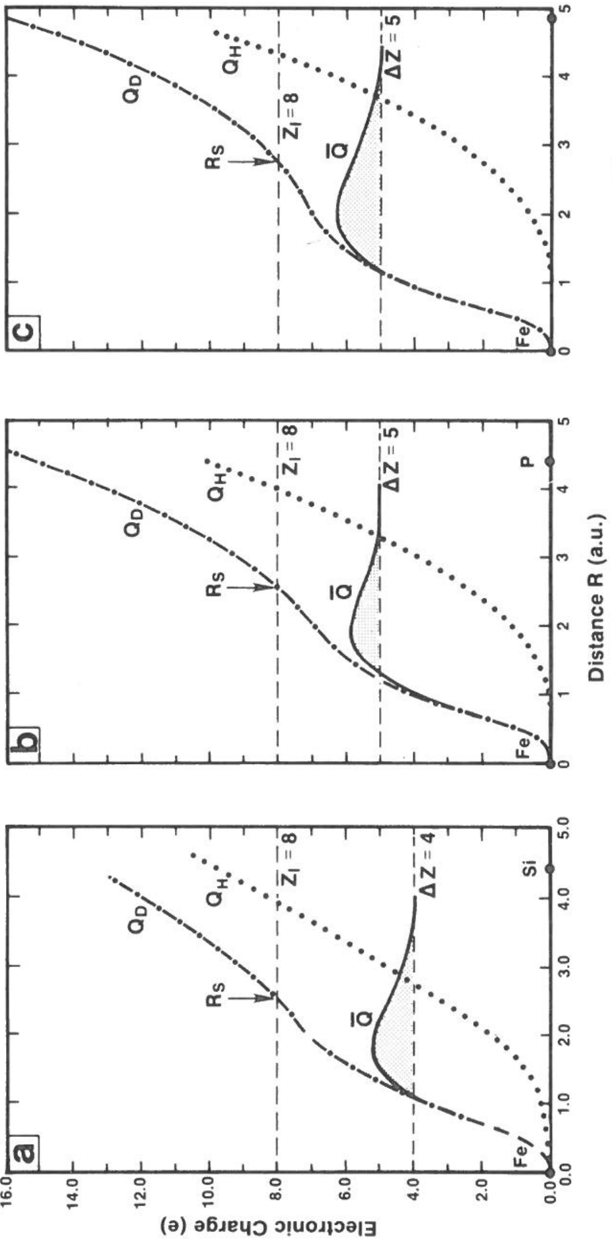

FIG. 34. We show for three substitutional impurity systems [(a) Si:Fe, (b) GaP:Fe, and (c) InP:Fe] the rate $Q_D(R) = \int_0^R \rho_D(\mathbf{r})\, d\mathbf{r}$ at which charge density is accumulated around the impurity site in the defect (D) containing systems, the rate $Q_H(R) = \int_0^R \rho_H(\mathbf{r})\, d\mathbf{r}$ at which charge density is accumulated around a host (H) cation site in the pure host system, and the net impurity-induced charge $\bar{Q}(R) = Q_D(R) - Q_H(R)$. The shaded areas denote regions where the impurity-induced charge $\bar{Q}(R)$ exceeds its asymptotic limit ΔZ ("screening overshoot"). R_S denotes the effective radius of a bonded impurity atom, enclosing in it the nominal impurity valence charge Z_I; i.e., $Q_D(R_S) \equiv Z_I$. The solid dots on the abscissa denote the position of the nearest-neighbor host atom. The Fe impurity is at the origin. [After V. Singh and A. Zunger, *Phys. Rev. B* **31**, 3729 (1985).]

where

$$Q_{\text{gap}}(R) = \sum_i^{\text{gap}} N_i \int_0^R |\psi_i|^2 \, d\mathbf{r} \tag{20.2}$$

is the contribution of the impurity-induced gap wave functions ψ_i with occupation numbers N_i (numbers shown in parentheses in Fig. 25), and $\Delta Q_{\text{VB}}(R)$ is the contribution of the displaced valence-band charge (calculated as $Q_D^{\text{VB}} - Q_H$, where Q_D^{VB} is the portion of Q_D arising from the perturbed valence-band states alone). ΔQ_{VB} constitutes the self-consistent screening response of the host to the bare impurity perturbation [$\Delta V_{\text{ext}}(\mathbf{r})$ of Eq. (10.4)]. The results are shown in Fig. 35 for substitutional (b) and interstitial (a) Si:Mn. As expected, at a large distance from the impurity the electrons occupying the gap levels produce all of the impurity charge $\bar{Q}$; i.e., [$\bar{Q}(\infty) = Q_{\text{gap}}(\infty) = \Delta Z$], whereas the valence band resumes its unperturbed density [$\Delta Q_{\text{VB}}(\infty) = 0$]. However, Fig. 35 shows that the impurity has already attained the charge-neutrality limit $\bar{Q}(R) = \Delta Z$ at a radius $R \cong 3$–5 a.u., *where the gap electrons contribute only ~50% (for interstitials) to ~75% (for substitutional) of* $\bar{Q}$. Figure 35 shows that the difference is made up by a rearrangement of the VB charge (shaded area denoting ΔQ_{VB}). As a result of an effective displacement of VB charge into the central cell, the system achieves local charge neutrality already at the cell boundary, *despite the rather extended nature of the gap wave functions.* Figure 35 also shows the distinguishing features of substitutional impurities. Their gap charge Q_{gap}

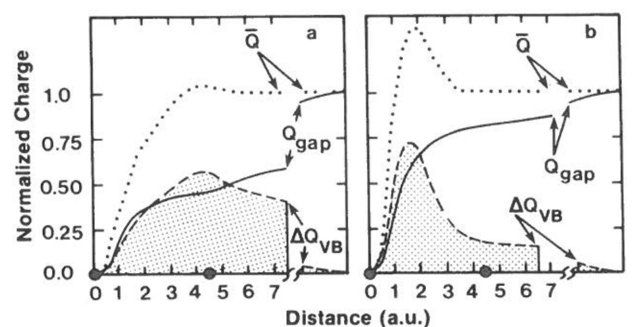

FIG. 35. Decomposition of the net impurity charge $\bar{Q}(R)$ into the band-gap contribution $Q_{\text{gap}}(R)$ and the valence-band contribution $\Delta Q_{\text{VB}}(R)$ [Eq. (20.1), shown here as the shaded area] for (a) interstitial, and (b) substitutional Mn^0 in Si. The charge is normalized by ΔZ. The radial impurity charge $\bar{Q}(R)$ approaches ΔZ (unit in this figure) at a large distance R from the impurity. At smaller distances $Q_{\text{gap}}(R)$ accounts for only a fraction of $\bar{Q}(R)$, the rest being contributed by the charge $Q_{\text{VB}}(R)$ of the rearranged valence-band resonances. [From A. Zunger and U. Lindefelt, *Phys. Rev. B* **26**, 5989 (1982).]

tracks the impurity charge $\bar{Q}$ considerably more closely than in the interstitial case. Also, the polarizing displacement of the VB charge occurs in the substitutional case within a significantly shorter distance. For comparison, recall that free atoms or $3d$ impurities in oxides show a perfect tracking $\bar{Q}(R) \equiv Q_{gap}(R)$ (all localized orbitals contribute to the atomic charge, thus ionizing some of them accordingly changes the effective charge $\bar{Q}$), and that shallow impurities (e.g., Si:P) manifest a very slow tracking $Q_{gap} \ll \bar{Q}$ in the central cell, (i.e., ionization does not alter the effective charge in the central cell).

Figure 36 compares $Q_{gap}(R)$ and $\Delta Q_{VB}(R)$ for neutral (substitutional) Mn in Si (A^0 with occupation e^3) and negatively charged Mn (A^- with occupation e^4). It shows that, whereas $Q_{gap}(R)$ increases as an electron is added to the gap level, $\Delta Q_{VB}(R)$ *shows a compensating decrease.* Much like a pool below a waterfall, the VB resonances rearrange in response to adding charge to the gap level so that VB charge leaks out of the central cell. We find that this remarkable "self-regulating response,"[196] first envisioned by Haldane and Anderson[234] (see similar results derived also by Fleurev and Kikoin[235]), leads to a nearly neutral central cell ($Q_{gap} + \Delta Q_{VB} \approx \Delta Z$ in Fig. 36) even for impurities with a nonzero formal charge. This self-regulation phenomenon has a number of interesting implications. *First*, since the effective charge $\bar{Q}(N)$ on the impurity depends only weakly on the number N of "active" electrons, the classical description of formal oxidation and charge states cannot be interpreted to imply a real *physical charge*: In fact, a T^{N_H+q} impurity is closer to neutrality [$\bar{Q}(N) \approx 0$] than to the ionic limit. *Second*, since the mean-field Mott–Hubbard Coulomb energy $U_{MF}(A^q)$ expresses the rate of increase in total energy with occupation N, the weak dependence of $\bar{Q}$ on N also implies a small effective U. Calculations for GaP[54] and Si[19] indeed reveal that in the solid, U is reduced up to two orders of magnitude relative to its free-ion values (Tables VII and IX); e.g., for Si:Mn$_s$ we have $U = 0.18$ eV, for GaP:Cr, $U =$ 0.6–0.7 eV, and for GaP:Ni, $U = 1.0$ eV. *Third*, a small U implies that the one-electron orbital energies $\epsilon(N) \cong \epsilon(0) + U\bar{Q}(N)$ also have a small dependence on occupation. This is illustrated in Fig. 37a,[196] which shows the opposing variations of Q_{gap} and Q_{VB} and the resulting weak dependence of ϵ_{gap} on N (Fig. 37b), and hence, small U. This explains why many charge states can coexist in a narrow energy range (Table VII). It has been suggested[39,47,234] that the same mechanism may be responsible for the ability of Fe to easily switch oxidation states in heme systems. *Fourth*, the self-regulating response mechanism implies that, whereas in low oxidation and charge states much of

[234] F. D. M. Haldane and P. W. Anderson, *Phys. Rev. B* **13**, 2553 (1976); P. W. Anderson and F. D. M. Haldane, unpublished results. I thank P. W. Anderson for drawing my attention to his unpublished work regarding the catalytic significance of this mechanism.

[235] V. N. Fleurev and K. A. Kikoin, *J. Phys. C* **9**, 1673 (1976); **17**, 2357 (1984).

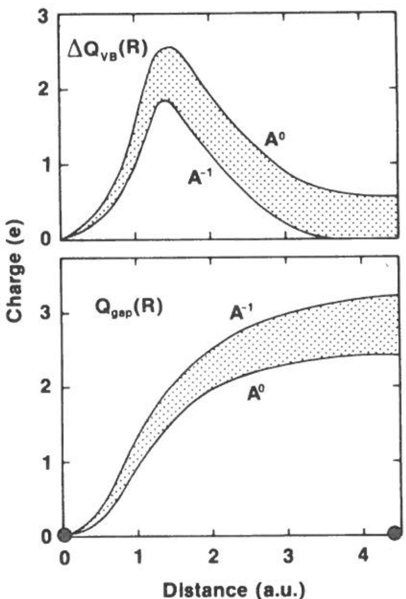

FIG. 36. Radial variations in the band gap $Q_{gap}(R)$ and valence band $\Delta Q_{VB}(R)$ contributions to the impurity charge for neutral (A^0) and negatively charged (A^-) substitutional Si:Mn. Shaded areas denote the charge redistribution in the $A^0 + e \rightarrow A^-$ process. Note that while addition of an electron to the gap level (in the $A^0 + e \rightarrow A^-$ process) raises $Q_{gap}(R)$ of A^- relative to that in A^0, the same process leads to a reduction in $\Delta Q_{VB}(R)$ for A^0 relative to A^-. This feedback, "self-regulating response" leads to a similar total net charge $\bar{Q}(R) = Q_{gap}(R) + \Delta Q_{VB}(R)$ for both A^0 and A^-. [From A. Zunger and U. Lindefelt, *Phys. Rev. B* **26**, 5989 (1982).]

the impurity charge extends over the *ligands*, when the oxidation and charge states are increased by ionizing gap levels, charge must flow *from the ligands to the impurity*, making up for the charge that was lost on the impurity site by ionization. In contrast, since no self-regulating response is available to $3d$ impurities in ionic media (as no strong VB resonances exist), in this case ionizations act to change the charge on the impurity itself (resulting in relaxations and polarizations[147]). This suggests[39] that in covalent materials the impurity Mössbauer isomer shift will depend only weakly on doping (i.e., ionization) relative to the situation in ionic crystals. *The real change of charge with ionization will occur on the ligands.* This agrees with the data surveyed in Part III,4.

One can inquire further about the chemical origin of the "leakage" of valence-band states from the central cell. Figure 37d analyzes $Q_{VB}(N)$ in terms of the wave-function representations [Eq. (17.6)] contributing to it. Whereas the a_1 and t_1 valence states (much like those in a rigid-band model) remain

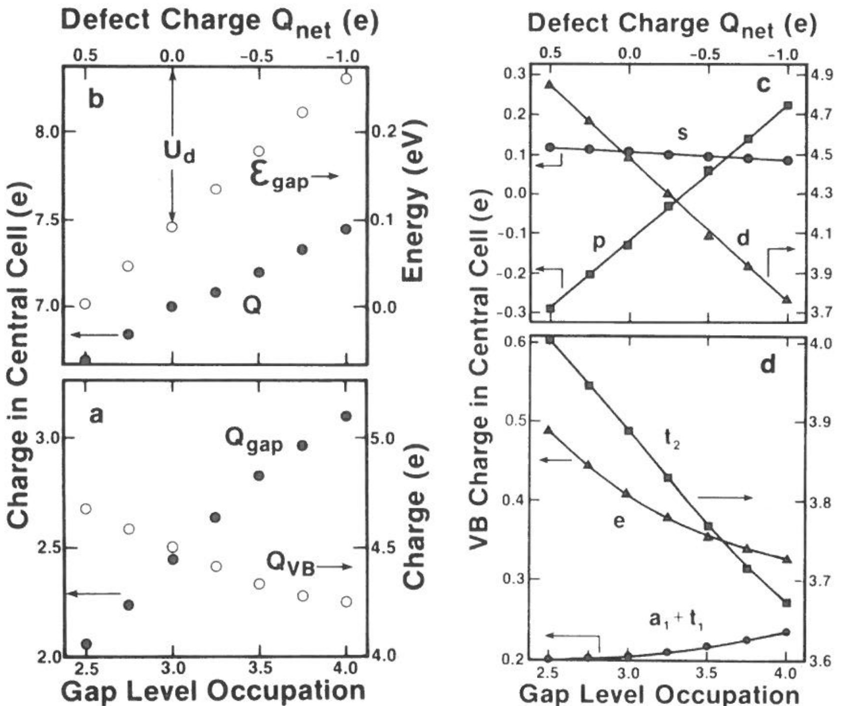

FIG. 37. Analysis of the changes in the electronic charge (enclosed in a nearest-neighbor sphere of radius 4.44 a.u.) around substitutional Si:Mn as a function of the occupation number of the gap level. (a) Q_{gap} and ΔQ_{VB} [Eq. (20.1)]: Note that as we increase the occupation of the gap level from 2.5*e* to 4.0*e* its contribution to the charge Q_{gap} increases too, but the valence-band charge Q_{VB} changes in the *opposite direction.* As a result, the sum $Q = Q_{gap} + Q_{VB}$ [part (b)] changes more slowly than Q_{gap} alone. This leads to a weak variation in the position of the band-gap energy level ϵ_{gap} with charge and to a small effective Mott–Hubbard energy U_d. (c) and (d) show the decomposition of ΔQ_{VB} into orbital charges ΔQ_l [Eq. (17.9)] and representation charges ΔQ^{α} [Eq. (17.8)]. This shows that the changes in ΔQ_{VB} are brought about by the reduction (increase) in the VB $d(p)$ charge, i.e., by *p-d* dehybridization. [From A. Zunger and U. Lindefelt, *Solid State Commun.* **45**, 343 (1983).]

largely unresponsive to the change in the gap-level occupation, the *e* and t_2 valence-band wave functions tend to leak out of the central cell as more electrons are added to the gap level. A partial-wave analysis of $Q_{VB}(N)$, depicted in Fig. 37c [using Eq. (17.5)], shows that the reduction in the valence-band contribution to the central-cell charge results from a strong attenuation of its *d* content (largely localized wave functions) accompanied by a smaller increase in the *p* content (largely delocalized wave functions), with almost no

response from the *s* states. I conclude that the remarkable features of 3*d* impurities in semiconductors are that they resist an ionic charge buildup in response to the addition of electrons by having their valence-band states leak out from the central cell, and that the system accomplishes this leakage by undoing its *p-d* hybridization (i.e., by dehybridization).

21. Effective Electronic Configurations

The small $U^{(dd)}(A^q)$ values for the 3*d* impurities in semiconductors have an interesting implication for the effective electronic configuration of the impurity atom. Whereas the large *atomic* $U^{(dd)}(T^{q+})$ values (Table IX) lead to the well-known preference for occupying the 4*s* subshell before the 3*d* subshell is completed, small *U* values in the solid may cause a population inversion in the ground state.

Figure 38 depicts, with the use of Eq. (17.8), the manner in which the atomic $s^m d^n = a_1^m(et_2)^n$ ground-state configuration is redistributed when the atom is placed substitutionally in silicon.[19] One sees (Fig. 38b) that most of the atomic a_1 electrons are depleted and redistributed into the *e* and t_2 representations. The *e* representation contains nearly four electrons for Zn through Fe, then 3, 2, 1, and 0 electrons for Mn, Cr, V, and Ti, respectively, as the e^{CFR} moves into the gap and is progressively emptied (Fig. 25a). The decrease in the occupation from Zn to Fe, for the t_2 representation, followed by a constant occupation of approximately four electrons thereafter, reflects the evacuation of the t_2^{CFR} level as it moves through the gap.

Figure 38a shows the variations with atomic number of the effective orbital configuration ΔQ_l of 3*d* impurities in Si [Eq. (17.9)]. The total number of impurity valence electrons Z_I is shown for comparison (dashed line in Fig. 38a). The interesting feature in this figure is that whenever the 3*d* subshell can also accommodate the *s* electrons (i.e., to the left of Ni d^8 in the periodic table), the latter are promoted into it. This trend is evident in Fig. 38a from the approach of the ΔQ_d line to the Z_I (dashed) line. *Transition-atom impurities in semiconductors therefore tend to approach a noble-metal configuration.* This is in marked contradiction to the Ludwig–Woodbury model,[1] which hypothesized (compare its underlying ligand-field model of Fig. 30) that, for substitutional 3*d* elements, the 3*d* electrons would be promoted into the *sp* subshell to form a tetrahedral hybrid (i.e., $d^n s^2 \rightarrow d^{n-2}s^1p^3$, or $d^{n+1}s^1 \rightarrow d^{n-2}s^1p^3$). We find that for the completely filled *d*-subshell elements Zn and Cu, where the 3*d* shell cannot accommodate any *s* electrons, the latter are being promoted into a *p* state, yielding for the substitutional case $\approx s^{0.24}p^{1.56}d^{10}$ for Zn and $s^{0.19}p^{0.84}d^{9.92}$ for Cu. The substitutional Ni

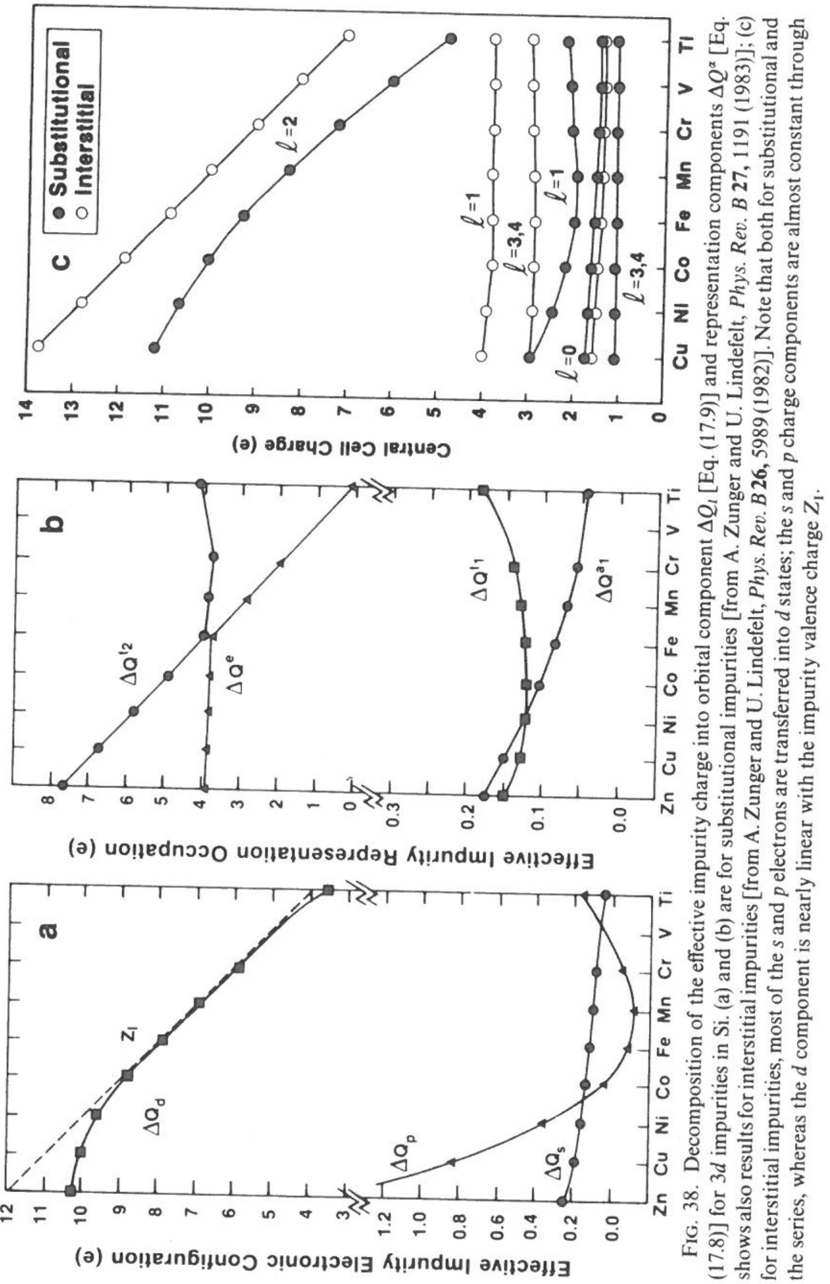

FIG. 38. Decomposition of the effective impurity charge into orbital component ΔQ_l [Eq. (17.9)] and representation components ΔQ^α [Eq. (17.8)] for 3d impurities in Si. (a) and (b) are for substitutional impurities [from A. Zunger and U. Lindefelt, *Phys. Rev. B* **27**, 1191 (1983)]; (c) shows also results for interstitial impurities [from A. Zunger and U. Lindefelt, *Phys. Rev. B* **26**, 5989 (1982)]. Note that both for substitutional and for interstitial impurities, most of the s and p electrons are transferred into d states; the s and p charge components are almost constant through the series, whereas the d component is nearly linear with the impurity valence charge Z_I.

impurity has the intermediate occupation of $s^{0.16}p^{0.38}d^{9.44}$; hence Ni in silicon forms a noble-metal-like compound with a nearly filled d subshell. This should be contrasted with the effective electronic configurations deduced for the bulk elemental metals[236] of $s^{1.3}d^{4.7}$, $s^{1.4}d^{6.6}$, $s^{1.3}d^{8.7}$, and $s^{1.3}d^{9.7}$ for Cr, Fe, Ni, and Cu, respectively, which show a much higher occupation of the s orbitals.

Figure 38c shows Q_l for interstitial impurities in Si, exhibiting an $s \rightarrow d$ population crossover. It shows that, although all non-d components of the central-cell charge density are small and nearly impurity independent, the d component is large and decreases rapidly with Z. We again see that whenever the d shell can accommodate more than its electrons (3d impurities lighter than Cu), the s electrons are promoted into the d shell, leading to an $\approx d^{n+m}$ configuration. These results for interstitial impurities confirm the classical hypothesis of Woodbury and Ludwig,[1] suggesting an $s \rightarrow d$ promotion for interstitial impurities, but contradict their assumption of a reversed $d \rightarrow sp$ promotion for substitutional impurities.

The predicted s-d population inversion[19,54] further suggests a simple explanation for the diffusion puzzle[10]: Whereas Ni is known to be an extremely fast interstitial diffuser in Si (diffusion constant[237] $D \sim 10^{-4}$ cm^2/sec, typical of *liquids*), the lighter 3d impurities like Ti are extremely immobile in silicon. It has been suggested[19] that this is so because Ni has an effective noble-atom-like closed-shell configuration $\approx d^{10}$ in silicon and is therefore both small and chemically passive. On the other hand, Ti and V exist in silicon as open-shell species with large perturbation radii, and hence they have a far greater propensity for both steric and chemical interactions with the host.

A calculation[19] of the charge-density components $\delta_l(r)$ of the effective impurity atom [Eq. (7.11)] shows them to be very similar to those of a free atom (in fact, almost indistinguishable on an ordinary plot), with somewhat compressed tails and a small nonspherical $\delta_3(r)$ term absent in the free atom. This analysis suggests a surprisingly simple chemical picture for the changes exerted on the crystalline environment by the impurity atom. Whereas the discrete atomic energy levels of the impurity atom undergo substantial changes in the solid—they split and broaden into structured resonances covering a wide energy range—the impurity's final effective charge density simply corresponds to that of a compressed atom with its s electrons excited into the p and d shells.

[236] R. M. Nieminen and C. H. Hodges, *J. Phys. F* **6**, 573 (1976).
[237] M. K. Bakhadyrkhanov, S. Zainabidinov, and A. Khamidov, *Fiz. Tekh. Poluprovodn.* **14**, 412 (1980) [*Sov. Phys. Semicon.* **14**, 243 (1980)].

22. The Bulk Analog of 3*d* Impurities in Semiconductors

a. 3*d* Bulk Chalcogenides, Pnictides, and Silicides

It is natural to consider bulk transition-atom silicides, phosphides, arsenides, and oxides as "concentrated-limit" analogs of 3*d* impurities in Si, GaP, GaAs, and ZnO, respectively.[54] I briefly indicate here the generic relation between the electronic structure in these two limits.

Starting with the rocksalt-structure 3*d* monoxides (e.g., NiO, CoO), having a sixfold-coordinated 3*d* ion, we find the band structures[150,151] to show a narrow e^{CFR}-type subband and a wider t_2^{CFR} subband, both inside the $\sigma \rightarrow \sigma^*$ band gap, which separates the oxygen-derived σ valence band from the metal–*s*-derived σ^* conduction band (cf. Fig. 30). The e^{CFR}-like and t_2^{CFR}-like bands have an octahedral ordering and are partially occupied, which leads to a multiplet structure and $d \rightarrow d^*$ internal transitions that are entirely analogous to those of 3*d* impurities in ZnO or in NaCl. As the atomic number *Z* of the 3*d* element decreases in going from NiO to FeO, VO, and TiO, these "gap levels" rise in energy[150] toward the CB, exactly as in Fig. 25. No dangling-bond hybrids occur in such systems, and all optical and magnetic properties are associated with the highly localized CFR bands. These are the prototypical systems of the Ludwig–Woodbury model.[1] As the anion becomes heavier in the O → S → Se → Te sequence, its outer *p* orbitals become shallower, leaving eventually the *d* orbitals of the transition atom *below* the ligand orbitals. The system as a whole acquires semiconducting properties with stronger metal–ligand overlap (and its attendant covalency). At this point ligandlike dangling-bond orbitals emerge, and the classical ionic ligand-field model (Part VI,18,d) is no longer the proper description of the system; our covalent model (Part VI,18,c) is. Typical to such systems are solutions of Mn in II-VI compounds.[238,239] The nearly continuous solubility of such systems allows one to join the impurity limit (e.g., CdTe:Mn, CdSe:Mn, etc.) with the bulk limit (e.g., $Cd_xMn_{1-x}Te$, $Cd_xMn_{1-x}Se$, etc.). Substitution of Mn leads to a continuous decrease in lattice constant[238] and increase in band gap,[238] until one reaches the composition where the lowest $d \rightarrow d^*$ transition of Mn^{2+} is exposed inside the gap. The crystal-field resonances are inside the valence band,[224–227] showing in excitation and photoluminescence [239] spectra the familiar $d \rightarrow d^*$ transitions. These semimagnetic semiconductors exhibit a range of interesting phenomena,[238] including spin-glass transitions, formation of antiferromagnetic clusters, spin–spin exchange between the localized magnetic moments and

[238] For review on Mn solutions in II-VI materials see: J. K. Furdyna, *J. Appl. Phys.* **53**, 7637 (1982); R. R. Galazka, Proc. Int. Conf. Phys. Semicond., *14th Edinburgh* p. 133 (1978).

[239] G. Ambrazevicius, G. Babonas, and Yu, V. Rud, *Phys. Status Solidi* **125B**, 759 (1984).

the band electrons, large Faraday rotation, and giant negative magnetoresistance associated with hopping conductivity.

As we move to Column-V anions, we encounter the 3*d* phosphides and arsenides.[155] All transition-metal phosphides attain a coordination number larger than 4 (akin to the unrelaxed GaP:3*d* impurity system) by adopting either the hexagonal ($B8_1$) NiAs structure (e.g., VP) or the orthorhombic (*B*31) MnP structure (all remaining phosphides). The band structure of transition-metal phosphides shows,[240–242] at low energies, a phosphorus 3*s* band (analogous to the lower valence band between $E_v - 9.8$ eV and $E_v - 12.4$ eV in Fig. 25b), separated by a heteropolar gap from the upper valence band above it. This upper valence band consists first of the bonding combinations of phosphorus 3*p* and the metal 3*d* orbitals (i.e., a t_2^{CFR}-like band). A narrow 3*d*-like nonbonding band (e^{CFR}-like) has also been identified.[240–242] The different properties of the 3*d* phosphides are explained[155,240–242] in terms of the location of the Fermi energy E_F relative to these bands. For MnP, E_F for the majority-spin states lies in the t_2^{DBH}-like antibonding band, whereas the E_F for the minority-spin states lies in the narrow nonbonding e^{CFR}-like states. This gives rise to a substantial exchange splitting, sizeable saturation moments (e.g., $1.29\mu_B$ in MnP[243]), and metallic behavior. In lighter transition-metal phosphides such as ScP,[241,242] the Fermi energy lies below the narrow nonbonding e^{CFR}-like band, but above the bonding t_2^{CFR} band.

As we move to Column IV we encounter the 3*d* silicides.[152,244] Their band structures[153,154] show a well-developed t_2^{CFR} bonding band, an antibonding t_2^{DBH}-like band, and a nonbonding e^{CFR} band between them. The Fermi energy lies inside the e^{CFR} band for the low-*Z* 3*d* silicides and in the t_2^{DBH} band for the high-*Z* silicides. These systems do not exhibit any significant localization effects (multiplet structure, large local magnetic moments), in analogy with the increased covalency in the sequence ZnO:3*d* → ZnS:3*d* → GaP:3*d* → Si:3*d*.

In going from the dilute Si:3*d* limit to the bulk silicide, *d*-*d* interactions increase, and metal–*d* silicon–*p* interactions decrease. Using the QBCF approach[21] and the mixed-basis band-structure method,[219] Zunger[245] investigated the trends in the orbital energies as a function of metal content by finding the electronic structure of a periodic supercell of Si containing in each cell $M = 4, 8, 16, 54$, and 250 Si atoms and one 3*d* atom. Metal *d*–*d* interactions decrease as the cell size increases, approaching thereby the isolated-impurity

[240] A. Yanase and A. Hasegawa, *J. Phys. C* **13**, 1984 (1980).

[241] P. G. Perkins, A. K. Marawaha, and J. J. P. Stewart, *Theor. Chim. Acta* (*Berlin*) **59**, 555 (1981); **59**, 569 (1981).

[242] E. Wimmer, A. Neckel, and K. Schwarz, *J. Phys. C* **12**, 5441 (1979); **12**, 5453 (1979).

[243] A. Takase and T. Kasuya, *J. Phys. Soc. Jpn.* **47**, 491 (1979).

[244] A. S. Berezhnoi, "Silicon and Its Binary Systems." Bureau of Standards, New York, 1960.

[245] A. Zunger, unpublished results (1984).

limit. The results were then fitted to a four-band tight-binding model (three t_2 levels and one e level), analogous in structure to the impurity three-level model of Part VI,18,c. The results[245] show that as the metal content increases, (1) the nonbonding e^{CFR} band broadens and rises in energy; (2) the antibonding t_2^{DBH} band located at higher energies narrows and is somewhat lowered in energy; and (3) as a result, the large e^{CFR}–t_2^{DH} gap that exists at small concentrations (cf. Fig. 25) vanishes when the metal-to-Si ratio exceeds a critical ratio of about $\approx\frac{1}{10}$–$\frac{1}{16}$; the system becomes metallic by band overlap. Bulk silicides hence have fewer of the localization-induced characteristics associated with 3*d* impurities in silicon, since the covalent network is completely disrupted and replaced by a metallic system.

b. *The Biological Analog: Heme Systems*

The only 3*d* "impurity" in covalent media of truly vital importance is the deep Fe center in heme systems.[246–256] Here, I briefly draw the reader's attention to the great similarity of the physical properties of this center to those of 3*d* impurities in conventional semiconductors. Depending on the particular heme molecule, iron is fourfold coordinated in such molecules by a variety of ligands, ranging from highly covalent to highly ionic. Calculations[246,247] and measurements[248–256] of various aspects of the electronic structure suggest the existence of both deep 3*d* states in the gap and states which resonate within the manifold of occupied molecular orbitals. The central iron atom can exist both in the Fe^{2+} and in the Fe^{3+} oxidation states with a small (pH-dependent) redox potential of ~0.3–0.5 eV[127] (4.5–4.7 eV with respect to vacuum), i.e., close to typical donor energies of Fe in semiconductors. The similar reduction of this ionization energies (relative to its free-ion value) observed both in heme proteins and in semiconductors led to the suggestion[39,47,234] that the self-regulating response mechanism (Part VI,20) might be operative in both systems. The positions of the ligand atoms

[246] T. Nozawa, M. Hatano, U. Nagashima, S. Obara, and H. Kashiwagi, *J. Chem. Soc. Jpn.* **56,** 1721 (1983), and references therein.
[247] R. G. Shulman, S. H. Glarum, and M. Karplas, *J. Mol. Biol.* **57,** 93 (1971).
[248] K. Wuthrich and R. G. Shulman, *Phys. Today* **April,** 43 (1970).
[249] G. C. Brackett, P. L. Richards, and W. S. Caughey, *J. Chem. Phys.* **54,** 4383 (1971).
[250] S. Rackovsky and D. A. Goldstein, *Proc. Natl. Acad. Sci. U.S.A.* **81,** 5901 (1984).
[251] P. O. D. Offenhartz, *J. Chem. Phys.* **42,** 3566 (1963).
[252] D. W. Smith and R. J. P. Williams, *Struct. Bond.* **7,** 1 (1970).
[253] M. Cerdonio, A. Congiu-Castellano, F. Mongo, B. Pispisa, G. L. Romani, and S. Vitale, *Proc. Natl. Acad. Sci. U.S.A.* **74,** 398 (1977).
[254] T. Iizuka and T. Yonetani, *Adv. Biophys.* **1,** 157 (1970).
[255] P. George, J. Bettlestone, and J. S. Griffith, *Rev. Mod. Phys.* 441 (1964).
[256] G. Lang and W. Marshall, *Proc. Phys. Soc.* **87,** 3 (1966).

have been observed[250] to change as the charge state of Fe changes (i.e., a lattice-relaxation effect akin also to 3*d* impurities in semiconductors). Absorption experiments[251–252] reveal both the familiar $d \rightarrow d^*$ internal transitions as well as charge-transfer bands, at the same spectral range as that characteristic of 3*d* impurities in semiconductors (Tables V and VII). Paramagnetic susceptibility[253] and EPR[254] experiments reveal[255] both a high-spin state of Fe (with a magnetic moment around $5\mu_B$) and a low-spin state (with ligand-dependent magnetic moments ranging around 2–3μB). EPR experiments distinguish clearly the high-spin state ($g_\parallel \cong 2, g_\perp \cong 6$) from the low-spin state ($g_x \cong 1.7, g_y \cong 2.2$, and $g_z \cong 2.8$), suggesting the lack of fourfold symmetry in the low-spin phase. Measurements of reaction equilibrium constants[255] reveal a ligand-dependent energy barrier to low-spin *vs* high-spin conversion, ranging from −0.16 to +0.45 eV. Proton NMR[248,249] and Mössbauer experiments[256] were further used to infer the ligand structure around Fe in its different spin and charge states.

Given the overall similarities in the properties of the deep Fe center in semiconductors and in heme systems, one cannot but hope that some of the modern impurity characterization techniques be used to unravel these intriguing analogies.

23. Breathing-Mode Lattice Distortions around the Impurity

Lindefelt and Zunger[140] (LZ) have studied the pattern of breathing-mode lattice distortions around 3*d* impurities in silicon. The results for interstitial impurities are summarized in Fig. 39. Their main findings are:

(1) At least four shells, containing 26 ligand atoms, show substantial distortions, the next three shells show modest distortions, and farther shells are essentially undistorted.

(2) The first shell, containing four Si atoms (located at a distance $d = 2.35$ Å from the interstitial site when the lattice is undistorted), moves *away* from the impurity. Averaging over the different impurities, LZ found the average outward displacement to be around 0.074 Å. For the six atoms in the second shell, which in the perfect crystal are at a distance of 1.155*d* from the interstitial site, the displacement is opposite to that of the first shell; i.e., the atoms move *toward the impurity.* The averaged inward displacement in this case is around 0.095 Å. Thus the distance between the two shells has, on the average, decreased from 0.365 to 0.19 Å, i.e., by a factor of two, *leading to an approximately tenfold-coordinated transition atom.* Remarkably, all three metallic bulk disilicide structure types[257] [the $TiSi_2$ (orthorhombic), $CrSi_2$

[257] A. F. Wells, "Structural Inorganic Chemistry," 4th Ed., p. 789. Claredon, Oxford, 1975.

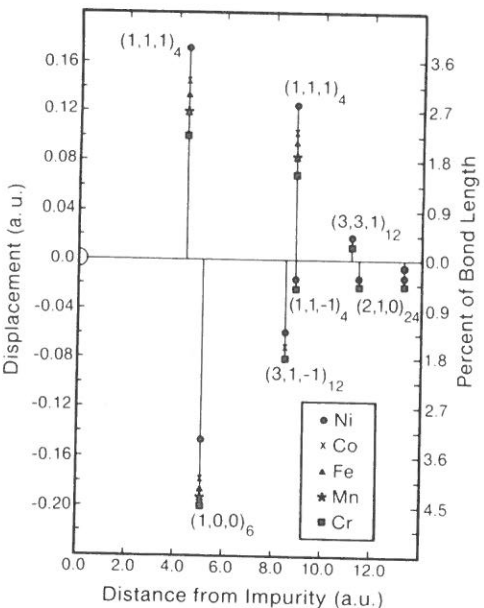

FIG. 39. Predicted breathing-mode lattice relaxations of the Si atoms in the $(h,k,l)_l$ shell (containing I atoms) around an interstitial $3d$ impurity (situated at the origin). Positive (negative) displacements denote outward (inward) relaxation of the nearest neighbors. Observe that the first shell of neighbors $[(1,1,1)_4]$ relaxes *outwards*, but the second shell of neighbors $[(1,0,0)_6]$ relaxes inwards. This leads to an approximately 10-fold-coordinated impurity atom. [From U. Lindefelt and A. Zunger, *Phys. Rev. B* **30**, 1102 (1984).]

(hexagonal), and $MoSi_2$ (tetragonal) structures] avoid the conventional close-packing coordination of 12 and assume an approximately 10-fold coordination around the transition atom, exactly like that of the dilute impurity limit.

(3) The chemical trend in the deformation pattern (Fig. 39) is that light $3d$ impurities (e.g., Cr) show the smallest *outward* movement of the first shell but the largest *inward* movement of the second shell, whereas heavier impurities (e.g., Ni) show just the opposite: the largest *outward* movement of the first shell but the smallest *inward* movement of the second shell. In both limits the net effect is to bring together ten Si atoms to form approximately 10-fold coordination. This suggests that the interstitial $3d$ impurity and its coordination shell, including ten ligands, should properly be viewed as a complex—an enlarged defect in its own right—rather than as a point impurity.

(4) Both for the first and the second ligand atom shells the anisotropic part of $\Delta\rho(\mathbf{r})$ (projected on the ligand site) gives rise to forces that pull the

neighboring atoms closer to the impurity. This contribution is, however, not strong enough to reverse the direction of distortion of the first shell.

(5) The Si:$3d_i$ system maintains a universal relaxation pattern, despite variations in the band filling, electronegativities, and ground-state configurations due to $s \rightarrow d$ population inversion. This process places all of the bonding s electrons in the d shell, producing nearly identically weak bonds for all $3d$ impurities.

(6) Since an interstitial $3d$ impurity forms weak directional bonds that did not exist in the unperturbed host crystal, the newly introduced charge anisotropy, for all $3d$s, produces forces that tend to shorten (stabilize) the bonds. In contrast, substitutional $3d$ impurities *disrupt* the directed covalency that existed in the unperturbed crystal by replacing a Si atom with an element that is less able to bond to Si (Figs. 31 and 32). Hence, the reduced charge anisotropy tends to increase (destabilize) the bonds, causing an overall *outward* relaxation both for the first and the second shells.

Recent EXAFS experiments[28] for Si:Fe have indicated an outward relaxation of the first shell by 0.1 ± 0.05 Å. Lindefelt and Zunger[140] predicted 0.068 Å (Fig. 39). While this agreement is encouraging, further experiments with greater accuracy are needed.

24. EFFECTS OF SPIN POLARIZATION

a. *Local Magnetic Moments*

Katayama-Yoshida and Zunger[39,47,217,258] (KYZ) have included spin-polarization effects in their self-interaction-corrected[215] local-spin-density calculation for interstitial $3d$ impurities in silicon. The spin-polarized local density of states of the neutral centers (Fig. 40) shows that these impurities in silicon introduce bonding (b) valence-band resonances of t_2 (t_+^b and t_-^b) and e (e_+^b and e_-^b) symmetries in the upper part of the valence bands (shaded areas) and that their antibonding (a) counterparts (t_+^a, t_-^a, e_+^a, and e_-^a) appear in the band gap or inside the conduction band. In addition, deep and nearly impurity-independent resonances (R) t_+^R, t_-^R, a_+^R, and a_-^R appear in the lower part of the valence bond. They find that these VB resonances control the impurity's charge distribution and magnetism. The decomposition of the local magnetic moment μ_{loc} in the impurity subspace into VB and gap contributions

$$\mu_{loc} = \mu_{gap} + \mu_{VB} \qquad (24.1)$$

[258] H. Katyama-Yoshida and A. Zunger, *Int. Conf. Magnetism, San Francisco* to be published (1985).

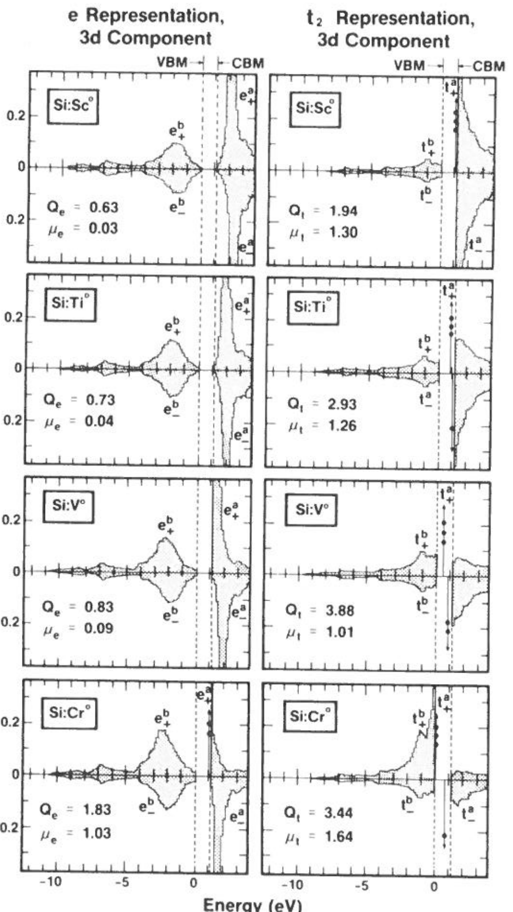

FIG. 40. Local density of states of spin-polarized, neutral interstitial $3d$ impurities in Si for the e (left panels) and t_2 (right panels) representations (calculated from local spin density functional Green's function method). Spin-up (down) are shown at the upper (lower) portions of each panel. Q_α and μ_α denote the contribution of representation $\alpha = e, t_2$ to the impurity charge and local magnetic moment, respectively. Dashed vertical lines denote the edges of the valence and conduction bands; gap levels are denoted by (●), showing their occupancy. The figure shows bonding (e^b, t^b) and antibonding (e^a, t^a) resonances. Note that much of the impurity charge and local magnetic moment originate from VB states. [From H. Katayama-Yoshida and A. Zunger, unpublished (1985).]

and its resolution into contributions of different angular momenta

$$\mu_{\text{loc}} = \sum_l \mu_l \qquad (24.2)$$

and representations

$$\mu_{\text{loc}} = \sum_\alpha \mu_\alpha \qquad (24.3)$$

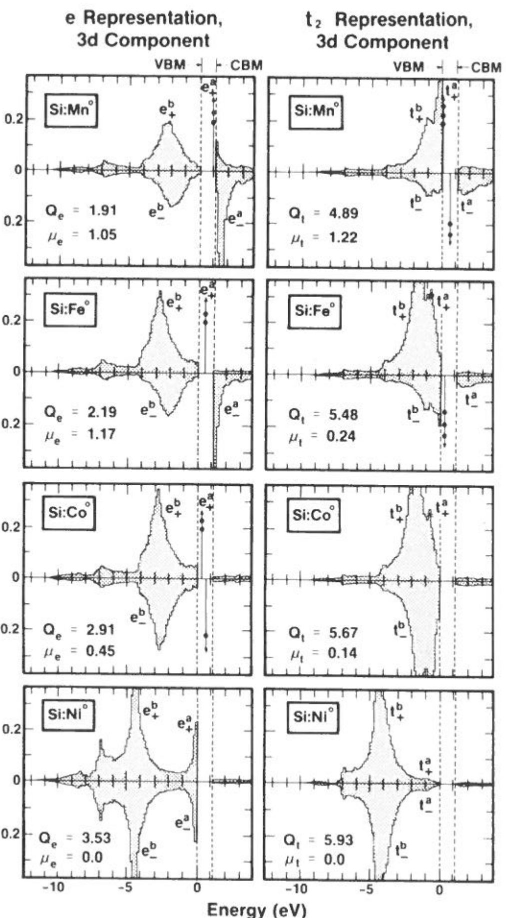

FIG. 40. (*Continued*)

is shown in Table XV. These results indicate that:

(1) The magnetism of the low-Z impurities is contributed by the gap levels, but that of the heavier neutral impurities is controlled mainly by impurity-induced valence-band resonances. In contrast, $3d$ impurities in wide-gap insulators have $\mu_{\text{loc}} \cong \mu_{\text{gap}}$. It is thus impossible to interpret ENDOR results for $3d$ impurities in semiconductors in terms of band-gap wave functions alone.[40]

(2) A comparison of the *local* magnetic moment with the *total* moment shows that only a fraction of the magnetic moment is localized on the impurity.

TABLE XV. LOCAL (loc) AND TOTAL (tot) MAGNETIC MOMENTS OF NEUTRAL INTERSTITIAL 3d IMPURITIES IN SILICON

Impurity	Spin	μ_{VB}	μ_{gap}	μ_s	μ_p	μ_d	μ_{a_1}	μ_e	μ_{t_2}	μ_{loc}	μ_{tot}
Sc^0	$\frac{3}{2}$	0.08	1.25	−0.00	0.02	1.30	−0.00	0.03	1.30	1.33	3.0
Ti^0	$\frac{2}{2}$	0.12	1.18	0.00	0.01	1.30	0.00	0.04	1.26	1.30	2.0
V^0	$\frac{1}{2}$	0.30	0.81	0.00	−0.01	1.17	0.00	0.09	1.01	1.11	1.0
Cr^0	$\frac{4}{2}$	1.14	1.51	0.00	−0.01	2.63	0.01	1.00	1.64	2.65	4.0
Mn^0	$\frac{3}{2}$	1.40	0.88	0.00	−0.01	2.25	0.01	1.05	1.22	2.28	3.0
Fe^0	$\frac{2}{2}$	1.61	−0.19	0.00	0.01	1.29	0.01	1.17	0.24	1.42	2.0
Co^0	$\frac{1}{2}$	0.28	0.32	0.00	0.00	0.49	0.00	0.45	0.14	0.60	1.0

[a] Calculated from local spin density Green's function method. H. Katayama-Yoshida and A. Zunger, unpublished (1985).

(3) Almost all of the local magnetic moment is contributed by the 3d orbital; other contributions (4s, 4p, 4d, 4f) are negligible.

(4) Both e and t_2 representations contribute to the magnetism; for the low-Z neutral impurities the t_2 contribution dominates, whereas for high-Z impurities the situation is reversed.

Figure 41[258] depicts for Si:Cr_i the variations with formal charge q of the gap and valence-band contributions to the local magnetic moment μ and impurity charge $\bar{Q}$. The remarkable result is that, whereas the gap and valence-band contributions to the *impurity charge* have opposing (hence partially cancelling) variations with the formal charge state (Part VI,20 and Fig. 37a), both the valence band and the gap contributions to μ vary in the same direction. We will see in Part VI,27 that this is a consequence of the fact that Coulomb-induced screening is far more effective than exchange-induced screening. Ionization transitions thus have only a small effect on the impurity *charge*, as a result of the self-regulating response,[196] but they can substantially change the *magnetic moment*. This highlights the qualitatively different variations with doping of the Mössbauer isomer shift[50–53] (measuring the *charge* on the impurity) and EPR or ENDOR (measuring the *spin density* on the impurity and the ligands). ENDOR experiments as a function of doping will be needed to examine such predictions.

Figure 42 shows the variation of the local magnetic moments along the interstitial Si:T^0 and Si:T^+ series. The normal trend expected from high-spin ground states (a single peak at $S = \frac{5}{2}$) is broken for V^+, Ti^0, V^0, and Co^{2+}, which exhibit minima in μ and a low-spin ground state. This is the first prediction[39] of a low-spin state for impurities in semiconductors, and is discussed next in more detail.

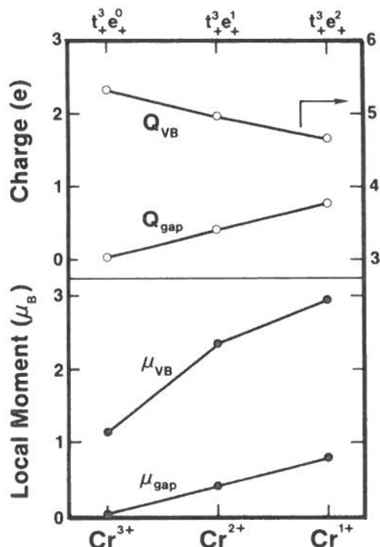

FIG. 41. Variations in the valence-band (Q_{VB}, μ_{VB}) and band-gap (Q_{gap}, μ_{gap}) contributions to the impurity charge (Q) and local magnetic moment (μ) of Si:Cr_i as a function of its formal charge state. Observe that, whereas Q_{gap} and Q_{VB} vary in *opposite* directions as the charge state is varied in the $Cr^{3+} \rightarrow Cr^{2+} \rightarrow Cr^{+}$ sequence (a "self-regulating response"), μ_{gap} and μ_{VB} vary in the *same* direction (i.e., an enhancement effect). [Calculated by H. Katayama-Yoshida and A. Zunger, *Int. Conf. Magnetism*, in press (1985) from local spin density Green's function method.]

b. *Exchange Splittings and Low-Spin Ground States*

The calculated[39] one-electron configurations of the interstitial 3d impurities in the T^0, T^+, and T^{2+} charge states in Si are depicted in Fig. 43. KYZ found that for the neutral centers T^0, contrary to the classical model,[1] the e_+^a level lies *above* the t_-^a level; i.e., one has a low-spin-like (LSL) level arrangement. For the charged centers T^+ and T^{2+}, the same is true for both the high-Z and low-Z ends of the 3d series. An LSL level arrangement at both ends of the 3d series has also been recently predicted[54,138,217] for substitutional 3d impurities in III-Vs, e.g., GaAs:V^{2+} (cf. Part IV,13) and for substitutional Cu, Ag, and Au in Si[232]. Spin-polarized Green's-function calculations[217] for GaAs: V^{2+} confirmed a low-spin ground state. Experimental testing of these unusual cases would be desirable. These results reflect the fact that $\Delta_x > \Delta_{CF}$ (see Part II,2) is not universally true. In contrast, a small-cluster calculation with spherical potentials[162,183] leads to an underestimation of directional covalency effects (hence Δ_{CF}), leaving the exchange coupling the only "strong interaction," so that $\Delta_x \gg \Delta_{CF}$. This resulted in a *universal* HSL level arrangement for all 3d impurities.[162,183] KYZ found in their LSD-SIC

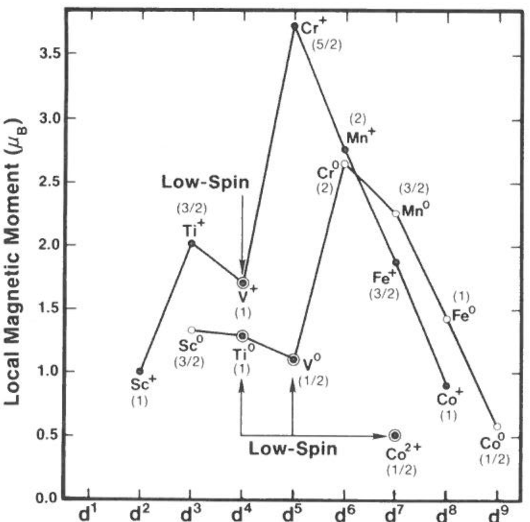

FIG. 42. Local magnetic moments of interstitial $3d$ impurities in Si for neutral and positive charge states. The impurity with the highest spin (Cr^+, with $S = \frac{5}{2}$) has also the largest local moment. The numbers in parentheses denote the total spin. The breaks at V^+, Ti^0, V^0, and Co^{2+} denote predicted low-spin ground states. [Calculated by H. Katayama-Yoshida and A. Zunger, unpublished (1985), from local spin density Green's function method.]

calculation that the ground-state spin values and multiplets (Fig. 43) conform to those suggested by LW (i.e., Hund's rule) for all impurities except Ti^0, Ti^-, V^0, V^+, and Co^{2+}, for which they predicted the low-spin multiplets ${}^3T_1$, ${}^2T_2$, ${}^2T_2$, ${}^3T_1$, and ${}^2E$, respectively, indicated in Fig. 43 by asterisks. No experimental data exist for these centers as yet; these would surely be critical experiments. Figure 44 summarizes the predictions of KYZ regarding the spin states of interstitial $3d$ impurities in Si.[39]

Defining the exchange splitting of the e and t_2 levels from Eq. (2.17) using the *bonding* levels (b), as $\Delta_x^{e,b} = \epsilon_{b,+}^e - \epsilon_{b,-}^e$ and $\Delta_x^{t_2,b} = \epsilon_{b,+}^{t_2} - \epsilon_{b,-}^{t_2}$, we see (Fig. 45) that: (1) The trends in Δ_x parallel the trends in the multiplet correction energies (Fig. 17b) and atomic exchange energies (Fig. 10b), except for the low-spin impurities. (2) Δ_x^e and $\Delta_x^{t_2}$ are similar for the neutral impurities, but, for the positively charged impurities, Δ_x^e is much larger than $\Delta_x^{t_2}$. (3) The exchange splittings are large at the center of the series (between $\frac{1}{3}E_g$ and E_g); hence, they are expected to overwhelm any tendency for spin pairing via Jahn-Teller distortions. On the other hand, the low-spin states at the two ends of the $3d$ series are characterized by low exchange energies; thus, they may exhibit JT distortions. (So far, only impurities at the center of the series have been carefully investigated experimentally, and no JT distortions were observed. They may occur at both ends of the $3d$ series, where exchange-correlation

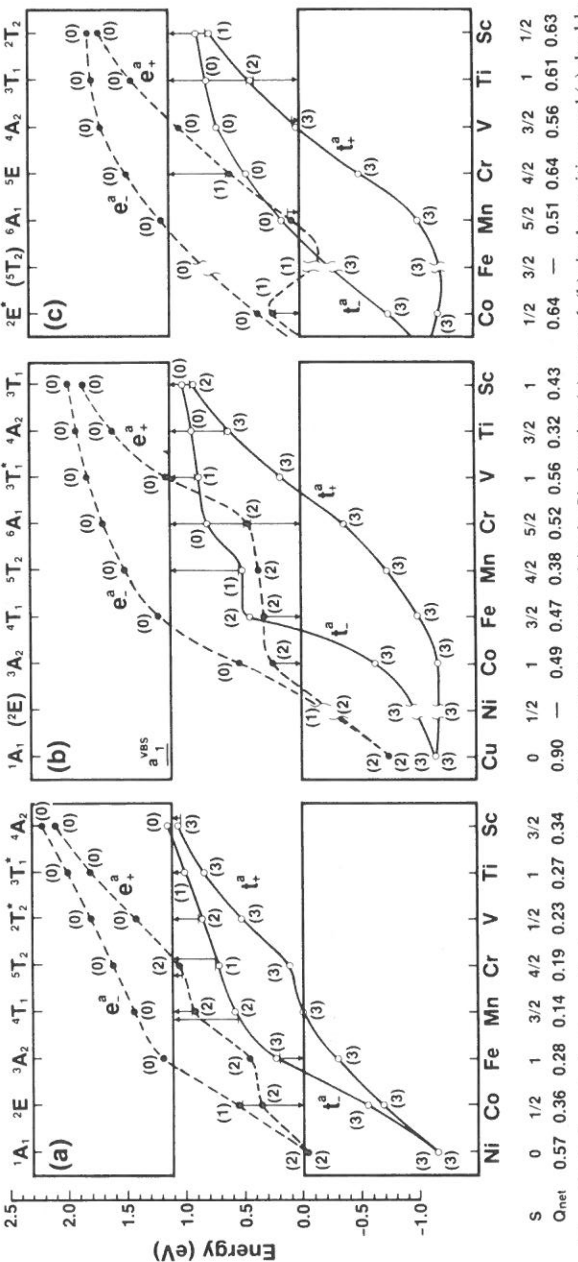

FIG. 43. Spin-polarized one-electron energy levels for interstitial $3d$ impurities in Si, showing (a) neutral, (b) singly positive, and (c) doubly positive centers. The vertical arrows indicate the levels which are ionized in the respective first, second, and third donor transitions [(a), (b), and (c), respectively]. The predicted multiplets are denoted on top; asterisks indicate predicted low-spin ground states. S and Q_{net} are, respectively, the spin and net charge in the impurity subspace. Numbers in parentheses show the occupation of the antibonding $e(e_+^a, e_-^a)$ and t_2 (t_+^a, t_-^a) levels. Observe the large shifts in the positions of the various energy levels as the occupation numbers are altered. Note also the occurrence of a low-spin-like level ordering (e_+^a above t_-^a) for many impurities. [From H. Katayama-Yoshida and A. Zunger, *Phys. Rev. B* **31**, 8317 (1985).]

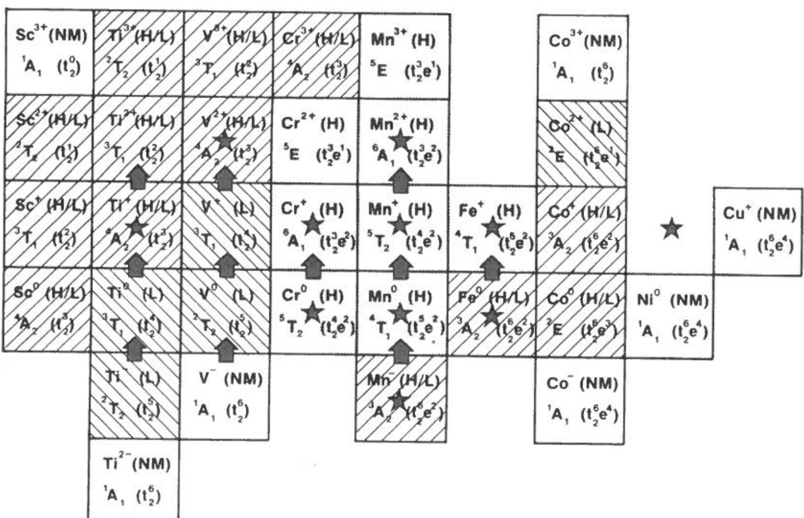

FIG. 44. Summary of observed (marked by a star) and calculated spin and charge states of interstitial 3d impurities in Si (see the results of Fig. 43). Arrows connect the two charge states for which an ionization transition has been observed in DLTS. Shaded areas denote high (H)-spin ground states, left cross-hatched areas denote low (L)-spin ground states, right cross-hatched areas denote states for which the high- and low-spin states are indistinguishable (H/L), and clear areas denote nonmagnetic (NM) ground states. Note that no EPR measurements exist for the charge states predicted to have a low-spin ground state. [From H. Katayama-Yoshida and A. Zunger, unpublished (1985).]

energies are small.) The recent[217] predicted occurrence of a low-spin ground state for GaAs:V^{2+} is illustrated in Fig. 46.

c. *Hyperfine Coupling Constants*

The hyperfine coupling constants for the various charge states of interstitial 3d impurities in silicon were calculated[39,47,184,217,258] [Eq. (5.2) and the text surrounding it]. The results are given in Table II. Table XVI shows the breakdown of the central contact hyperfine field into contributions of different s orbitals. The main conclusions follow. (1) The largest contributions are provided by the contact terms A_c, with only small corrections from A_L. (2) Covalent reductions (cf. Fig. 11) are apparent. (3) The sign of the hyperfine field is decided by the opposing effects of 1s and 2s contributions (negative) versus 3s and 4s contributions (positive). (4) The contact term, proportional to the spin density [Eq. (5.2)], also scales with the local magnetic moment: The changes in the contact term with the impurity's formal charge state (i.e., Cr in Table XV) parallel the changes of the local magnetic moment (Fig. 41). (5) The agreement between theory and experiment, when the latter is available

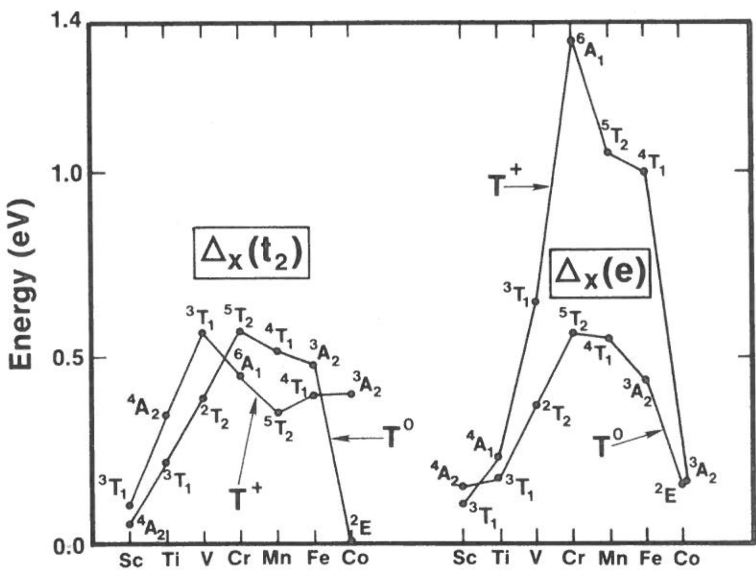

FIG. 45. Calculated exchange splittings for the t_2 bonding $\Delta_x(t_2) = \epsilon^{t_2}_{b,+} - \epsilon^{t_2}_{b,-}$ and e bonding $\Delta_x(e) = \epsilon^{e}_{b,+} - \epsilon^{e}_{b,-}$ energy levels of neutral (T^0) and positive (T^+) interstitial 3d impurities in Si. The general trend parallels that of the exchange splitting in free ions (Fig. 10b), but that the scale is reduced in the solid, and a few low-spin ground states break the simple trends observed in free ions. [From H. Katayama-Yoshida and A. Zunger, unpublished (1985), calculated from local spin density Green's function method.]

TABLE XVI. DECOMPOSITION OF THE CONTACT HYPERFINE FIELD (IN KG) OF INTERSTITIAL 3d IMPURITIES IN SI INTO ORBITAL COMPONENTS

Impurity	H_{1s}	H_{2s}	H_{3s}	H_{4s}	H_{tot}
Sc^0	−4.79	−80.13	22.79	3.42	−58.71
Ti^0	−6.52	−92.56	39.85	7.03	−52.20
V^0	−6.69	−94.01	40.67	3.37	−56.67
Cr^0	−32.35	−430.60	214.32	8.86	−239.77
Cr^+	−45.96	−611.82	304.52	12.59	−340.68
Cr^{2+}	−32.74	−435.84	216.93	8.96	−242.69
Cr^{3+}	−12.57	−179.33	88.84	3.67	−99.39
Mn^0	−27.25	−389.03	192.62	15.21	−208.45
Fe^0	−24.50	−278.52	179.17	8.18	−115.14
Co^0	−6.49	−74.07	47.70	2.19	−30.68

[a] Calculated by local spin density Green's function method. H. Katayama-Yoshida and A. Zunger, unpublished (1985).

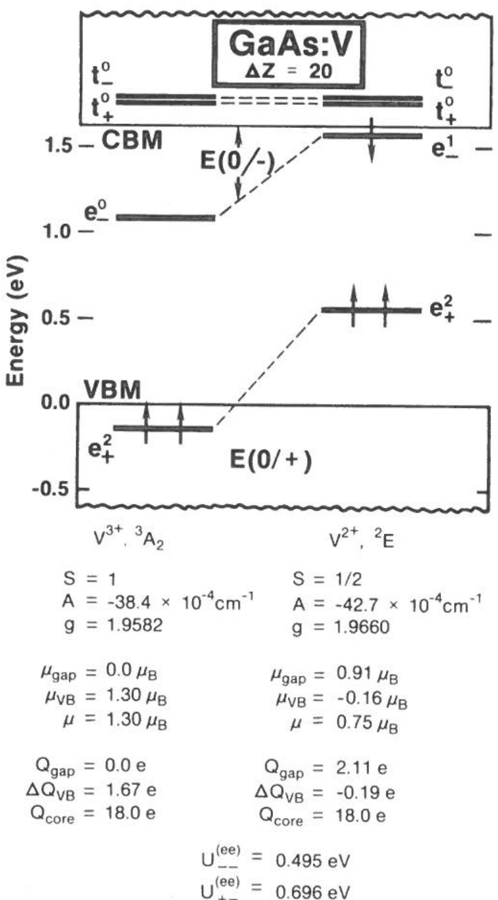

FIG. 46. Calculated[217] (spin-polarized Green's function local density approach) gap levels of GaAs:V^{3+} (left) and GaAs:V^{2+} (right), showing that the undistorted GaAs:V^{2+} has a low spin ground state. The figure summarizes the calculated spin (S), hyperfine coupling constants (A), g values (g), the contribution of bandgap-state (μ_{gap}, Q_{gap}) and valence band states (μ_{VB}, Q_{VB}) to the local magnetic moments (μ) and impurity charge (Q), as well as the e–e effective Coulomb energies for spins "up–up" [$U_{--}^{(ee)}$] and "up–down" [$U_{+-}^{(ee)}$]. The predicted acceptor level $E(0/-)$ is about 0.2 eV below the CBM; the predicted donor level $E(0/+)$ is inside the valence band.

(Table II), is good. In particular, theory predicted $A = +4.727 \times 10^{-4}$ cm^{-1} for Si:Ti^+ (a value[41b] not measured by LW), in good agreement with the recently reported value of $A = \pm 5.224 \times 10^{-4}$ cm^{-1}. Table II contains numerous predictions of values not yet observed.[39]

Figure 47 shows the calculated[47] spin density $\delta\rho(r)$ in the impurity orbital subspace for Si:Fe^0. At the impurity nucleus site, KYZ found a negative spin

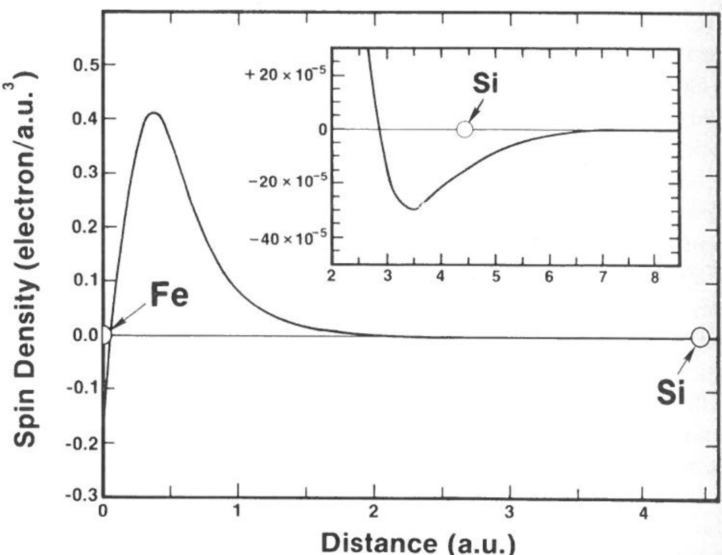

FIG. 47. Calculated spin density in the impurity subspace for neutral interstitial Si:Fe, using the LSD-SIC Green's-function approach. $\delta\rho(r) = \rho_+(r) - \rho_-(r)$. The insert shows on an enlarged scale the spin density past a distance of 2 a.u. from the impurity. The position of the Si nearest neighbor is denoted by the empty sphere. Note the negative spin density at the impurity nucleus, the positive spin density at the Fe core ($0.3 \leq r \leq 2$ a.u.), and the large depletion (negative spin density) past $r \gtrsim 3$ a.u. [H. Katayama-Yoshida and A. Zunger, *Phys. Rev. B* **32,** 7877 (1985).]

polarization that originates from the negative net core polarization. On the other hand, in the bond region at $r = 0.03$–2.9 a.u., a large positive spin polarization originates from the 3*d* polarization. Past $r \simeq 2.9$ a.u., there is a small negative $\delta\rho(r)$ caused by the extra localization of the up-spin *d* orbitals relative to the down-spin orbitals. The negative spin polarization contributed by 1*s* and 2*s* orbitals at the impurity nucleus is caused[47,258] by the covalent reduction in the Coulomb repulsion between $1s_\downarrow$ (or $2s_\downarrow$) and $3d_\uparrow$ orbitals, whereas the positive core polarization of the 3*s* and 4*s* orbitals is caused by a similar covalent reduction in the interaction of $3s_\downarrow$ (or $4s_\downarrow$) with the $3d_\uparrow$ orbital.

25. *g* VALUES

The *g* values for the various charge states of interstitial 3*d* impurities in Si were calculated[39,47,217,258] from Eq. (5.1) (and the text surrounding it) using the effective crystal-field splittings and wave functions obtained from the Green's-function calculation. The overall calculated trends (Table II) agree

with the published data; other values are offered as predictions. This calculation shows small spin-orbit contributions Δg_{LS} and a strong quenching of the angular-momentum component g_L for $L = 1$. Despite variations in the spin state (high *vs* low), the number and type of gap levels (Fig. 43), and their localization, KYZ found that covalency effects uniformly quench g_L. This is a consequence of the fact that substantial covalency is induced by the valence-band resonances that characterize all impurities. This finding suggests that there is no compelling reason to introduce for Si:3d alternative mechanisms (i.e., the dynamic Jahn–Teller effect[35]). As the covalency of the host crystal decreases in the Si → III-V → II-VI sequence, dynamical quenching of g_L is expected to increase relative to the covalent quenching mechanism. Quantitative calculations of the latter effect are needed to establish the extent of this effect in III-V's and II-VI's. Although admittedly difficult, it would also be of interest to establish an experimentally observable distinguishing feature between these two mechanisms for quenching g_L.

26. Donor, Acceptor, and Mott–Hubbard Energies

In the cases where sufficient data are available on internal $d \to d^*$ transitions (i.e., heteropolar semiconductors and insulators; *viz* Table V), it is possible to calculate the many-electron multiplet corrections both for internal and ionizing transitions (Part IV,12) and subtract these from the experimental transition energies, to obtain the mean-field components that can then be directly compared with the results of MF calculations. We will follow this approach for the prototype system GaP:3d. This approach is not possible for Si:3d, because its internal transitions have not yet been observed. For this system we use an alternative approach, where many-electron corrections are approximated by their single-configuration spin-only component, i.e., by using a spin-unrestricted approach. The results of FCZ suggest[138] that spin correlation is indeed the main contribution to the change in total correlation energy upon ionization.

The vertical transition energies of Eqs. (10.15), (10.18), and (10.20) are expressed as differences in total mean-field energies. A practical disadvantage of expressing transition energies as differences in *total* energies lies in the fact that each total energy in these equations contains a large, common term (the ground-state energy of the host crystal), but only a rather small difference (the change in $E_{\mathrm{MF}}^{(N)}$ that occurs when the occupation numbers of two levels are changed) is of interest. However, having identified the particular configuration changes $e^m t_2^n \to e^{m'} t_2^{n'}$ attendant upon the relevant transitions (Figs. 17, 19, and 20), one could construct approximate mean-field energy-level diagrams using Slater's transition-state construct.[214] Correct to second order, the difference in total energies attendant upon a change in electronic configuration $V^Q t^m \to V^{Q'} t^{m'}$ is given by the difference in the corresponding self-consistent density-functional orbital energies, computed at the intermediate occupation numbers $(Q + Q')/2$ and $(m + m')/2$

$$E_{\mathrm{MF}}[V^{Q'}t^{m'}] - E_{\mathrm{MF}}[V^{Q}t^{m}] \cong [\epsilon_V - \epsilon_t]_{V^{(Q+Q')/2},t^{(m+m')/2}}. \qquad (26.1)$$

This transition-state approach has been applied extensively[214] to transition atoms, reproducing the difference in total energies for 3d excitations to within $\gtrsim 0.1$ eV. Some of the properties of this approximation are: (1) The right-hand side of Eq. (26.1) is meaningful only for a given geometry of the impurity system; (2) it includes approximately the effect of electronic relaxation; (3) it incorporates not only the direct contributions of the levels V and t but also the indirect (screening) effects of all other levels included in the self-consistent calculation (e.g., valence-band resonances); and (4) it incorporates the lowest-order effects of the self-interaction correction.[214,215] Because of (1) above, our strategy will be as follows. We will calculate $\Delta E_{\mathrm{ver}}^{(N,N\pm1)}$ by performing separate self-consistent QBCF calculations for each transition-state configuration pertinent to the various donor and acceptor transitions. We will assume throughout the calculation the unrelaxed geometry of the ideal crystal. We will then compare our results for $\Delta E_{\mathrm{ver}}^{(N,N\pm1)}$ with the experimentally deduced mean-field energies. The discrepancies with experiments, where they exist, will reflect a combination of the amount by which the transition-state local-density model fails to be a perfect MF theory and the change in lattice distortions $\Delta E_{\mathrm{rel}}^{(N,N\pm1)}$ attendant upon the particular transition, which has been left out.

The transition-state analog of the mean-field excitation and ionization energies deduced from experiment are depicted in Fig. 8b. For example, the total energy difference attendant upon the first-acceptor transition in GaP:Fe [(−/0) in Fig. 8b], i.e., $[Fe^{2+}, d^6, A^-, e^3t_2^3, {}^5E] \leftrightarrow [Fe^{3+}, d^5, A^0, e^2t_2^3, {}^6A_1]$, is represented within the mean-field transition-state approximation [(−/0) MF in Fig. 8b] as the energy separation between the e level and the top of the valence band, using the intermediate $(\mathrm{VB})^{5.5}e^{2.5}t_2^{3.0}$ configuration for the self-consistent calculation. The second acceptor transition, $[Fe^{2+}, d^6, A^-, e^3t_2^3, {}^5E] \leftrightarrow [Fe^{+}, d^7, A^{2-}, e^4t_2^3, {}^4A_2]$ (Fig. 8b), likewise has a MF contribution represented by the energy separation between the conduction-band minimum and the e level, using the intermediate $(\mathrm{CB})^{0.5}\, e^{3.5}t_2^{3.0}$ configuration. The Mott–Hubbard Coulomb energy $U^{(ee)}(A^-)$ for the A^- center is then given by the separation of the two e-level energies in the first-acceptor and second-acceptor calculations (Fig. 8b). The intracenter excitation of the A^- center, $[Fe^{2+}, d^6, A^-, e^3t_2^3, {}^5E] \to [Fe^{2+}, d^6, A^-, e^2t_2^4, {}^5T_2]$ (Fig. 8b), is represented by the difference in t_2 and e-orbital energies, using the intermediate configuration $e^{2.5}t^{3.5}$ (Fig. 8b).

Figure 48 depicts the self-consistently calculated,[54,259] impurity-induced e and t_2 energy levels for GaP:3d in the vicinity of the fundamental band gap, using the occupation number pertinent to the transition-state $E\ (-/0)$ first acceptors. Along with the calculated levels (open circles), we give the mean-field energies deduced from experiment (solid circles) and indicate the correspondence between experiment and theory by arrows to guide the eye. An analysis of the data shows that the first-acceptor transitions for the impurities Zn, Cu, Ni, Mn, and Cr involve the ionization of the t_2^{DBH} electron, whereas the acceptor states of Co and Fe involve ionization of the e^{CFR} electron. This switch between Ni and Co, or Fe and Mn, cannot be deduced without acknowledging many-electron effects. Table XVII[54,259] compares the calculated values and the experimentally deduced values for the acceptor levels. The agreement with experiment is good, except for GaP:Cr, for which the calculated positions of the t_2 levels are about 0.4 eV *too high*. Interestingly, the GaP:Cr system for which our (lattice-unrelaxed) calculation shows a large discrepancy with experiment is also know to be distorted at least in its A^- state. It is therefore tempting to associate at least part of the discrepancy between theory and experiment for these two impurities to lattice relaxations $\Delta E_{rel}^{(N,N\pm1)}$. Such relaxations are indeed expected to *lower* the position of the (antibonding) t_2^{DBH} levels; the magnitude of $\lesssim 0.4$ eV energy lowering of such levels is consistent with data on similar systems (Part IV,10).

It is obvious from Fig. 48 that the experimentally deduced single-acceptor MF levels (solid circles) show a nonmonotonic trend with the impurity's atomic number (e.g., Mn has a shallower acceptor level than Fe). At the same time, it is clear from Fig. 48 that the mean-field t_2^{DBH} and e^{CFR} levels have a purely monotonic trend with the impurity's atomic number. The two observations are consistent for the following two reasons. *First*, the observed acceptor energies of Cr and Mn are associated with ionization of the t_2^{DBH} level, but that of Fe is associated with the e^{CFR} level (Fig. 47). This is a solid-state effect, absent from the free-ion ionization energies. *Second*, the many-electron multiplet correction (Fig. 19) for GaP:Mn is negative (making the acceptor energy *smaller* than the MF value), whereas the multiplet correction for GaP:Fe is positive (making the acceptor energy *larger* than the MF value).

[259] The QBCF calculation of Singh and Zunger[54] showed a mean-field acceptor energy of $E_v + 0.26$ eV for GaP:Ni and a double acceptor energy of $E_v + 1.53$ eV for GaP:Fe. At the time, these compared poorly with the mean-field results deduced from experiment[54]: $E_v - 0.24$ and $E_v + 1.70$ eV, respectively. Since then, the experimental results have been revised by Z. Liro (personal communication): the lowest $d \rightarrow d^*$ transition in GaP:Ni is at 0.82 eV (Table V), not 0.58 eV, and the observed second acceptor in GaP:Fe is at $E_v + 2.09$ (Table VII), not $E_v + 2.25$ eV. These revised experimental results lead to a much better agreement with theory: the experimentally deduced mean field first acceptor of GaP:Ni is $E_v + 0.25$ eV and the second acceptor in GaP:Fe is at $E_v + 1.54$ eV. Correspondingly, $U_{MF}(Fe^{2+}) = 1.44$ eV (not 1.60 eV), in better agreement with the calculated result[54] of 1.40 eV (Table XVII).

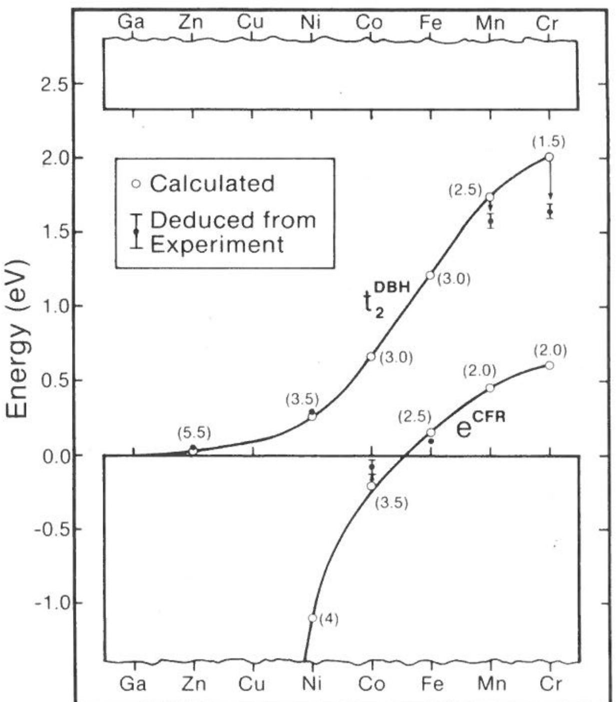

FIG. 48. Calculated acceptor $[H_{MF}(-/0)]$ levels (○) in GaP, compared with the mean-field values for acceptors deduced from experiment (●). Arrows connect the corresponding levels, to guide the eye. Numbers in parentheses indicate the (transition-state) occupation numbers pertinent to a first-acceptor transitions. The result for GaP:Cu is an interpolation. Observe that the acceptor transitions for Zn, Ni, Mn, and Cr commence from the t_2^{DBH} level, but those for Co and Fe commence from the more localized e^{CFR} level. [From spin-restricted QBCF calculation of V. Singh and A. Zunger, *Phys. Rev. B* **31**, 3729 (1985); see also Ref. 256.]

This effect exists also in the corresponding free ions, but its magnitude is attenuated in the solid five times.

Fazzio *et al.*[232] have recently compared the calculated trends in ionization energies of 3d, 4d, and 5d impurities (Cu, Ag, and Au in Si), finding the gap levels to steadily rise along this series. A similar trend in the $3d \rightarrow 4d \rightarrow 5d$ acceptor energies is expected in other materials.[196] This suggests that the 4d and 5d ionization energies [of those impurities whose 3d analogs have acceptor levels already close to the CBM (see Table V)] may be inside the conduction band, making such materials p-type.

The mean-field Coulomb repulsion energies[54] $U_{MF}^{(tt)}(A^-)$ are compared in Table XVII with values deduced from experiment.[259] They are within 0.2–0.5 eV of experimental values and are consistently too small. This suggests

TABLE XVII. CALCULATED[54] (calc) AND EXPERIMENTALLY DEDUCED MEAN-FIELD (MF) RESULTS FOR IONIZATION TRANSITIONS IN GaP:3d[a]

Impurities	Ionized level	First acceptor $E_{MF}(-/0)$	First acceptor $E_{calc}(-/0)$	Second acceptor $E_{MF}(-/2-)$	Second acceptor $E_{calc}(-/2-)$	Coulomb energies $U_{MF}(A^-)$	Coulomb energies $U_{calc}(A^-)$
Cr	t_2	$E_v + 1.65$	$E_v + 2.02$	$E_v + 2.69$	$E_v + 2.58$	1.04	0.56
Mn	t_2	$E_v + 1.59$	$E_v + 1.74$	—	—	—	—
Fe	e	$E_v + 0.10$	$E_v + 0.13$	$E_v + 1.54$	$E_v + 1.53$	1.44	1.4
Co	e	$E_v - 0.08$	$E_v - 0.20$	—	—	—	—
Ni	t_2	$E_v + 0.25$	$E_v + 0.26$	$E_v + 1.40$	$E_v + 1.26$	1.15	1.0
Cu	t_2	—	$E_v + 0.10$	—	—	—	—
Zn	t_2	$E_v + 0.07$	$E_v + 0.02$	—	—	—	—

[a] First acceptor $E_{MF}(-/0)$, second acceptor $E_{MF}(-/2-)$, and Coulomb repulsion energies $U_{MF}(A^-)$, given in eV. Results for GaP:Ni are modified relative to Ref. 54, using more recent experimental data of Z. Liro, unpublished (1985) (see Ref. 259).

that the A^- state (e.g., Cr^{2+}) is stabilized by lattice distortion more than the A^{2-} state is (e.g., Cr^+). The largest discrepancy in U occurs for GaP:Cr (0.48 eV). Indeed, its A^- state is a symmetric $^6A_1$ state and hence not subject to JT distortion. In general, one expects that polarization and electrostatic ion–ion interactions would result in a greater induced energy lowering for the higher oxidation state[147] (i.e., Cr^{2+} versus Cr^+).

A few observations can be made. *First*, the calculated[54] Coulomb repulsion energies in GaP:3*d* are about 2–4 times larger than those calculated[19] for substitutional Si:3*d*, consistent with the lesser covalency of GaP. *Second*, the Coulomb energies for the e^{CFR} orbitals (1.4 eV in GaP:Fe) are larger than those for the t_2^{DBH} orbitals (1.0 and 0.85 eV for Ni and Cr, respectively), consistent with the higher localization of the former. Finally, we notice that the Coulomb energies calculated here for GaP:3*d* are about 20 times smaller than those calculated for the free 3*d* ions (Table IX). Since the reduction factor for Si:3*d* is even larger than that in GaP:3*d*, it is tempting to speculate that the reduction factor for the Fe "impurity" in the highly covalent hemelike biological systems (hemoglobin, cytochrome *c*) would equal or even exceed that of the Si:3*d* system, explaining the ease of the Fe^{2+} and/or Fe^{3+} oxidation and/or reduction cycles in electron-transporting biological systems.

No systematic study of the internal $d \to d^*$ excitation energies has been attempted. However, for GaP:Fe, Singh and Zunger[54] find $\Delta_{eff}[e^3t_2^3; e^2t_2^4] = 0.87$ eV, significantly larger than the value 0.45 ± 0.03 eV deduced from experiment (Table XII). While cluster calculations which use spherical muffin-tin potentials[185,186] obtain generally smaller values of Δ_{eff}, and hence better agreement with experiment, this success cannot be reproduced if more general,

anisotropic potentials are used. The QBCF method can reproduce[20,54] the smaller Δ_{eff} if the appropriate nonspherical components of the potential are artificially zeroed, mimicking thereby MSX_α cluster calculations. The reason for the overestimation of Δ_{eff} in GaP:3*d* is currently not understood, but it might be related to intrinsic deficiencies in the way the local-density approximation describes localized *d* orbitals. Indeed, effective crystal-field energies are notoriously difficult to calculate from first principles.[70,171,172,178] Singh and Zunger[54] have further predicted the dependence $\Delta_{eff}(A^-) < \Delta_{eff}(A^0) < \Delta_{eff}(A^+)$ of the effective crystal-field splitting on the formal charge state (a slope of 0.1–0.2 eV was deduced) but were unaware of any experimental data to check their prediction. Calculation of λ_e [Eq. (11.3)] from the wave function obtained in Green's function calculations by Singh and Zunger[54] for GaP:Mn yielded a value of 0.86 ± 0.01, in excellent agreement with the experimentally deduced value of 0.86 ± 0.08 (Table XII).

The results obtained[47] for donors and acceptors for *interstitial* 3*d* impurities in Si by application of Slater's transition-state construct to the spin-unrestricted calculation are compared in Fig. 49, with the experimental data

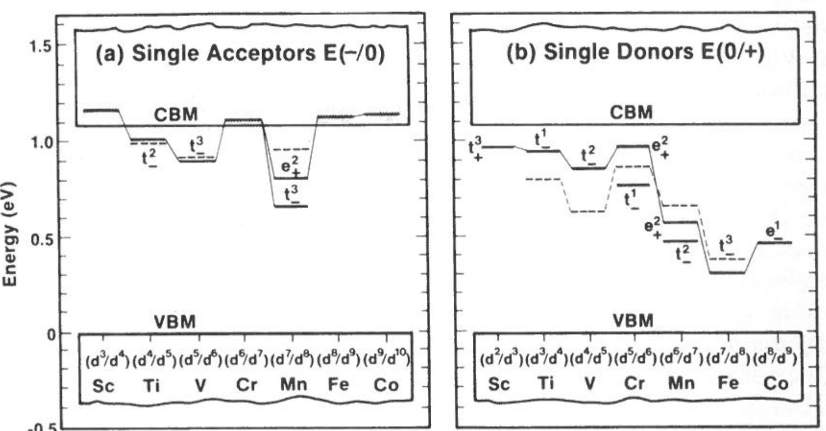

FIG. 49. Calculated (heavy solid lines) and observed (dashed lines, see Table VII) (a) single acceptors, and (b) single donors of interstitial 3*d* impurities in Si. The calculation assumes a spin-unrestricted model, neglecting orbital-correlation and lattice-relaxation effects. Experimental data include relaxation effects (i.e., thermal data are used), hence the observed energies are *higher* than the calculated ones. Shaded areas denote levels predicted to be resonances with the conduction band. In each case we indicate the one-electron level (t_-, e_+, e_-) being ionized in the respective transition. In a number of cases we show two possible ionization levels (e.g., Si:Mn, where either t_-^3 or e_+^2 can be ionized). Observe that, unlike the situation in free ions (Fig. 9a), no minimum occurs at the (d^4/d^5) acceptor transition for Si:Ti due to the occurrence of a low-spin ground state. [From H. Katayama-Yoshida and A. Zunger, *Mater. Res. Symp., San Francisco*, p. 117 (1985).]

(Table VII). Similar results have recently been reported by Beeler *et al.*[260] from their spin-polarized atomic-sphere-approximation (ASA) model. The vertical arrows in Fig. 43 denote the one-electron levels that can be ionized in the lowest-energy single, double, and triple donor transitions, respectively. Note that, in principle, impurities with two gap levels (e.g., Fe^0 with a t_+ level below e_+) could exhibit a photoluminescence transition (from the higher level to the CB) different from a DLTS transition (from the lower level to the VB). This idea awaits experimental testing.

The calculations[39,47,217] show that, whereas the first donor transition in Ti, V, and Fe commences from the t_-^a level, the same transitions in Sc, Cr, Mn, and Co commence from the t_+^a, e_+^a, e_+^a, and e_-^a levels, respectively. The calculated transition energies (Fig. 48) display the chemical trends apparent in the experimental data, in contrast with models that embody a universal HSL level ordering for all impurities.[183] For instance, KYZ found the occurrence of local minima (maxima) in the first donor energy of V d^4/d^5 (Cr d^5/d^6) to be a consequence of switching the initial state from t_-^a (in V) to e_+^a (in Cr), and the relative ease of ionizing the sixth electron in Cr^0, producing the exchange-stabilized half-filled shell of $Cr^+(d^5)$. On the other hand, the argument[1,4] that assumes a universal HSL ordering (cf. Hund's point in Fig. 9) will predict the first acceptor of Ti(d^4/d^5) to likewise be lower in the gap than the first acceptor of V(d^5/d^6), in contrast to the reversed trend observed. This reversal is naturally accounted for in the model of KYZ (Figs. 43 and 48) in terms of the *low-spin ground states* of Ti^0 and V^0. Note that, since the calculated values[39,47] correspond to an unrelaxed lattice (i.e., Franck–Condon optical transitions), they are higher in energy than the experimental values depicted in Fig. 49, which were obtained under equilibrium relaxed conditions (thermal excitations). Figure 49 contains a number of predictions for hitherto-unobserved transitions.

Our foregoing discussion of the calculated electronic structure of 3*d* impurities in semiconductors offers a resolution to the apparent dichotomy (described in Part III,9) between the covalently delocalized and the atomically localized models of such systems. First, different types of orbitals are responsible for "localized-like" and "delocalized-like" phenomena; e.g., the contact spin density and hyperfine field are decided by the hyperlocalized core orbitals (interacting with the 3*d* orbitals), the magnetism is largely contributed by the localized valence-band resonances, and so is the reduction in the Mott–Hubbard U, quenching of g_L and the spin-orbit splitting, and the relative constancy of the Mössbauer isomer shift, whereas the occurrence of many

[260] F. Beeler, M. Scheffler, and O. M. Anderson, *Mater. Res. Soc. Meet. on Microscopic Identification of Electronic Defects in Semiconductors*, pp. 117 (1985); *Bull. Am. Phys. Soc.* **30**, 303 (1984).

charge states in the band gap reflects the self-regulating response mechanism. Second, the inability of the e^{CFR} states to hybridize leads to the retention of many localized, atomiclike characteristics in the solid, including the multiplet structure and Hund's rule. Finally, the way that the delocalized and localized orbitals participate in certain physical observables defines a *competition* between opposing effects, e.g., localized-like high-spin states at the center of the 3*d* series *vs* delocalized-like low-spin states at its ends, and the change from Jahn–Teller quenching of g_L for more ionic semiconductors to a covalency quenching mechanism for Si. I conclude that there is no *dichotomy* in the problem, but *duality* is its underlying feature.

27. The Exchange-Correlation-Induced Negative "Effective U"

a. The Idea

The decomposition [Eq. (10.22)] of the effective $U^{(\alpha\alpha)}(A^q)$ into: (1) a vertical electronic "Hubbard U," $U_{ver}^{(\alpha\alpha)}$, (2) a relaxation correction $\Delta U_{rel}^{(\alpha\alpha)}$, and (3) a many-electron correction $\Delta U_{MC}^{(\alpha\alpha)}$ evokes the thought that perhaps a cancellation between different terms can occur. Lieb[261] has pointed out on formal grounds that the total energy $E(N)$ can have segments that are downward convex; i.e., $E(N+1)+E(N-1)>2E(N)$, or $U<0$. Anderson[144] had envisioned a situation in which a negative ΔU_{rel} overwhelms the positive $U_{ver}^{(\alpha\alpha)}$, leading to a negative "effective U." Considering a bond with harmonic force constant k_{yy} and an associated orbital that would accommodate $N-1=0$, or $N=1$, or $N+1=2$ electrons, he showed that if all of these electrons couple equally to the lattice [i.e., $n(N)=N$ in Eq. (10.23)], then N_{eff} of Eq. (10.28) is positive, leading to the possibility that the negative relaxation correction $\Delta U_{rel}=-V_y^2/2k_{yy}$ of Eq. (10.28) will overwhelm the positive Coulomb repulsion $U_{ver}^{(\alpha\alpha)}$ of the static bond, if V_y is sufficiently large. This mechanism has since been confirmed to occur in amorphous As_2S_3,[262] the silicon vacancy,[263] and in interstitial boron in Si.[264] The physical mechanics that lead to an occupation-dependent displacement force (ODDF) $f(N)$ of Eq. (10.23) can be diverse: a relaxation-induced bond formation in a charged $A^{q-1}-A^{q+1}$ defect pair[144,265] (e.g., As_2S_3), a Jahn–Teller force[137a] [the Si vacancy where

[261] E. H. Lieb, *Int. J. Quantum Chem.* **24**, 243 (1983).

[262] M. Kastner, D. Adler, and H. F. Fritzsche, *Phys. Rev. Lett.* **37**, 1504 (1976).

[263] G. D. Watkins and J. R. Troxell, *Phys. Rev. Lett.* **44**, 593 (1980); G. A. Baraff, E. O. Kane, and M. Schlüter, *Phys. Rev. Lett.* **43**, 956 (1979); J. R. Troxell and G. D. Watkins, *Phys. Rev. B* **22**, 921 (1980).

[264] R. D. Harris, J. L. Newton, and G. D. Watkins, *Phys. Rev. Lett.* **48**, 1271 (1982); H. J. Hoffmann, *Phys. Rev. Lett.* **51**, 1722 (1983).

[265] M. Kastner, *Phys. Rev. Lett.* **28**, 355 (1972); S. R. Ovshinsky, *Phys. Rev. Lett.* **36**, 1469 (1976).

$\hat{E}_{JT}$ of Eq. (10.28) is large and negative and $N_{eff} = 2$], or lattice polarization energy (e.g., polyvalent impurities in polar[266a,b] or ionic crystals,[147] where the charge in ion–ion interaction depends on occupation numbers[147]). Common to all such mechanisms is the requirement of atomic relaxations. This may pose severe restrictions on the occurrence of this type of negative-U center for the following reasons. *First*, lattice relaxations occurring with typical (phonon) frequencies of $\sim 10^{12}$ Hz are pertinent only to equilibrium (slow) experiments, unlike photoexcitations (occurring at typical frequencies of 10^{15} Hz), where only the initial state is relaxed.[143b] *Second*, Anderson's mechanism requires $N_{eff} > 0$ [Eq. (10.28)], but competition between energy lowering by JT coupling and spin polarization can lead to $N_{eff} < 0$. Such is the case for substitutional $3d$ impurities in tetrahedral sites with configurations $e^2t_2^1(^4T_1)$, $e^2t_2^2(^5T_2)$, and $e^2t_2^3(^6A_1)$ (e.g., GaAs:Cr in Fig. 4), where the spherical symmetry of the $^6A_1$ state leads to the suppression of JT coupling; hence, $n_{N+1} = 0$ and $N_{eff} = -7$. This is also the case for interstitial d impurities with $t_2^3e^0(^4A_2)$, $t_2^3e^1(^5E)$, and $t_2^3e^2(^6A_1)$ configurations (e.g., Si:Cr in Fig. 4), where $^4A_2$ and $^6A_1$ have no JT couplings, hence $n_{N-1} = n_{N+1} = 0$, but $t_2^3e^1$ could distort tetragonally. This gives $N_{eff} = -2$. In these cases, if a JT coupling exists, it acts to *increase* U_{ver} by $\Delta U_{JT} > 0$. Finally, this mechanism requires that activation barriers for atomic relaxation be surmountable, or else the instability may be too slow to observe (e.g., the suggestion of a "frustrated" negative U in amorphous Si[94]). These factors contribute to the relative paucity of this type of negative-U center.

A novel mechanism that may lead to a negative effective U has been suggested recently,[19,267,268] in which many-electron effects ΔU_{MC} act to render U negative. This idea was based on two results obtained earlier. *First*, calculations[19,39,47,54,140,196] indicated that localized impurities that interact with an itinerant network of covalent bonds show a very efficient self-regulating response to charging (Part VI,20), leading to a dramatic reduction of U_{ver} even in a static lattice. *Second*, calculation of many-electron corrections[138] indicated that these effects (ΔU_{MC} in Table VIII) contribute a negative term to U. This effect is already apparent in free ions (Table IX) where $U(d^3\text{-}d^4\text{-}d^5)$ is smaller than $U(d^4\text{-}d^5\text{-}d^6)$ by ~ 8 eV due to the exchange stabilization of d^5. However, in free ions this effect does not overcome the large (~ 20 eV) Coulomb energy U_{ver}. In such *isolated* systems (e.g., atoms) $U_{ver} \gg |\Delta U_{MC}|$, as can be verified from the values of the corresponding atomic integrals[269] (F^0 and F^4 in Slater's notation). Furthermore, this continues to be

[266] (a) K. Weiser, *Phys. Rev. B* **25**, 1408 (1982); (b) I. A. Drabkin and B. Ya. Moizhes, *Fiz. Tekh. Poluprovodn.* **17**, 969 (1983) [*Sov. Phys. Semicond.* **17**, 611 (1983)]; (c) G. M. Brown, S. F. Chan, C. Creutz, H. A. Schwarz, and N. Sutin, *J. Am. Chem. Soc.* **101**, 7638 (1979).

[267] M. Caldas, A. Fazzio, and A. Zunger, J. Electron. *Mater.* **14a**, 1035 (1985).

[268] H. Katayama-Yoshida and A. Zunger *Phys. Rev. Lett.* **55**, 1618 (1985).

[269] J. B. Mann, Los Alamos Scientific Report LA-3690, 1967, unpublished.

the case if the orbitals $\phi(r)$ used in such integrals are scaled (simulating, e.g., delocalization). Transition-atom impurities in insulators behave in this respect much like free atoms. The key point, however, is that when the atom is placed into a polarizable host system, its Coulomb and exchange-correlation interactions respond in a fundamentally different way to screening: The former, responding to long-wavelength (monopole) screening, is reduced far more than the latter (multipole screening).[270] This has been demonstrated experimentally in a recent, elegant set of measurements[271] for Mn impurities in noble metals, showing that, relative to the free atom, the Coulomb repulsion is reduced 20 times more than the exchange interactions.

This physical principle[267] has been analyzed by Katayama-Yoshida and Zunger[268] by computing the change in spin density $\Delta S(r) = S_{Cr^{2+}}(r) - S_{Cr^{3+}}(r)$ and in the electronic charge density $\Delta\rho(r) = \rho_{Cr^{2+}}(r) - \rho_{Cr^{3+}}(r)$ upon ionizing an interstitial Cr^{2+} impurity in Si to form Cr^{3+} (Fig. 50). Since the ionization takes place from the band-gap orbital $e\uparrow$ (having one and zero electrons, respectively, in Cr^{2+} and Cr^{3+}), the changes in spin and charge densities can be written, respectively, as $\Delta S(r) \equiv |\psi_e|^2 + \Delta S_h(r)$ and $\Delta\rho(r) \equiv |\psi_e|^2 + \Delta\rho_h(r)$, where $|\psi_e|^2$ is the orbital density of the gap level in Cr^{2+}, and $\Delta S_h(r)$ and $\Delta\rho_h(r)$ are (by definition) the changes in the spin and charge densities of all states below the valence-band maximum. Integrated over all space, the total change (over the macroscopic crystal) is $\int_0^\infty \Delta\rho(\mathbf{r})\,d\mathbf{r} = \int_0^\infty \Delta S(\mathbf{r})\,d\mathbf{r} = 1$. If the valence-band states were unresponsive to occupation of the gap level (i.e., as in a rigid-band, non-self-consistent model), then $\Delta S_h(r) = \Delta\rho_h(r) \equiv 0$. Similarly, in a spin-restricted calculation the charge density follows the spin density; hence, in this limit $\Delta S(r) \equiv \Delta\rho(r)$. Instead, Fig. 50 shows a strong screening of the *charge-density* change and a far weaker screening of the *spin-density* change: $\Delta\rho_h(r)$ equals approximately $-|\psi_e|^2$ in most of the bond region and thus cancels most of it. Consequently, $\Delta\rho(r)$ encloses only a small net charge in the impurity subspace, (of the order of $\lesssim 1/\epsilon_0$); the remaining charge is delocalized through the crystal. In contrast, most of $\Delta S(r)$ is confined to the bond region, like in a free ion, enclosing almost a full spin in this region. This is also evident from Fig. 41, which shows that the self-regulating response of the valence-band resonances ΔQ_{VB} acts to reduce the impurity *charge* (opposite trends in Q_{gap} and Q_{VB}), but not the *magnetic moment*.

This idea of an exchange-correlation-induced negative effective U may have far-reaching consequences. *First*, since the mechanism is electronic in nature, it could occur even under rigid-lattice conditions, i.e., in Franck–Condon optical excitations. *Second*, if $\Delta U_{rel} > 0$ but $U_{ver} + \Delta U_{MC} < 0$, one could

[270] C. Herring, *in* "Magnetism IV" (G. T. Rado and H. Suhl, eds.). Academic Press, New York, 1966.

[271] D. Van der Marel, G. A. Sawatzky, and F. U. Hillebrecht, *Phys. Rev. Lett.* **53**, 206 (1984); D. K. G. de Boer, C. Haas, and G. A. Sawatzky, *J. Phys. F* **14**, 2769 (1984).

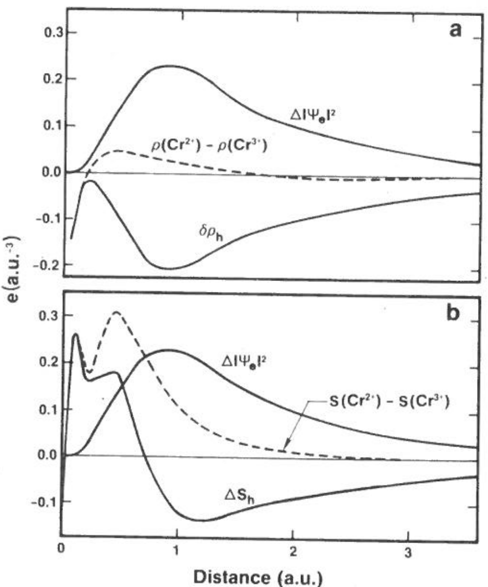

FIG. 50. (a) Change in charge density $\Delta\rho = \rho(Cr^{2+}) - \rho(Cr^{3+})$ (---) upon ionizing interstitial Cr^{2+} in Si. $\Delta|\psi_e|^2$ denotes the contribution to $\Delta\rho$ due to the change in the e gap level upon ionization, whereas $\delta\rho_h$ denotes the contribution due to the change in VB charge density. Note that $\Delta|\psi_e|^2$ and $\delta\rho_h$ nearly cancel each other in the bond region. This opposing trend in the two components of $\Delta\rho$ leads to a net small $\Delta\rho$, indicating a reduction in Coulomb repulsion effects. (b) Same as (a), but for spin densities. Note that, unlike $\Delta\rho$ in (a), the change in spin density upon ionization is localized, since the change $\Delta|\psi_e|^2$ in the gap orbital does not cancel the change ΔS_h in the valence-band spin density. This indicates ineffective exchange screening. [From H. Katayama-Yoshida and A. Zunger, *Phys. Rev. Lett.* **55**, 1618 (1985).]

encounter the interesting situation when in *thermal equilibrium experiments*, $U_{ver} + \Delta U_{rel} + \Delta U_{MC}$ is positive, but in *optical experiments*, $U_{ver} + \Delta U_{MC}$ is negative. *Third*, this mechanism holds the potential of explaining the phenomenon of "missing oxidation states,"[7] e.g., In^+ and In^{3+} exist, but In^{2+} is unstable, etc.[125]

b. Calculations

Katayama-Yoshida and Zunger[268] have examined this idea quantitatively for the three charge states of an unrelaxed interstitial Cr impurity in silicon: $Cr^{3+}(d^3)$, $Cr^{2+}(d^4)$, and $Cr^{+}(d^5)$, performing three separate self-consistent all-electron local-spin-density Green's-function calculations. They found for Si:Cr^{3+} (Fig. 51) that it has in its ground-state-unoccupied $e\uparrow$ and $t\downarrow$ levels in the gap and a triply occupied impurity-induced $t\uparrow$ orbital in resonance with the valence band. As the Fermi energy is raised, the e gap levels in Si:Cr^{2+} and

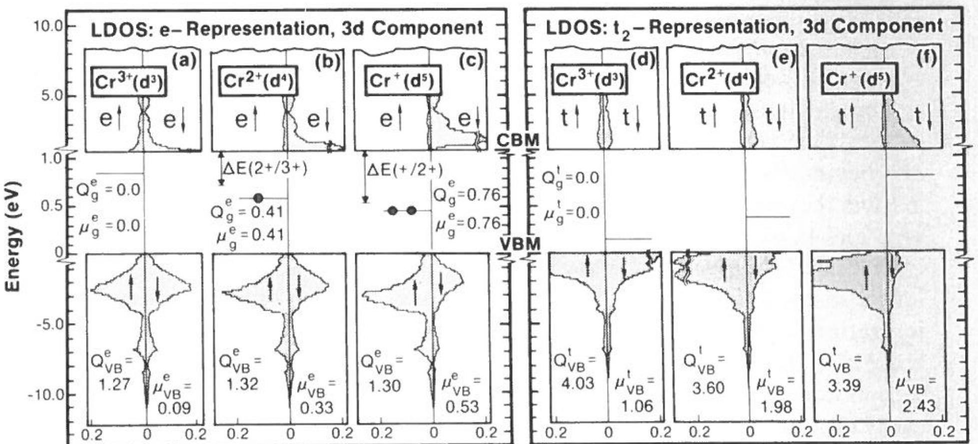

FIG. 51. Local density of states of unrelaxed interstitial Cr^{3+} [(a) and (d)], Cr^{2+} [(b) and (e)], and Cr^+ [(c) and (f)] in silicon, showing an exchange-correlation negative U; i.e., the third donor energy $E(2+/3+)$ is higher in the gap than the second donor energy $E(1+/2+)$. The shaded areas denote valence- and conduction-band resonances; $e\uparrow$, $t\uparrow$ denote up-spin states, whereas $e\downarrow$, $t\downarrow$ denote down-spin states. Thin horizontal lines show the position of the band-gap energy levels; solid dots indicate their occupation numbers. Q_g^α and μ_g^α show the contribution of representation $\alpha = e, t_2$ to the local charge (Q) and magnetic moment (μ) originating from the gap (g) levels; μ_{VB}^α and μ_{VB}^α show the respective contributions from the valence-band states (VB). Note that the exchange-correlation negative "effective U" is manifested by the fact that despite the increased occupancy of the e gap level of Cr^+ relative to Cr^{2+}, the energy position of this level is *lowered* in the gap. [From H. Katayama-Yoshida and A. Zunger, *Phys. Rev. Lett.* **55**, 1618 (1985).]

Si:Cr^+ is occupied by one and two electrons, respectively. The dominance of exchange over Coulomb interactions is evident in Fig. 51 from the fact that the orbital energy of the electron-rich orbital ($e\uparrow$ in Cr^+) is *lower* than that of the electron-poor orbital ($e\uparrow$ in Cr^{2+}). This leads to a negative $U^{(ee)}$ for the impurity e orbital. They calculated the Franck–Condon donor transition, respectively, $\Delta E^{c,e}(0/+) = E_c - 0.11 + \Delta E_{rel}(5,6)$ (the experimental value[272] is $E_c - 0.2$ eV, suggesting a small equilibrium relaxation $\Delta E_{rel}^{(5,6)} \cong -0.1$ eV), $\Delta E^{c,e}(+2/+) = E_c - 0.55 + \Delta E_{rel}^{(5,4)}$ and $\Delta E^{c,e}(2+/3+) = E_c - 0.36 + \Delta E_{rel}^{(4,3)}$. Consequently, they predicted for the Franck–Condon transitions ($\Delta E_{rel} = 0$) that Cr^+, Cr^{2+}, Cr^{3+} is an exchange-correlation negative-effective-U sequence with $U_{ver}^{(ee)} + \Delta U_{MC} = 0.36 - 0.55 = -0.19$ eV: The (vertical) double-donor transition is lower in the gap than the (vertical) triple-donor transition. They find $U_{ver}^{(ee)}(Cr^{2+}) = 0.12$ eV, and $\Delta U_{MC}(Cr^{2+}) = -0.31$ eV, whereas the sequence $Cr^{2+}(d^4)$, $Cr^+(d^5)$, and $Cr^0(d^6)$ is predicted to have a

[272] H. Feichtinger and R. Czaputa, *Appl. Phys. Lett.* **39**, 706 (1081); H. Conzelmann, K. Graff, and E. R. Weber, *Appl. Phys. A* **30**, 169 (1983); H. Feichtinger, personal communication.

normal positive-U behavior, with $U_{ver}(Cr^+) = 0.14$ eV and a larger $\Delta U_{MC}(Cr^+) = 0.3$ eV (since the d^6 configuration has two paired spins and hence a far weaker exchange energy).

The result $U_{ver} + \Delta U_{MC} < 0$ pertains obviously to the static lattice conditions. One can only speculate on the situation in equilibrium experiments. A few comments are in order, however. *First*, if JT distortions would have existed, they would *raise* U by ΔU_{rel}, since $N_{eff} = -2$ for $[Cr^{3+}, {}^4A_2]$, $[Cr^{2+}, {}^5E]$, and $[Cr^+, {}^6A_1]$. *Second*, the discussion of Part III,7 indicates that for interstitial $3d$ impurities JT energies are vanishingly small, but symmetric lattice distortions (Part VI,23) are not. Such distortions tend to lower the ionization levels in the gap by an amount proportional to the impurity charge[147] and hence may result in the disappearance of the highly charged second donor level into the valence band, in which case $U(Cr^{2+})$ cannot be easily measured. *Third*, despite the fact that the first donor of Cr is the highest in the gap of all $3d$ impurities in silicon (Table VII), no double donor (i.e., $Cr^+ \rightarrow Cr^{2+}$) or triple donor was found at equilibrium in the gap for any position of E_F[272] (although double donors have been observed for the neighboring elements V and Mn). While this is consistent with the proposed instability of Cr^{2+}, the failure to observe a triple donor under equilibrium conditions might suggest that it is inside the VB.

c. *Candidate Systems*

An exchange-correlation negative effective U of the d^3-d^4-d^5 type discussed here (equivalent also to the p^1-p^2-p^3 or the s^0-s^1-s^2 sequences) requires (1) all species to be in a high-spin configuration, (2) the individual transition energies $\Delta E(q/q-1)$ and $\Delta E(q+1/q)$ to be in the gap, (3) ΔU_{MC} to be sufficiently negative, and (4) JT energies to be sufficiently small, if $N_{eff} < 0$ (or sufficiently large if $N_{eff} > 0$). At least two other classes of impurities are isovalent with the d^3, d^4, d^5 sequence. *First*, we have other insterstitial $3d$ impurities in Si as well as the substitutional $3d$ impurities in an octahedrally coordinated system (e.g., MgO, CaO). Both appear as $t_2^3e^0({}^4A_2)$, $t_2^3e^1({}^5E)$, and $t_2^3e^2({}^6A_1)$ (i.e., $N_{eff} = -2$) and have small JT energies for the ${}^5E$ state. Their d^4 members are Fe^{4+}, Mn^{3+}, Cr^{2+}, and V^+. An extensive search for all interstitial $3d$ impurities in Si revealed[47] that V^0 and V^+ do not meet condition (1) [they are low-spin $t_2^5({}^2T_2)$ and $t_2^4({}^3T_1)$, respectively], and Mn^{3+}/Mn^{4+} and Fe^{4+}/Fe^{5+} do not meet condition (2) (the transitions are inside the host bands, much like the case for similar transitions[143,147] in MgO and CaO). Mn meets condition (3) best (most negative ΔU_{MC}). The *second* class is the *substitutional d* impurities in tetrahedral solids (e.g., GaAs, GaP, InP). They appear as the $e^2t_2^1({}^4T_1)$, $e^2t_2^2({}^5T_2)$, and $e^2t_2^3({}^6A_1)$ sequence, with $N_{eff} = -7$. Here, JT coupling

constants are higher than in the first class (leading to the stability of Cr^{2+} in GaAs); hence, $U_{ver} + \Delta U_{MC}$ have to overcome a bigger energy [cf. Eqs. (10.24), (10.28)] $+7(V_{JT}^2/2k)$ (unless the d^4 state converts to low-spin ${}^1A_1$ or ${}^1T_1$, yielding $N_{eff} = +1$). Fe^{4+}/Fe^{3+} does not meet condition (2) in II-V's and Mn^{3+}/Mn^{4+} is believed to be inside the VB of II-VI's. V^0 is probably in a low-spin configuration in II-Vs. The only outstanding candidate is GaAs:Mn, because of its small U_{ver} and large ΔU_{MC}.

The experimental situation for GaAs:Mn is intriguing. The relevant states here are $[Mn^{2+}, d^5, A^-, e^2t_2^3, {}^6A_1]$, $[Mn^{3+}, d^4, A^0, e^2t_2^2, {}^5T_2]$, and $[Mn^{4+}, d^3, A^+, e^2t_2^1, {}^4T_1]$. An acceptor transition $E(0/-)$ has been observed[273] at $E_v + 0.11$ eV (Table VII). EPR experiments (Table III) suggest spin-Hamiltonian parameters[274a] consistent with $[Mn^{2+}, d^5, {}^6A_1]$ even if the concentration of Mn exceeds that of the shallow dopants, i.e., even if most Mn should nominally be neutral $[Mn^{3+}, d^4, {}^5T_2]$. The latter state is isoelectronic with $[Cr^{2+}, d^4, {}^5T_2]$, which shows in GaAs a JT coupling and is detectable by EPR. No EPR signal of this type has ever been seen in GaAs:Mn (Andrianov *et al.*[30,111] interpreted their EPR and susceptibility data to be partially due to $[Mn^{3+}, d^4, {}^5T_2]$, but no fingerprint of a ${}^5T_2$-like EPR spectrum is apparent). Note that whereas a Mn^{3+} in *octahedral* symmetry (d^4, ${}^5E$, cf. Table I) has been postulated to exist in MgO to explain the phonon scattering contribution to the thermal conductivity,[275] no EPR imprint of a stable Mn^{3+} has been reported.

One possible explanation[12] for this puzzle is that $[Mn^{3+}, d^4]$ does not really exist in a ${}^5T_2$ state, but exists instead as a $[Mn^{3+}, (d^5 + \text{hole}), {}^6A_1]$-like species, showing only an ${}^6A_1$-like EPR, as $[Mn^{2+}, d^5, {}^6A_1]$ does. However, Clerjaud[14] pointed out that in this case there should be in the spin Hamiltonian a $J\mathbf{S}_1 \cdot \mathbf{S}_2$ exchange term between the d^5 electrons with $S_1 = \frac{5}{2}$ and a hole with $S_2 = \frac{3}{2}$. If J is not negligible, such a term will distort the EPR signal, but no such effect was observed. He concludes that the EPR spectra are due to $[Mn^{2+}, d^5, {}^6A_1]$, leaving the mystery of the absence of $[Mn^{3+}, d^4, {}^5T_2]$ unsolved.

Hennel *et al.*[276] suggested a different explanation for the absence of $[Mn^{3+}, d^4, {}^5T_2]$ and for the temperature independence of their Faraday rotation experiment: that $[Mn^{3+}, d^4]$ exists in a low-spin ${}^1A_1$ state rather than in a ${}^5T_2$ state; hence, it is EPR invisible. The calculations of Fazzio *et al.*[138,267]

[273] R. A. Chapman and W. Hutchinson, *Phys. Rev. Lett.* **18,** 443 (1967); W. Schairer and M. Schmidt, *Phys. Rev. B* **10,** 2501 (1974).

[274a] V. F. Masterov, S. B. Mikhrin, B. E. Samorukov, and K. F. Shtelmaleh, *Fiz. Tekh. Poluprovn.* **17,** 1259 (1983) [*Sov. Phys. Semicond.* **17,** 796 (1983)].

[274b] V. F. Masterov, Yu. V. Maltsev, and V. K. Sobolevskei, *Sov. Phys. Semicond.* **15,** 1235 (1981).

[275] L. J. Challis, A. A. Ghazi, and K. J. Maxwell, *J. Phys. C* **12,** 303 (1979).

[276] A. M. Hennel, A. Twardowski, and M. Godlewski, *Acta Phys. Pol.* **67A,** 313 (1985).

show that this may be the case for $[Cr^{2+}, d^4]$, where the excited $^1A_1$ state in GaAs, GaP, and InP is close (≤ 0.1 eV) to the $^5T_2$ ground state, but it is less likely to occur for $[Mn^{3+}, d^4]$, where the excited $^1A_1$ state is too high. Since, however, even $[Cr^{2+}, d^4]$ (at zero pressure) appears in a high-spin state, $[Mn^{3+}, d^4]$ should even more so exist as a high-spin species.

Caldas *et al.*[267] have pointed that a negative effective U for GaAs:Mn can explain the data in a natural way. They calculated $\Delta E_{MC}^{4,5} = -1.25$ eV, $\Delta E_{MC}^{3,4} = 0.6$ eV, and hence, $\Delta U_{MC}(A^0) = -0.65$ eV. Hence, if $U_{ver} + \Delta U_{rel} < 0.65$ eV, one has $U(A^0) < 0$. If this is the case, $[Mn^{3+}, d^4, A^0, e^2t^2, {}^5T_2]$ is never the ground state for any value of E_F: for low E_F, one has $[Mn^{4+}, d^3, A^+, e^2t_2^1, {}^4T_1]$ as the ground state, whereas after the transition point, $[Mn^{2+}, d^5, A^-, e^2t_2^3, {}^6A_1]$ is the ground state. They further pointed out the possibility that $U < 0$ *and* $E(0/-) < 0$; i.e., the conventional d^5/d^4 acceptor is inside the valence band. In this case, it is possible that $[Mn^{4+}, d^3, {}^4T_1]$ is never in the gap and only $[Mn^{2+}, d^5, {}^6A_1]$ exists in the gap for all E_F. This will happen if the multiplet correction $\Delta E_{MC}(0/-)$ to the acceptor energy outweighs the mean-field component. Note that in this "type-II negative U"[267] the *conventional* $E(0/-)$ (i.e., $^5T_2 \rightarrow {}^6A_1$ for Mn) is inside the valence band. In other words, the remaking of bonds cannot provide enough energy to transform the atom entering the crystal (d^5s^2 in Mn) into the neutral state (d^4) and lower energies are attained by the configuration $[A^- + \text{hole}]$. The *observed* (positive) acceptor, as suggested by Kaufmann and Schneider,[12] could correspond to this ground state of the type $[{}^6A_1 + \text{hole}]$, transforming into $^6A_1$. Note further that a "type-II negative U" is consistent with the fact that the A^- state is always observed by EPR in nominally p-type samples for GaAs, InP, and GaP. In GaAs:Mn another spectrum is also observed,[274b] corresponding to $g \cong 5.85$. I point out that this spectrum, interpreted previously[274b] as the $^4T_1$ ground state of interstitial Mn, d^7 could be interpreted equally well as the substitutional $[Mn^{4+}, d^3, A^+, {}^4T_1]$ (cf. Fig. 4). Note too that if the system is a type-II negative U, an observation of the d^5 configuration of Mn does not mean that the sample is n-type, as usually assumed.

The general mechanism suggested here for a negative effective U is operative whenever the two endpoint species are *electronically* stabilized (as opposed to *distortion*-stabilized species as in Anderson's mechanism). This includes therefore the s^0-s^1-s^2 sequence (where the endpoint species s^0 and s^2 are a closed-shell stability), e.g., $In^{3+}(s^0)$, $In^{2+}(s^1)$, and $In^+(s^2)$. Indeed, in centers in polar environment were suspected[266a,b] to form negative-U centers, where $In^{2+}(s^1)$ is unstable. Other examples of "missing oxidation states" due to disproportionation include manganese in acidic solutions (Mn^{3+}, d^4 unstable towards disproportionation[7]), gold complexes[7] (Au^{2+} unstable, forming $Au^+ + Au^{3+}$), and certain rhodium complexes (Rh^{2+}, d^7 unstable towards disproportionation[266c] into $d^6 + d^8$).

28. Universal Trends in Impurity Binding Energies

The understanding of the calculated trends in the one-electron gap levels in terms of a simple three-level model (Part VI,18,c) suggested to Caldas *et al.*[277] a simple universality rule. Since the energy shift ΔE of the (antibonding) gap level from its center of gravity $\bar{\epsilon} = \frac{1}{2}(\epsilon[t_2^0] + \epsilon[t_2^{VB}])$ is proportional to the energy difference $\Delta = (\epsilon[t_2^0] - \epsilon[t_2^{VB}])/2$ [Eq. (18.1)] as well as to the potential coupling matrix element $\beta = \langle t_2^0 | v | t_2^{VB} \rangle$, it is possible that the antibonding level will be approximately at a fixed distance from a host-independent reference point in different materials, since $\bar{\epsilon}$ and Δ tend to balance each other. For example, if $\epsilon[t_2^{VB}]$ is well above $\epsilon[t_2^0]$ as it is in ZnTe, then $\bar{\epsilon}$ is shallow but Δ is large, leading to a weak level repulsion $(\Delta^2 + \beta^2)^{1/2}$. If $\epsilon[t_2^{VB}]$ is closer to $\epsilon[t_2^0]$, as it is in ZnS, then $\bar{\epsilon}$ is deep but Δ is small, leading to a strong level repulsion. Hence, ϵ_{imp} will be similar in the two host crystals. Such a reference point may be taken as the intrinsic semiconductor vacuum level. To check this idea, Zunger[278] used his Green's function calculated levels of GaP:Fe and InP:Fe and referred all one-electron energy levels to the *electrostatic potential of each host crystal at its interstitial site*. The potential at the empty interstitial site has been shown to be a reasonable approximation to an internal (surface-independent) vacuum level, and had produced reasonable predictions for band alignments at interfaces.[279] Zunger found that, whereas the host-referred binding energies (HRBE) differ substantially ($E_c - 1.22$ and $E_c - 0.28$ eV, for GaP:Fe and InP:Fe, respectively), their vacuum-referred binding energies (VRBE) are much closer (-2.98 and -2.86 eV, respectively). Jaffe and Zunger[77] derived similar insight by analyzing the band-gap anomaly in ternary chalcopyrites.

Motivated by the above considerations, Caldas *et al.*[277] (CFZ) followed recent suggestions[280,281] and refer the experimentally determined HRBE of transition-atom acceptors [first $(0/-)$ and second $(-/2-)$] and donor $[(0/+)]$ levels in III-V and II-VI (Table VII) semiconductors to an approximate vacuum level, taken as the experimentally determined photothreshold Φ for the (110) surface [Eq. (8.1)]. They neglect material variations in surface corrections because (1) the experimental precision for surface corrections is poorer than for Φ, (2) Φ has proven to correlate well with E_{VBM} for a given sequence of common-cation compounds,[282] and (3) only relative *shifts* in the

[277] M. Caldas, A. Fazzio, and A. Zunger, *Appl. Phys. Lett.* **45,** 671 (1984).

[278] A. Zunger, unpublished results (1982).

[279] W. R. Frensley and H. Kroemer, *Phys. Rev.* **16,** 2642 (1977).

[280] L. A. Ledebo and B. K. Ridley, *J. Phys.* **15,** L961 (1982).

[281] P. Rojo, P. Leyral, A. Nouailhat, G. Guillot, B. Lambert, B. Deveaud, and R. Coquille, *J. Appl. Phys.* **55,** 395 (1984).

[282] W. A. Harrison, "Electronic Structure and Properties of Solids." Freeman, San Francisco, 1980.

vacuum level from one material to the other are needed here. I show in Fig. 52 the results for eight semiconductors for which reliable data exist, indicating the oxidation states that exist at each region of the gap. The remarkable result is that within a class of compounds, the VRBEs of each impurity are nearly constant, despite significant variations in HRBE.

A few chemical trends become apparent. (1) Shallow acceptors in CdTe and ZnTe [e.g., Cu, with $E(-/0) = E_v + 0.15$ eV] become deep acceptors in ZnS and ZnSe (around $E_v + 1.3$ and $E_v + 0.7$ eV, respectively, for Cu in ZnS and ZnSe)[283] merely because the VBM in the latter systems recedes, decreasing Δ and repelling ϵ_{imp} upwards, deep inside the gap. This is why CdTe can be made low-resistivity *p*-type by cation substitution, whereas sulfides cannot.[283] On the other hand, isovalent substitutional elements lacking a deep atomic energy $\epsilon[t_2^0]$ (e.g., Li, Na) can form shallow acceptors in II-VI's, thus having similar HRBE and different VRBE. The same is true for Mn acceptors in III-V's: They are deep in GaP but shallow in GaAs because $\Phi_{GaP} > \Phi_{GaAs}$. (2) Cr, Co, and Ni impurities that exist as deep donors in ZnS, ZnSe, and CdSe, but were not observed in CdTe and ZnTe, are predicted[277] to be indeed inside the valence band of the latter systems. (3) Iron impurity forms a midgap (semi-insulating) level in InP, but Cr is needed to form a midgap level in GaAs (despite the similarities in band gaps), since the VBM of InP is lower than that of GaAs. (4) Impurities in CdTe and ZnTe have similar HRBE (thus only one is shown in Fig. 52), since theeir Φs are nearly identical. Other common-anion semiconductors (e.g., InP and GaP) show variations in the HRBE of deep levels, since their Φs are different. This has also recently been experimentally confirmed for the $In_{1-x}Ga_xP$:Mn system,[89] where photoluminescence data suggest the acceptor transition to have a constant separation from vacuum for all compositions. (5) The failure to detect a V acceptor in InP (despite its existence in GaAs and GaP) is consistent with the prediction that it lies just above the CBM. (6) Cr in GaP can appear in the 1+ oxidation state, whereas it does not exist in GaAs and InP (but could be forced into the gap by applying pressure[108,165]) since the conduction-band minima of the latter materials are lower than in GaP.

Figure 53 shows[227] the universal trends in the VRBE of donors (T^{2+}/T^{3+}) in II-VIs and of acceptors (T^{3+}/T^{2+}) in III-Vs. (Similar trends are obtained for acceptors in II-VIs except that the jump is between Cr and Mn.) The overall trend, including the local minima in Mn, parallels that in free-ion ionization energies (Fig. 9a); the jump is larger in the more ionic II-VI systems since the impurity Mott–Hubbard Coulomb repulsion energies U are larger (Table VIII). The overall width of the distribution of VRBE is dictated by the host

[283] Y. S. Park and B. K. Shin, *in* "Electroluminescence" (J. I. Pankove, ed.), p. 131. Springer-Verlag, Berlin, 1977.

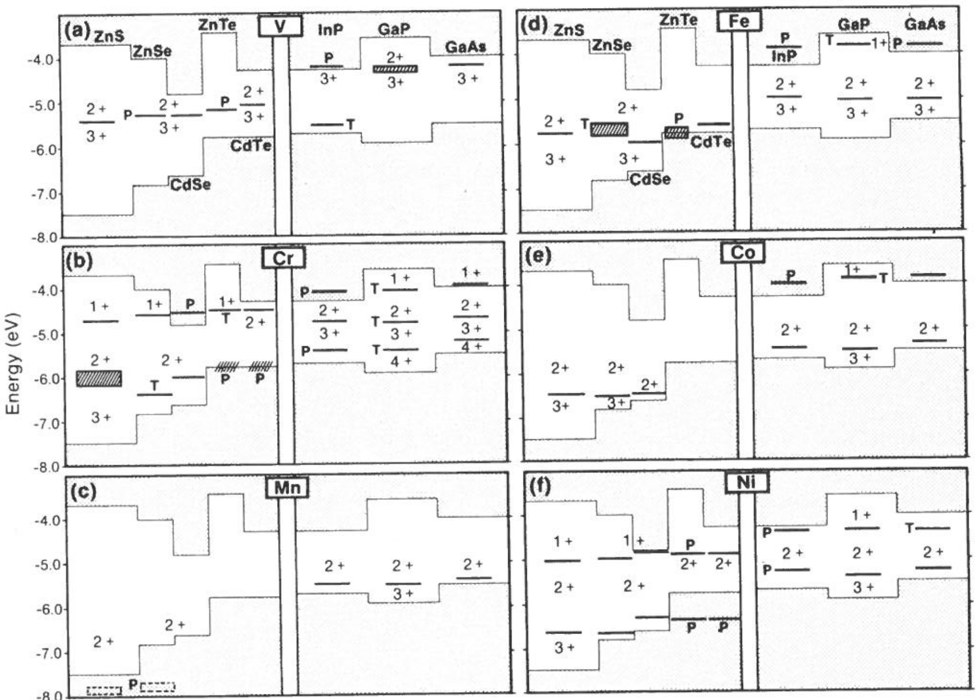

FIG. 52. Vacuum-related binding energies (VRBE) of donors and acceptors (Table VII) in various semiconductors, using work-function data of Eq. (8.1). Shaded areas denote the valence and conduction bands; cross-hatched areas denote uncertain experimental values. The numbers 1+, 2+, etc. denote stable oxidation states. T: tentative, P: predicted. Note that the VRBE values are nearly constant for a given impurity in various III-V and II-VI semiconductors. [After M. Caldas, A. Fazzio, and A. Zunger, *Appl. Phys. Lett.* **45,** 671 (1984), modified to include new data.]

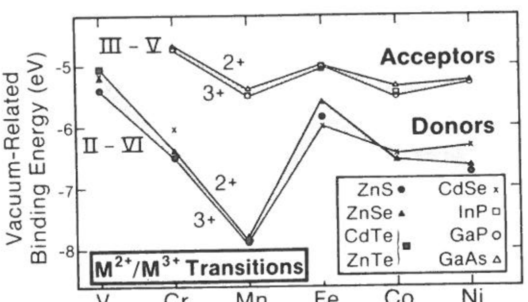

FIG. 53. Universal trends in acceptor and donor binding energies for 3*d* impurities, referred to the approximate host crystal vacuum level [Eq. (8.1)]. Shaded areas denote the existence domain of the ionization levels of a given impurity in different semiconductors. Note the local minimum at Hund's point (d^5/d^4 in Mn^{2+}/Mn^{3+}), similar to that observed in free ions (Fig. 9a). 2+ and 3+ denote the oxidation states. [After M. Caldas, A. Fazzio, and A. Zunger, *Appl. Phys. Lett.* **45,** 671 (1984).]

covalency. One hopes that the universality of VRBE could be used to predict the approximate location of unknown deep centers in crystals and alloys from a knowledge of Φ and the level position in related semiconductors. For example, the following values for donor energies can be used as rough guides to search for missing ionization energies: ZnS:Ti (2.4 eV); ZnS:Co (1 eV); ZnSe:V (1.6 eV), CdS:Fe (1.6 eV), CdS:Co (0.75 eV), CdTe:Ti (0.8 eV), and InP:Cr (0.3 eV). For the acceptors, we have GaP:Ti (1.5 eV).

29. Alloy Effects and Valence-Band Offsets

The vacuum pinning rule has a significant implication on the interpretation of alloy data[16,284] (Part III,6). Experiments on 3*d* impurities in $A_xB_{1-x}C$ alloys[85–92] reveal a linear composition (x) dependence of the transition energies $E(x)$ measured with respect to the VBM; i.e., $E(x) \cong E(0) + \bar{\alpha}x$ [Eq. (6.11)], where the slope $\bar{\alpha}$ is mostly *impurity independent*. For example, Samuelson *et al.*[89] found for $GaAs_{1-x}P_x$:Cu that $\bar{\alpha} = 0.43 \pm 0.03$ eV for different Cu-related (disorder-split) levels in this material. Recent results by the same group[91] show the same slope $\bar{\alpha}$ for Mn and Ag impurities in $GaAs_{1-x}P_x$. (A somewhat smaller slope of $\bar{\alpha} = 0.35$ eV was reported by the same group in Ref. 87.) In Al_xGa_{1-x}As:Fe, $\bar{\alpha} = 0.46$ eV was measured by Wang *et al.*[92] and Janssen *et al.*[90] found $\bar{\alpha} = 0.45$ eV for Al_xGa_{1-x}As:Cu. According to the vacuum pinning rule,[277] whereas levels of shallow impurities track closely the host-band edges closely, the *antibonding character* of deep cationic impurities leads, in different materials and alloys, to a constant separation of their binding energies from the *vacuum level* $\tilde{E}(x)$. This predicted impurity-independent universality, $\bar{E}^{(m)}(x) =$ const. for deep, antibonding, cation-site impurities, implies that[284] the apparent variations with the host crystal of VBM-referred binding energies $\epsilon_{imp}(x)$ are merely a consequence of variations $\Phi(x)$ in the position of the VBM with respect to vacuum, not an impurity effect. Hence, the conventional VBM-related binding energy $\epsilon_{imp}(x)$ is predicted to be $\epsilon_{imp}(x) = \Phi(x) - [\Phi(0) - \epsilon_{imp}(0)]$, or $\bar{\alpha} = \Phi(1) - \Phi(0)$ if we assume a linear composition variation of $\Phi(x)$. Using the observed difference in (110) photothresholds of GaP and GaAs [Eq. (8.1)], Zunger[284] showed for $GaAs_{1-x}P_x$, *independent of the cationic impurity* $\bar{\alpha} = \Phi(1) - \Phi(0) = 6.01 - 5.56 = 0.45$ eV (error bars of ± 0.05 eV), in excellent agreement with the results $\bar{\alpha} = 0.43 \pm 0.03$ eV of Samuelson *et al.*[89] He concluded[284] that their experiment measures essentially the difference in internal photothresholds of the two host materials, providing complementary information to that deduced from core photoemission of clean interfaces[285] (which include, however,

[284] A. Zunger, *Phys. Rev. Lett.* **54**, 848 (1985).
[285] H. Kroemer, *Proc. NATO Adv. Study Inst. Mol. Beam Epitaxy Heterostruct. Erice, Sicily, 1983.*

interface-specific effects). Knowledge of $\Phi(1) - \Phi(0)$ of two semiconductors and an impurity level $\epsilon_{imp}(0)$ in one of them is thus sufficient to predict the level position in the second material as well as its composition dependence in their alloys. Caldas *et al.*[277] predicted $\bar{\alpha} = 0.68 \pm 0.05$ eV for cation impurities in ZnS_xSe_{1-x}, in excellent agreement with the new results[88] for self-activated centers in this alloy, giving an average value $\bar{\alpha} = 0.61 \pm 0.04$ eV. This experiment further provides a critical test to the idea of Hjalmarson *et al.*[145] that the levels of deep cation-site impurities follow the composition variation of the cation vacancy level ("vacancy pinning"). The observation of Samuelson *et al.*[87,89] is in direct conflict with this suggestion: The calculated Ga vacancy-gap levels in GaP ($E_v + 0.15$ eV)[286] and in GaAs ($E_v + 0.06$ eV)[287] would suggest a slope of $\bar{\alpha} = 0.15 - 0.06 = 0.09$ eV, almost five times smaller than the observed slope.

The vacuum pinning rule can be reversed, using measured $\bar{\alpha}$ values for impurities to establish the difference between the *intrinsic* bulk work functions ΔE_v of the two semiconductors composing the alloy.[16,284] Zunger[16,284] had first suggested that measurements of a deep cationic impurity level in two semiconductors can serve to establish the *intrinsic* valence band offset in this pair of semiconductors. The valence-band offset ΔE_v contains a contribution ΔE_v^{bulk} that reflects the intrinsic difference in valence-band alignments of the two materials and a contribution ΔE_v^{inter} which is interface specific (hence, depends on orientation and deviation from ideality of the interface). The vacuum pinning rule[227] suggests[16,284] that ΔE_v^{bulk} can be obtained by measuring the electrical levels of the same impurity in two materials (or their alloy) from $\Delta E_v^{bulk} \cong \bar{\alpha}$. For instance, the results for Al_xGa_{1-x}As:Fe and Al_xGa_{1-x}As:Cu imply $\Delta E_v^{bulk}(Al_xGa_{1-x}As) \cong 0.45$ eV. This agrees with recent determinations[288] of the valence-band offset in AlAs–GaAs superlattice structures. Surprisingly, impurity data in alloys can be hence used to infer quantities such as ΔE_v. Note, however, that according to the theoretical model of Caldas *et al.*[277] the vacuum pinning rule can be used only for cation-substitutional antibonding levels (hence, this is not applicable to the EL2 center in GaAs which is not cationlike, or to hole excitations in GaAs:Mn which do not represent antibonding states). Furthermore, only the *intrinsic* bulk contribution to the valence-band offset can be obtained from this rule.

Data on impurity levels in different semiconductors can hence be used to deduce ΔE_v^{bulk}. Since, according to the vacuum pinning rule, the vacuum-related binding energy $-\Phi^{(H1)} + \Delta E^{(H1,I)}$ of impurity I in host H1 equals the

[286] M. Scheffler, J. Bernholc, N. O. Lipari, and S. T. Oantelides, *Phys. Rev. B* **29**, 3269 (1984).
[287] G. B. Bachelet, G. A. Baraff, and M. Schlüter, *Phys. Rev. B* **24**, 915 (1981).
[288] R. C. Miller, D. A. Kleinman, and A. C. Gossard, *Phys. Rev. B* **29**, 7085 (1984); W. I. Wang and F. Stern, unpublished results (1985).

VRBE $-\Phi^{(H2)} + \Delta E^{(H2,I)}$ of same impurity I in a different host H2, then

$$\Delta E^{(H1,I)} = \Delta E^{(H2,I)} + (\Phi^{(H1)} - \Phi^{(H2)}) = \Delta E^{(H2,I)} + \Delta E_v^{bulk}. \qquad (29.1)$$

Plotting $\Delta E^{(H1,I)}$ *vs* $\Delta E^{(H2,I)}$ for a series of impurities in two host crystals, H1 and H2 hence provides the average intrinsic valence-band offset ΔE_v^{bulk}(H1,H2) between them. This procedure does not use the observed photothreshold data which combine intrinsic and extrinsic contributions. Using the data of Table VIII, I find the expected transitivity, e.g.,

$$\begin{aligned}\Delta E_v^{bulk}(\text{GaP-InP}) &+ \Delta E_v^{bulk}(\text{InP-GaAs})\\ &= (0.18 \pm 0.02) + (0.22 \pm 0.03)\\ &= \Delta E_v^{bulk}(\text{GaP-GaAs}) = 0.40 \pm 0.05 \text{ eV}. \qquad (29.2)\end{aligned}$$

The value ΔE_v^{bulk}(GaP-GaAs) = 0.40 ± 0.05 eV deduced from impurity data in *pure* GaP and GaAs agrees with the values $\bar{\alpha} = 0.43 \pm 0.03$ eV[89] deduced from *alloy* experiments on $GaAs_{1-x}P_x$. We could now use these ΔE_v^{bulk} values to estimate the interface-specific contributions ΔE_v^{inter}, by using the Φ values of Eq. (8.1) (which combine both bulk and interface effects) to obtain $\Delta E_v^{inter} = \Delta\Phi - \Delta E_v^{bulk}$. This shows interface-specific effects to range between 0.05 to 0.25 eV, with an average of 0.15 eV. This represents the accuracy limit that can be expected from application of the vacuum pinning rule using the observed *extrinsic* phototreshold values (Fig. 51). Clearly, *intrinsic* values should be used, when available. Furthermore, this energy range represents the accuracy limit of all theoretical models of valence-band offsets which postulate transitivity.[289] Katnani and Margaritondo[290] have deduced empirically transitive valence-band offsets by fitting the best photoemission data. They find for GaP-InP, InP-GaAs, and GaP-GaAs the values 0.27, 0.36, and 0.63 eV, respectively. Compared with our bulk values of 0.18, 0.22, and 0.40 eV, respectively, we find again (linearized) interface-specific contributions of 0.09, 0.14, and 0.23 eV, respectively, or an average of $\Delta E_v^{inter} \cong 0.15$ eV.

VIII. Future Prospects

The substantial experimental and theoretical advances made over the past ten years in the field of 3*d* impurities in semiconductors have answered numerous questions and, at the same time, raised many new issues. The theoretical systematization of many of the observed ionization and $d \rightarrow d^*$

[289] W. A. Harrison, *J. Vac. Sci. Technol.* **14,** 1016 (1977); W. R. Frensley and H. Kroemer, *Phys. Rev. B* **15,** 2642 (1977); J. Tersoff, *Phys. Rev. B* **30,** 4874 (1984); and *Phys. Rev. Lett.* **52,** 465 (1984).

[290] A. K. Katnani and G. Margaritondo, *Phys. Rev.* **28,** 1944 (1983); see also G. Margaritondo, *Phys. Rev. B* **31,** 2526 (1985).

transition energies now provides clear indications as to which of the hitherto unobserved states (blank areas in Tables V and VII) should be, in principle, observable, and what is their approximate energy (cf. entries marked "gap" in Table VII and predicted values in Fig. 52). Qualitatively new features, characteristic of semiconductor host crystals and unmatched by the classical ionic systems, have been predicted theoretically to exist, including the occurrence of low-spin ground states for low-*Z* (Ti, V) and high-*Z* (Co) impurities, and the participation of impurity-induced valence-band resonances both in $d \rightarrow d^*$ transitions and in ionizations. In addition, the prediction of a self-regulating response mechanism has suggested additional *new phenomena*, including the occurrence of spin-stabilized "negative-*U*" centers in the d^3-d^4-d^5 sequence, the opposing movement of charge density on the impurity and ligand sites as the oxidation state is altered, and the qualitatively different responses of *spin* densities and *charge* densities to ionizations. The advancement of the "vacuum pinning rule" now offers new experimental means of observing *intrinsic* valence-band offsets in semiconductor heterojunctions and superlattices using impurity excitations as a probe. Many of the established intellectual tools used in the past to analyze the properties of 3*d* impurities in ionic crystals, and eventually extended to semiconductors have now been challenged—the use of the Tanabe–Sugano multiplet approach, the concept of crystal-field stabilization energy, the physical basis of the Ludwig–Woodbury model, the role of the Ham effect in explaining *g*-value quenching in Si and the significance of valence-band resonances in controlling ENDOR spin densities—to name a few. The new suggested concepts will have to be challenged and probed themselves, as new data and better theoretical models become available. The recent ability of theoretical models to go beyond cluster models, address both the one-electron *and* the many-electron aspect of the problem, predict wave-function-related and charge-density-related quantities (in addition to the more conventional observables related to energies alone), and address lattice-relaxation effects, suggest an optimistic outlook on even closer ties between theory and experiment. Recent advances and refinements in experimental impurity identification and characterization techniques promise in turn, to provide new challenges to theory.

Acknowledgments

It is a pleasure to acknowledge many discussions and collaborations with M. J. Caldas, A. Fazzio, H. Katayama-Yoshida, U. Lindefelt, V. Singh, and D. M. Wood. I am grateful to J. W. Allen, B. Clerjaud, A. Hennel, U. Kaufmann, J. Langer, H. J. Schulz, W. Ulrici, M. S. Skolnick, and Z. Liro for reviewing my compilations of experimental data and for many helpful suggestions. This work was sponsored by U.S. Department of Energy through SERI, under contract number DE-AC02-83CH10043, and by the office of Energy Research, Materials Science Division, U.S. Department of Energy, Grant No. DE-AC02-77-CHO-0178.

NOTE ADDED IN PROOF

Since the submission of this article, a number of additional articles relevant to the subject have appeared.

(1) *Electronic Structure.* F. Beeler, O. K. Anderson, and M. Scheffler (BAS) have applied their linear muffin tin orbital (LMTO) Green's function method to study interstitial $3d$ impurities in Si within the local spin density formalism [*Phys. Rev. Lett.* **55**, 1498 (1985)]. Their method differs in details from that used previously by Katayama-Yoshida and Zunger[39,47,217,258], for example, BAS have utilized the frozen core and the atomic sphere approximations (whereas KYZ have treated the core orbitals dynamically and involved no spherical approximations); BAS have shifted upward rigidly the host crystal conduction band to fit the observed fundamental Si band gap, hence their band structure wavefunctions are no longer eigenfunctions (KYZ have instead adjusted the host pseudopotential to fit the first five interband energies; their band wavefunctions diagonalize the host crystal Hamiltonian, as required by the basic Green's function formalism[21]). Finally, BAS have not applied the self-interaction correction[215] to the impurity potential, since it does not improve on the $d \rightarrow s$ and $d \rightarrow p$ atomic (interconfigurational) excitation energies, but KYZ have used this correction since it dramatically improves on all other properties of $3d$ ions, including[215] the orbital energies, ionization energies, orbital localization, spin densities, and magnetic moments. These properties (and not the $d \rightarrow s, p$ excitation energies, absent altogether in the impurity system) can directly affect the calculated properties of Si:$3d$. The calculation of BAS confirms many of the results of KYZ, including the occurrence of *low-spin* ground states for interstitial Ti^0, V^+, Ti^-, V^0 (p. 436), the prediction of the absence of a Hund-point in Si, Ti (p. 440), the mechanism for the occurrence of a crystal field splitting (p. 411), and trends in the electrical levels (Fig. 49 here and Fig. 2 in BAS). This provides strong support for both methods. However, some differences in results exist, including the prediction by BAS that Cr^0 and Cr^+ are low spin (in contrast with experiment) and that the highly charged impurities appear in BAS very low in the band gap (or inside the valence band). Hence, Cr^{3+} is inside the valence band, so the possibility of "negative U" (p. 452) cannot be examined in their calculation.

Recently, R. Broer, G. Aissing, W. C. Nieuwpoort, and L. F. Feiner (in press) also presented a Hartree–Fock cluster study of Ti, V, Cr, and Mn interstitial impurities in Si. Only Ti^0 was found to be in a low-spin ground state.

(2) *Alloy Effects and Valence Band Offsets.* J. M. Langer and H. Heinrich [*Phys. Rev. Lett.* **55**, 1414 (1985)] have extended the method of Ref. 284 (see also Ref. 16) for deducing intrinsic valence band offsets of semiconductors from $3d$ impurity levels (Part VI,29) by including a more extensive data base of experimental data. J. Tersoff [*Phys. Rev. Lett.* **56**, 675 (1986)] elaborated on the significance of this correlation to the theory of Schottky barriers.

Subject Index

A

Acceptor hole emission, 401
Acceptor-state occupation numbers, 401
Acceptor states, 442–449
  acceptor transition in Mn of GaAs:Mn, 455
  deep acceptors in ZnS and ZnSe, 458
  shallow acceptors in CdTe and ZnTe, 458
"Active impurity electrons," 277, 278, 280, 292–293, 303–304, 312, 378
Admittance matrix, 251
Adspace representation, 396
Aging, 135, 151, 159, 166–168, 182–183
  below 440 K, 151
  and electrical resistivity, 163, 183
  and hardness, 183
  kinetics of, 159
  re-aging kinetics, 182
Aggregation, kinetic theory of, 235–238
  generating function, equation for, 236
  gold colloid, experiments with, 241–244
  kernels, 237–238
  as a percolation problem, 238
Airy stress-function analysis, 39
Alloy decomposition, metastable stages in, 131–134
Alloy effects and valence-based offsets, $3d$ impurities in alloys, 460–462
Alloys, Guinier–Preston zones in, 131–206
Aluminum–copper alloys, 159–186
  aging scheme, 161
  change in zone size and density with aging time, 183
  cluster distribution, computer simulation of, 164
  distortions in the initial stage, 173–178
  displacements for interatomic vectors in GP zones, 176
  displacements normal and parallel to GP zone, 177
  strains normal to single layer zones, 173–174
  structured models, table of, 175
  elastic scattering, 162
  enthalpy of formation and of binding, 165
  EXAFS of, 149
  free energy versus composition, schematic of, 134
  the initial stage, 167–172
  the later stage, 178–186
    effects of aging, 180–181
  nucleation and growth, 184–185
  pair potential versus interatomic distance, 165
  phase diagram, Al-rich corner, 161
  resistivity changes in, 184
  solid solution, 159–166
  strains normal to zone faces, graph, 185
  vacancy contribution, 165
  the zones, 166–167
    aging, 166
Aluminum–silver alloys, 150–156
  chemical nature of clusters, 150–156
    phase diagram, 150
  GP zone in, 153
  local distortions, 156
  temperature dependence of faceting, 155
Aluminum–zinc alloys, 156–159
  pair probability, 157
  phase diagram, 158
  zone shape, 156–158
  zone-size distribution, 159
Anderson negative U, 353